Residual Axial and Lateral Load Carrying Capacity of Pile Supported Marine Terminal Exhibiting Seismically-induced Local Buckling in Inground Plastic Hinges

Theresa Richards

José I Restrepo

Sergio Suarez

Machel Morrison

Department of Structural Engineering

University of California, San Diego

National Institute of Standards and Technology (NIST) and

National Science Foundation (NSF)

NIST FAA Number: 70NANB22H061

Residual Axial and Lateral Load Carrying Capacity of Pile Supported Marine Terminal Exhibiting Seismically-induced Local Buckling in Inground Plastic Hinges

Theresa Richards
Department of Structural Engineering
University of California, San Diego

José I Restrepo
Head of R&D at Nabih Youssef Associates
Professor Emeritus of the University of California, San Diego

Sergio Suarez
Department of Structural Engineering
University of California, San Diego

Machel Morrison
Assistant Professor, Department of Structural Engineering
University of California, San Diego

National Institute of Standards and Technology (NIST) and
National Science Foundation (NSF)
NIST FAA Number: 70NANB22H061

June 2025

ABSTRACT

Steel pipe piles have been increasingly used to support new marine terminals along the seismically active west coast of the US. These structures are being designed using the first generation of performance-based seismic design requirements incorporated into the ASCE-COPRI 61 “Seismic Design of Piers and Wharves” Standards. For structures essential to the regional economy, post-event recovery response, or that require a level of seismic performance beyond life-safety protection, the standard prescribes performance-level checks for three seismic hazards and provides strain limit-states for these piles. These limit-states were borne-out using engineering judgment. To date, minimal to no physical testing or computational simulation has ever been conducted on these types of piles specific to this application to verify the critical life-protection performance level that could occur when a pile loses the gravity load-carrying capacity after the pile develops an inertia loading-induced inground plastic hinge and exhibits local buckling. This research evaluates the in-ground hinge performance of steel pipe piles commonly used in marine applications.

ACKNOWLEDGMENTS

This project was sponsored mainly by the National Institute of Standards and Technology (NIST) and the National Science Foundation (NSF) under award number 70NANB22H061. The Naval Facilities Engineering Systems Command (NAVFAC) provided additional financial support. The Port of Los Angeles, Port of Long Beach, Moffatt & Nichol, and Earth Mechanics Incorporated (EMI) provided material and in-kind technical support throughout the project.

The experiment was conducted at the University of California, San Diego Englekirk Structural Engineering Center (ESEC) with support from ESEC and UCSD Powell Laboratory technical support staff.

The blind prediction contest was accomplished with the direct support of the Pacific Earthquake Engineering Research Center (PEER).

Any opinions, findings, and conclusions or recommendations expressed in this material are those of the authors and do not necessarily reflect those of NIST/NSF, NAVFAC or others.

TABLE OF CONTENTS

APPENDICES

LIST OF TABLES

LIST OF FIGURES

1. Introduction

In 2014, after a public review cycle and balloting, the ASCE-COPRI 61 committee approved a Standard titled "Seismic Design of Piers and Wharves" [8] which incorporated first-generation performance-based seismic design requirements. The standard prescribes performance-level checks for three seismic hazards which is critical for structures essential to the regional economy, post-event recovery response, or that require a level of seismic performance beyond life-safety protection. The checks identified in the standard are (i) Minimal damage for the Operating Level Earthquake, having a 50% probability of exceedance in 50 years; (ii) Controlled and repairable damage for the Contingency Level Earthquake having a 10% probability of exceedance in 50 years; and (iii) Life-safety protection for the Design Earthquake, which the standard makes it the same as the design earthquake in the ASCE 7-05 Standard [6].

Marine structures built on sloping mudlines or dikes often include a subset of landside piles commonly referred to as seismic piles. These piles represent a fraction of the total foundation system but typically have shorter unsupported lengths, making them the primary contributors to the structure's lateral stiffness and resistance. During seismic events—or in the post-event phase—these piles experience significant lateral demands, which can lead to the formation of plastic hinges either at the pile-to-deck connection or below the mudline, within the embedded portion of the pile.

In seismic-prone marine environments, steel pipe pile-supported structures are commonly designed with a reinforced concrete pile-to-deck connection that integrates into the pile cap or deck. This connection is detailed to accommodate inelastic behavior in the concrete plug, which acts as a structural fuse—intentionally yielding to dissipate energy while protecting the rest of the system. As a result, local buckling of the steel pile is primarily expected to occur below or near the mudline, depending on the surrounding soil conditions.

For hollow (i.e., close-ended) or soil-infill (i.e., open-ended) steel pipe piles, the ASCE-COPRI 61 Standard [8] prescribes the compressive strain limits for Minimal damage, Controlled and Repairable Damage, and for Life-safety protection performance-levels listed in Table 1. Due to limited research, these strain limits were born out of engineering judgment. In the past two decades, steel pipe piles have become a preferred deep-foundation system chosen for many marine terminals and other marine structures in the high seismic regions of the US, particularly on the West Coast, and the need to have research-supported design recommendations has become dire.

In the development of the second generation of performance-seismic design provisions for pile-supported marine structures in ASCE-COPRI 61 [8], the following questions have arisen: (i) What do the prescribed strain-limits represent in the physical world? The onset

of local buckling? Fracture? Loss of gravity load carrying capacity? (ii) Testing has shown the pile diameter to wall thickness ratio may be an important variable to assess the onset of local buckling. Is such a variable important, or the main variable that should be considered to assess the pile loss of gravity load carrying capacity? (iii) If local buckling is the right metric to define one of the strain limits, why is a compressive strain prescribed and not the range between the peak tensile to peak compressive strain instead? (iv) do open-ended and close-ended pipe piles behave differently and require different strain limits? (v) shouldn't the pile loss of gravity load-carrying capacity of piles subjected to lateral inertial loading be the governing performance criterion for life-safety protection, at least, in the second generation performance-based seismic design of marine structures? Further research work could incorporate the effect of pile redundancy, where damaged piles can redistribute gravity loading to adjacent piles in the structure.

Table 1 ASCE-COPRI 61-14 [8] Compressive Strain* Limits for Steel Pipe Piles

Performance Level	Inground	Deep Inground
Minimal Damage	0.010	0.010
Controlled/Repairable Damage	0.025	0.035
Life-safety protection	0.035	0.050
* Compressive strain is assumed positive in ASCE-COPRI 61-14		

The objective of this research is to investigate these questions both experimentally and through detailed nonlinear finite element simulations, with the aim of distilling simple design recommendations for consideration and potential adoption into the ASCE-COPRI 61 standard [8]. The scope of the research is confined to examining the effects of lateral inertial loading on seamless, single, and double-welded steel pipe piles driven into soils that are not prone to liquefaction. Due to the periodic anisotropy present in spiral welded steel pipe piles, the findings from this study will not directly apply to these piles.

Between August 2022 and May 2024, four large-scale tests were conducted at UC San Diego to evaluate the performance of in-ground hinges for steel pipe piles with diameter-to-thickness (D/t) ratios ranging from 22 to 43. The purpose was to address knowledge gaps regarding the recommended critical strains for the in-ground hinge of steel pipe piles. Over the past two decades, industry practitioners, particularly those within the American Society of Civil Engineers/Coasts, Oceans, Ports & Rivers Institute (ASCE/COPRI) and Permanent International Association of Navigation Congresses (PIANC) standards committees, have debated whether the current ASCE/COPRI 61-14 [8] (ASCE/COPRI, 2014) recommended in-ground strain limits for the seismic design of

steel pipe pile-supported waterfront structures are appropriate or potentially unconservative.

Harn et al. [29] and Sadowski et al. [41] compared critical strains for hollow and filled steel pipe piles in literature against proposed design equations and the ASCE/COPRI 61-14 [8] recommended steel pipe pile in-ground strain limits. Figure 1 recreates the "D/t Effect on Critical (Buckling) Strain" figure from Harn et al. [29], with blue lines illustrating the D/t ratios of the four tests, thereby demonstrating the anticipated performance assuming in-ground plastic hinge behavior aligns with prior findings.

The test program was executed at the Soil-Structure Interaction (SSI) Test Facility North Soil Pit at the University of California, San Diego (UCSD) Englekirk Structural Engineering Center (ESEC). Four steel pipe piles underwent reversed cyclic lateral loading using an increasing amplitude displacement loading protocol to achieve very large lateral displacements. Anticipated outcomes included in-ground local pipe buckling, degradation in flexural strength, and significant axial shortening.

Concurrent with the test program, detailed nonlinear finite element models were developed to identify the primary parameters leading to potential loss of gravity load-carrying capacity in piles subjected to lateral loading. These computational models validated one or more of the field tests conducted. An extensive evaluation of in-ground hinge performance, post-peak pile performance, and axial shortening will be vital in providing future design recommendations to the industry.

The overall test program was divided into two phases, funded by three agencies: (i) the joint research program between the National Institute of Standards and Technology (NIST) and the National Science Foundation (NSF); (ii) the Naval Facilities Engineering Systems Command (NAVFAC) via the ASCE-COPRI Institute; and (iii) the Port of Long Beach. Additionally, the analytical portion of the research, including finite element modeling, was supported by the Pacific Earthquake Engineering Research Center (PEER). The Port of Long Beach provided test specimens, the Port of Los Angeles supplied material testing samples, and Earth Mechanics Inc. (EMI) offered geotechnical support services. Guidance for the project was provided by an Advisory Board comprising industry experts.

Three hollow steel pipe piles with an outer diameter of 10.75 inches and wall thicknesses of either 0.25 inches or 0.5 inches were tested under the NIST/NSF-funded project. One hollow steel pipe pile with an outer diameter of 12.75 inches and a wall thickness of 0.375 inches was tested with the support of both NIST/NSF and NAVFAC funding. This study evaluates variables such as diameter-to-thickness ratios and constant axial loading. All test piles are specified according to API X52 standards [5] and are instrumented with strain gages, inclinometers, vertical and lateral string potentiometers, accelerometers, and digital image correlation (DIC) to monitor their behavior during testing.

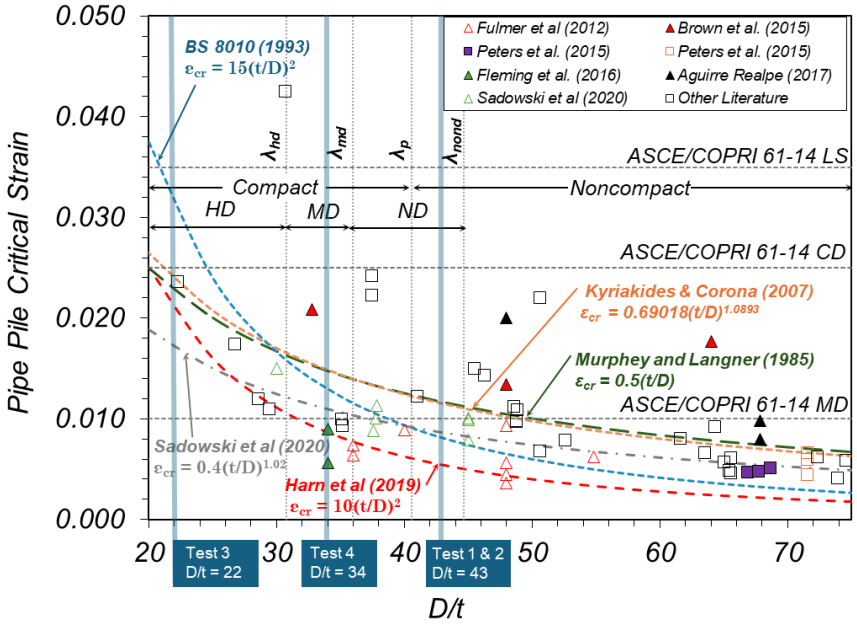

Figure 1: Pipe Pile Critical Strain in terms of D/t Ratio (Harn et al Recreation) [29]

2. Literature Review

In marine applications, steel pipe piles with different diameter-to-thickness ratios are driven vertically, with their ends either closed or open, serving as structural support for vertical and lateral resisting systems. Over the past decade, the marine structural engineering community has shown increasing concern regarding the seismic performance of driven steel pipe piles.

In the design of piers and wharves located in seismic regions, performance-based and displacement-based design methods are used in the structural seismic analysis. Pile-supported structures are designed in the United States in accordance with ASCE/COPRI 61: Seismic Design of Pile-Supported Piers and Wharves (ASCE/COPRI 61, 2014) [8].This standard recommends structures to be designed to withstand three different performance hazard levels; operational level earthquake (OLE), contingency level earthquake (CLE) and design level earthquake (DE). These levels are defined by the probability of exceedance for ground motion and performance levels, categorized as minimal damage (MD), controlled and repairable damage (CD), and life safety protection (LS). Unlike building structures, wharves are designed so that plastic hinges form in the pile rather than in the deck structure, thereby protecting the deck—hence the design principle of "strong deck - weak pile." Plastic hinges are specific regions within the pile where inelastic deformations concentrate due to the material surpassing its yield strength under seismic loading. These plastic hinges typically develop in three regions: at the pile head (within the deck-to-pile connection), at the soil-pile interface at mudline, and/or within the embedded pile length, i.e., in-ground.

In design, wharf structures are typically modeled using simplified beam-elements using programs such as SAP2000. The stiffness properties for pile beam elements are determined through moment curvature analysis of the pipe cross-section. Nonlinear properties determine plastic hinges within beam elements by considering moment-curvature relationships, material properties, confinement effects, axial load levels, and the plastic hinge length as specified in ASCE/COPRI 61 (2014) [8]. The in-ground plastic hinge length is typically taken as two pile diameters unless detailed modeling or experimental tests provide justification for a different length. The maximum plastic hinge zone strain demands are calculated by converting rotations at the hinges to curvatures and then converting curvature to strain. These strains are then checked against the prescribed strain limits in ASCE/COPRI 61 (2014) [8]. This approach to estimating material deformation demands assumes that plane sections remain plane and that curvature distributions are uniform strain field along the plastic hinge length. This assumption is consistent with concrete pile testing performed by Blandon [11] and has proven to be accurate based on reinforced concrete-filled steel tube testing conducted by Brown et al. [15]. However, unlike concrete piles, the wall of a hollow steel pipe-pile is

susceptible to local buckling, which in some cases may occur at relatively low levels of plastic rotation. This local buckling invalidates the plane-sections hypothesis used to calculate strain demands, however, the occurrence of local buckling does not necessarily constitute failure of the pile i.e. complete loss of lateral and axial load carrying capacity.

2.1 The Evaluation of Local Buckling on Buried Pipelines

Early research assessed the behavior of buried steel tubes under bending for oil and gas pipeline applications. These pipelines are subjected to external earth pressures, internal pressures, and substantial deformations due to soil movements. The performance of the steel tube is highly dependent on the pile diameter-to-wall thickness ratio, known as the D/t ratio. Several experimental tests conducted in the 1970s and 1980s by Sherman [41], Zayas et al. [48], Sherman [43], and Gresgnigt [28] evaluated pressurized and unpressurized buried steel tubes with D/t ratios ranging from 18 to 110. Except for Zayas et al. [48], all studies examined the performance of buried tubes under monotonic loading in three or four-point bending tests subjected to flexure. Zayas et al. [48] investigated six A36-grade steel braced tubes under cyclic axial loading. The walls of the tubes buckled locally once the first yield moment occurred, leading the section to perform plastically and redistributing the internal moments in the steel pipe. Large D/t tube pipes under cyclic loading displayed a rapid decline in structural capacity after the onset of buckling due to the thin wall thickness.

Steel tube ovalization, as shown in Figure 2 and local buckling within the plastic region was widely unknown prior to the early experimental research on buried pipeline specimens. Gresnigt [28] conducted numerous monotonic three-point air tests on both pressurized and unpressurized steel tubes, with D/t ratios ranging from 20 to 110. The onset of buckling, which occurs at the maximum bending moment, was influenced by the internal pressure within the steel tube. Higher internal pressures delayed the onset of buckling. Tubes with high internal pressures significantly affected the critical buckling curvature.

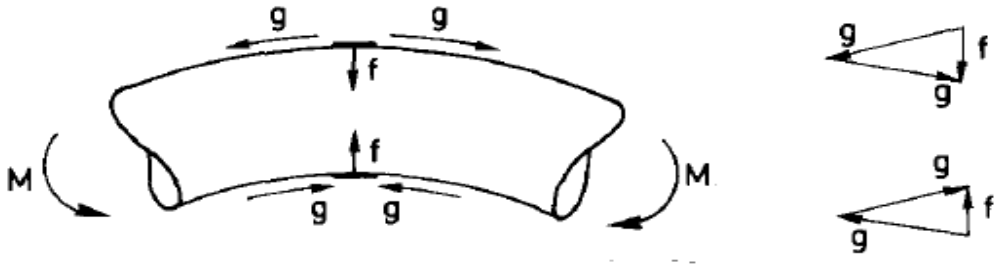

Figure 2: Local Ovalization Forces of Steel Tube (Gresnigt, 1986) [28]

Dorey et al. [20] were among the few researchers to apply a constant axial force to a steel pipe in a full-scale test, taking into account temperature-induced eigen-forces. The tests

involved thirty-eight plain and girth welded steel tubes subjected to monotonic loading, with consideration given to the eccentric axial load applied to a pressurized steel tube while assessing post-buckling behavior. The study concluded that axial strain is crucial in determining critical bending strain. The D/t ratio isn't the only factor affecting pipe buckling; internal pressure, yield strain, and circumferential girth welds are also important.

2.2 The Evaluation of Local Buckling on Tested Hollow Steel Pipe Piles

Local buckling, as shown in Figure 3, is more susceptible to occur on hollow piles. Fulmer et al. [26] assessed the performance of eight hollow spiral-welded steel pipe piles with D/t ratios ranging from 36 to 55. These piles were tested in-air and subjected to four-point bending under cyclic loading conditions. They found that local buckling reduced overall member strength by 20% but did not assess the residual axial loading.

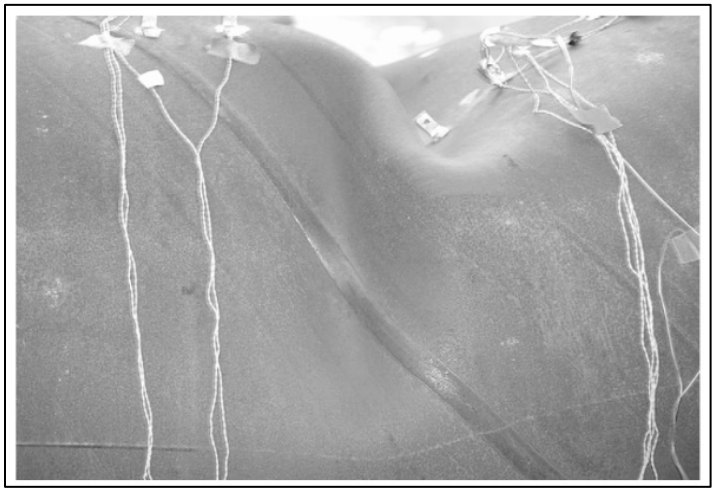

Figure 3: Local Buckling of Hollow Steel Pile with Spiral Weld (Fulmer et al. [25])

In 2016, two experimental research programs were simultaneously conducted to assess the behavior of steel tubes in marine applications. Van Es et al. [45] performed an investigation on fifteen large-scale four-point bending tests of hollow steel tubes, focusing on pre-existing geometric imperfections and material properties. The study observed the occurrence of local buckling at the locations of girth or coil connection welds, or at geometrical imperfections that developed during fabrication. While the residual axial capacity was not specified, a significant amount of bending capacity remained after the onset of buckling, diminishing only gradually with increased post-buckling.

Winkel [46] conducted an investigation on eight large-diameter steel piles commonly utilized in the design of breasting and mooring dolphins for marine terminals. These piles were subjected to single point lateral loading during field tests at the Port of Rotterdam. Due to their large diameter, these pipes have thin walls, resulting in slender piles with substantial D/t ratios ranging from 92 to 250, which heightens the risk of failure. Large-diameter piles are typically driven with either open or closed ends. When driven with open-

end tips, soil plugs form below the mudline. The density of these soil plugs, whether loosely or densely packed, influenced the location where buckling initiated. Winkel [46] identified four critical locations within the mudline to five pile diameters (5D) below as potential risks for the onset of local buckling: (i) the location of maximum bending moment, (ii) the maximum soil pressure, (iii) the mudline elevation, and (iv) the top of the soil plug elevation.

Fleming et al. [24] tested two piles with the same D/t ratio under cyclic loading in both improved and unimproved clay soil. The pile in improved soil yielded within 1 foot below ground and showed local buckling above due to low cycle fatigue. In unimproved soil, initial yielding occurred at a depth of 4 feet.

Sadowski et al. [41] performed three-point bending tests on nine cold-formed hollow steel pipes, with seven of these specimens tested to the point of failure. The steel tubes were of grade S355J2H and had diameter-to-thickness ratios ranging from 30 to 45, in compliance with EN 10210 standards. Failure was detected in the initial cycle by observing a decline in the load-displacement curve. The results obtained were corroborated using an ABAQUS model, excluding considerations of soil conditions and external axial loads.

2.3 The Experimental Testing of Filled Steel Pipe Piles

Marine applications often use reinforced concrete-filled steel tubes (RCFSTs), concrete-filled steel tubes, and sand-filled steel tubes. In-air tests in literature evaluate the buckling performance of these filled steel tubes.

Montejo et al. [34] studied the behavior of RCFSTs with different D/t ratios using a four-point bending air test. Based on these tests, they proposed reduced strain-based damage control limits for implementation into the Port of Los Angeles Code for Seismic Design [19].

Brown et al. [15] conducted twelve four-point bending reversed cyclic loading tests on RCFST with D/t ratios ranging from 32 to 192. They noted a reduction in bending capacity following local buckling and subsequent fracture of the tube wall. The study found that the tensile strain of the tube affects its resistance to local buckling under compression, with higher D/t ratios requiring lower tensile strain limits at buckling onset. Brown et al. [15] suggested a tensile strain limit for high D/t ratios, which they determined to be suitable for low D/t ratios as well. This recommendation was adopted by the Alaska Department of Transportation.

Aguirre and Realpe [2] and Kowalsky [30] performed twelve half-scale RCFST tests in the soil, as shown in Figure 4. The tests conducted were similar to the four-point bending test described by Brown et al. [15], but with variations in axial load ratio and soil stiffness due to embedding in soil. Local buckling is significantly influenced by the D/t ratio of the

tube. However, the occurrence of fractures was independent of the D/t ratio, manifesting under a constant strain. Specimens with imperfections, such as welding defects, are prone to quicker onset of buckling due to these imperfections. Indeed, the D/t ratio impacts the tube, exhibiting a greater influence on the strength rather than the stiffness of the tube. Additionally, the aboveground length-to-diameter ratio and soil stiffness have implications for the strength and displacement characteristics of the system [2].

A study conducted by SBRCUnet, as referenced by van Es et al. [45], examined twelve sand-filled steel tubes with diameter-to-thickness (D/t) ratios ranging from 72 to 119 in four-point bending tests. It was observed that, unlike hollow tubes, sand-filled tubes exhibited outward local buckling due to the internal sand pressure exerted on the tube walls. Gresnigt [28] noted that this internal pressure mitigated ovalization, thereby delaying the onset of local buckling [45]. The moment capacity of sand-filled tubes was reduced by 15% to 25%, which is comparable to or less than the reduction observed in hollow piles as reported by van Es et al. [45].

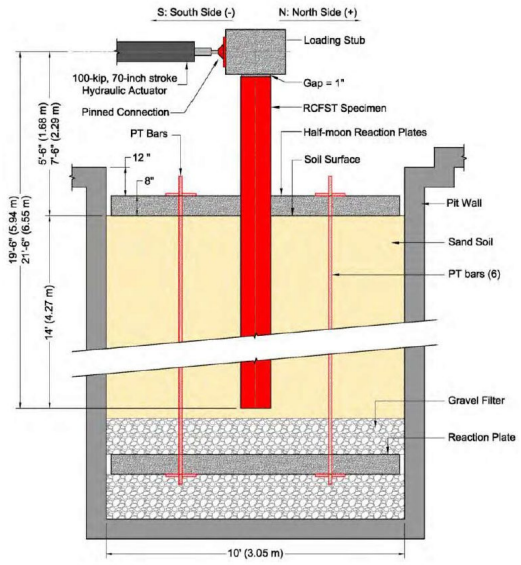

Figure 4: RCFST Tube in Soil Test Setup (Kowalsky, 2019) [30]

2.4 Literature Proposed Critical Strains

Piers and wharves are constructed of stockier steel pipe piles with D/t ratios ranging from 20 to 60. Harn et al. [29] analyzed test results published for both hollow and filled steel tubes, asserting that hollow piles in piers and wharves may experience premature buckling at the in-ground hinges before attaining the strain limits prescribed by design codes. Figure 5 illustrates the idealized force-displacement response of pipe piles in pier and wharf applications, demonstrating that local buckling can occur at varying force-displacement demands depending on the D/t ratios and soil types. Ductile piles,

characterized by low D/t ratios, should ideally attain point 3 on the curve, reflecting the compactness of the section.

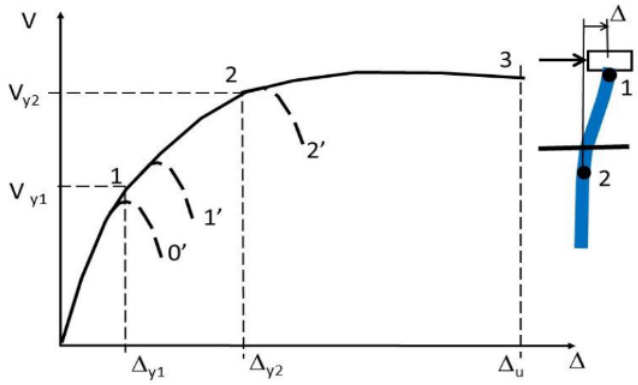

Figure 5: Idealized Force-Displacement Response for Pier/Wharf Pipe Pile (Harn et al., 2019) [29]

The location of the initial hinge in pile-supported structures is significantly influenced by the ductility of the structural system. In performance-based design, the placement of the initial hinge should correspond with the performance levels. For MD and CD, it is optimal for hinges to develop within or below the deck, as this area is more accessible for repairs. The top-of-pile deck connection detail for steel pipe piles typically includes a reinforced concrete plug embedded into the concrete deck. Seismic pile connections to the deck are generally designed as partial-moment-connections, causing the anticipated yield point to occur within the concrete plug connection below the deck [27]. However, if the pile has a relatively short unsupported length above mudline with surrounding stiff soil conditions, there is a possibility that a plastic hinge could form in-ground at low performance levels. This research examines the performance of the in-ground hinge and the specified strain limits utilized in designing seismic piles for marine structures.

The current strain limits presented in ASCE/COPRI 61-14 [8] are conveyed in the commentary as being developed from full-scale test programs supplemented with numerical analyses. However, there is no test programs referenced which support the current in-ground hinge strain limits for steel pipe piles provided in ASCE/COPRI 61-14 [8]. Table 1 summarizes the ASCE/COPRI 61-14 [8] in-ground and deep in-ground hinge strain limits for steel pipe piles. Recent studies have examined the flexural behavior of steel pipe piles and have compared experimentally measured critical strains, i.e. maximum strains developed prior to the onset of local buckling, to the code specified strain limits. Many of these studies were in-part motivated by the NCHRP Synthesis 440 [36], which first compared the material strains presented in Port of Los Angeles (POLA) [19] Seismic Design Guidelines, Port of Long Beach (POLB) [38] Wharf Design Criteria and the California Building Code Chapter 31F Marine Oil Terminals Engineering and Maintenance Standards (MOTEMS) [33]. It should be noted that the ASCE/COPRI 61-14

standard [8] presents strain limits identical to those presented in POLB Wharf Design Criteria and POLA Seismic Code.

The NCHRP Synthesis 440 [36] determined that the existing codes and guidelines did not adequately address the relationship between strain and damage. Specifically, for steel pipe piles, it was not evident which limit state was associated with the physical performance of the pipe, such as preventing bulging, buckling, or tearing. Furthermore, the codes lacked supporting justification and research for the established strain limits, suggesting that these limits were based on engineering judgment and conservative estimations [36].

Harn et al. [29] and Sadowski et al. [41] evaluated the relevant experimental research on the critical strains of hollow and filled steel pipe piles and directly compared the results against recommended ASCE/COPRI 61-14 [8] absolute compressive strain limits. Figure 6 shows the D/t effect on critical (buckling) strain figure presented by Sadowski et al. [41]. The figure presents pipe pile critical strains for piles with D/t ratios ranging from 10 to 100. Results include four in-air tests performed by Fulmer et al. [26], Brown et al. [15], Peters et al. [37] and Sadowski et al. [41], as well as two in-soil tests performed by Fleming et al. [24] and Aguirre et al. [2]. Empty and solid symbols in Figure 1 indicate hollow pipes and filled pipes, respectively, whereas squares and triangles represent monotonic loading and cyclic loading, respectively. Table 2 summarizes the test set-up, pile type, loading protocol, material specification, D/t ratios, average recorded material yield strength and soil conditions, if applicable, for the tests presented in Figure 1. The recommended ASCE/COPRI 61-14 [8] absolute compressive strain limits and the limiting width-to-thickness ratios for compression elements in accordance with AISC 341-16 [3] and AISC 360 [4] considering a material yield strength of 50ksi are presented. Member designations, such as compact and non-compact defined per AISC 360 [4] and highly ductile (HD), moderately ductile (MD) and non-ductile members (ND) defined per AISC 341 [3], are identified for the range of D/t ratios presented. Design equations proposed by researchers are also presented in Figure 6 as a function of D/t, including the Harn et al. [29] proposed simplified equation, $\varepsilon_{LS} = 10(t/D)^2$ for defining the LS strain limit. All equations consider only the D/t ratio, ignoring the post-buckling effects of the pile, specifically, the residual axial and lateral load capacities.

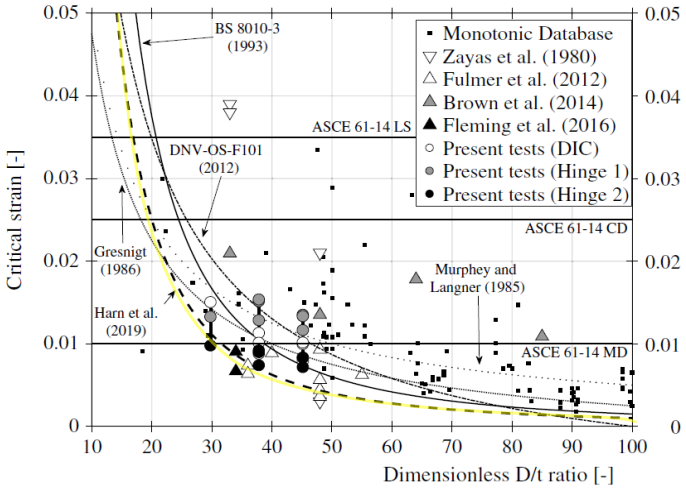

Figure 6: Effect of D/t on Pipe Critical Buckling Strains (Sadowski, 2020) [41]

While the test parameters, boundary conditions, loading protocols, and critical strain definitions differed amongst the various studies, as can be observed in Figure 6, most pipe piles were not able to attain the life safety (LS), or the controlled and repairable damage (CD) strain limits prescribed in ASCE/COPRI 61 [8] prior to the onset of local buckling. Furthermore, noncompact piles with D/t ratios equal to or greater than 40 (as defined per AISC 360-16 [4] assuming 50ksi steel) are shown to experience local buckling prior to the development of the minimal damage (MD) strain limit prescribed in ASCE/COPRI 61 [8].

The data presented in Figure 6 shows considerable variability, which can be attributed to differences in test parameters. It appears that critical strains generally decrease as the D/t ratio increases. Pipes filled with soil, sand, or concrete typically experienced larger strains before local buckling occurred, with reinforced concrete-filled piles achieving higher critical strains than those filled with soil.

Based on the analysis of the data presented in Figure 1, Harn et al. [29] proposed a revised life safety strain limit equation in which the life safety strain limit was formulated as a function of D/t. Frandsen and Nguyen [24] assessed the implications of designing a marine structure using the critical strain equation proposed by Harn et al. [29]. Their findings indicate that the revised strain limits lead to a 30% reduction in predicted seismic performance, necessitate the use of more compact piles, and potentially require an increase in the strength of reinforced concrete pile-to-deck connections. This raises concerns regarding the economic feasibility of employing steel pipe piles for marine applications. Furthermore, the development of these strain limits does not account for the effects of cyclic loading, loading history, residual gravity load-carrying capacity of the pile post-buckling, or the overall performance of the structure.

3. Experiment Design

The large-scale test program consists of a series of in-soil single steel pipe pile tests performed at the UC San Diego. The objective of the test program, for the first time, evaluated the performance of in-soil driven steel pipe piles of different D/t ratios under lateral cyclic loading under combined shear, flexure, and axial loading.

The tests were performed within north soil pit at the Soil-Structure Interaction (SSI) Test Facility North Soil Pit at the University of California, San Diego (UCSD) Englekirk Structural Engineering Center (ESEC). To identify trends, four steel pipe piles were installed within two days such that approximately 68% of the pile length embedded in the soil pit. The single steel pipe pile tests each had the same set up; a free-head configuration. Each pile was subjected to axial loading at the top of the pile using a steel apparatus with repurposed reinforced concrete blocks. The piles were subjected to displacement controlled reversed cyclic lateral loading applied near the pile top by a hydraulic actuator. Other words, the top of the pile was loaded laterally by a large stroke/large force capacity actuator fastened to both a loading apparatus installed on top of the pile and a steel beam extension post-tensioned to a concrete reaction wall. This set-up was consistent for each of the four piles. Figure 7 shows a schematic rendering of Test 1.

Test limitations, when compared to piles supporting waterfront structures, were as follows:

- Soil limitations
  - Existing soil was identified as stiff sandy soil with little variation within the in-ground pile length.
  - No slope protection such as riprap or rock protection was placed in the soil pit.
  - The test pit in its current set up cannot accommodate fully submerged soil conditions since it is not contained/sealed on the sides or at the bottom.
- Reduced scale (1:3) of pile test results in nonlinear scaling. Thus, the nonlinear effects can be missed due to size reduction.
- Applied lateral loading protocol considers testing piles under quasi static loading, in which inertial loading effects are not present and rate effects present in the materials are minimal.
- There are differences between the test set-up boundary conditions and those which exist in realistic marine structures. For example, the boundary condition at top of the pile in the test is “free” while this is not the case in a marine structure where the top of the pile would likely be connected to a concrete deck.
- System level effects (such as the redistribution of axial load) are not considered in the tests. In addition, the effect of sloped mudlines and multidirectional loading and subsequent events (aftershocks) are also not considered.

The boundary condition at the top of the pile was designed to consider zero bending moment. The test layout and set-up was designed to minimize multiple mobilization and demobilization of pile installation and reduce multiple loading apparatus to accommodate the testing interests.

Three (3) hollow steel pipe piles with an outer diameter of 10.75-in and a wall thickness of 0.25-in or 0.5-in were tested under the NIST/NSF-funded project. One (1) hollow steel pipe pile with an outer diameter of 12.75-in with a wall thickness of 0.375-in was tested with both NIST/NSF and NAVFAC funding support. Table 2 summarizes the steel pipe properties and test parameters. The variables being evaluated are diameter-to-thickness ratios and constant axial loading. All test piles are specified in accordance with API X52 [5] and will be instrumented with strain gages, inclinometers, vertical and lateral string potentiometers, accelerometers, and digital image correlation (DIC) to record the pile behavior during testing.

Table 2: Steel Pipe Parameters[1]

Test No.	Funding Source	Outside Diameter [in] (mm)	Wall Thickness [in] (mm)	D/t Ratio	f_y[2] [ksi] (MPa)	Axial Load		Test Pile Length [ft] (m)	AISC 360[4]
						P_{axial}/P_y[3] %	[kips] (kN)		
1	NAVFAC	10.75 (273)	0.250 (6.4)	43	62.8 (433)	4%	23 (102)	28.00 (8.5)	Non-Compact
2	NIST / NSF		0.250 (6.4)	43	71.4 (492)	13%	78 (345)	28.00 (8.5)	Non-Compact
3			0.500 (12.7)	22	70.8 (488)	7%	78 (345)	28.00 (8.5)	Compact
4		12.75 (324)	0.375 (9.5)	34	69.6 (480)	8%	78 (345)	28.00 (8.5)	Compact

Notes:
[1] Port of Long Beach (POLB) provided piles.
[2] Steel yield strength, f_y, is based on steel coupons tensile test of the test piles performed at UCSD.
[3] $P_y = F_y A_g$, where F_y was determined from the UCSD material test stress-strain curves, A_g is the gross pile cross-sectional area. P_{axial} is the applied axial load on the pile, including two-thirds of the actuator weight.

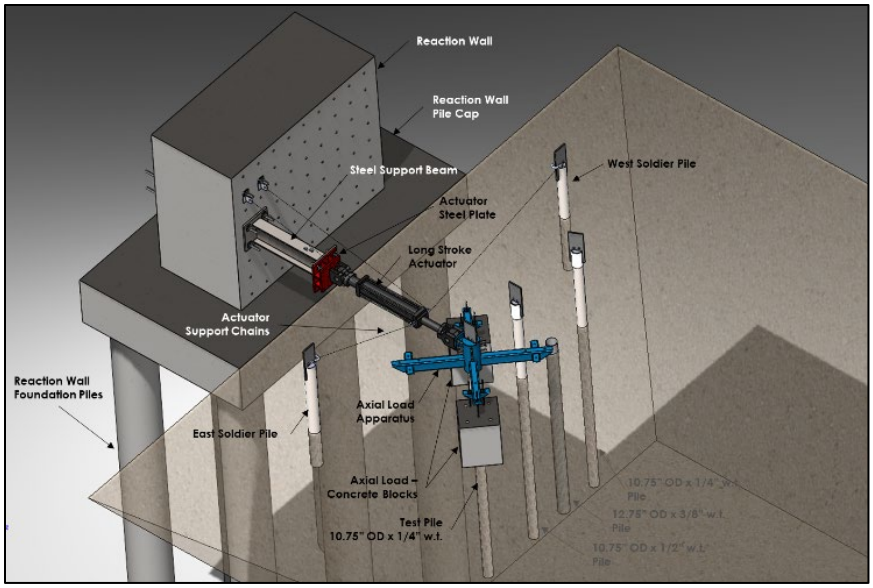

Figure 7: Schematic Rendering of Experiment (Test 1)

4. Test Set-Up

The experiment consisted of four (4) 28-ft long piles installed approximately 19-ft in the ground with the remaining 9-ft extending above the ground. All four piles were instrumented and installed at the same time to optimize contractor mobilization. The top of pile elevation for the four test piles was controlled by the fixed location of the through holes on the reaction wall where the actuator applying the lateral load was anchored. Two shorter soldier piles were installed to resist the out-of-plane movement of the actuator during in-plane loading. The soldier piles consisted of remaining pile material from the test specimens after material testing specimens and test specimens were removed.

The width of the reaction wall in addition to the loading apparatus influenced the test pile(s) locations. The edge-to-edge width of the loading apparatus including the concrete blocks is 17.15-ft. The 45-deg rotation of the apparatus crossbeam gives limited clearance between the concrete blocks and the adjacent test piles during testing. Therefore, the order of the testing was critical to the test set-up. Test 4 directly interferes with Test 2 and Test 3, requiring the Test 4 pile to be cut 5-in above ground. The top portion of Test 4 was reinstalled using a welded splice technique after the completion of Tests 2 and 3, both of which will be cut at mudline to perform Test 4. Test 1 had to be cut at the mudline to perform Test 3.

The piles were extensively instrumented from 6-in above ground to 6.67-ft below ground with 40 single-element type strain gauges and up to four Direct Coupling (DC) accelerometers. Additionally, above-ground instrumentation included three string potentiometers to measure lateral displacement, two string potentiometers to measure axial displacement, an inclinometer and up to two DC accelerometers. The pile and supporting soldier piles were installed into the existing fill soil in the North Pit on January 6, 2023, using an ABI TM22 mobile ram rig with a vibratory hammer.

The constant axial and lateral loading were applied directly to the steel pipe pile through a uniquely designed steel loading apparatus installed at the top of the pile. The lateral load was applied to the pile by using a 220-kip 48-in stroke MTS actuator. The actuator transferred either the cyclic lateral loading to the pile by way of a plate welded to a steel jacket and then by threaded rods to the exterior pile face. Four (4) bolts connected the actuator to a 2-in thick actuator plate welded to the steel jacket. The other end of the actuator was anchored to the 2-in thick built-up actuator plate bolted to an 8-ft long steel support beam post-tensioned to the reaction wall. Two chains served as secondary axial support for the actuator, with one end anchored to the reaction wall and the other to the actuator. The actuator was also supported with a secondary lateral restraint in the out of applied load direction by two chains, one connected on both sides of the actuator and the other end anchored to either the east or west soldier pile. The constant axial load is applied to the pile by direct bearing at the top of the pile. Two or four concrete blocks were

suspended from the steel loading apparatus. A schematic rendering of the test set up is shown in Figure 8. Test 1 was the only test which did not require the concrete blocks be contiguous with the soffit of the steel apparatus arms.

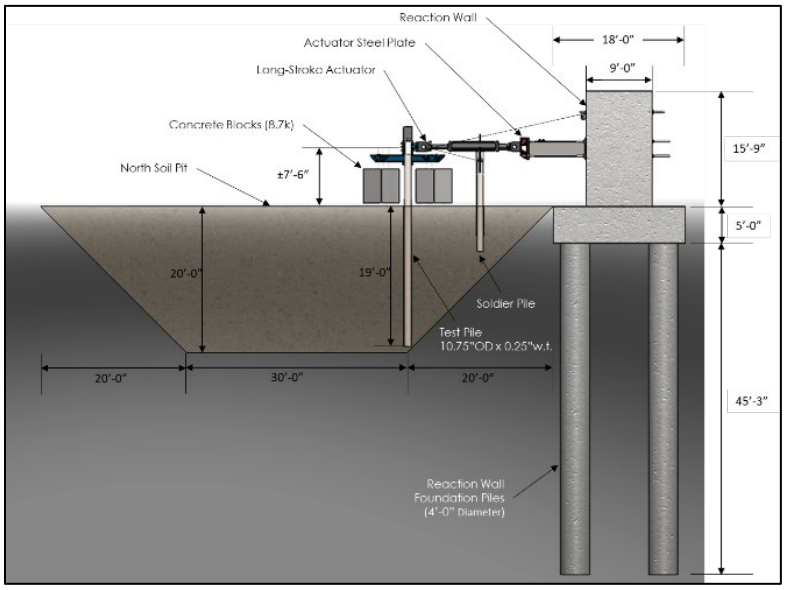

Figure 8: Schematic Cross-Section of Test 1

a) Elevation of Pile Test 01

b) Pile Test 03 Set up in April 2024

c) Pile Test 01 – Post Test Layout

d) Direct overview of Test Pile 04

Figure 9: Field Images of Test and Test Set-up

4.1 Existing Site Conditions & Soil Characterization

The SSI facility consist of two soil pits positioned just west of the 360-degree shake table at the UC San Diego ESEC. These two soil pits, identified as the north and south soil pits, were constructed in the early 2000s. A reaction wall was designed between the pits. A schematic of the reaction wall is presented n Figure 10. The reaction wall consists of four concrete blocks measuring 19-ft long by 9-ft wide by 4-ft high, stacked on top of each other and post-tensioned to a 5-ft deep concrete pile cap. The pile cap is supported on six 4-ft diameter reinforced concrete piles. The reaction wall was designed with 2.625-in diameter through holes spaced at 2-ft on-center to allow for prestressing high-strength bars up to 225-kips each.

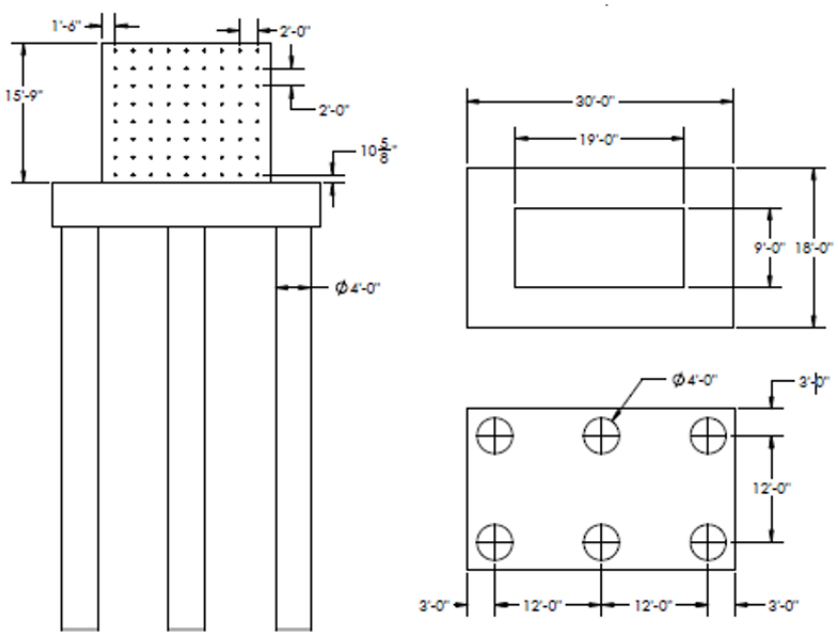

Figure 10: Schematic Sketches of Test Facility Reaction Wall

The north test pit was designed as a refillable inverted trapezoidal pit. The top of the pit is dimensioned as approximately 70-ft by 70-ft with a depth of 20-ft and a 30-ft by 30-ft floor base.

The pit was initially filled in 2005 by a Caltrans-funded abutment test with two different soil types, clayey sand, and silty sand, both of which were imported from sites within San Diego. The material was compacted to a relative compaction of 90% and 95%, respectively, or more (Bozorgzadeh, 2007) [12].

A preliminary geotechnical investigation of the soil in the north soil pit was conducted on September 26, 2022 approximately 10 months prior to testing Test #1. The test pile and soldier piles were installed in January 2023. Unfortunately, the weather conditions were

increasingly wet after pile instrumentation between November 2022 and January 2023, during pile installation and shortly thereafter. Damage to the in-ground instrumentation was observed several weeks after installation once the weather calmed. The damage was assumed to be due to pile installation methods with consideration of the extremely wet conditions. Therefore, the piles had to be re-instrumented, requiring the existing top 8-ft of surrounding soil to be excavated and later backfilled.

The excavation of the north soil pit was performed over several days in mid-June 2023. Approximately 200 cubic yards of existing in-situ soil was removed and stock-piled and stored southeast of the reaction wall. As recommended by the supporting geotechnical engineer (EMI), a maximum depth of 8-ft and a perimeter wall slope no steeper than 1.5H:1V was implemented. Figure 11 demonstrates the excavation plan of the pit. Soil was removed by hand within a 2-ft radius (clear distance) of the test pile. The two soldier piles remained unexposed with the same driven depth. The backfill of the original soil was performed in mid-July 2023. The Contractor was instructed to backfill the existing material in 8-in lifts compacted to 90% of maximum dry density per ASTM D1557. Hand compaction equipment was used within 2-ft of the test pile. Figure 11 shows field photos of the excavation and backfill.

A second geotechnical investigation was completed in April 2024, approximately 8 months after pile Test 1 and weeks before pile Test 3. This investigation included four cone penetration tests (CPTs) and two seismic CPTs (SCPTs) in addition to soil sampling through bore holes. The seismic CPTs included shear wave velocity soundings. Figure 13 depicts the locations of the four CPTs, two SCPTs and two boreholes performed in April 2024. The initial investigation performed in 2022 determined the estimated depth to the pit bottom to be 20-ft, which was determined as the interface between fill material and native soils, and the refusal depth of the CPTs averaged 30-ft shows the CPT results for cone/tip resistance and sleeve friction. Pore pressure and friction ratio were recorded along the depth but are not shown here. Minimal pore pressure was observed, and the friction ratio varied from 1% to 8%.

Soil laboratory tests were performed by EMI and included grain size analysis, direct shear test and unconsolidated undrained test, refer to Appendix A. Based on visual observation, the top four to six inches of the soil surrounding the pile was not well compacted. The soil near the piles was hand-compacted with an individual hand-compactor during the backfill operations performed in July 2023. Given the top feet of soil has no additional loading applied and no overburden, the first few inches of soil is not as well compacted as the deeper soil layers and thus the top several inches of soil is considered loose. Based on the geotechnical characterization the soil was classified as a medium stiff to very stiff mixture of sand/silt/clay.

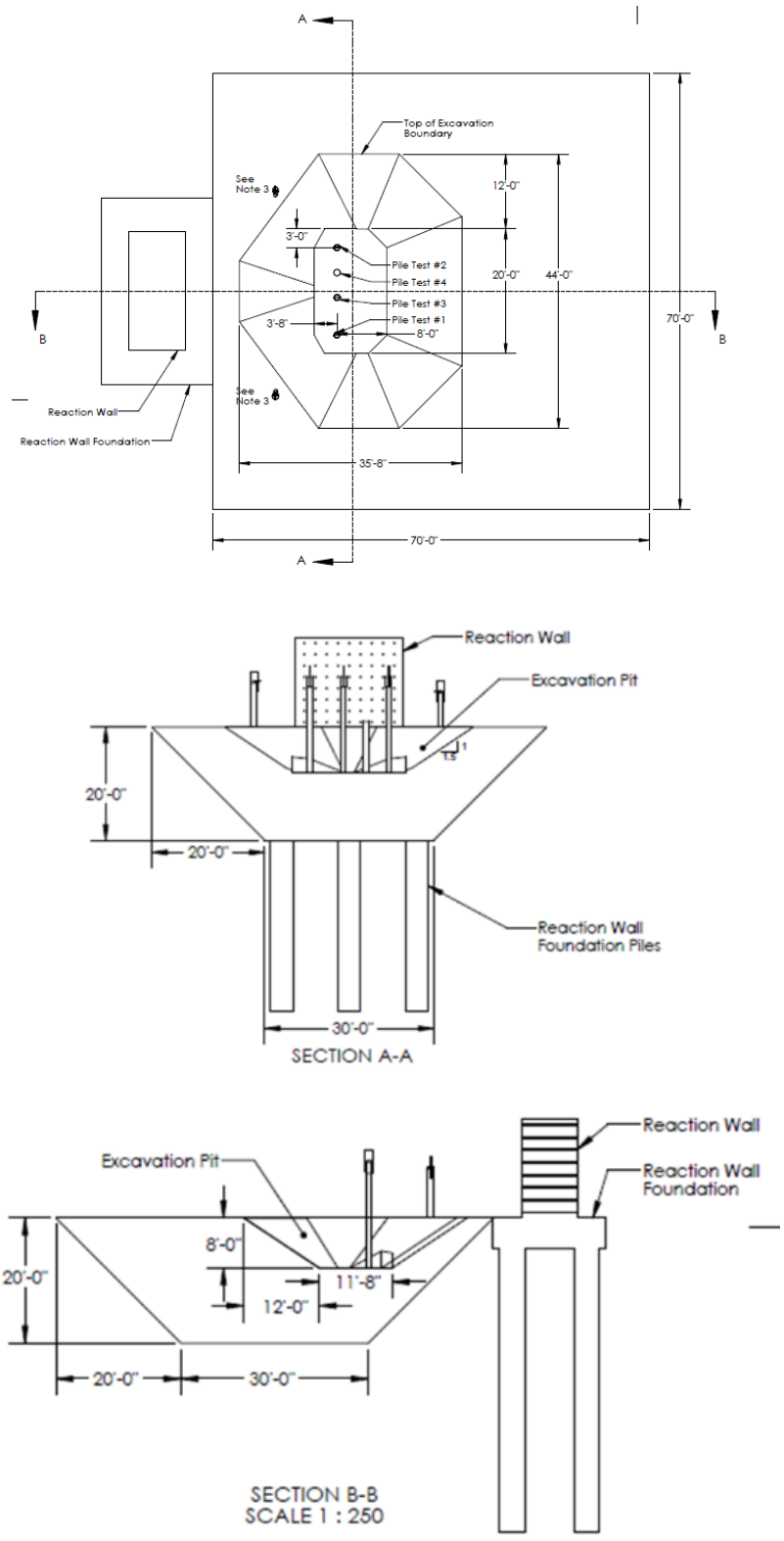

Figure 11: North Pit Excavation Plan

(a) Soil Pit Excavation – Day 1

(b) Final Soil Pit Excavation

(c) Soil Pit Excavation Overview

(d) Backfill Soil Pit – Day 1

(e) Backfill Soil Pit

(f) Backfill Soil Pit

Figure 12: ESEC North Pit Soil Excavation and Backfill Photos

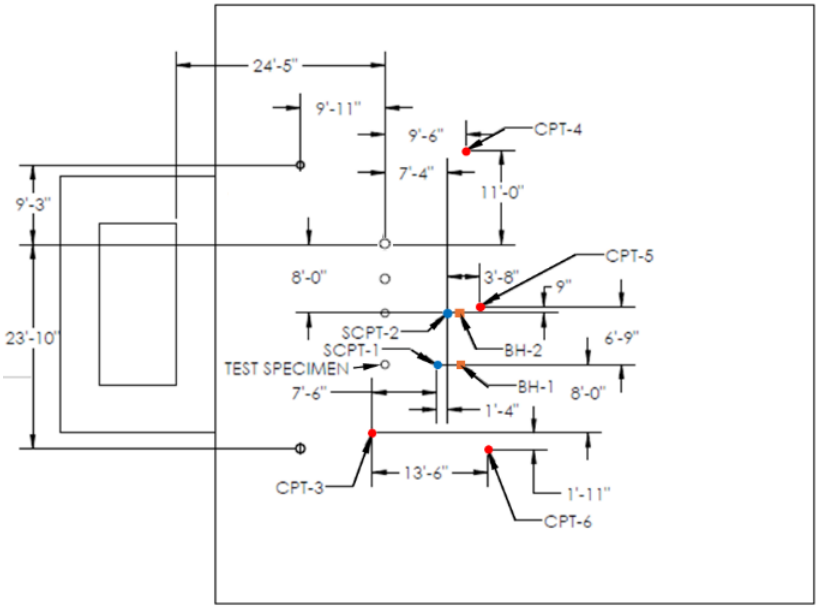

Figure 13: ESEC North Pit Soil Characterization Plan

Due to the low-rate single quasi-static reversed cyclic loading application and soils surrounding piles being primarily granular, EMI does not expect excessive pore water pressure to build up during pile loading. Thus, the pore water pressure would have negligible effects on the test results. During the 30-ft deep CPT soundings, water was not encountered at any depth. A well was drilled the same day as the borings were performed and no water was observed.

Figure 15 shows the recommended soil parameters based on the CPT and SCPT information obtained. The soil characteristics are summarized as determined by EMI from the SCPTs, CPTs and soil laboratory tests from the boring samples.

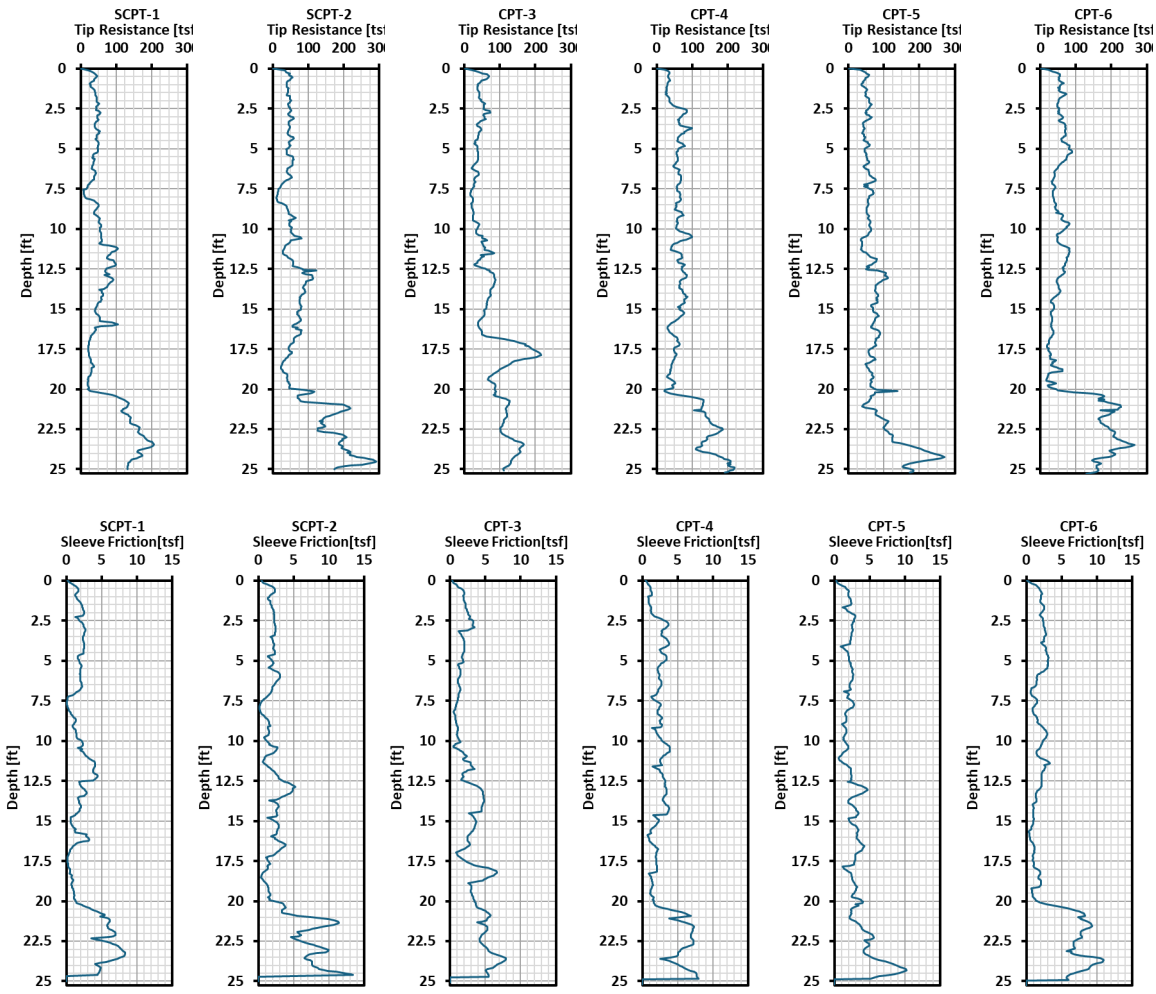

Figure 14: CPT Cone/Tip Resistance & Sleeve Friction Results (Kehoe Testing: April 2024)

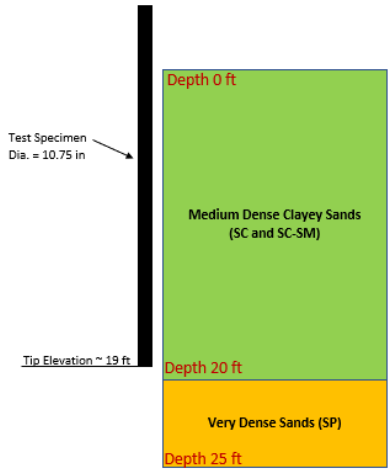

Boring No .	Sample No.	Sample Depth (ft)	Soil Identification (group symbol) ASTM D2488/D2487	Moisture Content ASTM D2216 (%)	Total Unit Weight ASTM D2937 (pcf)
BH-1	*D-1*	0	SC	13.8	126.0
BH-1	*T-2*	2.5	SC	11.7	136.6
BH-1	*D-3*	5	SC	15.3	126.5
BH-1	*T-4*	7.5	SC-SM	11.6	119.3
BH-1	*D-5*	10	SC	13.6	130.2
BH-1	*D-6*	12.5	SC	10.8	117.8
BH-1	*D-7*	15	SC-SM	14.2	124.4
BH-1	*D-9*	20	SC	12.9	126.8
BH-2	*D-1*	0	SC	13.4	126.4
BH-2	*T-2*	2.5	SC	11.8	131.9
BH-2	*D-3*	5	SC	14.6	130.2
BH-2	*T-4*	7.5	SC-SM	11.4	117.7
BH-2	*D-5*	10	CL to SC	13.5	125.4
BH-2	*D-6*	12.5	SC	11.3	124.5
BH-2	*D-7*	15	SC	14.3	130.8
BH-2	*D-9*	20	SC	12.7	129.8

(a) Generalized Soil Profile *(b) Summary of Laboratory Results from April 2024 Borings*

Figure 15: Generalized Soil Profile for North Soil Pit and Summary of Laboratory Results (Produced by EMI, 2024)

4.2 Pile Installation

The test piles and two supporting soldier piles were installed using an ABI TM22 mobile ram rig with a vibratory hammer on January 6th and January 9th of 2023. Figure 16 shows the piles being installed with the ABI TM22 mobile ram rig.

a) Pile Installation D/t 22 & D/t 43 *b) Pile Installation Pile #2 with Vibratory Hammer*

Figure 16: Pile Field Installation

A single 16-in wide 1.5-in thick knife plate was welded into the top of each pile to allow for the hammer jaws (clamps) to grip the pile for installation. The test pile was positioned such that the knife was perpendicular to the outer face of the reaction wall and in plane of the axis of loading. The position of the knife plate was parallel to the outer face of the reaction wall for the two soldier piles. Each test pile was initially installed in the ground 9-ft then operations were paused to measure the depth to top of soil plug during installation and then continued until the pile hit refusal or in-ground tip elevation of approximately 19-ft. To obtain the estimated depth of soil plug, a weighted probe was dropped into the pile. Only test pile #1 experienced minor walking of the pile tip and out-of-plumbness during installation.

Table 3 summarizes the pile in-ground depth, the above-ground pile height, the top of pile elevation, and the calculated soil plug height for each pile at 9-ft in-ground and final in-ground depth after driving. The soil plug clear height, the measured height from the top of the ground surface to the top of the soil plug, was determined in feet and pile diameters. Refer to Figure 17 for field measurement schematic sketch of the pile. Therefore, no inner pile confinement of the soil is observed within the anticipated location of plastic hinging for all test piles. The height of the plug was observed to remain unchanged from installation to test-date.

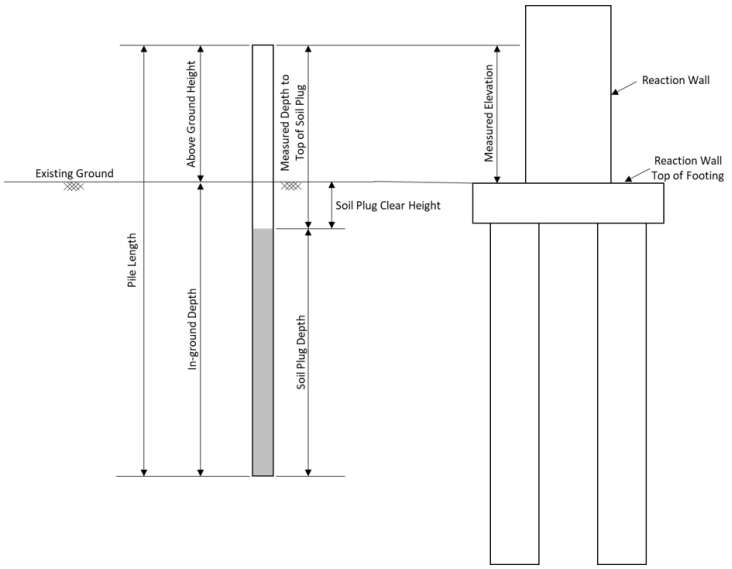

Figure 17: Pile Field Measurements Schematic Sketch

Table 3: Pile Field Installation and Soil Plug Field Measurements

Date	Pile (Nominal Dim.)		Test No.	Total Pile Length	In-Ground Pile Depth	Above Ground Pile Height[1]	Top of Pile EL.[2]	Top of Soil Plug Depth[3]	Soil Plug Clear Height[4]		Soil Plug Depth[5]	Soil Plug to Pile In-ground Ratio[6]
	D	t										
	[in]	[in]		[ft]	[ft]	[ft]	[ft]	[ft]	[ft]	[Dia]	[ft]	
1/6/2023	12.75	0.375	Soldier Pile (E)	12	4	8	8.04	8.17	0.17	0.2	3.83	0.96
1/6/2023	10.75	0.5	Soldier Pile (W)	12	4.17	7.83	-	9.71	1.88	2.1	2.29	0.55
1/6/2023	10.75	0.5	Soldier Pile (W)	12	6.17	5.83	6.39	7.92	2.08	2.3	4.08	0.66
1/6/2023	10.75	0.5	3	28	8.92	19.08	-	24.79	5.71	6.4	3.21	0.36
1/6/2023	10.75	0.5	3	28	19.29	8.71	8.95	19.44	10.73	12.0	8.56	0.44
1/6/2023	10.75	0.25	1	28	9.00	19.00	-	23.50	4.50	5.0	4.50	0.50
1/6/2023[7]	10.75	0.25	1	28	19.00	9.00	9.29	18.42	9.42	10.5	9.58	0.50
1/9/2023	12.75	0.375	4	28	9.00	19.00	-	22.23	3.23	3.0	5.77	0.64
1/9/2023	12.75	0.375	4	28	19.31	8.69	8.99	14.17	5.48	5.2	13.83	0.72
1/9/2023	10.75	0.25	2	28	9.00	19.00	-	22.02	3.02	3.4	5.98	0.66
1/9/2023	10.75	0.25	2	28	19.08	8.92	8.94	12.97	4.05	4.5	15.03	0.79

Notes:
[1] Measured above ground height of the pile from the top of in-situ soil.
[2] Measured top of pile elevation from the reaction wall top of footing. (i.e., Reaction wall top of footing is El. 0+00)
[3] Measured depth of the soil plug from the top of the pile.
[4] Calculated soil plug clear height.(i.e., Soil Plug Clear Height = Top of Soil Plug Depth - Above Ground Pile Height)
[5] Calculated depth of the soil plug. (i.e., Soil Plug Depth = Total Pile Length - Top of Soil Plug Depth)
[6] Calculated soil plug to pile in-ground ratio. (i.e., Ratio = Soil Plug Depth / Pile In-ground Depth)
[7] In-Ground Pile Depth at start of cyclic testing increased 4.5 in, thus above ground pile height was 8.625ft and in-ground pile depth was 19.375ft.

4.3 Instrumentation

To evaluate the performance of the pile and the post-buckling behavior the test specimens were densely instrumented with nearly 63 channels of data acquisition. The instrumentation included an array of 40 large-strain electrical-foil strain gages, three lateral string potentiometers, two axial string potentiometers, and one inclinometer. Additionally, four to five DC accelerometers were installed along the pile to evaluate static and dynamic acceleration. Digital images were taken to evaluate the top translation and rotation of the pile through digital image correlation (DIC). Refer to the pile instrumentation plan, provided in Appendix A. The plan does not show the DIC or the control string potentiometers, as they were not installed just prior to load application.

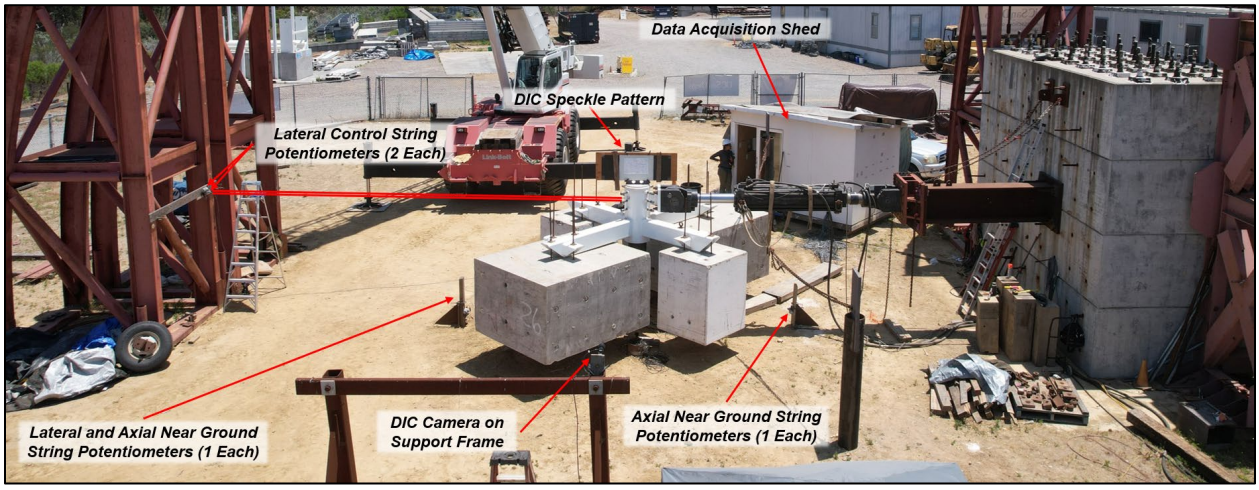

Note: Inclinometer is on the eastern face of the Test 2 pile and therefore, is not shown.

Figure 18: Overall Test Above Ground Instrumentation Test 2

4.3.1 Strain Gauges

The test piles were initially instrumented with 40 single-element type YEFLA-5 strain gauges, SGX01 to SGX40 (which “X” is the pile tested), manufactured by Tokyo Measuring Instruments Lab in November/December 2022. The strain gauges were distributed along the north and south faces of the pile, 20 gauges per face, with a ±30-deg clockwise offset from the axis of lateral loading and location of extreme fiber. The first strain gauge was installed on both sides approximately 6-in above the ground surface, and the last gauge approximately 7-ft below the top above-ground gauge. The center-to-center gauge spacing varied between 4-in and 6-in vertically, with the tighter spacing in the region of anticipated hinge location. The gauges were mounted on the outside surface of the piles with wires oriented in the direction towards the top of pile. As previously mentioned, due to pile installation occurring during extreme wet conditions, more than half of the strain gauges were determined non-viable, and thus a majority were replaced in June/July 2023 after excavation. The location of the strain gauges remained

unchanged for the re-instrumentation. Figure 19 shows the in field photos of the re-instrumentation of the pile.

A continuous 20-ft long steel angle, L2x2x1/8, was initially mounted to the exterior face of the pile to protect the strain gauge wires during pile installation. During the instrumentation of the piles, an approximate length of 8-ft 4-in of the angles was removed from the ground surface to the excavation base elevation. These angles were not replaced before backfilling. In lieu of the angle, extensive waterproof adhesive tape was placed on each strain gauge for protection. High strength duct tape was applied circumferentially as reinforcement to reduce tension on the wires during backfill. The duct tape was roughly spaced 4-in vertically.

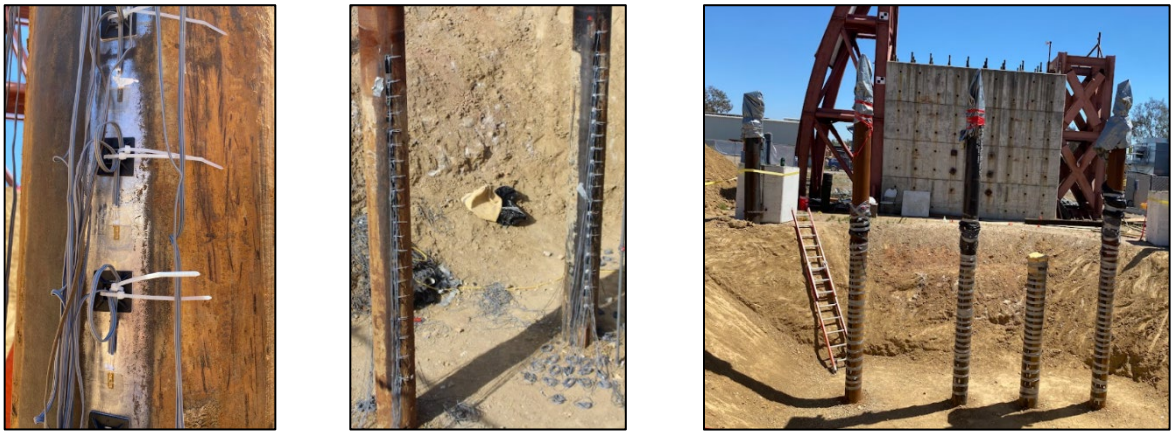

(a) 4-in Gauge Spacing *(b) Strain Guage Profile* *(c) Final Strain Gauge Instrumentation*

Figure 19: Strain Gauge Instrumentation

4.3.2 Accelerometers

Five DC accelerometers (AC) were installed along the south external face of the piles, refer to Figure 20. Two were installed above ground with three below ground. The top accelerometer was placed roughly 20-in from the top of pile, just below the knife plate. A second accelerometer was placed within 6-in above the ground elevation. Three accelerometers were strategically placed within the embedded length of the pile, approximately 2.75-ft, 5-ft and 7.5-ft below the ground. The DC accelerometers are capable of tri-directional sensing, measuring static acceleration of gravity in tilt-sensing applications and dynamic acceleration due to vibration or motion. The accelerometers were installed to understand dynamic response during the free vibration tire tests, which was added at the last minute and only performed for Pile Test 1 and Pile Test 3. Covers were designed and created using a 3-dimensional printer. The purpose of the covers was to reduce damage to the accelerometers during soil backfill and during the test.

a) Bottom DC Accelerometer Mounted

b) DC Accelerometer with Cover

c) In-ground DC Accelerometers

Figure 20: DC Accelerometer Instrumentation

4.3.3 String Potentiometers

Two lateral string potentiometers, SPTLX01 and SPTLX02 (which "X" is the pile tested), were used to monitor the lateral movement. The string potentiometers were mounted on the north face of the steel load apparatus, equally offset from the center of lateral loading, approximately 1-in apart. The top string potentiometer, SPTLX01, was a 5-in string potentiometer capable of measuring movements up to 2.5-in in either direction. This string potentiometer was used to monitor the lateral displacements at the top of the pile during the small amplitude cycles up to ±1.1-in. The remaining cycles used SPTLX02, which was a 50-in rated string potentiometer capable of measuring up to 25-in in either direction. These top of pile lateral string potentiometers were mounted to a rigid steel frame approximately 25-ft from the external face of the steel load apparatus.

A third lateral string potentiometer, SPTLX03, was mounted on the north face of the pile, in plane with the lateral loading, approximately 7-ft 7-in from the top of the pile and roughly 13-in from the ground surface. SPTLX03, was a 50-in string potentiometer capable of measuring movements up to 25-in in either direction. The instrument itself was mounted to a rigid steel angle approximately 6-ft from the external face of the pile anchored in the soil.

Two lateral string potentiometers, SPGAX04 and SPGAX05) were used to record the axial shortening of the pile by way of a pulley system. The string end of the system was connected to an eye bolt welded to the external face of the pile approximately 6-ft 8-in from the pile top. The string was then suspended vertically through a pulley mounted 6in from the eye bolt. The string was then extended laterally and connected to the string potentiometer mounted to the rigid steel angle anchored in the soil approximately 6-ft from

the external face of the pile. The pulley system was installed on both the north and south face of the pile in the plane of lateral loading.

4.3.4 Inclinometers

A single inclinometer, INCGX06, was installed at the same elevation, approximately 13-in above top of ground, as the third string potentiometer at a 90-deg offset on the eastern external face of the pile. The recorded data of the inclinometer along with the SPTLX03 string potentiometer was used to estimate the location of the in-ground plastic hinge of the pile by using the recorded pile rotation at this location.

Above ground instrumentation layout and photo is shown in Figure 21.

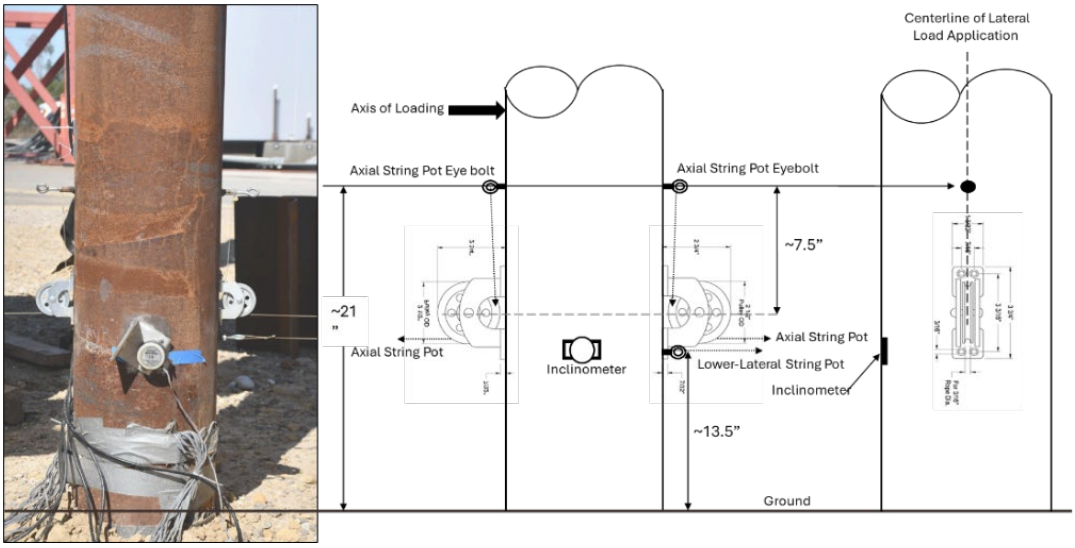

Figure 21: Near-Ground Instrumentation Elevation Plan

4.3.2 Digital Image Correlation (DIC)

DIC was sampled above the top of the steel load apparatus on the knife plate for all tests, refer to Figure 22. The steel load apparatus was designed to transfer both the axial and lateral loading to the pile. The apparatus is positioned at the top of the pile and is discussed in detail in the subsequent section. A single high-resolution monochromatic Chameleon3 USB3 camera and a NIST-traceable calibration panel were installed approximately 12-ft away from the eastern or western side of the test pile, whichever was practical for the test-setup and access. The 2.8-megapixel camera have a 1928 x 1448 resolution with a maximum throughput of 13 frames per second. The camera has a 1/1.8 charge-coupled device (CCD) sensor with a 3.69 µm pixel size. The images are post-processed using the commercially available DIC software DaVis by LaVision. The DIC technique relies on a "recognizable" speckle pattern distributed along the surface where the displacement fields were determined. The data recorded from the DIC was used to evaluate the axial shortening on the pile from the top during testing. In the instance which

the axial load was determined negligible, the impact of axial shortening at 0-lateral pile displacement was generally smaller than the resolution of the measuring device.

Figure 22: Top of Pile DIC Instrumentation

4.4 Load Application Design

The constant axial and lateral loading was applied directly to the steel pipe pile through a uniquely designed steel loading apparatus installed at the top of the pile. The loading apparatus was constructed as a reusable jacket system designed to (1) support up to four (4) concrete blocks used to apply axial load and (2) to transfer the lateral loading applied using a 220-kip 48-in stroke MTS actuator.

To obtain the axial loads for each test up to four concrete blocks, two larger blocks and/or two smaller blocks were supported from the crossbeams of the steel apparatus. All four blocks were repurposed from the ESEC material yards from past research projects. The blocks were reinforced with minimum requirements. The two small concrete blocks were rectangular with approximate dimensions of 3.5-ft by 3.5-ft by 4.7ft. Three 1.875-in diameter holes were drilled strategically in a triangular layout centered on one of the 3.5-ft by 3.5-ft face for the installation of post-installed Grade 80 No. 6 all threaded rods with high strength grout. The two large concrete blocks were rectangular with approximate dimensions of 7.4-ft by 6.0-ft by 4.1ft. Four 1.875-in diameter holes were drilled strategically in a square layout rotated 45-deg and centered on one of the 7.4-ft by 6.0-ft face for the installation of post-installed Grade 80 No. 6 all threaded rods with high strength grout.

The jacket was designed with a slot to accommodate the knife plate required for pile installation and removal. An initial 0.625-in cap plate sat on top of the pile; however, this

was later replaced with a 1.5-in thick cap plate during Test 2 setup. Twelve (12) holes sized to accommodate a 1.25-in diameter threaded rod with three (3) hex nuts were drilled around the 18-in OD jacket oriented at 45-deg, 135-deg, 225-deg and 315-deg. The application of lateral loading was denoted as 0-deg. A strategic orientation of tightening was required during installation of the loading apparatus was required to reduce uneven loading on the pile and ensuring a flat interface between the semi-HSS sleeve and the outer top edge of the test pile. The lateral loading was applied to the test pile through contact of the threaded rods and the axial load through the bearing of the cap plate.

The actuator attached to the loading apparatus by four (4) bolts connected to the 2-in actuator plate welded to an HSS 8x8 tube welded to the jacket. The other end of the actuator was anchored to a 2-in built up actuator plate assembly which is bolted to an 8-ft long steel support beam post-tensioned to the reaction wall. The actuator was laterally restrained, for safety, in the out-of- applied load plane direction by two chains, one connected on both sides of the actuator and the other end anchored to the soldier pile.

The two small concrete blocks were suspended from the loading apparatus with a maximum distance of 6-in above finished ground for Test 1. For the remaining tests, the four concrete blocks were secured in direct contact with the steel crossbeam soffit, providing maximum clearance between the concrete blocks and the ground surface. The concrete blocks were pre-existing from previous projects performed at ESEC. A combination of threaded rods, couplers, hex nuts, plates, and leveling washers were designed to develop a post-installed adhesive anchorage in the block and the top connection with the loading apparatus HSS member. The leveling/spherical washer at the threaded rod-HSS top connection allowed for a maximum angle of correction of 3-deg. The washer was oversized, at least ¼-in diameter larger than the threaded rod, to allow for additional rotation. The connection was designed to accommodate a rotation of no greater than 6-deg.

Drawings of the loading apparatus and the concrete blocks are provided in Appendix B.

(a) Concrete Block Anchorage Installation

(b) Steel Loading Apparatus

(c) 48-in Stroke Hydraulic Actuator

(d) Complete Test Set-up

Figure 23: Components of Test Set-up for Application of Axial and Lateral Loading

5. Material Properties

5.1 Structural Steel – Pipe Piles

The steel pipe pile test specimens were provided by the Port of Long Beach (POLB). These piles were electric resistance welding (ERW)/high frequency welding (HFW) longitudinal line pipe manufactured in accordance with API 5L Standard Grade X52 [5] and delivered at lengths between 40-ft to 42-ft. The piles were cut into three segments: test pile, material testing, and non-test pile lengths, as shown in Table 4.

Tensile tests were performed on material coupons from the material testing pile lengths. Standard tensile tests were performed on all coupon specimens to develop the stress-strain curves, shown in Figure 24. The material properties for each pile is provided in Table 5. The material yield stress listed for each specimen was determined from the stress-strain curves. The material yield stress was determined by one of two methods; yield plateau and 0.2% offset. Test 1 and Test 2 pile material tests exhibited yield plateaus, allowing for the material yield stress (strength), f_y, to be taken as the average of values within the plateau. For Test 3 and Test 4 piles, the materials stress-strain curves had no yield plateau, the yield strength was then determined as the intersection of the stress-strain curve and offsetting the initial young's modulus by a 0.2% offset.

The elastic modulus, E_s, was determined by calculating the initial slope from the first four measurements in the curve. The yield strain, ε_y, was determined as E_s / f_y. The uniform strain at the tensile point was defined as ε_u. The tensile stress f_u maximum tensile stress obtained in the test.

Gradual strain hardening was evident with strength degradation observed at high strain values, greater than 0.05. Strain Hardening modulus, E_{sh}, and strain hardening strain, ε_s, were determined from the difference of the ultimate and yield stress and strain determined. Minimal strain hardening was observed for these specimens and stress reduction after ultimate stress. All determined stress-strain curves are reported as engineering stress and strain. All curves exceed the minimum specified yield strengths and ultimate tensile strengths required in the specifications.

Table 4: Steel Pipe Pile Test Segments

Test No.	Outside Diameter [in] (mm)	Wall Thickness [in] (mm)	D/t Ratio	Pile Lengths			
				Delivered [ft]	Test Pile [ft]	Material Testing [ft]	Non-Test Pile [ft]
1	10.75 (273)	0.250 (6.4)	43	40.70	28 (8.5)	0.70 (2.3)	12.00 (39.4)
2	10.75 (273)	0.250 (6.4)	43	40.75	28 (8.5)	0.75 (2.5)	12.00 (39.4)
3	10.75 (273)	0.500 (12.7)	43	42.04	28 (8.5)	1.79 (5.9)	12.25 (40.2)
4	12.75 (324)	0.375 (9.5)	22	40.33	28 (8.5)	0.50 (1.6)	11.83 (38.8)

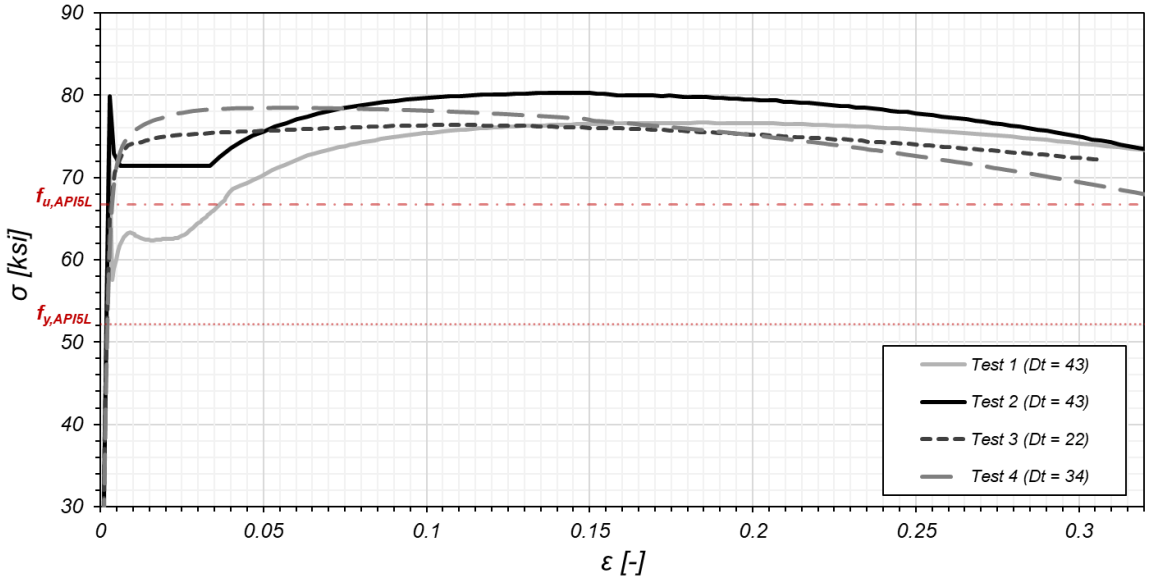

Figure 24: Test Specimen Stress-Strain Relationship of Material Coupons

Table 5: Steel Pipe Pile Test Specimen Material Properties

Test No.	Outside Diameter [in] (mm)	Wall Thickness [in] (mm)	D/t Ratio	f_y [ksi] (MPa)	E_s [ksi] (GPa)	ε_y [-]	ε_{sh} [-]	E_{sh} [ksi] (GPa)	ε_u [-]	f_u [ksi] (MPa)
1	10.75 (273)	0.250 (6.4)	43	62.8 (433)	29100 (201)	0.0024	0.181	76.4 (0.53)	0.183	76.7 (528)
2	10.75 (273)	0.250 (6.4)	43	71.4 (492)	28200 (195)	0.0025	0.131	67.1 (0.46)	0.134	80.3 (553)
3	10.75 (273)	0.500 (12.7)	43	70.8 (488)	29400 (203)	0.0024	0.106	52.8 (0.36)	0.108	76.4 (527)
4	12.75 (324)	0.375 (9.5)	22	69.6 (480)	27500 (190)	0.0025	0.048	195.7 (1.3)	0.051	78.5 (541)

5.2 Structural Steel – Loading Apparatus

The loading apparatus was mainly composed of structural steel, round and rectangular HSS members, plates and threaded rods. The HSS members were fabricated according to ASTM 500 Grade B. Plates were specified according to ASTM A572 Grade 50. Fabricated threaded rods were specified to ASTM F1554 Grade 55 or ASTM A307 Grade B. Other hardware was specified to ASTM A563.

Once fabricated the steel loading apparatus was then coated with shop primer and white color with a minimum applied film thickness of 3 mils to protect the steel during outdoor storage before, during and after performing tests.

5.3 Other Material

The material properties of repurposed components such as the concrete blocks were unknown and were not considered given the influence on the test outcome was anticipated to be negligible.

6. Test Protocol

6.1 Dynamic Tire Vibration Loading

Dynamic tire tests were performed on two of the four test piles, Test 1 and Test 3. The steel apparatus was applied to the top of pile and a standard vehicle rubber tire was hung from a forklift and positioned at various distances from a 2-in loading plate attached to the steel apparatus. The pendulum height was approximately 15-ft to 20-ft from the impact point. The tire was released, striking the plate in a single impact and causing the pile to oscillate freely.

To adequately evaluate the dynamic behavior of the piles, four levels of impact distances were conducted, refer to Table 6. Each level consisted of a minimum of 10 tests, each applied roughly at the same location with the same release speed, however this was not measured for each test. Figure 25 shows the tire just before impact on the 2-in plate.

Table 6: Tire Impact Distances

Test Pile	Distance of Tire Edge to Loading Plate (inches)			
	Level 1	Level 2	Level 3	Level 4
Pile 1 (D/t =43)	15	27	60	96
Pile 3 (D/t = 22)	12	48	96	144

Figure 25: Dynamic Tire Test on Test 1

6.2 Constant Applied Axial Loading

A constant axial load was applied for all tests as shown in Table 7. The constant axial load consists of the weight of the actuator, the weight of the steel load apparatus, and the concrete blocks. The self-weight of the pile is anticipated to contribute to the axial loading, however negligible to the load applied and thus is not included in calculations. Due to the stiffness of the support beam connected to the reaction wall, only two-thirds of the actuator weight is considered on the pile.

The concrete blocks, whether two blocks or four blocks, were suspended in the air from the steel built-up cross beam apparatus. As previously discussed, the steel apparatus is designed as a fixed jacket system, transferring the axial load through directly bearing atop the pile. Applying the axial load in this manner has the advantage of maintaining the axial load on the pile through lateral cyclic loading. The material take-off for the steel load apparatus estimated its total weight to be approximately 2.8 kips. The large-stroke MTS actuator is estimated to weigh a total of 5.2-kips.

The axial load ratios presented in Table 7 are calculated as the applied load, P_{ax}, divided by the pile axial yield capacity, P_y. The axial yield capacity, P_y, is calculated using the nominal cross-sectional area of the pile and the yield stress measured through material coupon tests.

Table 7: Constant Axial Loading

Pile Test	Units	Test 1	Test 2	Test 3	Test 4
Total Block Weight	kips	17.2	71.7	71.7	71.7
Actuator (2/3)	kips	3.5			
Steel Apparatus Weight	kips	2.9			
Total Constant Axial Load = Block + Actuator + Apparatus	kips	23.5	78.0	78.0	78.0
F_y (per material testing)	ksi	62.8	71.4	70.8	69.6
$P_y = F_y A_g$	kips	518	589	1140	1015
P_{ax} / P_y	%	4	13	7	8

The axial load was fully applied to the test overnight, with testing performed within 24-hr of load application.

6.3 Cyclic Lateral Loading

The cyclic lateral loading for each test was applied by an MTS servo-controlled hydraulic actuator with a 220-kip and ±24-in stroke capacity. Preliminary calculations, presented in Table 8 determined the maximum lateral reaction, F_p, of the pile would not exceed 30-kips, about 15% of the actuator's force capacity.

This force, F_p, was calculated as the plastic moment of the pile section, M_p, divided by the measured above ground height of the pile to load application, L. M_p is the product of material yield strength, from material coupon testing, multiplied by the pile plastic section modulus, Z.

Table 8: Anticipated Peak Lateral Load

Pile Test	Unit	Test 1	Test 2	Test 3	Test 4
A_g = Pile Gross Area	in^2	8.25	8.25	16.10	14.58
F_y (per material coupon testing)	ksi	62.8	71.4	70.8	69.6
$P_y = F_y A_g$	Kips	518	589	1140	1015
Z = Plastic Sect. Modulus	in^3	27.6	27.6	52.6	57.4
$M_p = F_y Z$	kip-in	1733	1971	3724	3995
L = exposed pile height above ground + 2.5 x pile diameters	ft	10.07	10.61	10.66	11.07
$F_p = M_p / L$	kip	14.3	15.5	29.1	30.1

The lateral loading protocol, as shown in Figure 26, was determined following FEMA 461 [23] unidirectional testing displacement-based loading history for a single specimen test, using an increasing amplitude displacement loading protocol. The targeted smallest and maximum lateral displacements of 0.4-in and 22.68-in are considered and fall within the capacity of the actuator. The lateral displacement amplitude, a, of each cycle was determined as $a_{i+1} = 1.4a_i$, where $_i$ is the preceding step. The pile was loaded following this protocol until it exhibited significant (> 50%) degradation of lateral strength, the maximum displacement of the actuator was reached or the clearance of the base of the concrete blocks and the top of ground was within ½-in.

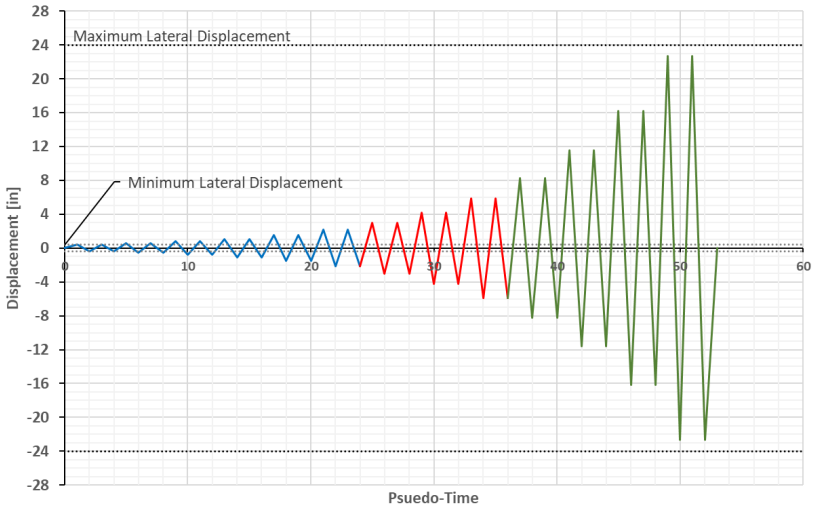

Figure 26: Displacement-Based Loading Protocol Per FEMA 461, 2007 [23]

The loading protocol was divided into phases with different actuator velocities for each phase. The velocities in Test 1 and Test 2 were at a slower rate than that of the remaining two tests.

For Test 1 and Test 2, the lateral loading protocol was divided into three phases. The first phase, shown in blue in Figure 26, included the first six loading cycles and had a velocity targeted at 2in per minute. The second phase, shown in red, included cycles seven, eight, and nine with a velocity targeted at 4-in per minute. The remaining cycles were included in the third phase, shown in green, with a velocity of 8-in per minute.

For Test 3 and Test 4, the lateral loading protocol was divided into two phases. The first phase included the first four loading cycles and had a velocity targeted at 4in per minute. The second phase included the remaining nine cycles to maximum displacement with a velocity targeted of 8-in per minute.

The targeted velocity did not have an impact on the pile performance.

The actuator was held for 1-min on average at each peak amplitude. The test was occasionally paused at amplitude peaks or zero displacement to allow for photos, visual observations, and measuring of soil gapping and/or removal of soil to provide additional clearance for the suspended concrete blocks used for axial loading at higher amplitude cycles. The total test duration varied between two to three hours from start to finish, including all pauses.

7. Data Processing

The instrumentation which fed into the data acquisition system and was post-processed as described in this section is presented in Section 4.3.

7.1 Data Acquisition

A data acquisition system capable of operating at 256 Hz was used to interpret signals from the instrumentation channels and convert them into a digital format for post-processing. The system consisted of a single chassis (or nodes), which was loaded with an embedded controller based on Windows XP running Lab View applications and eight SCXI-1520 signal conditioning modules and had the capability to support sixty-four channels. The data recording was initiated before the command signal was sent to the control system which powered the actuator.

8. Free Vibration Tests

A tire test was performed on Test 1 and Test 3. The purpose of the tire test was to evaluate the free vibration response of the system. Test 1 and Test 3 are considered given the specimens are the upper and lower bounds of the test program. Test 1 and Test 2 have the highest D/t ratio of 43, defined as a non-compact pile in accordance with AISC 360, with Test 1 having a lower material yield strength. Test 3 has the lowest D/t ratio of 22, defined as a compact pile per AISC 360.

The natural period and damping of the pile system were determined from post-processing the top accelerometer data considering Chopra (2017) [18] free vibration mathematical approach. The tire impact disrupts the pile's static equilibrium causing it to oscillate in free vibration. The effective viscous damping ratio controls the rate at which the vibration decays, bringing the system back to equilibrium.

The effective viscous damping ratio, ζ, was determined from the top accelerometer data, located near the application of tire impact. The effective viscous damping was calculated assuming a free vibration harmonic response decay, refer to Figure 27. The peak response was identified, and subsequent peaks were within 50% of the peak response. The response was normalized, such that the peak response was 1 and the response decay less than 1. Due to the low frequencies from the tire impact the natural frequency, ω_n and the natural frequency of damped vibration ω_D are equivalent. Thus,

$$\rho = \sqrt{1 + \zeta^2} \tag{2}$$

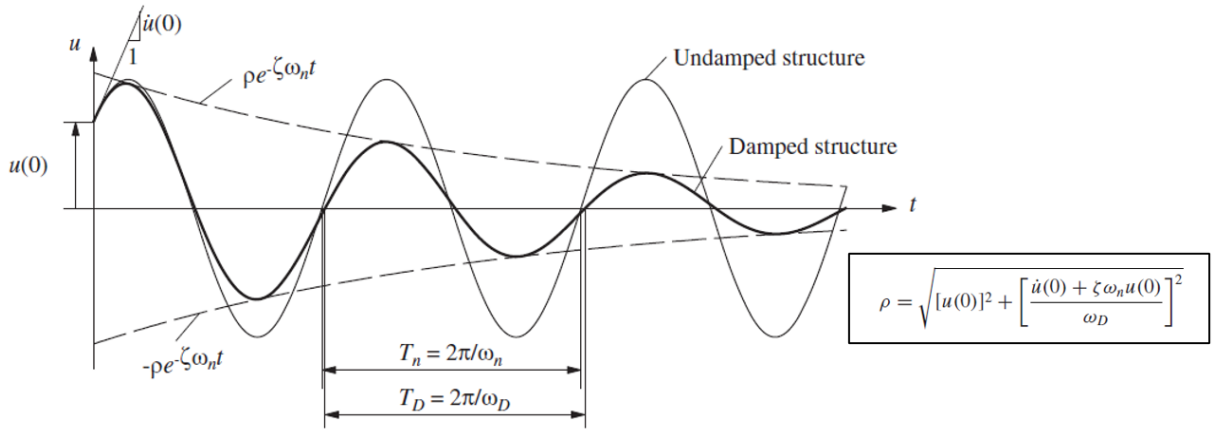

Figure 27: Effect of Damping on Free Vibration (Chopra, 2017) [18]

The system's stiffness, k can be back calculated, using the natural frequency of vibration,

$$T_n = 2\pi\sqrt{m/k} \tag{3}$$

Thus, deriving k as

$$k = {}^{m}/_{(T_n/2\pi)^2} \quad (4)$$

The cross-sectional bending stiffness of the pile is taken as

$$k_b = \frac{EI}{L} \quad (1)$$

The moment of inertia, E_s, was taken as provided from the material tests in Table 5. For simplicity the pile length was taken as the full pile length, 28ft. This is neglecting the contribution of the soil.

For more flexible systems, the pile curvature profile was determined from the strain gauge data recorded along the top 8-ft of the in-ground pile depth. The curvature was calculated by subtracting the peak recorded strains in each test recorded on opposing faces at the same elevation. This was only possible where both strain gauges produced readable data on both external faces of the pile. If a single gauge was inactive or shunted for any reason, that elevation was removed. If the tire impact's dynamic response was within the system's noise level, the strain gauge data could not be used to assess the pile curvature.

The first two peaks of the strain profile for the north and south face was determined for the top 8-ft off the in-ground pile depth. Theoretical strains were computed considering the applied mass of the steel loading apparatus and half the pile self-weight with the maximum recorded acceleration for the first and last test in Level 4.

8.1 Test 1 Dynamic Response

The bending stiffness of the pile was calculated as 9848 kip-in.

The dynamic test for Pile 1 consisted of the tire impact at four distances, i.e. four levels with up to 14 tests in a level. Refer to Table 6 for tire impact distances.

The effective viscous damping ranged from 1.65% to 2.5% with a fundamental period ranging from 0.23 to 0.25 seconds with averages of 2% and 0.24-sec, respectively. Figure 28 shows the calculated effective viscous damping ratio and fundamental period for the four levels.

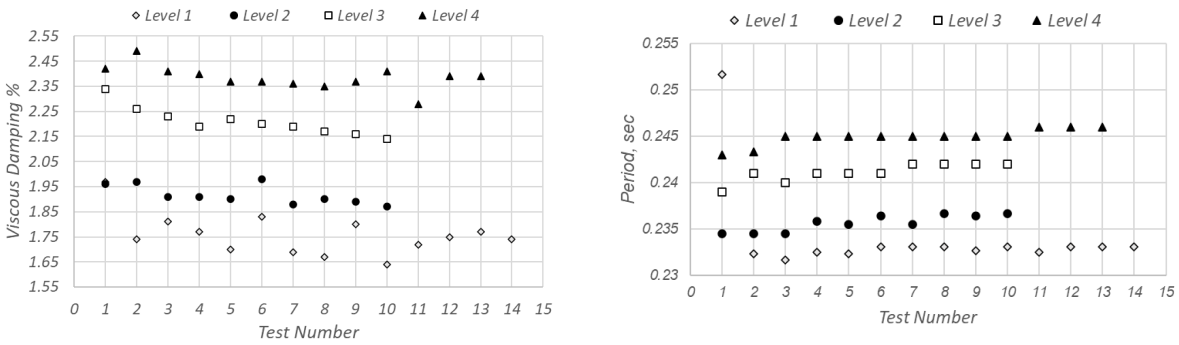

(a) Effective Viscous Damping Ratio *(b) Fundamental Period*

Figure 28: Test 1 Dynamic Response: Viscous Damping and Fundamental Period

The system's stiffness, k, for Test 1 was calculated as 0.06 k/in.

Test 1 strain profile is shown in Figure 29 for the first and last test performed in Level 4. The theoretical strains, ε_T, was defined as f_s/E_s. The stress, f_s, due to the tire impact was computed as the moment at ground divided by the pile's elastic section modulus. The moment was the product of the force imposed on the pile by the tire impact, considering the mass of the steel apparatus, times the maximum recorded acceleration in the test, times the pile's above ground height. Figure 30 shows the respective curvature profile from load application to the last in-ground strain gauge elevation.

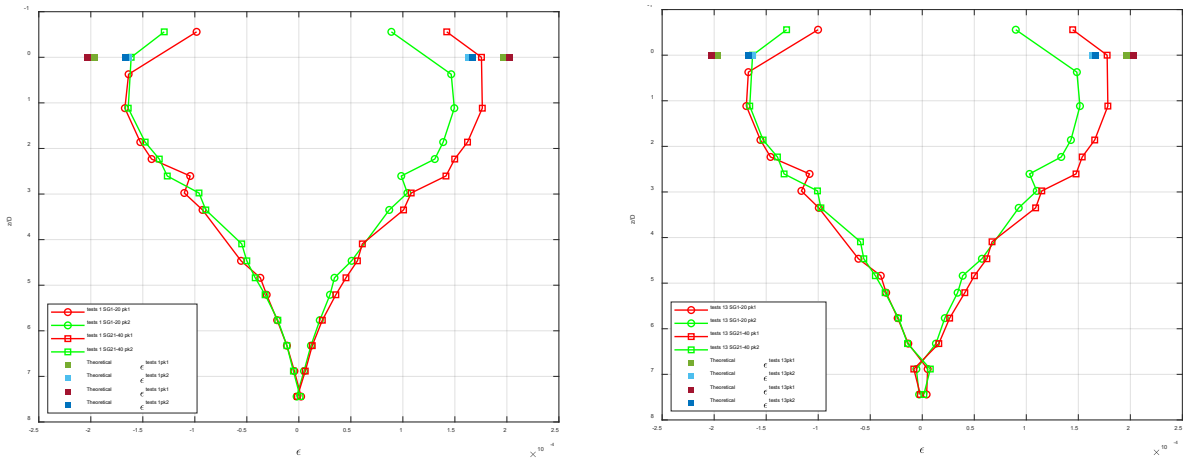

(a) Level 4 Test 1 Strain Profile *(b) Level 4 Test 13 Strain Profile*

Figure 29: Test 1 Dynamic Response: Level 4 Test 1 and 13 Strain Profile

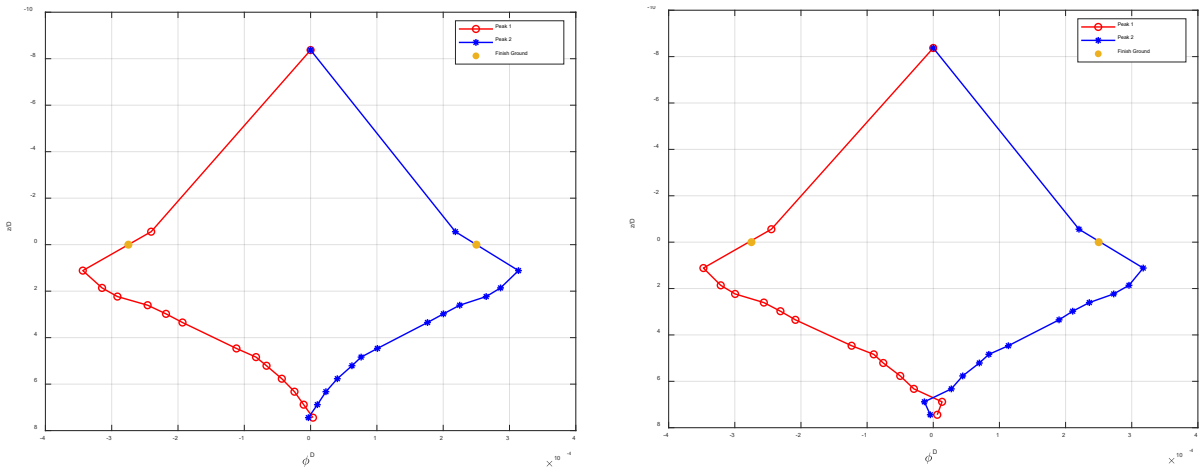

(a) Level 4 Test 1 Curvature Profile *(b) Level 4 Test 13 Curvature Profile*

Figure 30: Test 1 Dynamic Response: Level 4 Test 1 and 13 Curvature Profile

8.2 Test 3 Dynamic Response

The bending stiffness of Test 3 was calculated as 18546 kip-in. The moment of inertia, E_s, was taken as provided from the material tests in Table 5. For simplicity the pile length was taken as the full pile length, 28ft, neglecting the contribution of the soil.

The dynamic test for Pile 3 consisted of the tire impact at four distances, i.e. four levels with up to 10 tests in a level. Refer to Table 6 for tire impact distances.

The effective viscous damping ranged from 1.4% to 2.8% with a fundamental period ranging from 0.05 to 0.2 seconds with averages of 2% and 0.12-sec, respectively. Figure 31 shows the calculated effective viscous damping ratio and fundamental period for the four levels.

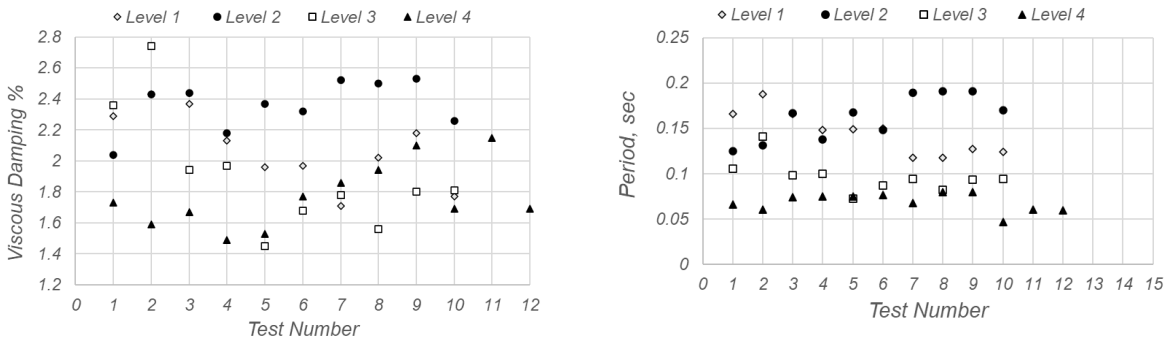

a) Effective Viscous Damping Ratio *b) Fundamental Period*

Figure 31: Test 3 Dynamic Response: Viscous Damping and Fundamental Period

The system's stiffness, k, for Test 3 was calculated as 0.28 k/in.

The strain gauge time histories for Test 3 were analyzed; however, due to the increased pile stiffness, many of the in-ground strain gauges recorded signals fell within the system's noise level. Therefore, the strain data could not be used to generate strain or curvature profiles.

9. Quasi-static Cyclic Test Results

9.1 Test 1: Cyclic Response

Test 1 involved a noncompact pile section, as defined by AISC 360 [4], with a D/t ratio of 43 and a constant applied axial demand approximately 4% of the maximum allowable axial cross-section capacity. As a noncompact section, it is expected to reach the full yield stress in its compression elements prior to the onset of local buckling; however, it lacks the ductility to achieve a rotation capacity of three times its yield rotation. As a result, local buckling is expected to initiate shortly after yielding, thereby limiting the section's ability to sustain significant plastic deformation.

The recorded actuator displacement and force time histories for Test 1 are presented in Figure 33Figure 41. The test completed 11 full loading cycles before the post-peak applied lateral force fell below 80% of the peak lateral force.

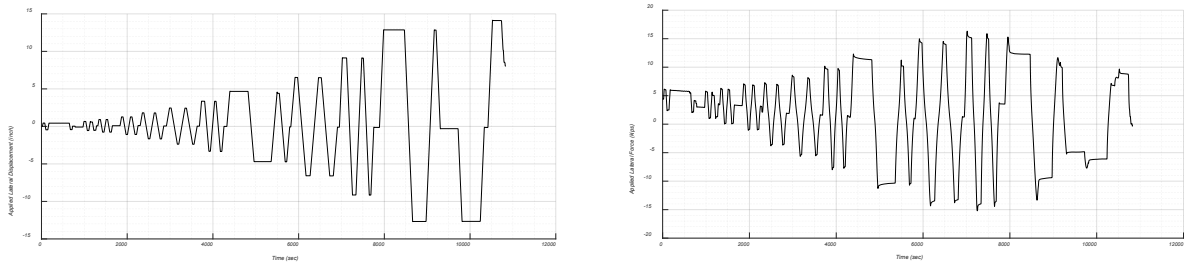

(a) Applied Lateral Displacement *(b) Recorded Actuator Applied Force*

Figure 32: Test 1 Applied Lateral Displacement and Force Time History

The cyclic force displacement curve, shown in Figure 33(a), was converted to a normalized moment rotation curve shown in Figure 33 (b). The y-axis was converted from actuator force to bending moment at estimated plastic hinge location normalized by the calculated plastic moment of the pile section. The x-axis was converted to chord angle, calculated from the recorded lateral displacement over the depth to observed plastic hinge. Refer to Figure 34 for the representative free-body diagram of Test 1 for reference.

The bending moment was determined in the deformed configuration by taking the moments about the estimated hinge location observed in the field, approximately 24.7-in below the ground surface. The free pile height of the lateral loading at zero displacements above ground was measured at 7.88-ft, resulting in an above ground moment arm of 9.96-ft. The first yield moment, M_y, is when the extreme fiber of the section reaches yields at 1263 kip-in. The plastic moment, M_p, was calculated as 1727kip-in. Material properties presented in Table 5 were used in the discrete fiber calculation of the pile capacity considering the P-delta effects induced by the axial load application.

As shown in Figure 33(b), the first yield moment, M_y/M_p, was reached at a chord angle of 0.04 within cycle 8. The plastic moment, M_p/M_p, was reached at a chord angle of 0.065 prior to reaching the first peak amplitude in cycle 10.

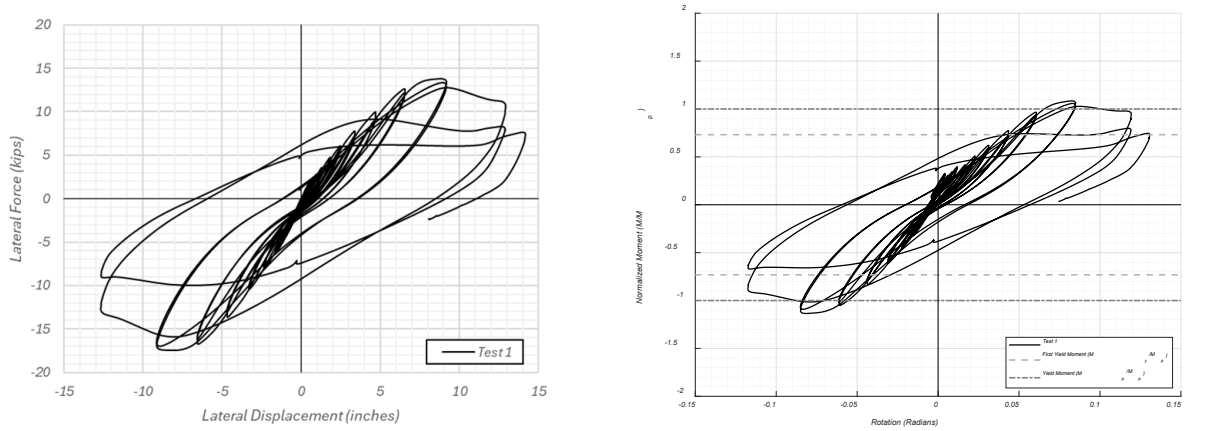

a) Actuator Force- Displacement Curve *b) Normalized Moment vs. Pile-Rotation Response*

Figure 33: Test 1 Hysteretic Response

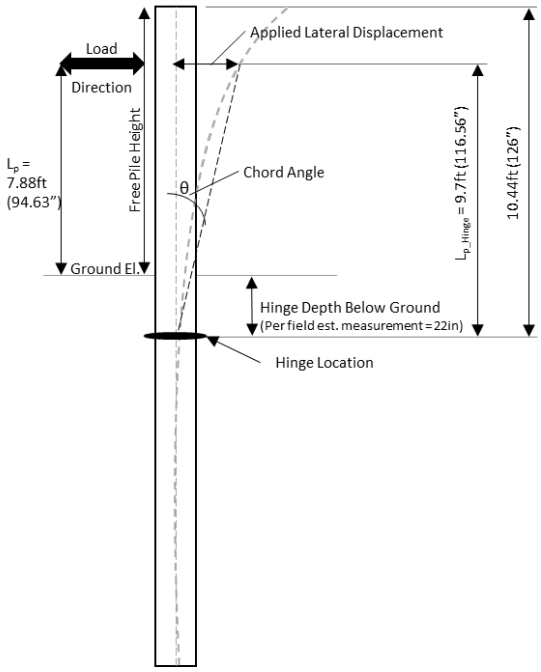

Figure 34: Schematic Free-Body Diagram of Pile

Pile Strains

The normalized strain profile for the first positive and negative peaks for cycles 1-11 are shown in Figure 35 and Figure 36. Figure 35 shows the first and second positive and negative peaks along the pile depth. Figure 36 shows the maximum compressive and

tensile strains within each test amplitude cycle for a given elevation. Figure 35 will be used to verify the experiment against the finite element model. All other test will summarize the maximum compressive and tensile strains per cycle.

After evaluation of the recorded strain data, of the 40 strain gauges installed, 35 were determined viable for post-processing. However, only 11 strain gauge pairs (22 strain gauges) at 11 elevations/depths were used in this report. The depth is normalized by the pile diameter, and the strains are presented in micro-strains. The strain profile only considers the instrumented pile length and not the entire length of the test pile. The theoretical yield strain was determined as the $\varepsilon_y = f_y/E_s$. The red "x" shown in the strain profile indicates either the loss of the strain gauge due to damage or the strain recording exceeding the maximum recordable reading per the manufacturer, approximately 10% - 15 % in the subsequent cycle for that amplitude peak. As shown in Figure 35 and Figure 36, when looking at the behavior at the first positive peak, strain gauges SG102, SG104, SG105, SG106 and SG109 on the north face were either damaged or exceeded the maximum recordable strain as they have "x" occurring either in cycles 9, 10 or 11. The south face experienced more loss of gauges or exceedance of maximum recorded strain at the first negative peak, losing strain gauges SG122, SG124, SG125 and SG126.

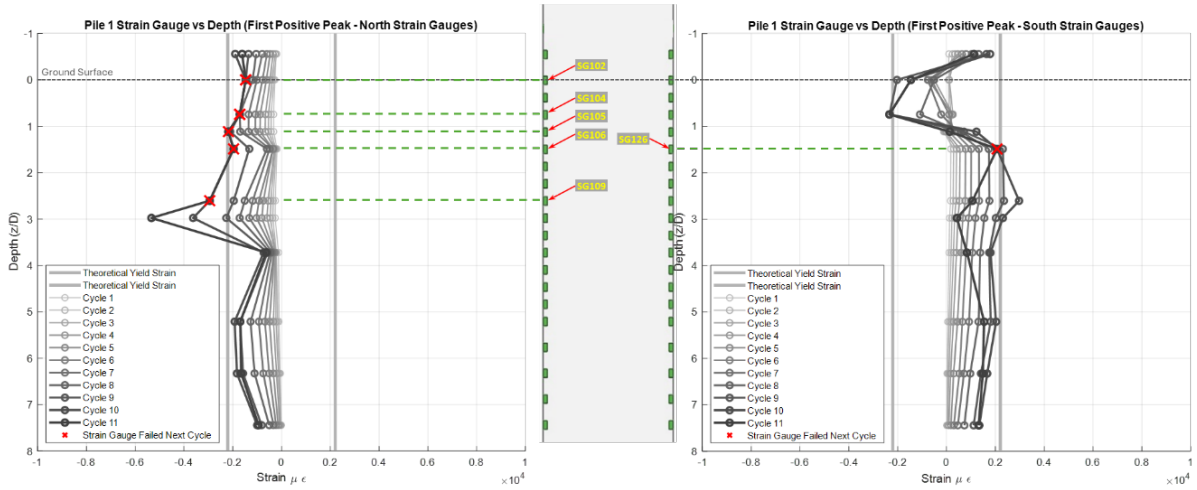

a) First Positive Peak North (left) and South (right) Strain Gauge vs. Depth Profiles

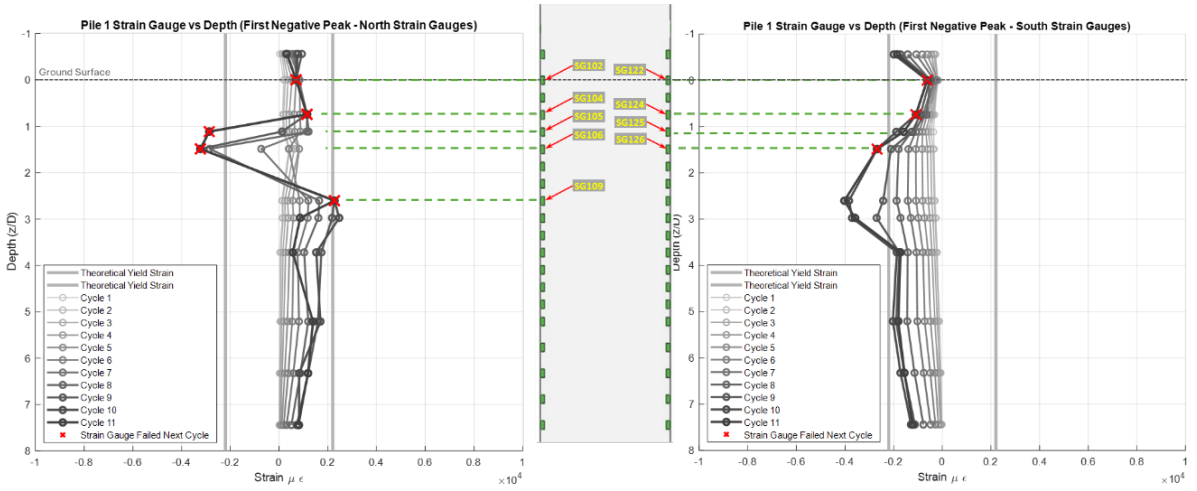

b) First Negative Peak North (left) and South (right) Strain Gauge vs. Depth Profiles

Figure 35: Pile 1 Strain Gauge vs. Depth Profiles

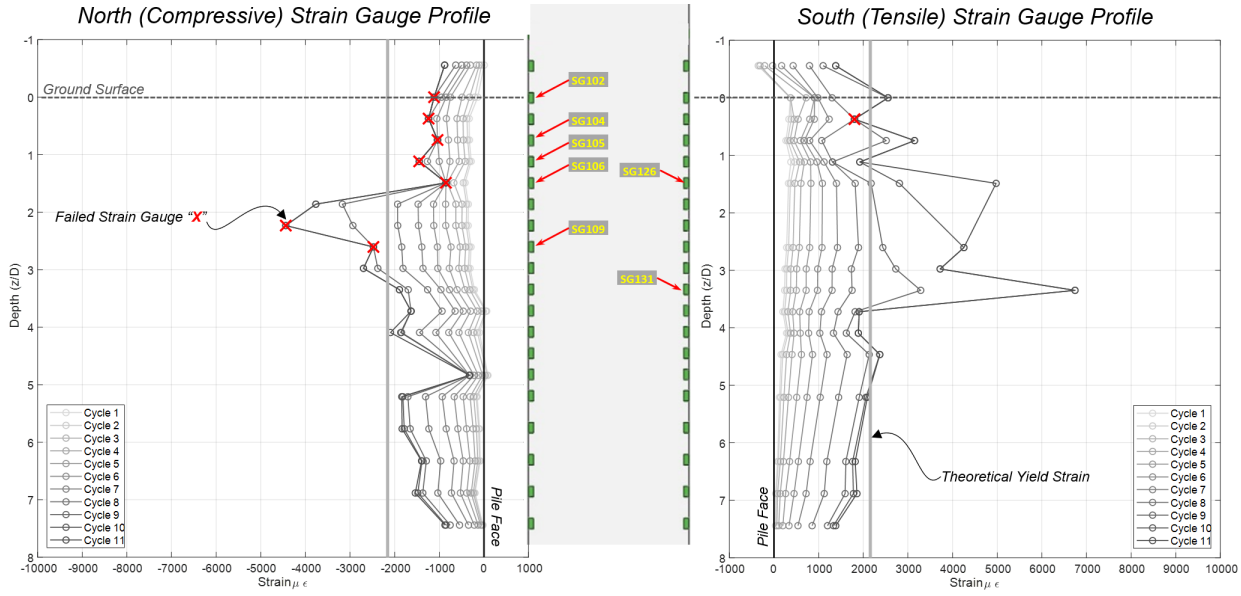

a) Cycle Peak North Compressive and South Tensile Strains vs. Depth Profiles

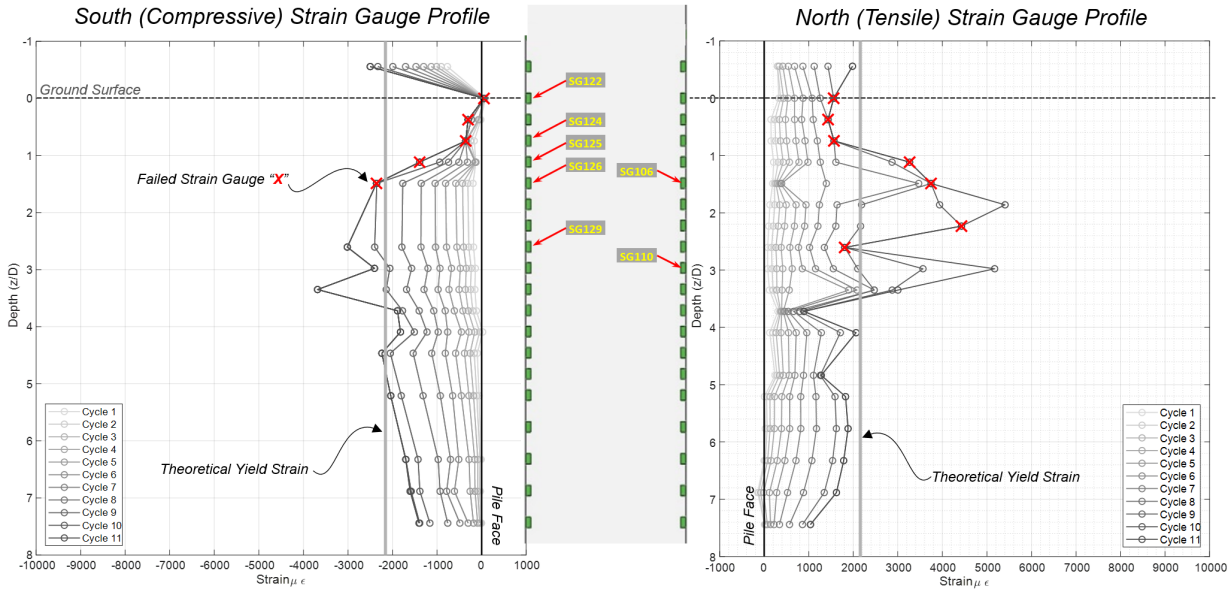

b) Cycle Peak South Compressive and North Tensile Strains vs. Depth Profiles

Figure 36: Test 1 Maximum Peak Compressive and Tensile Strain vs. Depth Profiles

Observed Buckling

The local buckling at the in-ground hinge was initially observed after testing using a plumber's camera. The camera was attached to the end of a strong flexible cable providing live video feed. The camera head was inserted into the pile at the top and lowered into the pile. The cable was marked at 10ft increments, however, to accurately measure the depth of the bulked region, a flexible measuring table was attached to the

camera end. Once the bulked region was observed on the camera the depth was recorded. Prior to excavation the soil pit, the pile had been cut approximately 13.5-in above grade. A top-down visual of the in-ground buckled pile is shown in Figure 37(a). To verify the accuracy of the depths observed, the soil pit was excavated in August 2024, making the buckle region visible and accessible. The buckled region of the pile was extracted and the dirt and debris were removed from the pile using a laser cleaner, refer to Figure 37(b). The piles were painted light grey and 360-degree photos were taken to produce a 3D point cloud model of the pile using AutoCAD ReCap Photo, refer to Figure 37(c).

An outward buckle was observed on the southern face of the pile; this could also be visible from above ground. The center of the buckle was determined as 18.5-in (1.72 pile diameters, D) from initial top of ground. An inward buckle was observed with the plumber's camera and later, once extracted, on the northeastern face. This inward buckle was measured 8-in below the outward buckle, 26.5-in (2.5D) from the initial top of ground. The depth of buckling for performance analysis and processing of the results was taken as an average between the south and north buckles determined as 22-in, roughly two pile diameters (2D). The length from top of south buckle and bottom of north buckle can be defined as the buckled region, measuring roughly 1-ft in length.

(a) In-ground Top View *(b) Laser Cleaned Elevation* *(c) Point Cloud Model*

Figure 37: Observed Location of In-Ground Pile Buckling of Test 1

The location of the observed buckle corresponds to the strain behavior illustrated in Figure 35 and Figure 36. During large displacement cycles, strain measurements from 1D to 4D below ground level exceed the theoretical yield strain. The highest strain values are recorded by gauges SG106 to SG111 on the north face, as well as SG226 to SG 131 on the south face. Note SG127 and SG128 demonstrated nonviable readings and therefore was removed for post processing.

All ten strain gauges exceeded the theoretical yield strain during the test. SG126 on the south face is the closes viable reading near the observed south buckle with a maximum tensile strain of 0.005 and a compressive stain of 0.0024. Whereas the north observed buckle is near strain recordings SG108 and SG109, both of which significantly exceeded the gauges' measurement capacities during larger displacement cycles, potentially indicating the initiation and progression of local buckling. Maximum compressive and tensile strains recorded for SG108 were 0.175 and 0.004, respectively. For SG109 the maximum compressive and tensile strains recorded was 0.0025 and 0.325, respectively.

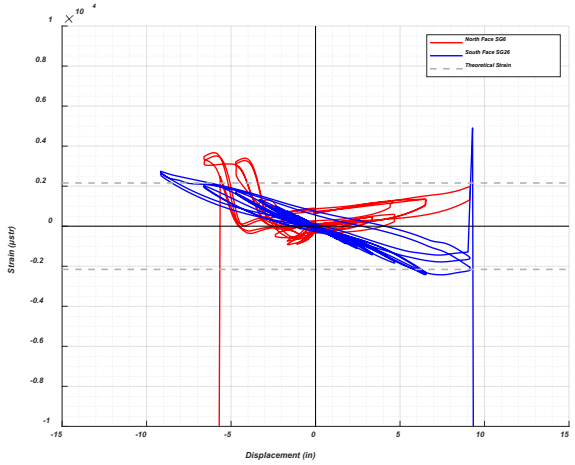

a) SG106 & SG126 at 1.5D below Grade

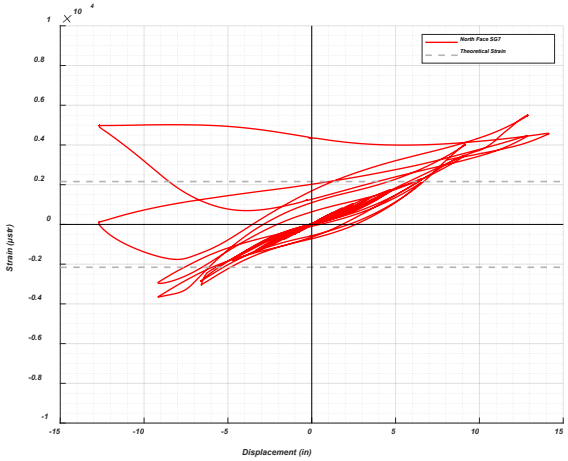

b) SG107 at 1.9D below Grade

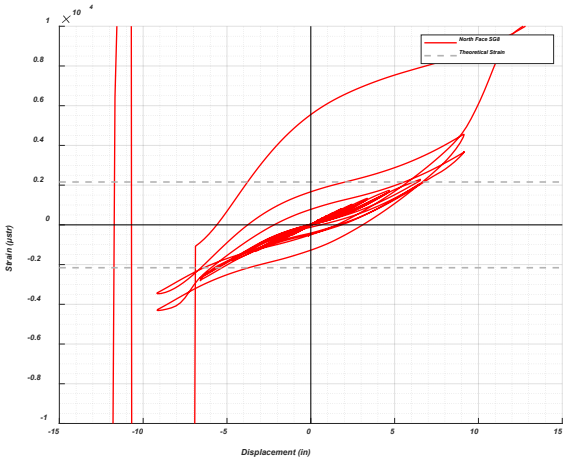

c) SG108 at 2.2D below Grade

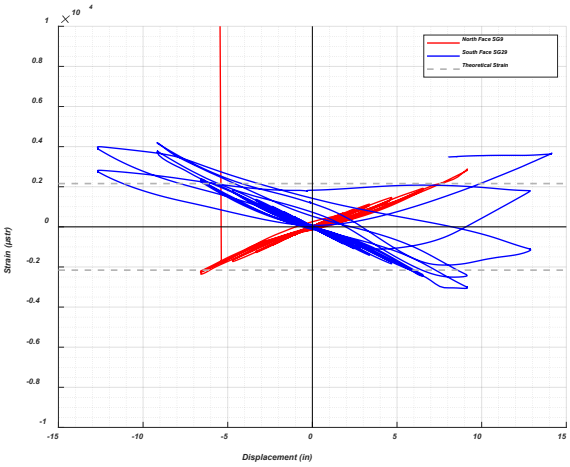

d) SG109 & SG129 at 2.6D below Grade

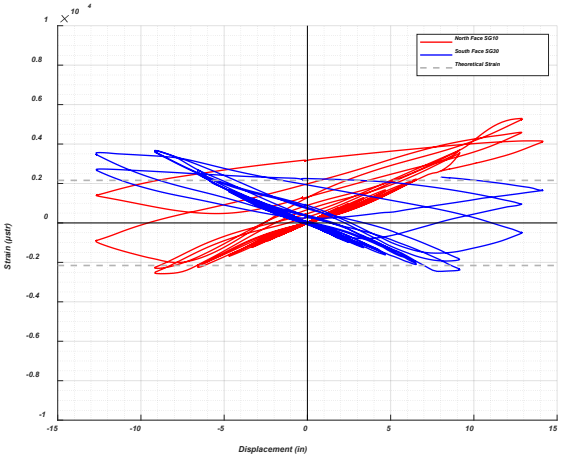

e) SG110 & SG130 at 3.0D below Grade

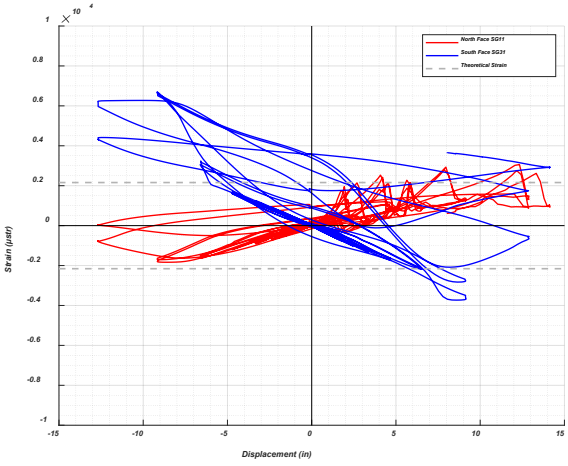

f) SG131 at 3.3D below Grade

Figure 38: Test 1 Strain vs Applied Displacement within Buckled Region

Topsoil Gapping

To evaluate the impacts of the surrounding soil in the pile buckling region, the soil gapping at ground surface was visually evaluated and measured after the first peak of cycles 7, 8, 9, 10, and 11 when the pile displacement returned to zero. The test was paused at the first peak to allow for observations and gapping measurements. The measured soil gapping for these cycles is shown in Figure 39. The depth of the soil gapping was observed and measured as approximately 32-in after the first peak of cycle 8 and 52-in after the first peak of cycle 11. These depth measurements are estimates since granular soil, obstructions such as small rocks and debris can fall into the gap and lead to inaccurate depth measurements. Furthermore, the inner soil plug, as determined in Table 3, is not present for the top 10D, where D equals the pile diameters. Thus, the increase in soil gapping and the presence of a deep soil plug indicates that at higher lateral displacement amplitudes there is limited soil influence on the pile for up to 2D to 4D below the ground surface.

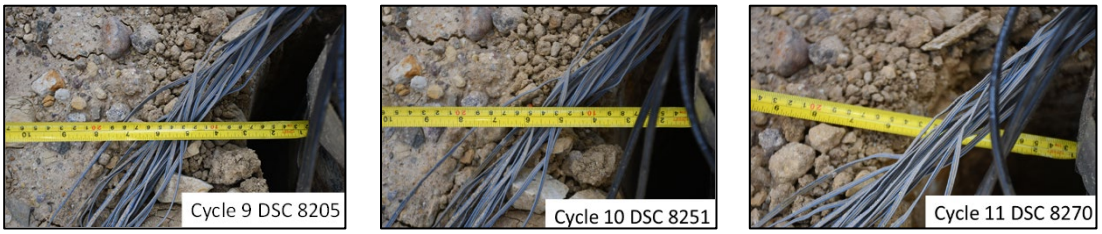

Figure 39: Test 1 Soil Gapping Field Measurements at First Peak Amplitude

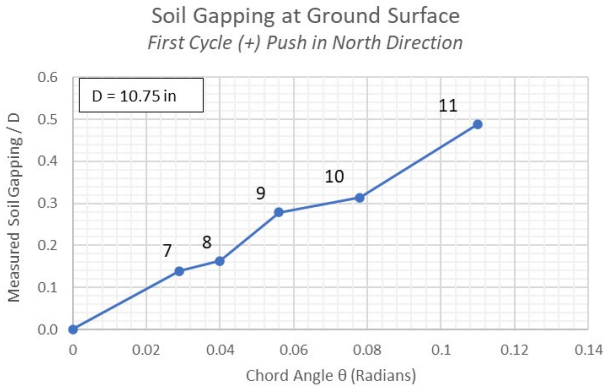

Figure 40: Test 1 Soil Gapping verse Chord Angle

9.2 Test 2: Cyclic Response

Test 2 involved a noncompact pile section, as defined by AISC 360 [4], with a D/t ratio of 43 and a constant applied axial demand approximately 13% of the maximum allowable axial cross-section capacity. As a noncompact section, it is expected to reach the full yield stress in its compression elements prior to the onset of local buckling; however, it lacks the ductility to achieve a rotation capacity of three times its yield rotation. As a result, local buckling is expected to initiate shortly after yielding, thereby limiting the section's ability to sustain significant plastic deformation.

The recorded actuator displacement and force time histories for Test 2 are presented in Figure 41. The test completed 11 full loading cycles before the post-peak applied lateral force fell below 80% of the peak lateral force.

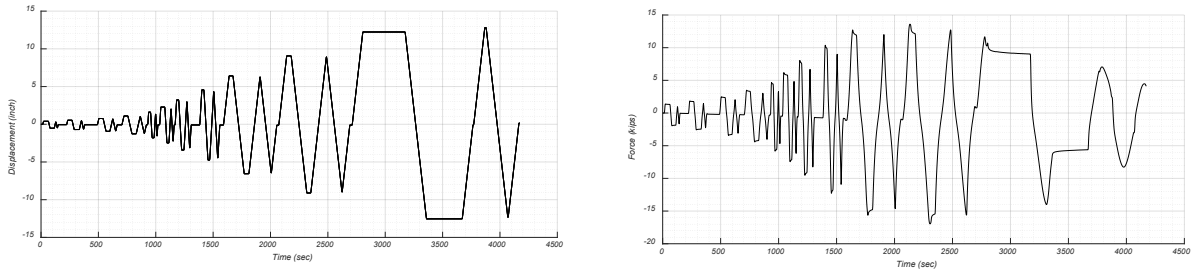

(c) Applied Lateral Displacement *(d) Recorded Actuator Applied Force*

Figure 41: Test 2 Applied Lateral Displacement and Force Time History

The cyclic force displacement curve, shown in Figure 42(a), was converted to a normalized moment rotation curve shown in Figure 42(b). The y-axis was converted from actuator force to bending moment at estimated plastic hinge location normalized by the calculated plastic moment of the pile section. The x-axis was converted to chord angle, calculated from the recorded lateral displacement over the depth to observed plastic hinge. Refer to Figure 34 for the representative free-body diagram of Test 1 for reference.

The bending moment was determined in the deformed configuration by taking the moments about the estimated hinge location observed in the field, approximately 24.7-in below the ground surface. The free pile height of the lateral loading at zero displacements above ground was measured at 7.62-ft, resulting in an above ground moment arm for the applied lateral load of 9.68-ft. The first yield moment, M_y, is when the extreme fiber of the section reaches yields at 1306 kip-in. The plastic moment, M_p, was calculated as 1924 kip-in. Material properties presented in Table 5 were used in the discrete fiber calculation of the pile capacity considering the P-delta effects induced by the axial load application.

As shown in Figure 42(b), the first yield moment, M_y/M_p, was reached at a chord angle of 0.025 within cycle 8. The plastic moment, M_p/M_p, was reached at a chord angle of 0.042 prior to reaching the first peak amplitude in cycle 10.

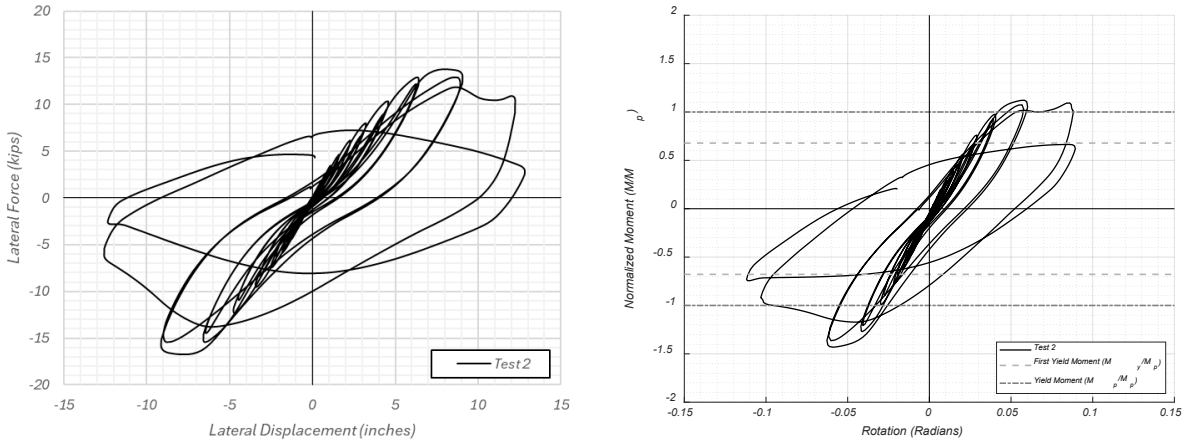

a) Actuator Force-Displacement Curve

b) Normalized Moment vs. Pile-Rotation Response

Figure 42: Test 2 Hysteretic Response Curves

Recorded Pile Strains

The normalized strain profile for the maximum positive and negative peaks for cycles 1-11 are shown in Figure 43. After evaluation of the recorded strain data, of the 40 strain gauges installed, 33 were determined viable for post-processing. However, only 13 strain gauge pairs (26 strain gauges) at 13 elevations/depths could be compared. The profile depth is normalized by the pile diameter, and the strains are presented in micro-strains. The strain profile only considers the instrumented pile length and not the entire length of the test pile. The strains shown are the maximum compressive and tensile strains observed in each cycle. Although shown in a single plot for each cycle, maximum strains at different elevations may have peaked at different times within the same cycle. The theoretical yield strain was determined as the $\varepsilon_y = f_y/E_s$, approximately 0.0025. The red "x" shown in the strain profile indicates either the loss of the strain gauge due to damage or the strain recording exceeding the maximum recordable reading per the manufacturer, approximately 10% -15% in the subsequent cycle for that amplitude peak. To eliminate step backs in the profile recording, any strain recorded in a cycle that was lower than the strain in the preceding cycle was interpreted as the maximum peak of the previous cycle. As shown in Figure 43, strain gauges SG202, SG203, SG204 and SG206 on the north face were either damaged during the test or exceeded the maximum recordable strain as they have "x" occurring in large displacement cycles. The south face also experienced loss of gauges or exceedance of maximum recorded strain at large displacement cycles, losing strain gauges SG223, SG224 and SG227.

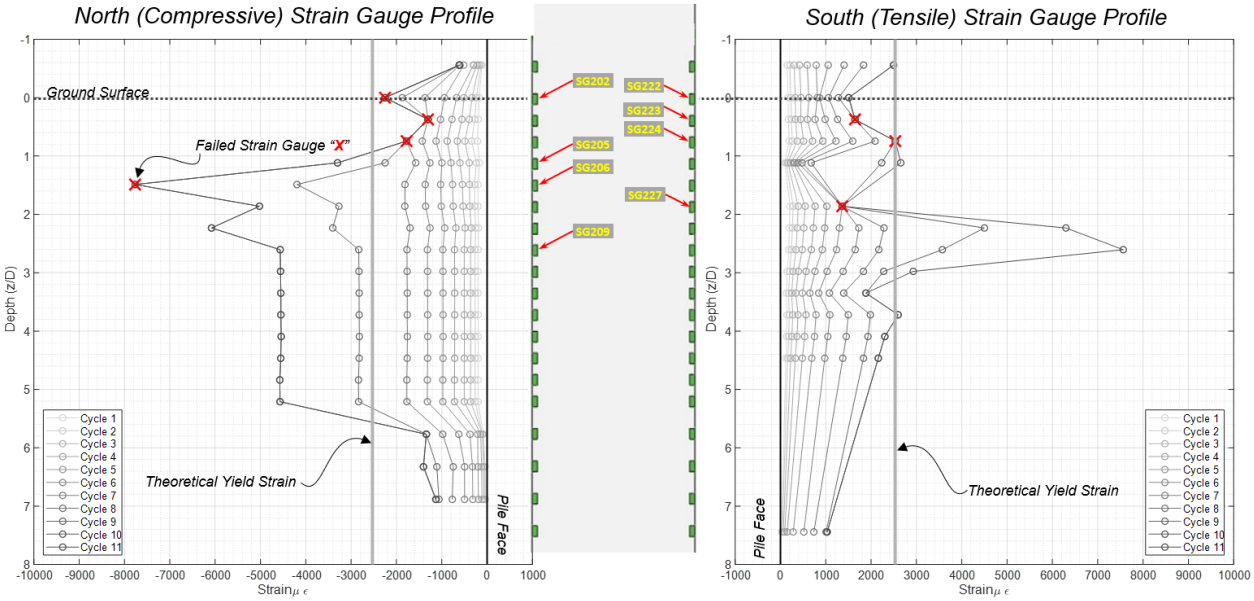

a) Cycle Peak North Compressive and South Tensile Strains vs. Depth Profiles

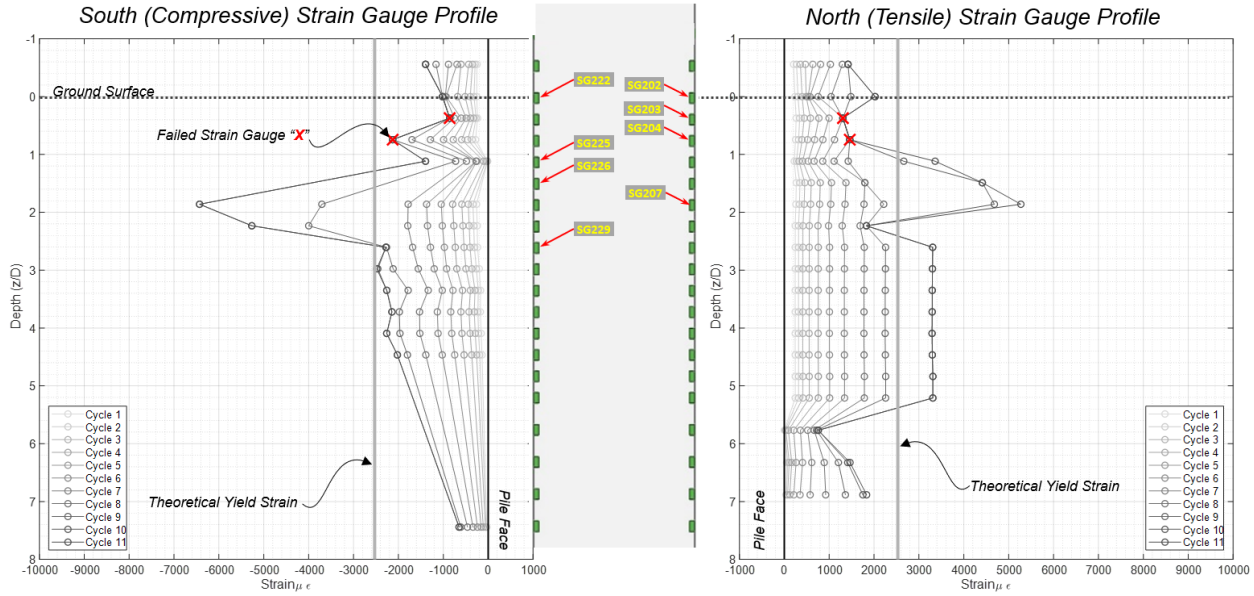

b) Cycle Peak South Compressive and North Tensile Strains vs. Depth Profiles

Figure 43: Test 2 Maximum Peak Compressive and Tensile Strain vs. Depth Profiles

Observed Buckling

The local buckling at the in-ground hinge was initially observed after testing looking down the pile once it was cut several inches above ground. Prior to post-test excavation of the soil pit, the pile had been cut approximately 9-in above grade. A top-down visual of the in-ground buckled pile is shown in Figure 44(a). To verify the accuracy of the depths observed, the soil pit was excavated in August 2024, making the buckle region visible and

accessible. The buckled region of the pile was extracted and the dirt and debris were removed from the pile using a laser cleaner, refer to Figure 44(b). The piles were painted light grey and 360-degree photos were taken to produce a 3D point cloud model of the pile using AutoCAD ReCap Photo, refer to Figure 44(c).

The pile experienced partial circumferential outward and inward buckling at multiple elevations between 20-in and 30-in below the initial ground elevation, approximately 1.9 to 2.8 pile diameters (D), respectively. Two inward buckles were observed on the south face occurring within 1.9 and 2.2 pile diameters below initial ground. An outward buckle was observed on the northern pile face approximately 2.8 pile diameters below initial ground. The depth of buckling for performance analysis and processing of the results was taken as an average between the observed buckles determined as 24.7-in, roughly 2.3 pile diameters (2.3D) below grade. The length from top of south buckle and bottom of north buckle can be defined as the buckled region, measuring roughly 1-ft in length.

(a) In-ground Top View *(b) Laser Cleaned Elevation* *(c) Point Cloud Model*

Figure 44: Observed Location of In-Ground Pile Buckling of Test 2

The location of the observed buckle corresponds to the strain behavior illustrated in Figure 43. During large displacement cycles, strain measurements from 1D to 5.5D below ground level exceed the theoretical yield strain. The highest strain values are recorded by gauges SG206, SG207, SG208, and SG209 on the north face, as well as SG227, SG228, and SG229 on the south face. Note SG226 demonstrated nonviable readings and therefore was removed for post processing.

All seven strain gauges shown in Figure 45 exceeded the theoretical yield strain during the test. SG206, SG207, and SG227 recorded strains significantly beyond the gauges' measurement capacities during larger displacement cycles, potentially indicating the initiation and progression of local buckling. This is particularly notable for SG227, which

was positioned near the top of the inward buckles observed on the southern exterior face of the pile, approximately 20-in or 1.9D from the top of ground. SG227 experienced a series of peak compressive strains, with a recorded maximum strain of 0.122 occurring in loading cycle 9. This gauge remained viable throughout the test duration.

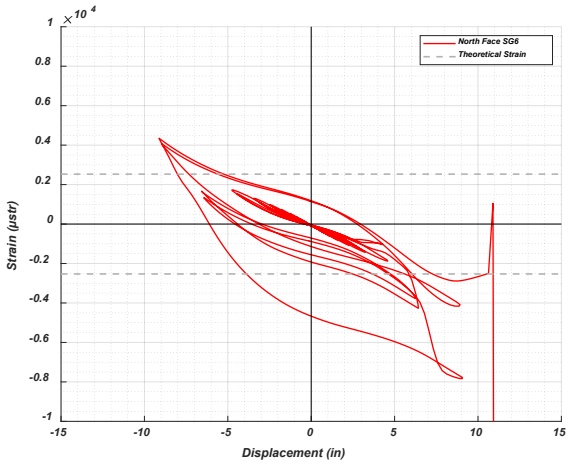

g) SG206 at 1.5D below Grade

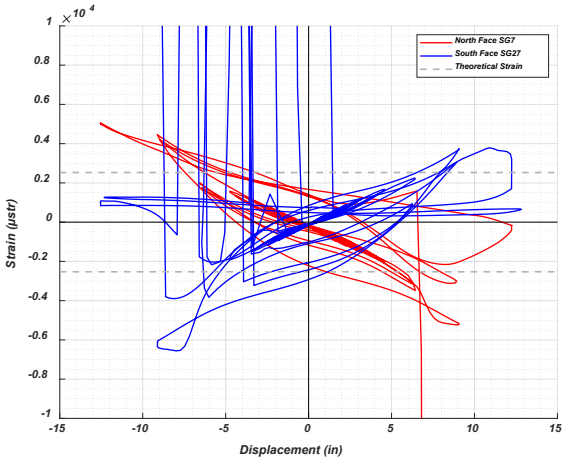

h) SG207 & SG227 at 1.9D below Grade

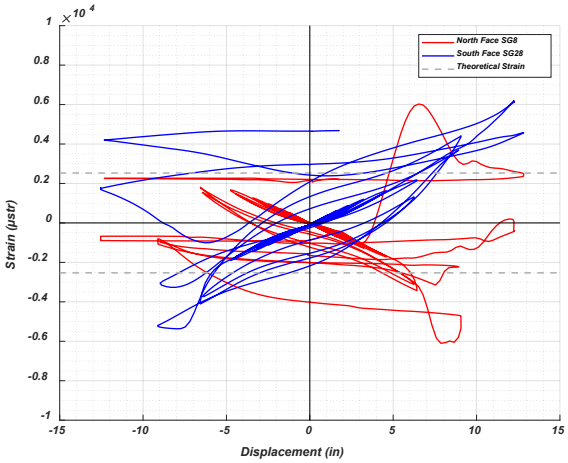

i) SG208 & SG228 at 2.2D below Grade

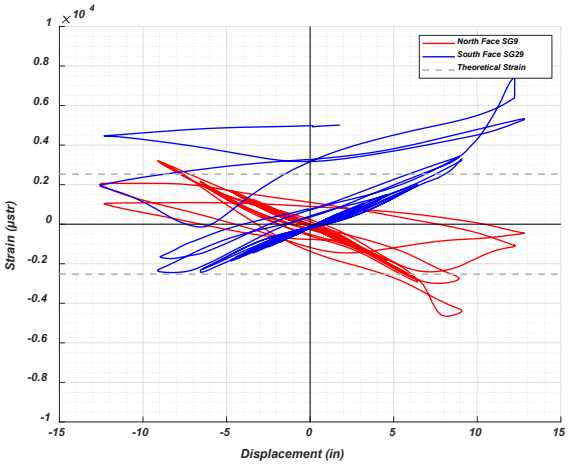

j) SG207 & SG227 at 2.6D below Grade

Figure 45: Test 2 Strain vs Applied Displacement within Buckled Region

Topsoil Gapping

To evaluate the impacts of the surrounding soil in the pile buckling region, the soil gapping at ground surface was visually evaluated for Test 2 using a near ground go-pro. The go-pro was programmed to take a series of photos within the duration of each cycle, capturing the pile displacement and soil heaving at the top of ground. This was installed as a backup measurement for Test 2. Unfortunately, the longitudinal and axial string potentiometers where installed with insufficient lengths to measure the near-ground

lateral and axial displacements at the large displacement cycles leading to the Go-pro photos being the only measuring tool. The near-ground measurements were determined using the photos and measuring tool in Bluebeam. The gapping was measured at every cycle peak. Figure 46 shows the measured gapping at the first north push peak for cycles 7, 8, 9, 10, and 11. Furthermore, the inner soil plug, as determined in Table 3, is not present for the top 4.5D, where D equals the pile diameters. Thus, the increase in soil gapping and the presence of a deep soil plug indicates that at higher lateral displacement amplitudes there is limited soil influence on the pile for up to 2D to 4D below the ground surface.

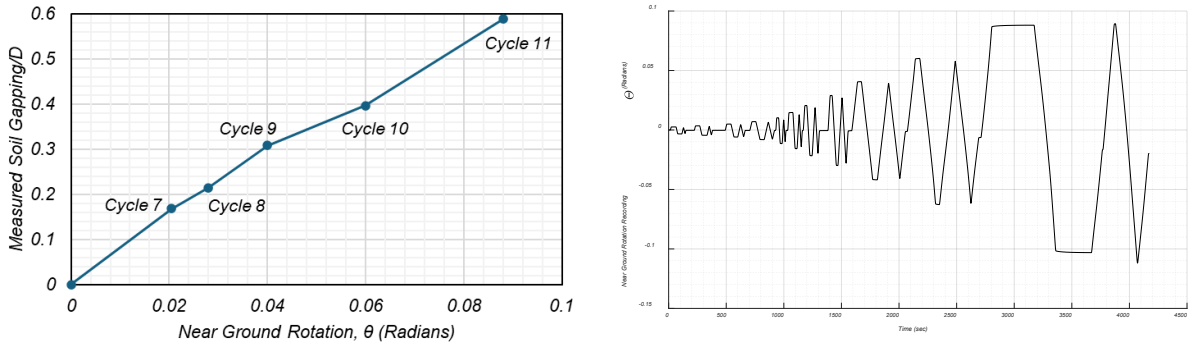

(a) Normalized Soil Gapping Measurements vs Near Ground Rotation Recordings

(b) Near Ground Rotation Recording

Figure 46: Test 2 Near Ground Measurements

9.3 Test 3: Cyclic Response

Test 3 involved a compact pile section, as defined by AISC 360 [4], with a D/t ratio of 22 and a constant applied axial demand approximately 7% of the maximum allowable axial cross-section capacity. As a compact section, it is expected to reach the full yield stress in its compression elements prior to the onset of local buckling; and have significant post-peak performance ductility, typically a rotation capacity greater than three times its yield rotation. As a result, local buckling is expected to initiate well after yielding, allowing the section's ability to sustain significant plastic deformation.

The recorded actuator displacement and force time histories for Test 3 are presented in Figure 47. The test completed 13 full loading cycles before the maximum displacement allowed for the actuator was achieved.

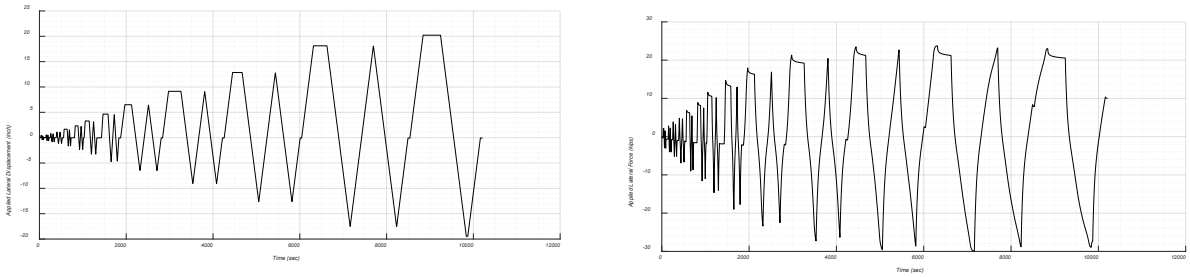

(a) Applied Lateral Displacement *(b) Recorded Actuator Applied Force*

Figure 47: Test 3 Applied Lateral Displacement and Force Time History

The cyclic force displacement curve, shown in Figure 48(a), was converted to a normalized moment rotation curve shown in Figure 48(b). The y-axis was converted from actuator force to bending moment at estimated plastic hinge location normalized by the calculated plastic moment of the pile section. The x-axis was converted to chord angle, calculated from the recorded lateral displacement over the depth to estimated plastic hinge. Given no buckling was observed in Test 3, the hinge location was estimated at 3D considering the behavior of previous tests. Refer to Figure 34 for the representative free-body diagram of Test 1 for reference.

The bending moment was determined in the deformed configuration by taking the moments about the estimated hinge location, assumed as 3.3D, 35.48-in below ground. The free pile height of the lateral loading at zero displacements above ground was measured at 7.67-ft, resulting in an above ground moment arm for the applied lateral load of 10.62-ft. The first yield moment, M_y, is when the extreme fiber of the section reaches yields at 2595 kip-in. The plastic moment, M_p, was calculated as 3700.4 kip-in. Material properties presented in Table 5 were used in the discrete fiber calculation of the pile capacity considering the P-delta effects induced by the axial load application.

As shown in Figure 48(b), the first yield moment, M_y/M_p, was reached at a chord angle of 0.046 within cycle 9. The plastic moment, M_p/M_p, was reached at a chord angle of 0.081 prior to reaching the first peak amplitude in cycle 11.

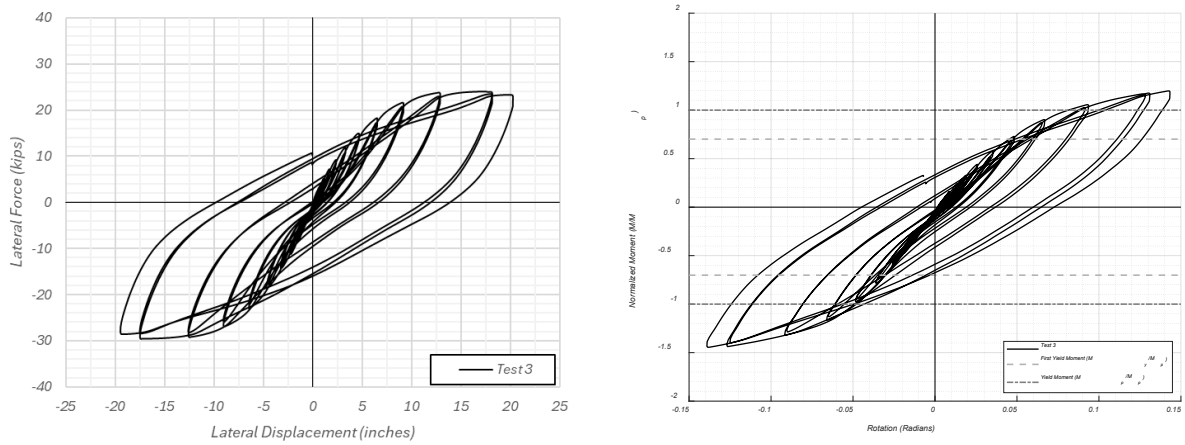

a) Actuator Force-Displacement Curve

b) Normalized Moment vs. Pile-Rotation Response

Figure 48: Test 3 Hysteretic Response

Recorded Pile Strains

The normalized strain profile for the maximum positive and negative peaks for cycles 1-13 are shown in Figure 49. After evaluation of the recorded strain data, of the 40 strain gauges installed, 30 were determined viable for post-processing. However, only 10 strain gauge pairs (20 strain gauges) at 10 elevations/depths could be compared. The profile depth is normalized by the pile diameter, and the strains are presented in micro-strains. The strain profile only considers the instrumented pile length and not the entire length of the test pile. The strains shown are the maximum compressive and tensile strains observed in each cycle. Although shown in a single plot for each cycle, maximum strains at different elevations may have peaked at different times within the same cycle. The theoretical yield strain was determined as the $\varepsilon_y = f_y/E_s$, approximately 0.0024. The red "x" shown in the strain profile indicates either the loss of the strain gauge due to damage or the strain recording exceeding the maximum recordable reading per the manufacturer, approximately 10% -15% in the subsequent cycle for that amplitude peak. To eliminate step backs in the profile recording, any strain recorded in a cycle that was lower than the strain in the preceding cycle was interpreted as the maximum peak of the previous cycle. As shown in Figure 43, strain gauges SG301 to SG308 on the north face were either damaged during the test or exceeded the maximum recordable strain as they have "x" occurring in large displacement cycles. The south face also experienced loss of gauges

or exceedance of maximum recorded strain at large displacement cycles, losing strain gauges SG322, SG323, SG325, SG327 and SG335.

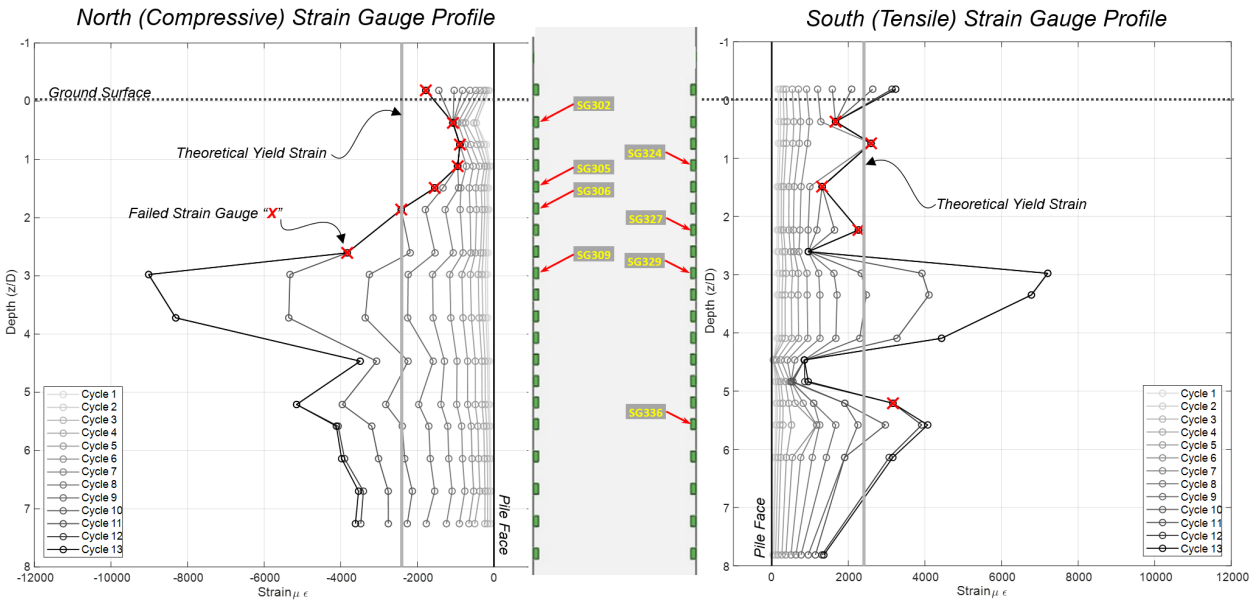

a) Cycle Peak North Compression and South Tensile Strain vs. Depth Profiles

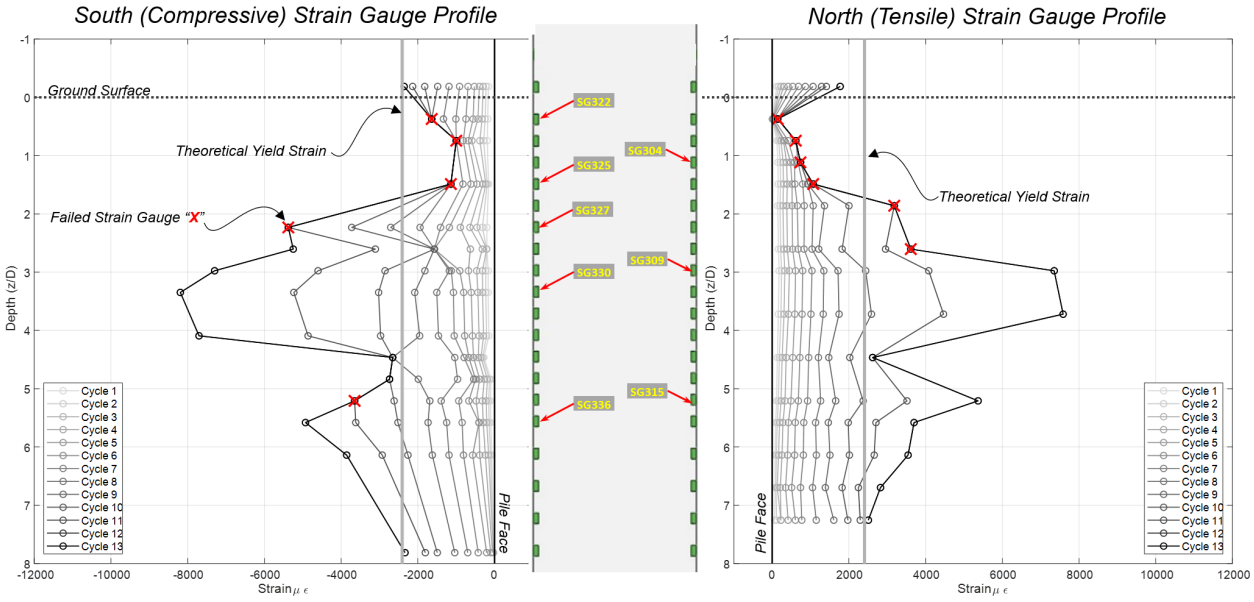

b) *Cycle Peak South Compression and North Tensile* vs. Depth Profiles

Figure 49: Test 3 Maximum Peak Compressive and Tensile Strain vs. Depth Profiles

Observed Buckling

Although, Test 3 exhibited no visible buckling. Pile strains at large displacement cycles well exceeded the theoretical yield strain. Strain measurements from 1.9D below ground

to the last in-ground strain at 7.8D below ground exceed the theoretical yield strain. The highest strain values are recorded by gauges SG308, SG309 and SG311 on the north face, as well as SG328, SG329, SG330 and SG332 on the south face. Note SG226 demonstrated nonviable readings and therefore was removed for post processing.

All seven strain gauges shown in Figure 50 exceeded the theoretical yield strain during the test. SG309, SG311, SG329 and SG330 recorded strain time histories demonstrated no exceedance of the gauges' measurement capacities or exhibit gauge failure during the test. The recorded strains of SG308 and SG328, however, significantly exceeded the gauges' measurement capacities during larger displacement cycles, potentially indicating the initiation and progression of local buckling or loss of gauge due to damage. SG328 experienced a series of peak compressive strains, with a recorded maximum strain of 0.325 occurring in loading cycle 9. This gauge remained viable throughout the test duration.

Topsoil Gapping

To evaluate the impacts of the surrounding soil in the pile buckling region, the soil gapping at ground surface was visually evaluated for Test 3 using a near ground go-pro. The go-pro was programmed to take a series of photos within the duration of each cycle, capturing the pile displacement and soil heaving at the top of ground. The longitudinal string potentiometers was installed with insufficient lengths to measure the near-ground lateral and axial displacements at the large displacement cycles which preceded those of Test 1 and Test 2 leading to the Go-pro photos being the only measuring tool. The near-ground measurements were determined using the photos and measuring tool in Bluebeam. The gapping was measured at every cycle peak for the larger amplitude displacement in cycles 7 to 13. Figure 51 shows the near surface soil gapping, heaving and hole depth measurement at the higher amplitude displacements. The measured depth of the developed hole was nearly seven pile diameters deep, indicating that full instrumented depth of the pile was within the gapping boundaries. Figure 52 shows the normalized soil gapping measurements determined from the Go-Pro Photos vs. the calculated chord angle assuming a hinge 3D, where D equals the pile diameters, below the surface. Unfortunately, the inclinometer recordings near ground were determined nonviable. Furthermore, the inner soil plug, as determined in Table 3, is not present for the top 12D. Thus, the increase in soil gapping and the presence of a deep soil plug indicates that at higher lateral displacement amplitudes there is limited soil influence on the pile for up to 7D below the ground surface.

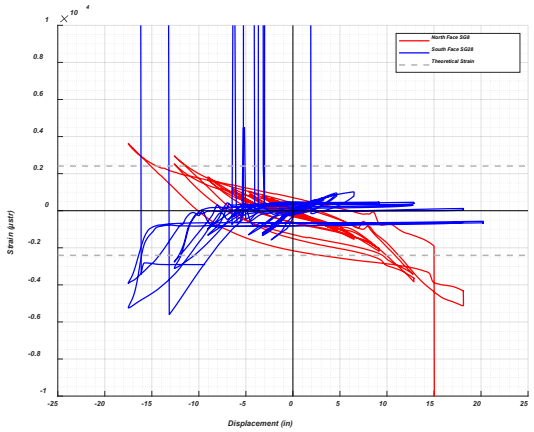

a) SG308 & SG328 at 2.6D below Grade

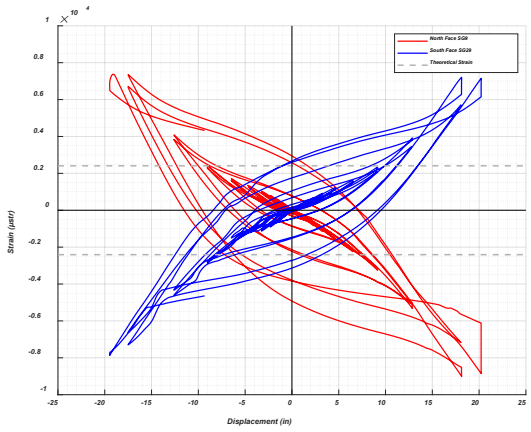

b) SG309 & SG329 at 3D below Grade

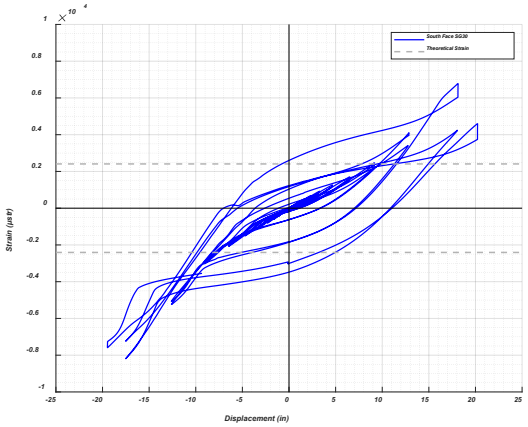

c) SG330 at 3.3D below Grade

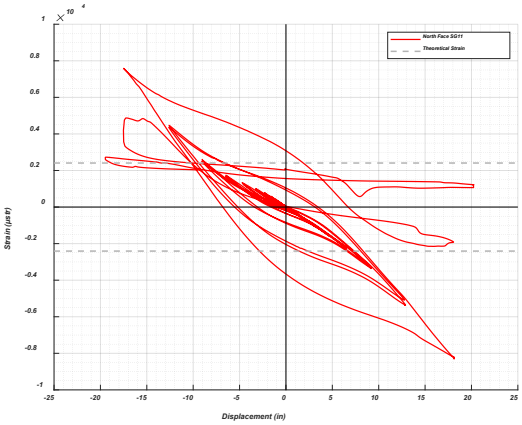

d) SG311 at 3.7D below Grade

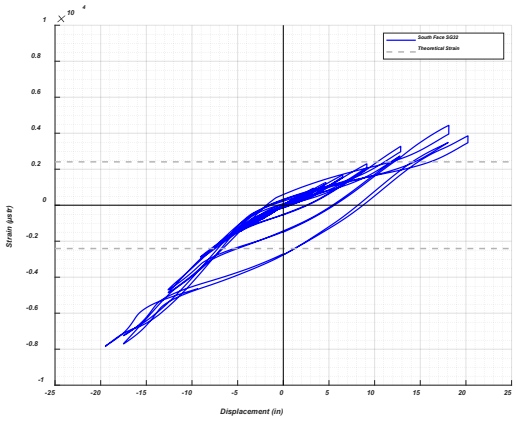

e) SG332 at 4.1D below Grade

Figure 50: Test 3 Strain vs Applied Displacement within Buckled Region

(a) Soil Gapping Field Photo at Large Amplitude Displacements

(b) Final Field Soil Gapping Depth Measurement

Figure 51: Test 3 Near Ground Field Measurements

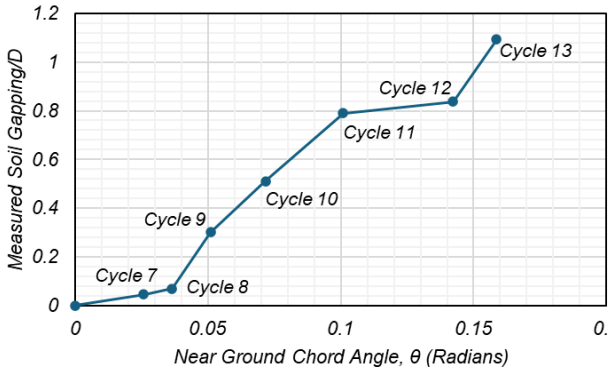

(a) Normalized Soil Gapping Measurements vs Near Ground Chord Angle

Figure 52: Test 3 Near Ground Measurements

9.4 Test 4: Cyclic Response

Test 4 involved a compact pile section, as defined by AISC 360 [4], with a D/t ratio of 34 and a constant applied axial demand approximately 8% of the maximum allowable axial cross-section capacity. As a compact section, it is expected to reach the full yield stress in its compression elements prior to the onset of local buckling; and have significant post-peak performance ductility, typically a rotation capacity greater than three times its yield rotation. As a result, local buckling is expected to initiate well after yielding, allowing the section's ability to sustain significant plastic deformation.

The recorded actuator displacement and force time histories for Test 4 are presented in Figure 53. The test completed 13 full loading cycles before the maximum displacement allowed for the actuator was achieved, as shown in Figure 54.

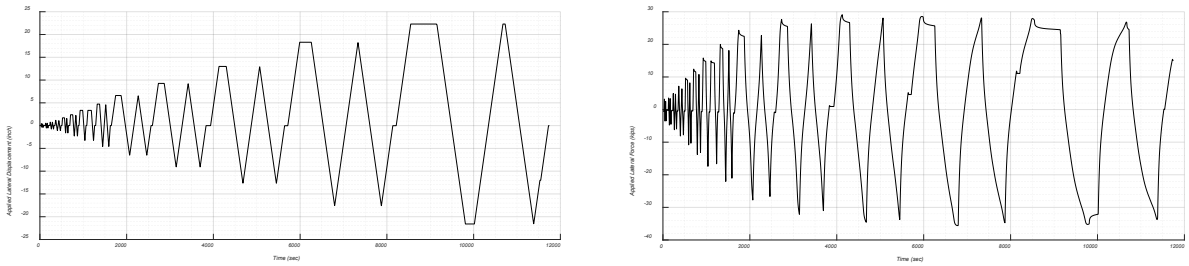

(c) Applied Lateral Displacement *(d) Recorded Actuator Applied Force*

Figure 53: Test 4 Applied Lateral Displacement and Force Time History

Figure 54: Test 4 Maximum Amplitude Displacement

The cyclic force displacement curve, shown in Figure 48(a), was converted to a normalized moment rotation curve shown in Figure 55(b). The y-axis was converted from actuator force to bending moment at estimated plastic hinge location normalized by the

calculated plastic moment of the pile section. The x-axis was converted to chord angle, calculated from the recorded lateral displacement over the depth to estimated plastic hinge. Given no buckling was observed in Test 3, the hinge location was estimated at 3D considering the behavior of previous tests. Refer to Figure 34 for the representative free-body diagram of Test 1 for reference.

The bending moment was determined in the deformed configuration by taking the moments about the observed hinge location of 2.4D, 30.6-in below ground. The free pile height of the lateral loading at zero displacements above ground was measured at 7.67-ft, resulting in an above ground moment arm for the applied lateral load of 10.22-ft. The first yield moment, M_y, is when the extreme fiber of the section reaches yields at 2808 kip-in. The plastic moment, M_p, was calculated as 4074 kip-in. Material properties presented in Table 5 were used in the discrete fiber calculation of the pile capacity considering the P-delta effects induced by the axial load application.

As shown in Figure 55(b), the first yield moment, M_y/M_p, was reached at a rotation of 0.030 prior to reaching the first peak of cycle 9 in the push direction. However, the first yield was achieved in the pull direction in the prior cycle, cycle 8, at a rotation of 0.024. The plastic moment, M_p/M_p, was reached at a chord angle of 0.057 just prior to reaching the first peak amplitude displacement in cycle 10.

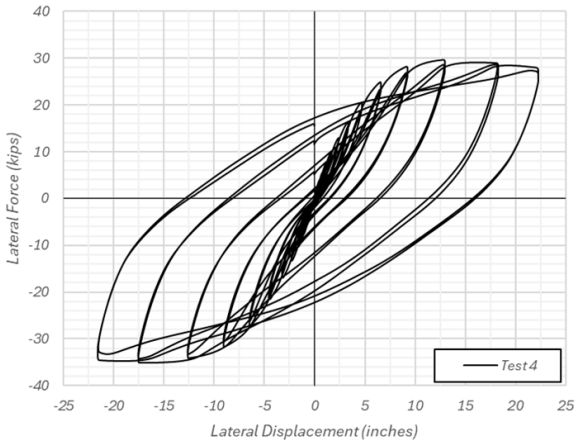

a) Actuator Force-Displacement Curve

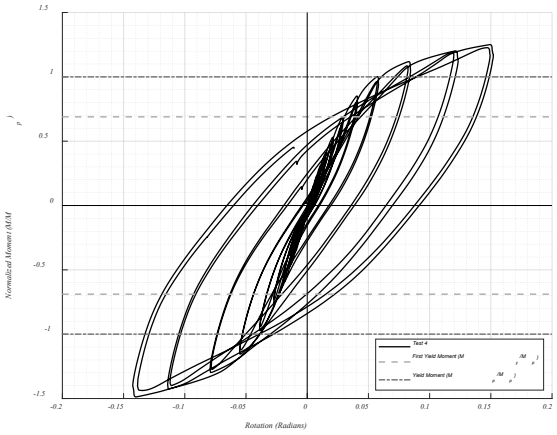

b) Normalized Moment vs. Pile-Rotation Response

Figure 55: Test 4 Hysteretic Response

Recorded Pile Strains

The normalized strain profile for the maximum positive and negative peaks for cycles 1-13 are shown in Figure 56. After evaluation of the recorded strain data, of the 40 strain gauges installed, 30 were determined viable for post-processing. However, only 11 strain gauge pairs (22 strain gauges) at 11 elevations/depths could be compared. The profile

depth is normalized by the pile diameter, and the strains are presented in micro-strains. The strain profile only considers the instrumented pile length and not the entire length of the test pile. The strains shown are the maximum compressive and tensile strains observed in each cycle. Although shown in a single plot for each cycle, maximum strains at different elevations may have peaked at different times within the same cycle. The theoretical yield strain was determined as the $\varepsilon_y = f_y/E_s$, approximately 0.0025. The red "x" shown in the strain profile indicates either the loss of the strain gauge due to damage or the strain recording exceeding the maximum recordable reading per the manufacturer, approximately 10% -15% in the subsequent cycle for that amplitude peak. To eliminate step backs in the profile recording, any strain recorded in a cycle that was lower than the strain in the preceding cycle was interpreted as the maximum peak of the previous cycle. As shown in Figure 56Figure 43, strain gauges SG402, SG405 to SG410 on the south face were either damaged during the test or exceeded the maximum recordable strain as they have "x" occurring in large displacement cycles. The north face also experienced loss of gauges or exceedance of maximum recorded strain at large displacement cycles, losing strain gauges SG421 to SG424, SG426 to SG428, SG431 and SG433.

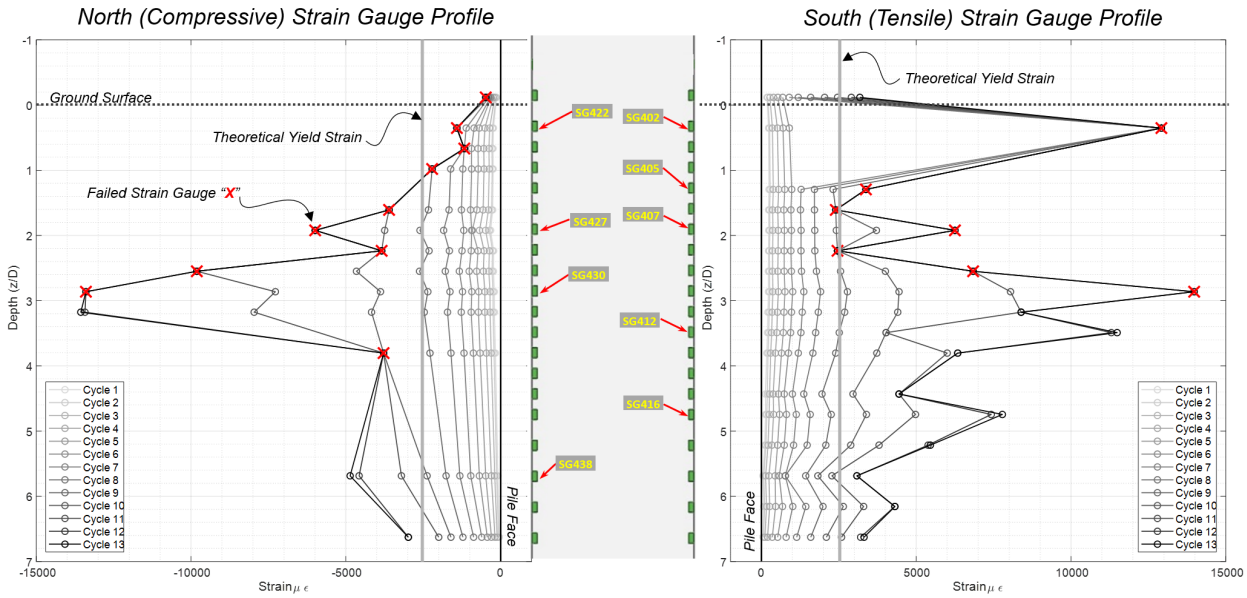

a) *Cycle Peak North Compression and South Tensile vs. Depth Profiles*

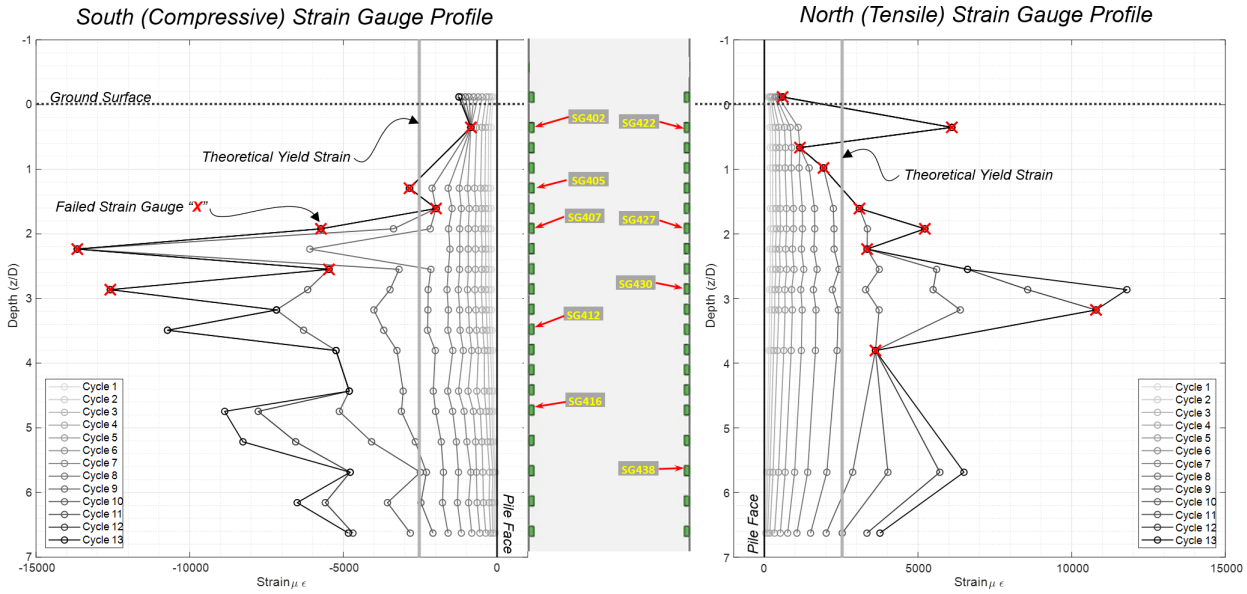

b) *Cycle Peak South Compression and North Tensile* vs. Depth Profiles

Figure 56: Test 4 Maximum Peak Compressive and Tensile Strain vs. Depth Profiles

Observed Buckling

The minor local buckling was observed after the post-test excavation of the soil pit, making the buckle region visible and accessible. The buckled region was observed more as an inundation of the pile exterior and not a complete collapsed buckle, which differed from the buckling observed for the noncompact piles. The buckle region of the pile was extracted and the dirt and debris were removed from the pile using a laser cleaner, refer

to Figure 57(a). The piles were painted light grey and 360-degree photos were taken to produce a 3D point cloud model of the pile using AutoCAD ReCap Photo, refer to Figure 57(b).

The visual buckle was observed on the south face approximately 2.35 pile diameters, 30.5-in, below the ground. This depth location was considered processing of the results. No other buckling was visually observed on the pile.

a) Field Cleaned Elevation *b) Point Cloud Model*

Figure 57: Observed Location of In-Ground Pile Buckling of Test 4

The location of the observed buckle corresponds to the strain behavior illustrated in Figure 56. During large displacement cycles, strain measurements from 1.6D below ground level to the last strain gauge installed at 6.6D exceeded the theoretical yield strain. The highest strain values are recorded by gauges SG408 and SG410 on the south face, as well as SG430 and SG431 on the south face. Note SG410 and SG431 demonstrated remained intake demonstrating complete time histories.

All four strain gauges exceeded recorded strains from the previous tests in larger displacement cycles, potentially indicating the sections notably higher ductility prior to the occurrence of local buckling. The gauges within the observed local buckling region were SG408 on the south face and SG428 on the north face at 2.2D below the ground and SG409 and SG429 at 2.5D below the ground. The maximum recorded absolute strain at this elevation on the south face were 0.326 for SG408 and 0.0065 for SG409. The maximum recorded absolute strain at this elevation on the south face were 0.262 for SG428 and 0.026 for SG429.

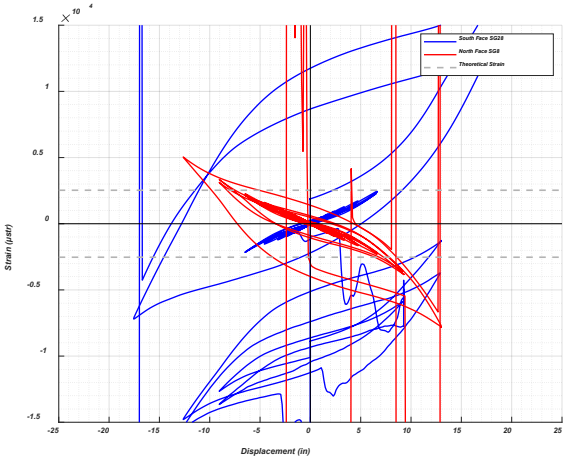

a) *SG408 & SG428 at 2.2D below Grade*

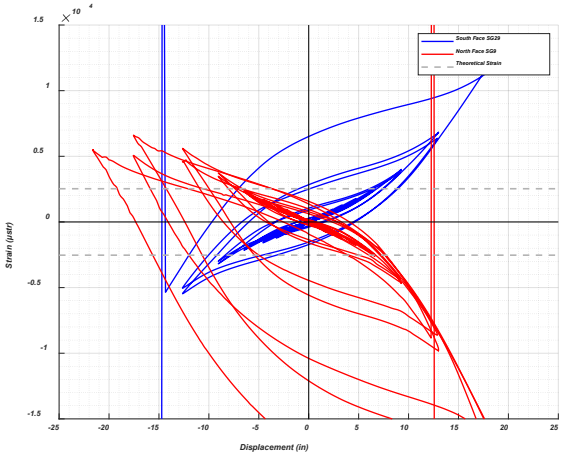

b) *SG409 & SG429 at 2.5D below Grade*

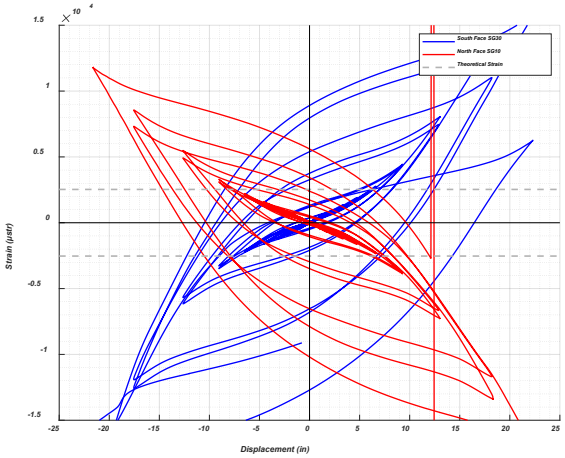

c) *SG410 & SG430 at 2.9D below Grade*

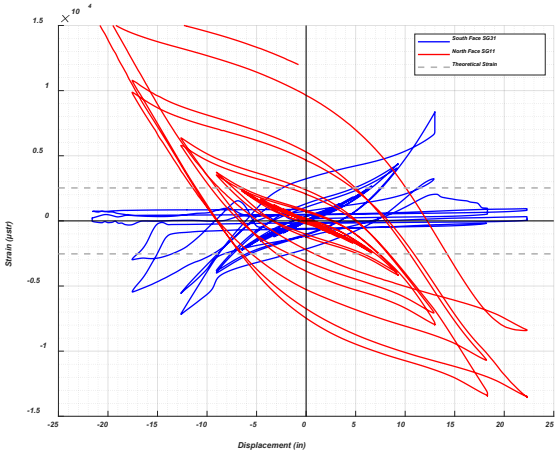

d) *SG411 & SG431 at 3.2D below Grade*

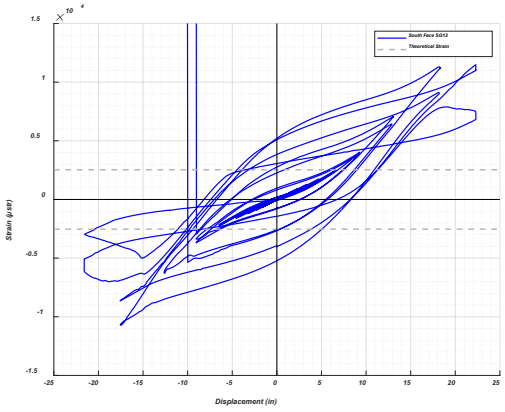

e) *SG412 at 3.5D below Grade*

Figure 58: Test 4 Strain vs Applied Displacement within Buckled Region

Topsoil Gapping

To evaluate the impacts of the surrounding soil in the pile buckling region, the soil gapping at ground surface was visually evaluated for Test 4 using a near ground go-pro. The go-pro was programmed to take a series of photos within the duration of each cycle, capturing the pile displacement and soil heaving at the top of ground. However, in test 4 the Go-Pro only captured the near soil gapping up to seven displacement amplitude cycle. Therefore, no measurements are summarized. However, similar near surface soil gapping and heaving were observed as seen in the previous tests. Figure 59 shows field photos of the soil gapping at the first cycle peak amplitude of cycle 13. Figure 60 shows the near ground rotation measurements recorded by the above-ground inclinometer.

(a) Near Ground Go-Pro Photo Looking West *(b) Looking from above the Concrete Blocks*

Figure 59: Test 4 Field Photos of Soil Gapping at First Peak of Cycle 13

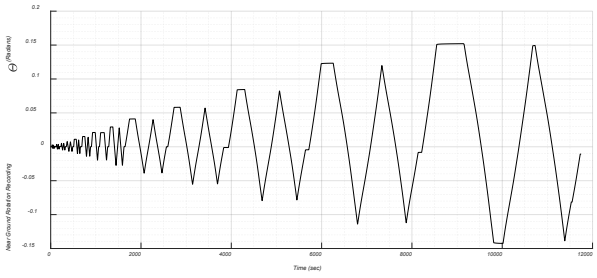

Figure 60: Test 4 Near Ground Rotation Time History Recordings

9.5 Summary

Four steel pipe pile specimens were tested in the North Soil Pit at the ESEC NHERI Testing Facility at UCSD. Each test was subjected to flexural and axial forces induced by a constant axial load and unidirectional cyclic lateral loading. All piles exhibited behavior as expected. Figure 61 shows the first quadrant response envelopes of the hysteretic soil-pile response. The two non-compact piles, Test 1 and Test 2, had limited ductility in the post-peak response. Enabling the soil-pile system to resist the larger amplitude displacements while resisting more than 80% of the peak lateral load. Both piles experienced partial circumferential inward and outward in-ground buckling at multiple elevations. The constant axial loading was maintained given the partial circumferential buckling of the cross-sectional area of the pile. The compact piles, Test 3 and Test 4, demonstrated a more ductile post-peak performance. Failure of the soil-pile system performance, as defined for these tests as the inability to resist at least 80% of the peak lateral force, was not possible due to the constraints of the test set-up. Figure 61 demonstrates both Tests 3 and 4 require high rotations to experience in-ground buckling and component failure.

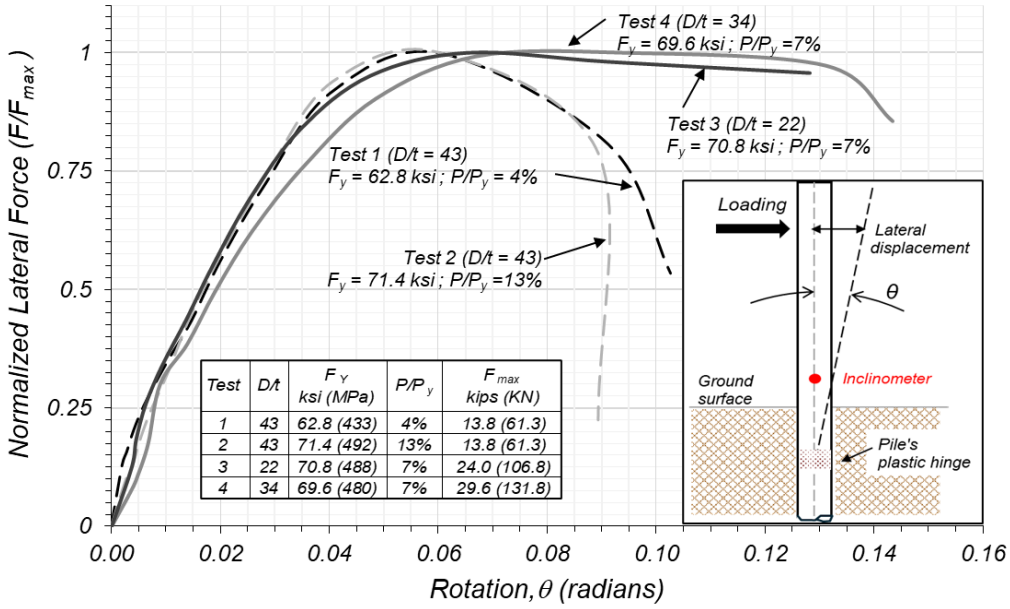

Test	D/t	F_Y ksi (MPa)	P/P_y	F_{max} kips (KN)
1	43	62.8 (433)	4%	13.8 (61.3)
2	43	71.4 (492)	13%	13.8 (61.3)
3	22	70.8 (488)	7%	24.0 (106.8)
4	34	69.6 (480)	7%	29.6 (131.8)

Figure 61: Normalized Lateral Force- Rotation Response Envelopes

Table 9 and Figure 63 compares the in-ground buckling observed in the three of the four tests that had visible buckling. The maximum strains provided in Table 9 are also defined as the critical strains for these tests. These critical strains were obtained from strain gauge time histories near or at the observed buckle elevation before a 20% reduction in lateral load or occurrence of peak strain recording, typically over 0.04. Both compressive and tensile strains are noted alongside their respective cycles. For the tests with visible

buckling, all peak strains occurred in post-yield cycle, typically within the cycle in which peak lateral load was reached. The inground depth of observed buckling showed a pattern for the available data, averaging at 2.5 pile diameters below ground. Axial load was sustained throughout all four tests and may have affected the depth of buckling along with other factors such as material strength.

Table 9: In-Ground Local Buckling Observation Summary

Pile Test	Buckle Depth Below Top of Ground *(where D is pile diameters)*			Strain Gauge	Max Strain Recorded[1] (ε)	Observed Loading Cycle
	Average	North	South			
1 [43]	2.0D	2.5D	1.7D	8	Comp. = 0.0043 Tens. = 0.010	Cycle 10 Cycle 11
2 [43]	2.3D	2.8D	2.2D	27 29	Comp. = 0.0066 Tens. = 0.0074	Cycle 10 Cycle 11
3 [22]	N/A	-	-	-	-	-
4 [34]	2.4D	-	2.4D	8	Comp. = 0.018 Tens. = 0.017	Cycle 10

[1] This is the maximum strain recorded in the time history prior to any outlier spikes indicating buckling or loss of gauge. In some SGs the strain exceeds the gauge capacity implying large unrecordable strains or potential occurrence of buckling. The largest is the first maximum recorded strain in the observed hinge region.

Figure 63 demonstrates were Test 1, 2, and 4 pile critical strains fall in relation to literature findings. Given the lack of internal soil plug in the ground withing the hinge region and the presence of soil gapping, the test performance aligns with the results concluded from in-air tests.

Instrumentation data to determine axial shortening effects, although available, were not included in this report. No noticeable shortening was visually observed. Data processed for Test 1, with the smallest applied axial loading, indicated axial shortening as less than 0.1-in in total even after the soil-pile system could no longer resist 80% of the peak lateral force. This is negligible to overall pile performance and therefore was not further evaluated from the DIC and axial string potentiometers in this report.

(a) Test 1 [D/t = 43] (b) Test 2 [D/t = 43] (c) Test 4 [D/t =34]

Figure 62: Comparison of Observed In-Ground Pile Buckling

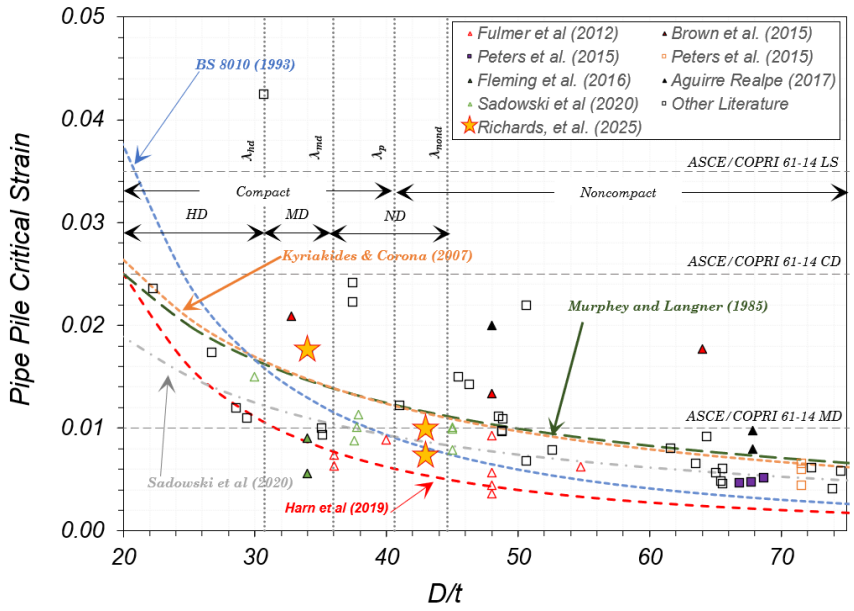

Figure 63: Comparison of Critical Strain *(Recreated Harn et al, 2019)*

10. Finite Element Analysis Validation

A detailed finite element model (FEM), refer to Figure 64, was developed in LS Dyna R9.3.1 (LSTC, 2016) [32] to simulate the pile's behavior under quasi-static lateral cyclic loading and constant vertical loading. The dimensions used to develop the FEM reflect those shown in Figure 7(b). To address the nonlinear nature of soil-pile interaction, an explicit solver was used to overcome convergence difficulties associated with implicit time integration schemes. The finite element model accounted for sources of nonlinearity such as contact, soil and steel plasticity, and large deformations in both the soil and pile (e.g., soil gapping and pipe-wall buckling). Simulation time was expedited through selective mass scaling, while ensuring that kinetic energy remained low relative to internal energy throughout the solution.

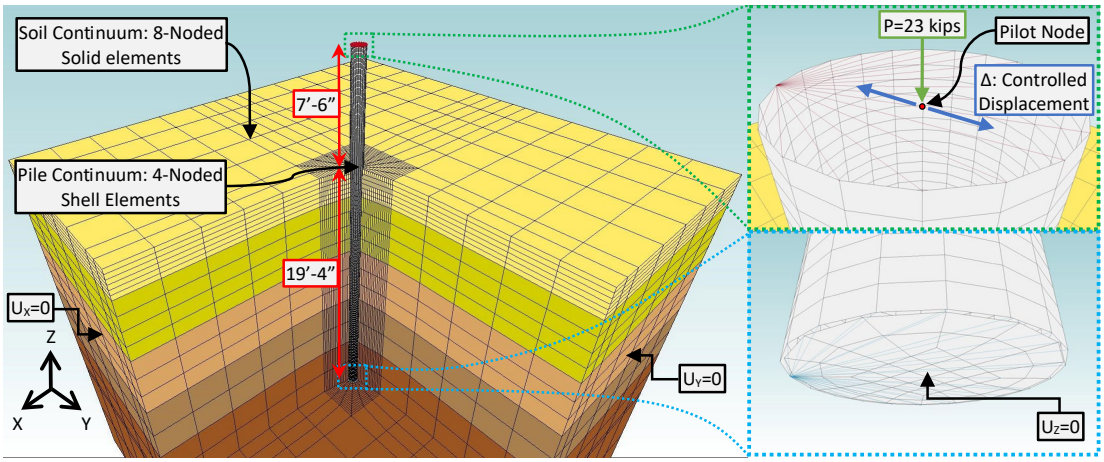

Figure 64: Finite Element Model

Eight-noded solid elements with reduced integration (ELFORM 1) and four-noded shell elements with reduced integration (ELFORM 2) and hourglass control were adopted for representation of the soil and pile continuum, respectively. Shell elements were defined with three integration points through the thickness. The nodes of the shell elements are defined at the mid-plane of the shells with half of the pile wall thickness projecting towards both sides of the shell. Nodes lying on the four sides of the soil block are restrained against motion normal to each side; and translation in all directions is prevented for nodes at the bottom of the block. Vertical translation is restricted for shell nodes at the bottom of the pile. At the top of the pile, a pilot node is defined at the cross-section center and a kinematic constraint is applied to enforce no distortion of the cross-section. The pilot node is used to prescribe the lateral displacement history and apply the vertical load. Nonlinear contact, accounting for Coulomb friction, is defined at the soil-pile interface using the AUTOMATIC_SURFACE_TO_SURFACE definition in LS Dyna. The contact in LS-Dyna is defined by identifying primary and secondary surfaces to which contact segments are defined and associated. The contact segments themselves are defined like shell elements

(e.g. 4-noded primary and secondary nodes) but have no stiffness or property association themselves. Linear springs are defined from the secondary nodes to the primary segment, whose stiffness is dependent on the nodal mass and time step. The contact algorithm searches the master segments for any penetrations by the secondary nodes, and upon detection, the algorithm computes the penetration distance normal to the primary segment. A contact force is applied to the secondary node equal to the product of the spring stiffness and the penetration distance. This contact force is also applied to the primary segment in the opposite direction and distributed to the primary nodes based on iso-parametric shape functions. Furthermore, LS-Dyna computes an effective coefficient of friction, μ_c, using Eq. 5.

$$\mu_c = \mu_d + \left(\mu_{s,\text{soil}-\text{steel}} - \mu_d\right)e^{-DC|v_{rel}|} \quad (5)$$

It should be noted that due to negligible relative velocities, v_{rel}, between the soil and pile (v_{rel} approximately 0), the definition of the coefficients of dynamic friction (μ_d) and exponential decay (DC) are redundant; however, the coefficient of static friction, $\mu_{s,soil\text{-}steel}$, is defined in Table 10 along with other LS-Dyna inputs required to model the soil material behavior.

Table 10: Soil model constants and coefficients of static friction

Simulation	Depth Range [ft]	γ [lb/ft^3]	ν	K_{LS}	Φ [°]	C [psf]	ψ [°]	$\mu_{s,soil\text{-}steel}$
Sim. 1	0-2	130	0.3	0.8	50	100	17	0.25
	2-20	120	0.35	0.8	38	1500	0	0.25
	20-30	135	0.3	0.8	45	100	12	0.25
Sim. BE	0-20	125	0.35	0.8	37	200	4	0.25
	20-25	135	0.3	0.8	42	100	9	0.25

The soil and steel material behavior are modeled with the Drucker-Prager (MAT-193) and Chaboche (Chaboche, 1986) [17] (MAT-153), constitutive models, respectively. For the first simulation, Sim. 1, Geotechnical Engineering practitioners at EMI used the CPT data from September 2022 to estimate the secant shear modulus, friction angle, and cohesion profiles shown in Figure 66(a)-(c) and the tabulated material model parameters corresponding to Sim.1 in Table 3, according to the recommended approaches discussed in (Bolton 1986) [13] and (Brandenberg et al. 2010) [14]. Furthermore, Table 10 summarizes the depth-varying parameters unit weight (γ), Poisson's ratio (ν), shape factor (K_{LS}), friction angle (φ), cohesion (C), dilation angle (ψ), and $\mu_{s,soil\text{-}steel}$ for input into MAT-193. It should be noted that for Sim. 1, the parameters used correspond to upper

estimates, and the secant shear modulus for the top two feet of soil (upper layer) were additionally reduced by a factor of 0.5 based on engineering judgement.

Following the April 2024 CPT campaign, soil data was made available. In response, EMI updated the secant shear modulus, friction angle, and cohesion profiles to their best estimate (BE) as shown in Figure 66(a)-(c). Consequently, an additional simulation using the BE parameters was performed (Sim. BE) to evaluate the effects that the updated soil model parameters have on the force-displacement response and buckling mode.

The steel was modeled using nonlinear kinematic hardening by superimposing three nonlinear backstresses described by the parameters in Table 11 and illustrated by the simulated cyclic engineering stress-strain response shown in Figure 67(a).

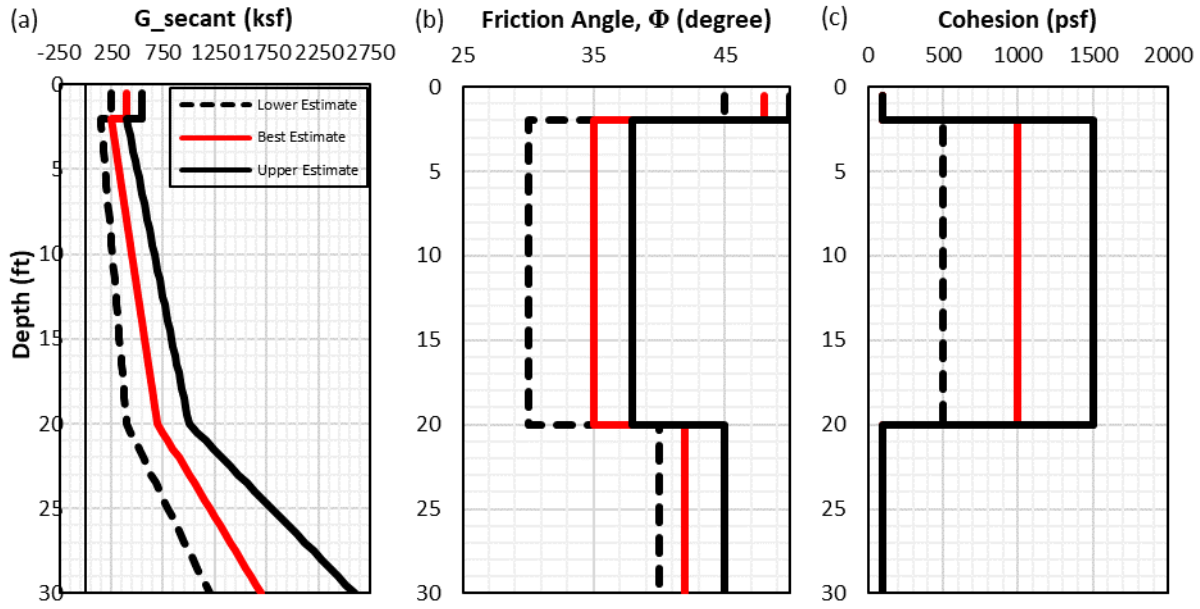

Figure 65: Profiles for (a) secant shear, (b) friction angle and (c) cohesion used in Sim. 1 (Prepared by EMI)

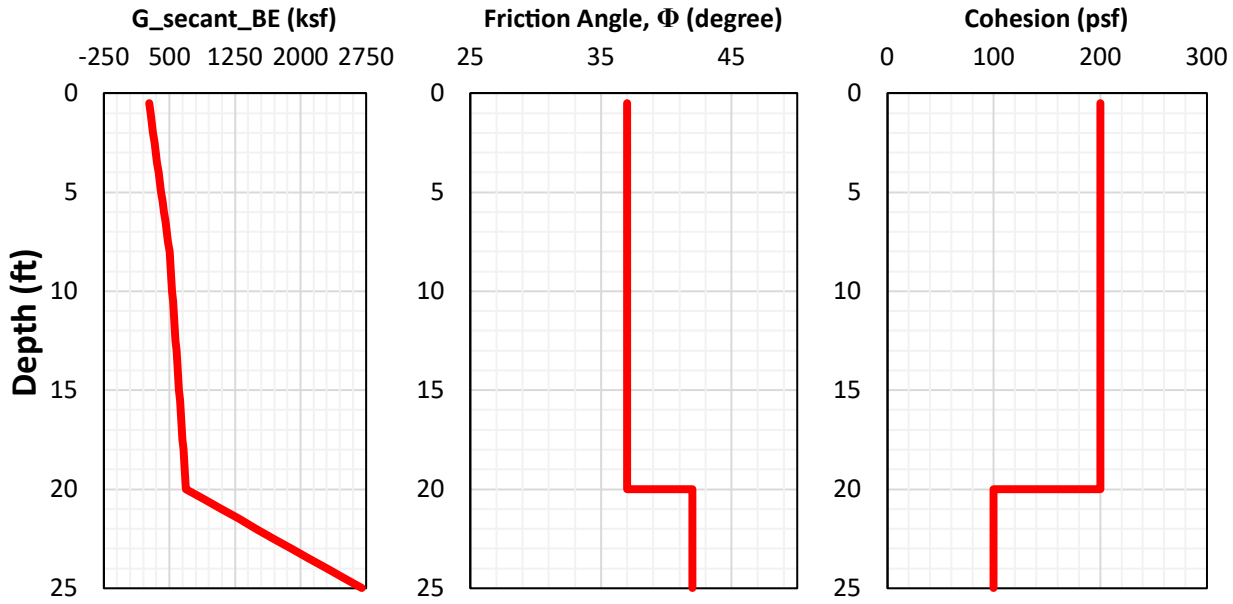

Figure 66: Profiles for (a) secant shear, (b) friction angle, (c) cohesion used in Sim. BE (prepared by EMI)

Table 11: Chaboche constitutive model parameters for steel pile

Physical properties		Elastic constants				Kinematic hardening					
γ [lb/ft^3]		ν	E [ksi]	σ_o [ksi]		C_1 [ksi]	γ_1	C_2 [ksi]	γ_2	C_3 [ksi]	γ_3
503		0.3	29153	42		27412	3525	12618	763	2451	394

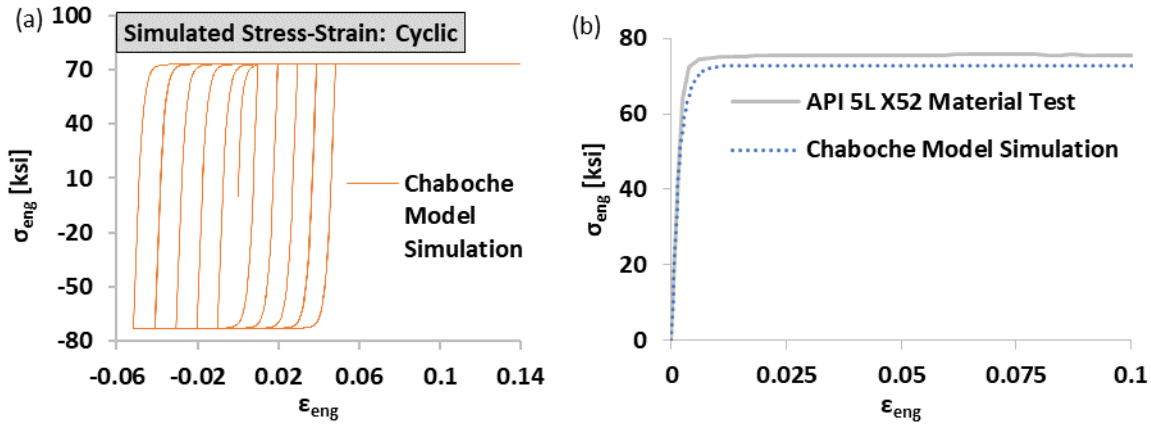

Figure 67: Steel engineering stress-strain response: (a) simulated cyclic and (b) tensile test-simulation comparison.

Residual stresses and initial imperfections in pile are not modeled; nor is the skin friction developed from driving, inertial forces, or ERW weld material and geometry. The soil is

represented as continuum rather than discrete particles, which is representative of a cohesive continuum, or soil having some degree of cohesion. The soil parameters were obtained from CPT rather than from direct testing, and the CPT was conducted prior to excavation and instrumentation repair. Hence, the FEM assumes that the excavation's disturbance did not affect the soil properties. Additionally, the geometry of top hat loading apparatus is not directly accounted for to simplify the modeling and the boundary condition as illustrated by the pilot node in Figure 67.

The detailed FEM quantifies key metrics of in-ground hinge behavior which are hard to measure experimentally. Metrics include critical strains (ε_{cr}), depth of plastic hinge (D_{ph}), and in-ground plastic hinge responses like moment and plastic rotations.

The marine structures engineering community has yet to agree on what constitutes ε_{cr} or how to quantify it experimentally. Sadowski et al. 2020) [41] conducted 3-point cyclic bending tests on hollow steel tubes to idealized expressions for curvature evaluated at the buckling moment while also using DIC data to fit a polynomial curve describing the displacement field and taking the second derivative of this curve to determine curvature as an alternative method. These curvatures were used to determine strains based on plane sections theory. Fulmer et al. (2012) [26] and Brown et al. (2015) [15] studied 4-point bending performance, determining ε_{cr} with Optotrak LED instrumentation. This instrumentation was used to compute strains through displacements and identify the instance the pipes violated plane sections theory. The value of ε_{cr} was taken as the largest tensile strain achieved prior to this violation; however, Fulmer et al. (2012) [26] used the Optotrak grid nearest to the buckling location to evaluate ε_{cr}, while Brown et al. (2015) [15] averaged the strains determined by all Optotrak grids in the constant moment region. Winkel et al. (2017) [47] also studied the effects of sand infill on the 4-bending performance of steel tubes but used a 10% drop in bending moment to characterize the instance of buckling and used the measured jack elongation to quantify ε_{cr}. Regardless, in all investigations ε_{cr} is commonly associated with the onset of pipe wall buckling.

In this report, the FE analysis is used to calculate ε_{cr} for the cyclically loaded pile. The ε_{cr} obtained from the FE analysis is defined as the maximum compressive strain sustained by a shell element in the valley of the buckled region prior to the onset of buckling. Furthermore, the onset of buckling is identified as an instance prior to bifurcation of the inner, mid-plane, and outer integration points' longitudinal strains; this procedure is presented in Figure 68(a). The depth to plastic hinge, D_{ph}, is taken as the elevation difference between the undisturbed upper soil surface and an averaged location of the buckles occurring on either side of the pile as illustrated in Figure 68(b).

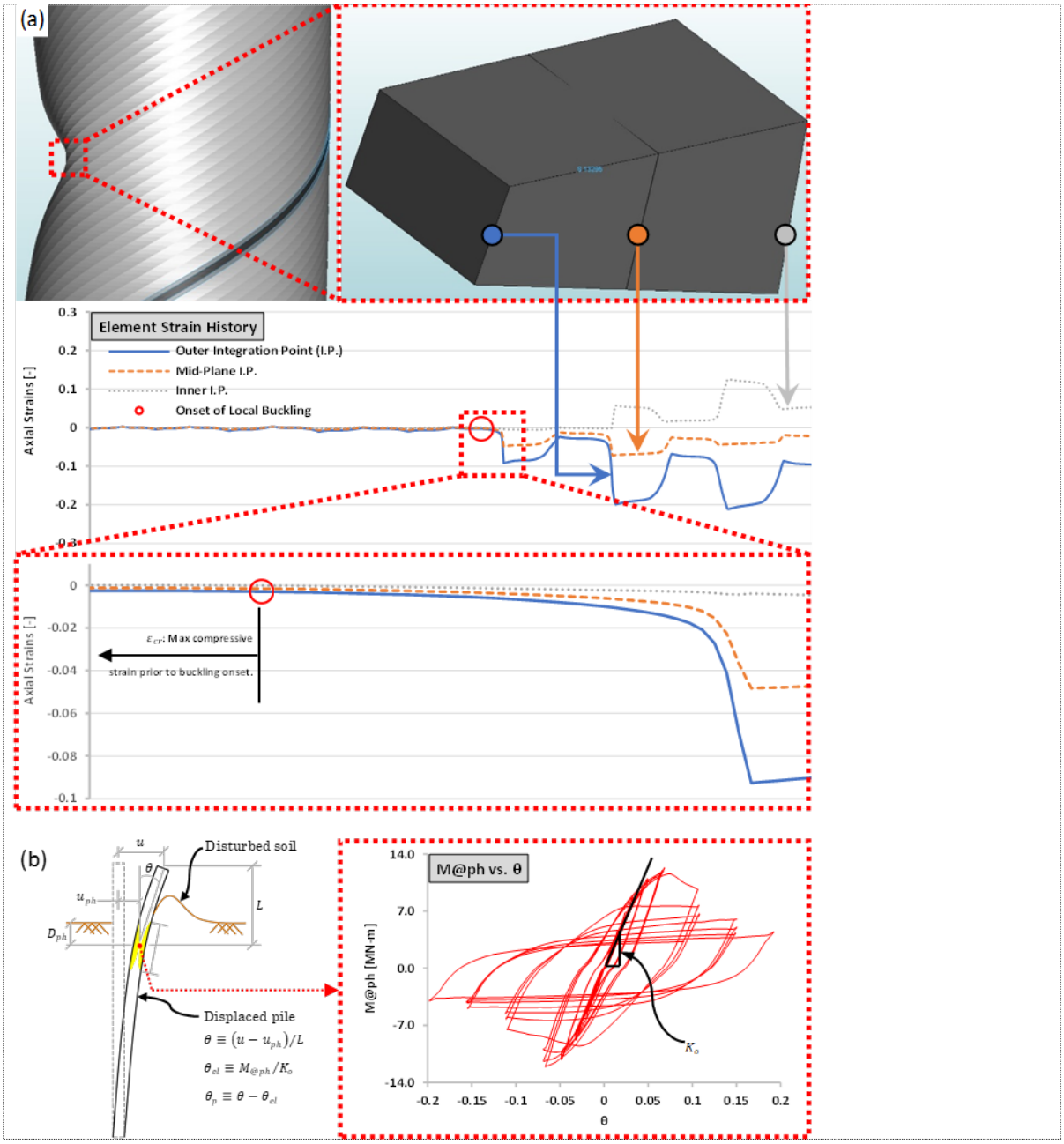

Figure 68: Definition of (a) ε_{cr} and (b) D_{ph} and θ_p

10.2 FEA Validation

The model was subjected to the loading protocol applied in the experiment with a slight modification. The experiment was initiated with an approximate preexisting lateral load of 4 kips and an unverified displacement; as such, an effective mean displacement of 1.25 inches was approximated by using the initial stiffness to extrapolate the point on the experimental force-displacement response, corresponding to zero displacement and 4-kip loading, towards a zero-loading condition; and subsequently increased to 1.75 inches.

The numerical displacement protocol was obtained by shifting the experimental loading protocol in the positive direction by the mean displacement of 1.75 inches, see Figure 69.

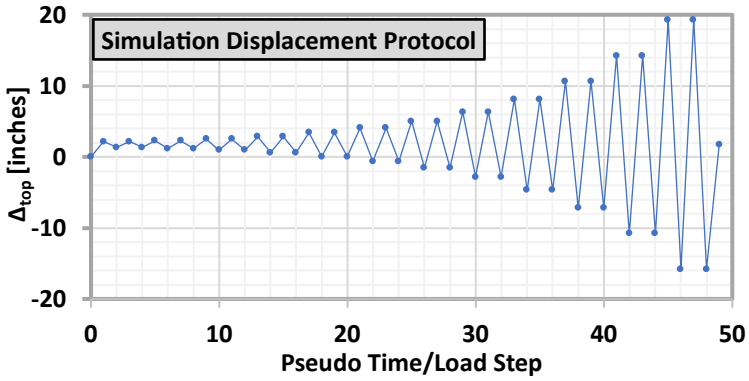

Figure 69: Simulation Displacement Protocol

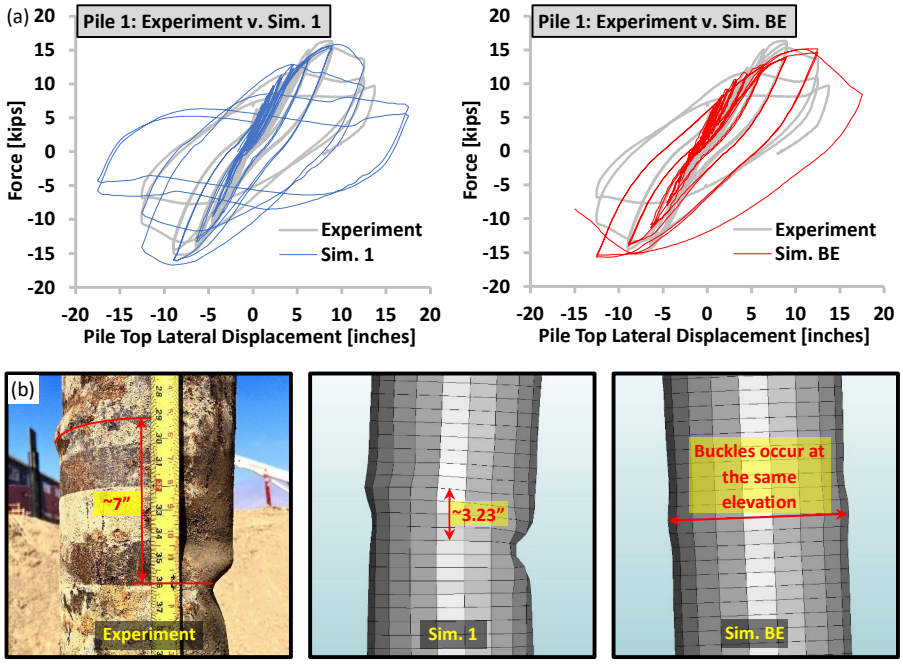

Figure 70: Comparison Between Experimental and Simulated (a) Hysteretic Force-Displacement Responses and (b) Local Buckling

Figure 70(a) compares the experimental and simulated force-displacement responses and Figure 70(b) compares the local buckling of the pile and suggests that the FEM results for Sim. 1 are in better agreement with the experimental observations than Sim. BE. Sim. 1 captures the force-displacement response better than Sim. BE since the force values at peak displacements more closely resemble those observed in the cyclic experiment. Moreover, Sim. 1 more accurately captures the instance of buckling, which

is marked by the cycle at which strength degradation initiates for both push and pull directions. The pile's strength in Sim. BE does not degrade until an entire cycle set after the one observed in the experiment. For clarity, the hysteretic responses are decomposed into the twelve cycle sets.

Figure 70(b) illustrates the comparison of the buckling modes between the experiment and both simulations. The local buckling in Sim. 1 is qualitatively representative of what is observed in the experiment: both showing an outward buckle on the South side at a higher elevation and an inward buckle on the North side at a lower elevation. It is noted, however, that the vertical distance between the North and South buckles differs for the experiment and Sim. 1 as shown. Sim. BE, on the other hand, exhibits outward buckles on both the South and North sides of the pile at the same elevation. Although the soil parameters used in Sim. BE were obtained from soil testing conducted closer in date to the cyclic experiment, they were conducted after the experiment was performed therefore potentially introducing inconsistencies due to the heavily disturbed nature of the soil surrounding the pile. Hence, Sim. 1 is selected to further study the pile responses in the following discussions.

Although the experiment was stopped prematurely when the specimen experienced considerable post peak strength degradation, the Sim. 1 was allowed to complete the 12^{th} cycle set. Additionally, the simulated pile buckled at nearly the same instances for both the push and pull directions and the simulated location of the plastic hinge is approximately 24 inches below the soil surface, which is approximately 1.5 inches smaller than the average buckle depth for the test (i.e. 22 inches). However, in the pull (South) loading direction, the simulation slightly overpredicts the strength of the soil-pile system. This inconsistency may be attributed to the offset in the simulated loading protocol in Figure 69. Also, observation of the experimental hysteresis shows that towards the end of the 12.5-inch amplitude cycles, an increase in lateral force is exhibited, which may potentially be due to the slight loss of axial load that occurred when the concrete blocks encountered the soil during these large displacement cycles; this slight loss of axial load was not modeled.

The strain profiles for the first positive peaks and the first negative peaks are presented in Figure 71 and Figure 72, respectively. Parts (a) and (b) for these figures correspond to observations of the North and South strains, respectively. For clarity, these figures are separated into three plots each containing cycle sets 1-4, 5-8, and 9-11 corresponding to the first, second, and third plots. In the experiment, the strain gauges on the North and South sides of the pile were instrumented at a 30° offset from the axis of lateral loading. However, to maintain reasonable simulation times for the FEM, the mesh was refined such that the nearest set of element integration points corresponded to a 36° offset. For this same reason, the mesh refinement along the pile does not allow for strain observations at the same elevations along the instrumented pile.

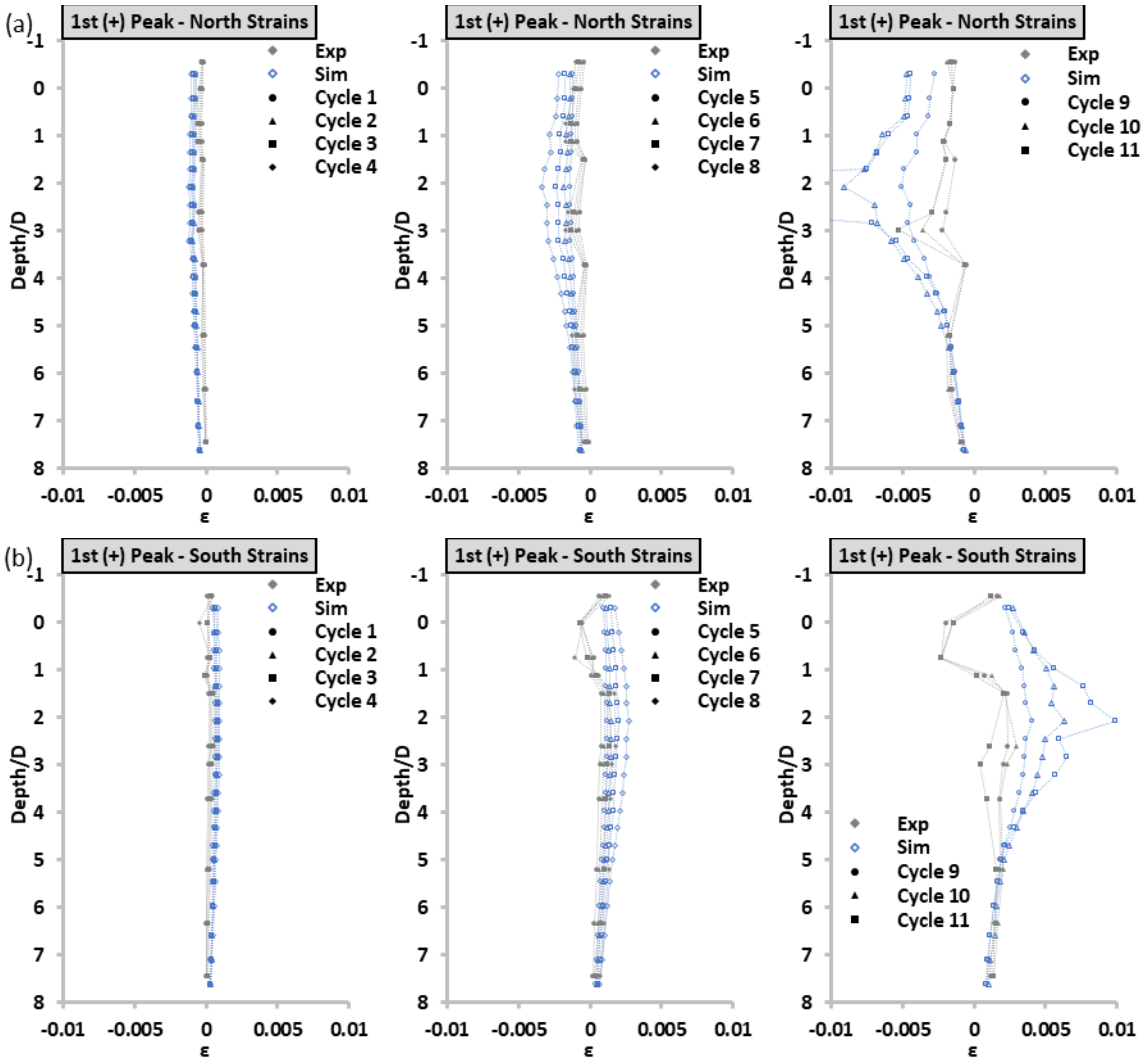

Figure 71: Strain profiles at first positive (North) peaks in cycle sets.

In general, the simulation tends to overpredict the strain profiles in the vicinity of the buckled region; this is particularly pronounced for the larger displacement cycles (e.g. cycle sets 9, 10, and 11). The strains at locations farther away from the region of buckling are better predicted. For the north strain profiles at the first negative peaks of the lower cycles (e.g. cycle sets 1-4) in Figure 72(a), the simulation registers compressive (negative) strains; initially this seems counterintuitive as the fibers on the North side of the pile would ideally be in tension when the specimen is pulled towards the South. However, this observation in the FEM is consistent when considering the adjustment made to the simulation's loading protocol previously discussed. For example, the mean displacement in the loading protocol results in compressive strains on the North side of the pile for cycles at small displacement amplitudes. Furthermore, the strain profiles on both the North and South sides of the piles appear to be better estimated for the negative peak displacements. It should be noted that some of the strain gauges in the vicinity of

local buckling suffered failure prior to achieving the large displacement cycle sets (e.g. Cycles 9-11), so the experimental strain data shown in Figure 71 and Figure 72 may not accurately reflect the actual strains in this region at these cycles.

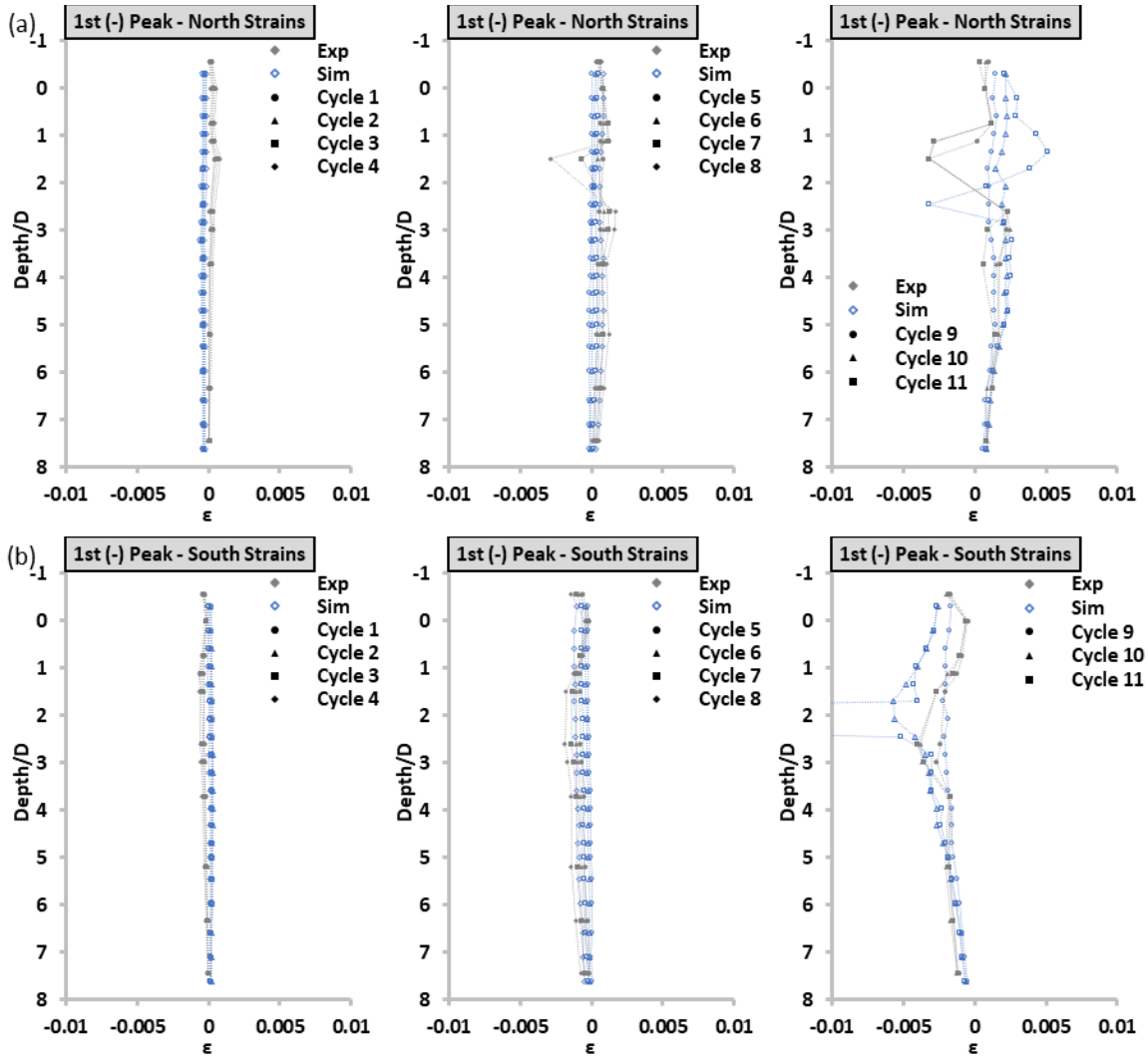

Figure 72: Strain profiles at first negative (South) peaks in cycle sets.

10.3 FEA Results and Discussion

In the previous section, the FEM is shown to reasonably estimate the pile's local and global responses. This section focuses on evaluating, and placing into perspective, the pile's performance in regard to the metrics described in ε_{cr}, D_{ph}, and θ_p. Harn et al. 2019 surveyed the literature on primarily in-air bending performance of steel pipes in the absence of axial load to compile data on ε_{cr} and plotted the values as a function of D/t. The study revealed that ε_{cr} generally decreases as D/t increases and that pipes undergoing cyclic bending tend to buckle at lower strains than pipes under simple monotonic bending tests. A similar effect is generally observed when comparing hollow to

filled pipes (e.g. concrete or sand filled pipes). Nevertheless, the study highlighted that only a few monotonic in-air bending tests can achieve the life safety (LS) strain limit stipulated in (ASCE/COPRI 61-14). This questions the validity of the strain limit and raises concerns about whether port structures designed under the current governing design standard lack conservativeness.

To address some of the drawbacks and inconsistencies of ε_{cr} quantification, the authors conducted a parametric study, (Suarez et al. 2024), which aimed to numerically investigate performance metrics associated with component-level capacity design metrics of steel pipe piles, such as ε_{cr} and D_{ph}, under realistic loading and boundary conditions of steel pipe piles using the model presented in Figure 73. The parametric study results reiterated here are for piles in an idealized dense sand profile. The findings underscore the insensitivity of ε_{cr} to axial load and the over-conservative limit that the metric imposes on piles' ductility. The simulated pile's performance is also evaluated and discussed in light of the parametric study findings. All simulated results presented here are quantified with the procedures described in Figure 68. Figure 73(a) plots the ε_{cr} as a function of D/t. The horizontal lines are strain limits tabulated in the ASCE/COPRI 61-14, and the curves are evaluations of ε_{cr} functions of D/t proposed by Kyriakides and Corona 2007), Harn et al. 2019), and Sadowski et al. 2020). The gray markers are a recreation of the survey presented in Harn et al. 2019. The blue round markers pertain to the parametric study results presented in Suarez et al. 2024 and the red crossed marker represents the results for the simulation of the pile presented herein. The figure suggests that the simulated ε_{cr} from the parametric study (blue solid circular markers) are comparable to pipe bending experiments from literature. Furthermore, it is noted that the ε_{cr} of 0.0105 for the simulated pile under consideration (i.e., the ESEC test, D/t=43) also falls in good agreement with the predicted and experimentally observed values of ε_{cr}. However, both experimentally and numerically observed ε_{cr} exhibit a significant degree of scatter with respect to D/t and reinforce the notion that code-stipulated LS strain limit is, generally, unachievable by pipes with D/t ratios commonly used to support marine structures. However, in Figure 73(a) the ESEC test is the only one subjected to axial load. Figure 73(b) places the pile's ε_{cr} in comparison with that of piles from the parametric study of D/t=48 and varying axial load (P/P_y). Again, it is emphasized that ε_{cr} is insensitive to the presence of axial load.

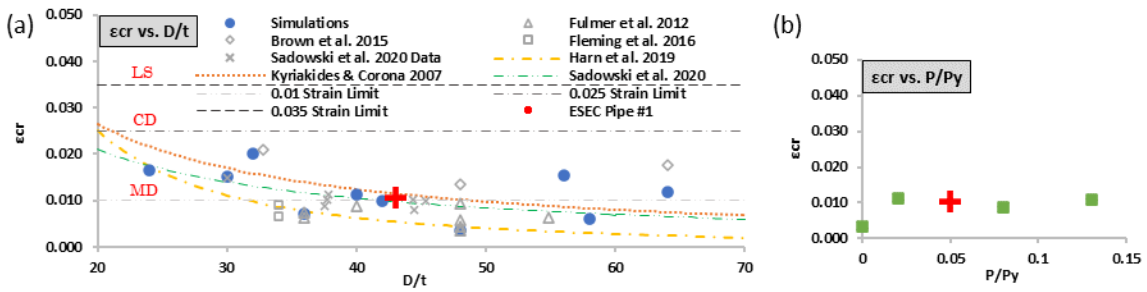

Figure 73: Critical strains, ε_{cr} versus (a) D/t and (b) P/P_y

The depth of plastic hinge, D_{ph}, results are presented in Figure 43. Figure 43(a) varies the D/t ratio while Figure 43(b) varies the axial load ratio, P/P_y. The pile's simulated D_{ph} appears to slightly overpredict what past simulations have estimated. However, it should be noted that not all parameters are consistent between the tested pile simulation and the piles studied in the parametric study. For example, the above ground length to diameter ratio (L_a/D) is larger for this cyclic test specimen than for the parametric study. Furthermore, the soil secant shear modulus and parameters are also not the same. For Figure 43(b), the green square markers pertain to a pile with D/t ratio of 48 rather than 43, for which a larger D_{ph} should be expected based on the trend of Figure 43(a).

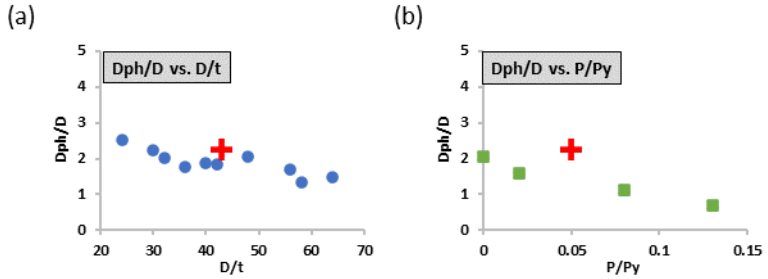

Figure 74: Depth of plastic hinge, D_{ph} versus (a) D/t and (b) P/P_y

The procedure in Figure 68(b) is used to develop the normalized moment-plastic rotation response of the simulated pile and presented in , where the moment is normalized by the expected plastic moment ($M_{pe}=F_{y,0.2\%}Z$). It is important to note that the ESEC test pile (D/t=43) would be considered non-compact according to AISC 360-16 [4] Table B4.1(b) case 20; hence the design flexural strength according to AISC 360-16 [4] would not be M_p, but instead M_n (AISC 360-16 [4] Eq. F8.2), see Eq. 5:

$$(\text{Eq. } 5): M_n = \left(\frac{0.021E}{\left(\frac{D}{t}\right)} + F_y\right)S$$

Where E, F_y, and S are the Young's modulus, nominal yield strength, and section modulus of the steel pile, respectively. Despite the ESEC pile being considered non-compact

according to AISC 360-16 [4], the simulated pile results shown in Figure 75 achieved full theoretical plastic moment.

The horizontal lines in Figure 75 show where 80% of the peak response lies in both the positive and negative lateral loading direction. The pairs of vertical lines represent the range of plastic rotations achieved by four different criteria subsequently described. For criteria 1 (yellow dashed double-dotted lines), the ε_{cr} is determined by the equation proposed by Harn et al. 2019 [29] ($\varepsilon_{cr} = 10(D/t)^2$) and for criteria 2 (black dashed dotted lines) the ε_{cr} is determined following the procedure described previously. In summary, the plastic rotation ranges for criteria 1 and 2 are those successfully completed prior to achieving said ε_{cr} values, and by virtue of this, reflect the ductility predicted by strain-based failure criteria. The figure suggests that imposing ε_{cr}, by either Harn's [29] recommended equation or the procedure proposed here, is rather conservative and would not allow designers to leverage available ductility of the pile. Criteria 3 (green dashed lines) defines the plastic rotation ranges associated with the peak responses in both directions. Evaluation under this criterion considerably increases the plastic rotation ranges that may be utilized in design. Criteria 4 (red dotted lines) correspond to the plastic rotations associated with a 20% post-peak strength degradation of the backbone curve and inspired by the criteria used to qualify special moment frame (SMF) beam-column connections (AISC 341-16 [3]). Since both steel pipe piles and SMF connections dissipate seismic-induced energy primarily through flexural yielding of members in bending, a similar approach is adopted to study the post-peak performance of the steel piles. Figure 75 shows that a drastic increase in plastic rotation ranges is achieved when capitalizing on the post-peak response of the pile. Plastic rotation capacities, θ_{pc}, are subsequently defined as half of the plastic rotation ranges in Figure 75. The strain-based capacity criteria significantly limits θ_{pc} of steel pipe piles to 0.0098 radians (criterion 1) and 0.016 radians (criterion 2), whereas criterion 3 results in θ_{pc} of 0.034 radians and criterion 4 results in θ_{pc} of 0.079 radians.

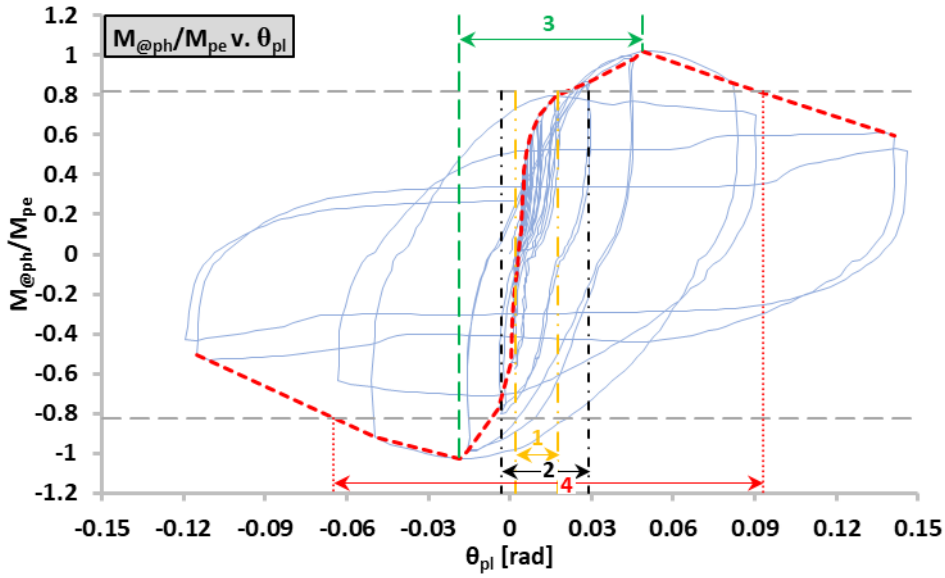

Figure 75: Normalized moment-plastic rotation response

11. Blind Prediction

A blind prediction contest organized by Pacific Earthquake Engineering Research (PEER) Center welcomed practitioners and academics to compete in two analysis categories, limited and comprehensive, in the evaluation of key response for Test 2. The intent of the contest was to evaluate the influence of engineer judgment on the modeling outcomes in the predicted performance of the in-ground hinge behavior. Detailed information regarding the test set-up, steel material properties, soil boring logs, cone penetration test results, soil laboratory testing, and axial and lateral loading were provided. Appendix C provides all distributed documentation for the contestants.

Eight contestants participated in the contest, each using a different analysis approach and software. The two categories allowed contestants to either use a simplified analysis approach (limited) or capture the full cyclic response and predict the dynamic response (comprehensive). Six of the contestants modeled the soil using p-y springs or similar, which is common practice in Port design. Two contestants modeled the soil as a continuum, participating in the Comprehensive Analysis category.

The categories of the blind prediction were as follows:

- Comprehensive Analysis: This category recommended practitioners and researchers intending to model the test specimens and test setup to capture the full cyclic response of the test specimens and to predict overall and dynamic response parameters.

  For the two contestants that participated in the comprehensive analysis, it was required of them to complete three sections:

  - Free Vibration Validation
  - Cyclic Response Validation
  - Hysteretic Energy Validation

- Limited Analysis: This category recommended practitioners and researchers intending to use simple computational models to capture the main response parameters.

  For the six contestants that participated in the limited analysis, it was required of them to complete one section, the validation of the cyclic response.

This section summarizes the results received from the contestants and compared against the Test 2 results. The test lateral loading protocol provided differs slightly from that shown in Figure 26. The recorded actuator displacement was provided, divided into small displacements and large displacements as shown in Figure 76.

Table 12: Blind Prediction Contestant Summary

#	BP Entry	BP Category	Program Used	Comments
1	BPC 2	Limited	Plaxis 3D Monopile Designer	API Sand model
2	BPC 3	Limited	SAP2000	P-Y Spring Model
3	BPC 4	Limited	Ensoft LPile v2022.12.12	Static pushover targeted to sub-cycle peak displacement
4	BPC 5	Comprehensive	FLAC3D	Soil Continuum
5	BPC 7	Limited	OpenSees	Beam on Nonlinear Winkler Foundation
6	BPC 8	Comprehensive	OpenSeesPy	P-Y Spring Model
7	BPC 10	Limited	Oasys Alp	P-Y Spring Model
8	BPC 11	Limited	NVShaft (UNV Reno)	P-Y Analysis Model

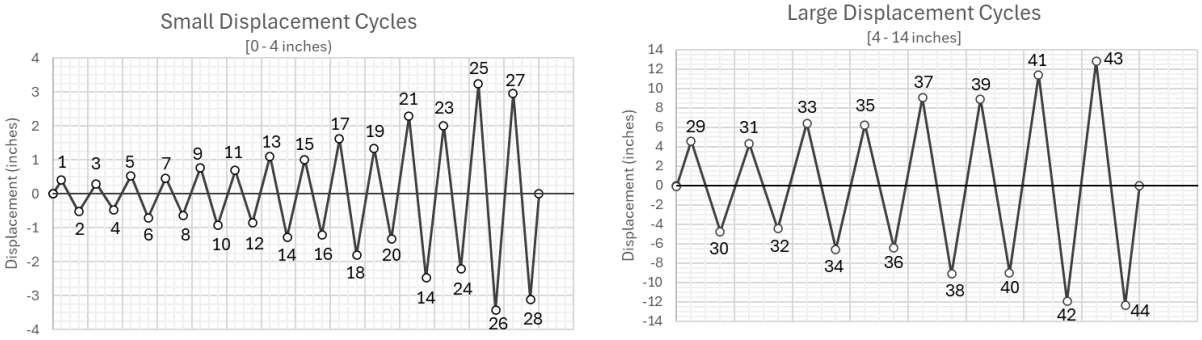

(a) Small Displacement up to Semi-Cycle 28 *(b) Large Displacement from Semi-Cycle 29 to 44*

Figure 76: Test 2 Recorded Actuator Lateral Displacements

11.1 Free Vibration Validation – Comprehensive Analysis

As Test 1 and Test 2 had similar cross-sectional geometric properties, contestants were asked to use the provided information of Test 2 to determine the dynamic response of Test 1 pile specimen. The elastic modulus determined from the material tests, Table 5, shows a 5% difference from the two tests, thus the anticipated dynamic response can be assumed similar. The maximum displacement of 0.260-inches from Level 4 Test 12 of the Test 1 dynamic tire test was provided for the contestants to apply at the top of the pile. The axial Load Apparatus mass was provided, and the contestants were required to determine the fundamental period of free vibration and the effective viscous damping ratio.

Figure 77 displays the displacement decay of the free vibration response. Figure 78 displays the determined fundamental period and viscous damping ratio. Although, Contestant 8 overdetermined the effective viscous damping ratio, of the two contestants the displacement decay and fundamental period was more accurately estimated.

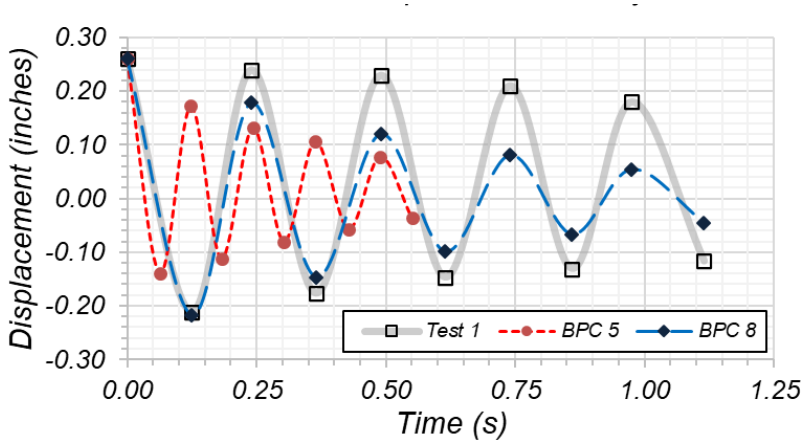

Figure 77: Free Vibration Validation – Displacement Decay

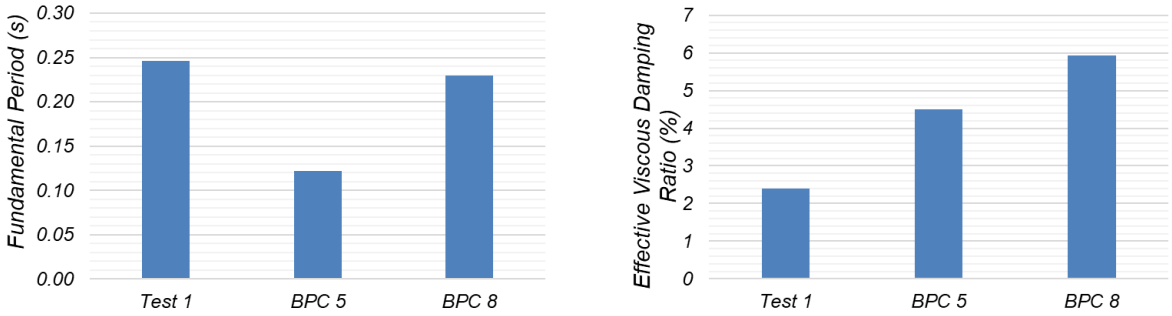

(a) Fundamental Period *(b) Effective Viscous Damping*

Figure 78: Free Vibration Validation – Fundamental Period & Viscous Damping Ratio

11.2 Cyclic Response Validation – Limited & Comprehensive Analysis

All eight contestants participated in the Cyclic Response Validation. Each contestant filled a predefined table based on the results of their simple or comprehensive analysis. A graphical demonstration of the cyclic response was developed of Test 2 per their respective analysis. Figure 79 displays the response envelopes of the eight contestants against that of Test 2. Figure 80(a) and (b) displays the peak lateral force and calculated moment of each response compared to that seen in Test 2. Half of the responses overpredicted performance, and some failed to conduct a simple quality assurance check that the lateral force could not exceed the upper bound given by the pile section plastic moment divided by the pile's length above the ground. Only two responses, Contestant 4 and Contestant 8, were determined to be acceptable despite underprediction.

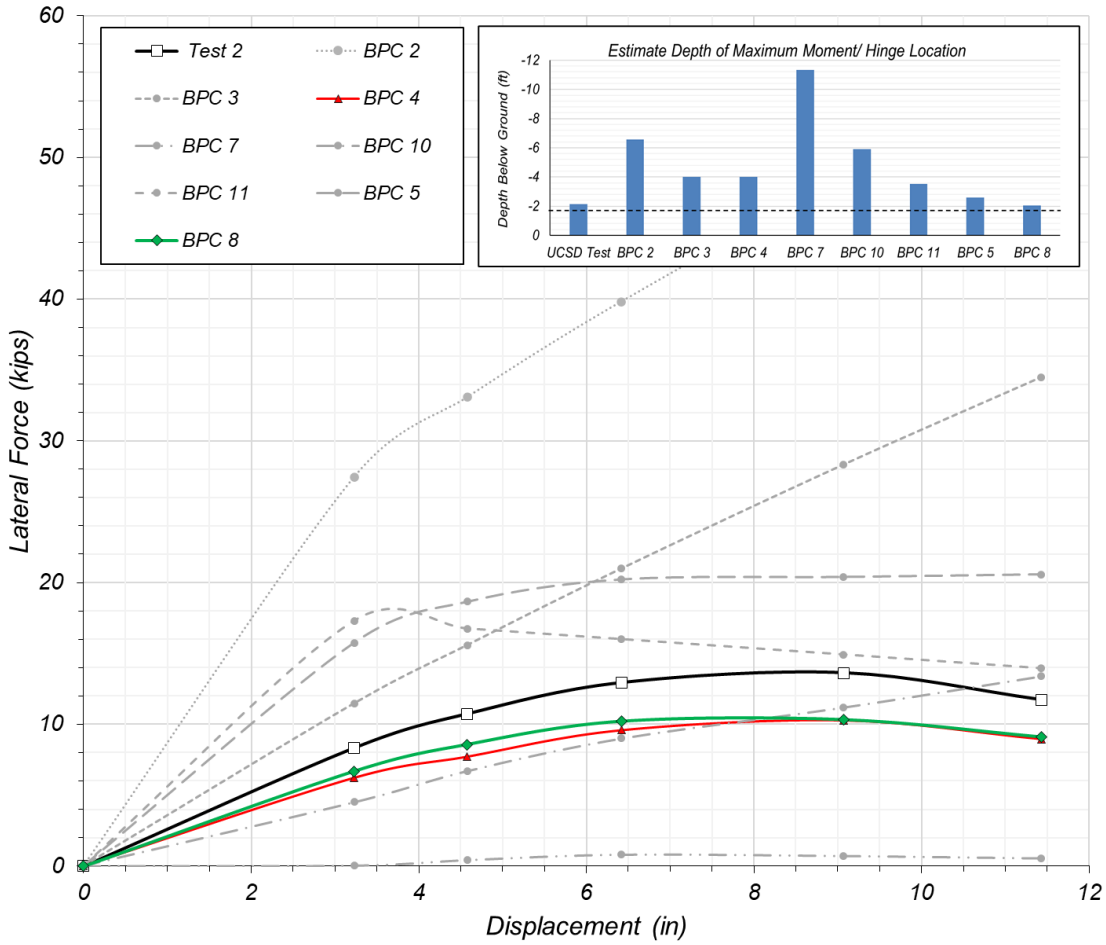

Figure 79: Blind Prediction Response Envelopes and Depth of Hinge Results for Pile Test 2

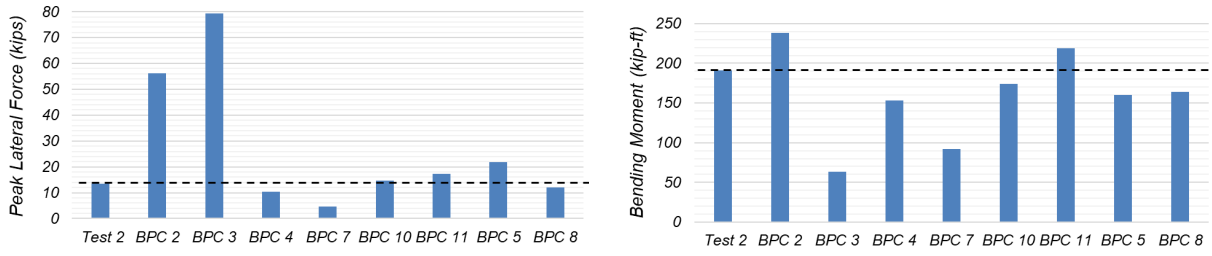

(a) Peak Lateral Force *(b) Bending Moment*

Figure 80: Free Vibration Validation – Peak Lateral Force & Bending Moment

11.3 Hysteretic Energy Validation - Comprehensive Analysis

The contestants were asked to calculate the hysteretic energy of the response for cycles 25-26, 33-34 and 37-38 of Figure 76. Hysteretic energy is determined by the shaded area enclosed by the start point and end point of the respective cycle, consisting of the first positive and negative peaks, as shown in Figure 81. Figure 82 shows the hysteretic energy of Test 2 for the respective cycles. Figure 83 compares Test 2 hysteretic response against that calculated by the contestants. Contestant 8 predicted the hysteretic energy within 55% of the test response, whereas contestant 5 calculated energy was overpredicted by almost three times.

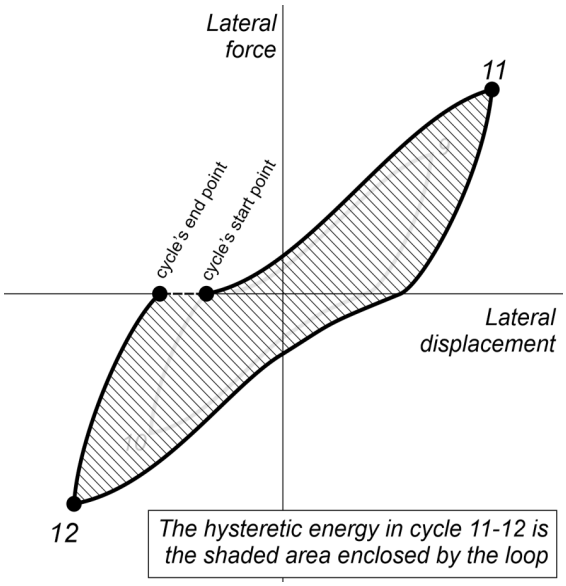

Figure 81: Hysteretic Energy Example

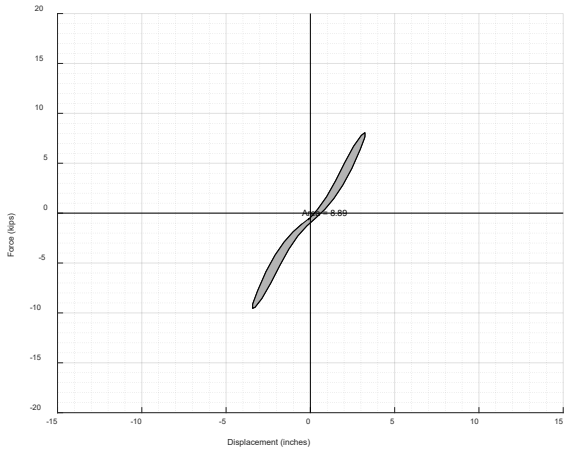

(a) Cycle 25-26 Hysteretic Energy

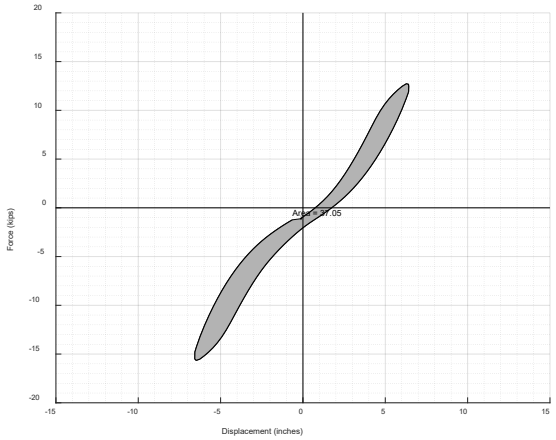

(b) Cycle 33-34 Hysteretic Energy

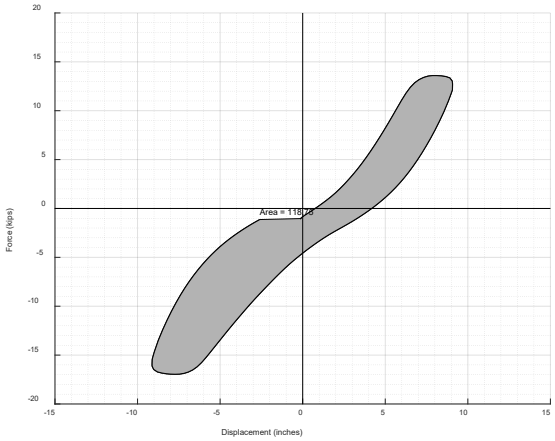

(c) Cycle 37-38 Hysteretic Energy

Figure 82: Test 2 Hysteretic Energy

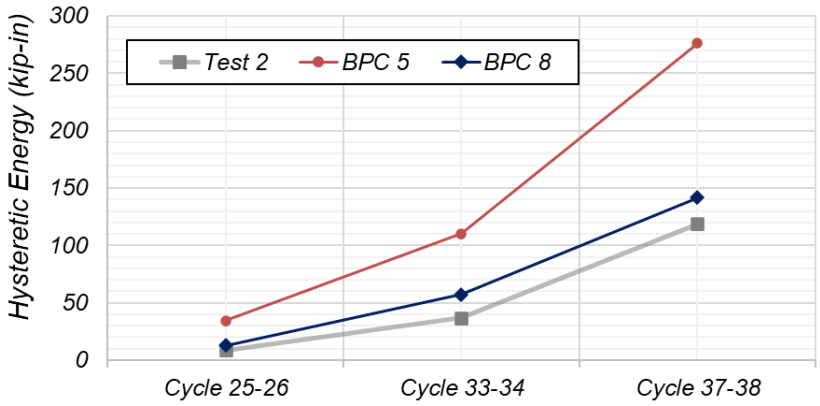

Figure 83: Hysteretic Energy Validation Comparison

12. Conclusions

Experimental tests were performed and accompanied by limited analytical validation to verify the steel pipe pile seismic strain limits used in waterfront facilities design. The in-ground steel pipe pile strains were evaluated for steel pipe piles with three diameter-to-thickness ratios: 22, 34 and 43 subjected to a constant axial loading less than 15% of the pile's elastic axial capacity in addition to quasi-static lateral. The tests were set up such that the pile had a free-head embedded in stiff sandy soil with the lateral and axial loads applied at the top of pile to establish appropriate in-ground strain limits. The piles were loaded until significant strength degradation due to formation of a plastic hinge was evident. Local buckling in the location of the plastic hinge was visually confirmed where observed on three of the four piles after the completion of the four tests. A detailed FEM of the Test 1 was developed and validated against the measured local and global responses. The FEM was subsequently used to analyze in detail the mechanical behavior of the pile component.

The results of the experiments indicated that all steel piles tested exhibited the expected ductile response as defined by AISC 360 [4]. Compact piles, Tests 3 and 4, displayed ductile performance with gradual post-peak strength degradation at large displacements after the pile section had ceased to be elastic. For Test 1 and Test 2, both with D/t ratios of 43, the piles reached displacements in the test that corresponded to significant strength reduction after the plastic moment was achieved. At large displacements, the Test 2 pile experienced a substantial loss of lateral strength. Leading to rotations which exceeded those generally considered in design. However, despite the degradation of approximately 50% in lateral load carrying capacity, the piles continued to sustain the applied gravity load. Test 4 demonstrated subtle loss of strength at large displacements and was unable to reach significant degradation due to the test limitations. Test 3 saw limited to no noticeable loss of strength as the necessary displacement exceeded those capable for the test.

Buckling was observed for the three piles with D/t ratios 34 and 43. The buckling locations were isolated to approximately 1/3 of the pile circumference and at various depths along the applied loading face. None of the piles demonstrated an elephant's foot collapse in which the entire pile section at a single elevation was compromised. Test 1 and 2 saw buckling on both the north and south face, whereas Test 4 only had visible buckling on the north face, positive push direction. This allowed axial stiffness in the pile wall sections not in the plane of lateral loading to remain after plastic moment was reached and resulted in a relatively small axial shortening of the pile due to the in-ground buckling observed.

Interior soil was observed to be absent for the top several feet of the in-ground pile length after driving the pile, thus the pile had a hollow core during testing. Soil gapping was observed during testing and increased significantly at higher displacement amplitudes

due to the cohesion in the soil. Although gapping formed at the soil-pile interface, at the onset of strength degradation corresponding to significant local pipe wall buckling, the face of the pile which buckled was in contact with the soil. Hence, it is unlikely that the soil gapping played a significant role in the local buckling and associated strength degradation.

The finite element modeling was performed to validate the in-field experimental results for Test 1. Based on the results, the critical strain is comparable to that in past experiments and numerical simulations performed in literature. Albeit these past experiments were conducted under 3- and 4-point in-air bending, thus suggesting the soil conditions had very little impact on the critical strain. While the critical strain predicted is consistent with findings from prior investigations, as a capacity metric it would significantly overburden the pile's design by limiting its design ductility, or available plastic rotations. Alternative basis for plastic rotation capacity, namely peak and post-peak strength degradation targets, are defined and demonstrated to considerably amplify the available ductility of the pile.

Based on the outcomes of this test, UCSD recommends future investigations on steel pipe piles for marine applications to consider the following.

- Top of pile connection.
- Spiral welded pipes fabricated according to ASTM A252 [9]
- Bidirectional lateral loading.
- Behavior under saturated and submerged soil conditions
- Effect of riprap.
- Multi-pile system behavior under seismic excitation.

13. References

[1] 8010, British Standard BS. 1993. "Code of Practice for Pipelines, Part 3. Pipelines Subsea: design, construction and installation," British Standards Institution, London.

[2] Aguirre Realpe, D.A. 2018. "Seismic Performance and Displacement Capacity of RCFST Drilled Shafts," North Carolina State University (NCSU), Raleigh.

[3] American Institute of Steel Construction (AISC). 2016. ANSI/AISC 341-16: Seismic Provisions for Structural Steel Buildings, Chicago, Illinois: AISC.

[4] American Institute of Steel Construction (AISC). 2016. ANSI/AISC 360-16: Specification for Structural Steel Buildings, Chicago, Illinois: AISC.

[5] American Petroleum Institute (API). 2018. API Specification 5L, 46th Edition: Line Pipe, Washington, DC: API.

[6] American Society of Civil Engineers (ASCE), "ASCE 7 Minimum Design Loads and Associated Criteria for Buildings and Other Structures," ASCE Standards, Reston VA, 2005.

[7] American Society of Civil Engineers (ASCE), "ASCE 7 Minimum Design Loads and Associated Criteria for Buildings and Other Structures," ASCE Standards, Reston VA, 2016.

[8] American Society of Civil Engineers (ASCE). 2014. Seismic Design of Piers and Wharves (ASCE/COPRI 61-14), Reston, Virginia: ASCE.

[9] ASTM International. 2019. "ASTM A252 / A252M-19: Standard Specification for Welded and Seamless Steel Pipe Piles," West Conshohocken, PA.

[10] Applied Technology Council et al. 2007. Interim testing protocols for determining the seismic performance characteristics of structural and nonstructural components (FEMA 461). Federal Emergency Management Agency.

[11] Blandon, C., Restrepo, J.I., and Jaradat, O. 2013. "Displacement Demands and Shear Key Forces in Pile-Supported Marginal Wharves with Strong Lateral-Torsional Coupling," *ACI Special Publication 295, American Concrete Institute*, pp. 1-18.

[12] Bozorgzadeh, A., et al. 2008. "Experimental and Analytical Investigation on Stiffness and Ultimate Capacity of Bridge Abutments," SSRP 7, (59).

[13] Bolton, M.D. 1986. "The Strength and Dilatancy of Sands," Geotechnique, 36(1): 65-78.

[14] Brandenberg, S.J., Bellana, N., and T., S. 2010. "Shear wave velocity as function of standard penetration test resistance and vertical effective stress at California bridge sites," Soil Dynamics and Earthquake Engineering, 30(10): 1026-1035.

[15] Brown, N.K., Kowalsky, M.J., and Nau, J.M. 2013. "Strain Limits for Concrete Filled Steel Tubes in AASHTO Seismic Provisions," Alaska Department of Transportation & Public Facilities, North Carolina State University, Raleigh, NC.

[16] Brown, N.K., Kowalsky, M.J., and Nau, J.M. 2015. "Impact of D/t on Seismic Behavior of Reinforced Concrete Filled Steel Tubes," *Journal of Constructional Steel Research*, 107: 111-123.

[17] Chaboche, J.L. 1986. "Time-Independent Constitutive Theories for Cyclic Plasticity," *International Journal of Plasticity*, 2(2): 149-188.

[18] Chopra, A.K. 2017. Dynamics of Structures: Theory and Applications to Earthquake Engineering. 5th ed., Pearson Education

[19] City of Los Angeles Harbor Department. 2010. "Port of Los Angeles Code for Seismic Design, Upgrade and Repair of Container Wharves (POLA Seismic Code 2010)." May.

[20] Dorey, A.B., Murray, D.W., and Cheng, J.R. 2000. "An Experimental Evaluation of Critical Buckling Strain Criteria," in 2000 International Pipeline Conference (IPC), Calgary, Alberta, Canada.

[21] Elsherbiny, Z.H., El Naggar, M.H., and Elgamal, A. 2017. "Helical piles foundation for wind turbines: full-scale testing of a single helical pile in sand." Proceedings of the 3rd international conference on performance-based design in earthquake geotechnical engineering (PBD-III), Vancouver, Canada.

[22] Ensoft Inc. 2022. Computer Program LPILE 12.09, A Program for the Analysis of Piles and Drilled Shafts Under Lateral Loads.

[23] Federal Emergency Management Agency (FEMA). 2007. "FEMA 461: Interim Testing Protocols for Determining the Seismic Performance Characteristics of Structural and Nonstructural Components." Washington, D.C.

[24] Fleming, B.J., Sritharan, S., Miller, G.A., and Muraleetharan, K.K. 2016. "Full-Scale Seismic Testing of Piles in Improved and Unimproved Soft Clay," Earthquake Spectra, 32(1): 239-265.

[25] Frandsen, H. and Nguyen, D. 2019. "Seismic Design of Pile-Supported Wharves: Effect of New Steel Strain Limits in ASCE 61-19," in Proceedings, Ports 2019, Reston.

[26] Fulmer, S.J., Kowalsky, M.J., Nau, J.M., and Hassan, T. 2012. "Reverse Cyclic Flexural Behavior of Spiral DSAW and Single Seam ERW Steel Pipe Piles," *Journal of Structural Engineering*, 138(9): 1099-1109.

[27] Goel, R.K. 2010. “Simplified Procedure for Seismic Evaluation of Piles with Partial-Moment Connection to the Deck in Marine Oil Terminals.” *Journal of Structural Engineering*, 136(5), May 2010.

[28] Gresnigt, A. 1986. "Plastic Design of Buried Steel Pipes in Settlement Areas," Heron, 31(4): 113.

[29] Harn, R., Ospina, C.E., and Pachakis, D. 2019. "Proposed pipe pile strain limits for ASCE 61-19," in Proceedings, Ports 2019, Reston.

[30] Kowalsky, M. J. 2019. "Seismic Behavior of Reinforced-Concrete-Filled Steel Tubes," *ASPIRE Spring 2019,* pp. 32-33.

[31] Kyriakides, S. and Corona, E. 2007. Mechanics of Offshore Pipelines: Buckling and Collapse, vol. 1, Burlington, MA: Elsevier.

[32] LSTC. 2016. LS-DYNA: Keyword User's Manual, 9.0 ed., vol. 1, Livermore: Livermore Software Technology Corporation (LSTC).

[33] MOTEMS (Marine Oil Terminal Engineering and Maintenance Standard). 2011. "Marine Oil Terminal Engineering and Maintenance Standard, Title 24 California Code of Regulations, Part 2, California Building Code, Chapter 31F (Marine Oil Terminals)," vol. 2, Washington, D.C.: International Code Council.

[34] Montejo, L.A., Gonzalez-Roman, L.A., and Kowalsky, M.J. 2012. "Seismic Performance Evaluation of Reinforced Concrete-Filled Steel Tube Pile/Column Bridge Bents," Journal of Earthquake Engineering, 401-424.

[35] Murphey, C.E. and Langner, C.G. 1985. "Ultimate Pipe Strength Under Bending, Collapse, and Fatigue," in Proceedings of the 4th International Conference on Offshore Mechanic and Arctic Engineering Symposium, Dallas.

[36] National Cooperative Highway Research Program (NCHRP). 2013. "Synthesis 440: Performance-based Seismic Bridge Design," Transportation Research Board, Washington, D.C.

[37] Peters, D.J., Broos, E.J., Gresnigt, A., and van Es, S.H. 2015. "Local Buckling Resistance of Sand-filled Spirally Welded Tubes," in Proceedings of the Twenty-fifth, Kona.

[38] POLB (Port of Long Beach). 2021. Port of Long Beach Wharf Design Criteria (POLB WDC) version 5.0. Long Beach, CA: POLB.

[39] Richards, T.L., Suarez, S., Restrepo, J.I., and Morrison, M.L. 2022. "Steel Pipe Pile Strain Limits for Performance-Based Seismic Design of Marine Structures," in PORTS 22, Honolulu.

[40] Richards, T., Rahmani, A., Suarez, S., Restrepo, J., Morrison, M., and Jaradat, O. 2025. "Large-Scale Test Progress and Assessment of the In-ground Hinge Development of Steel Pipe Piles," in PORTS 25, Rhode Island.

[41] Sadowski, A.J., Wong, W.J., Li, S.C., Malaga-Chuquitaype, C., and Pachakis, D. 2020. "Critical buckling strains in thick cold-formed circular-hollow sections under cyclic loading."

[42] Sherman, D.R. 1976. "Tests of Circular Steel Tubes in Bending," Journal of the Structural Division, Proceedings of the American Society of Civil Engineers, 102(ST11): 2181-2195.

[43] Sherman, D.R. 1983. "Bending Capacity of Fabricated Pipes," College of Engineering and Applied Science, University of Wisconsin, Milwaukee.

[44] Suarez, S., Richards, T., Morrison, M.L., and Restrepo, J. 2024. "In-ground Plastic Hinge Behavior of Steel-Pipe Piles for Piers and Wharves." Marine Structures, 1-15 (IN PREPARATION).

[45] van Es, S. 2016. "Inelastic Local Buckling of Tubes for Combined Walls and Pipelines," TUDelft, 08 07 2016. [Online].
Available: https://doi.org/10.4233/uuid:48e61e69-a35f-43d5-a417-b393cbacaa98.

[46] Winkel, J. 2016. "Large diameter dolphin piles: The effect of the inner soil on their local buckling resistance," MSc Thesis, Delft University of Technology.

[47] Winkel, J., Kostis, N., Peters, D.J., and van Es, S.H.J. 2017. "05.31: Experiments and FEM Simulations of Local Buckling of Sand-Filled Tubular Piles," ce/papers, 1(2-3): 1305-1314.

[48] Zayas, V.A., Popov, E.P., and Mahin, S.A. 1980. "Cyclic Inelastic Buckling of Tubular Steel Braces," Report No. UCB/EERC-80/16, University of California, Berkeley, Earthquake Engineering Research Center, Springfield, VA.

Appendix A Instrumentation

Instrumentation Plans, Sketches and Photos

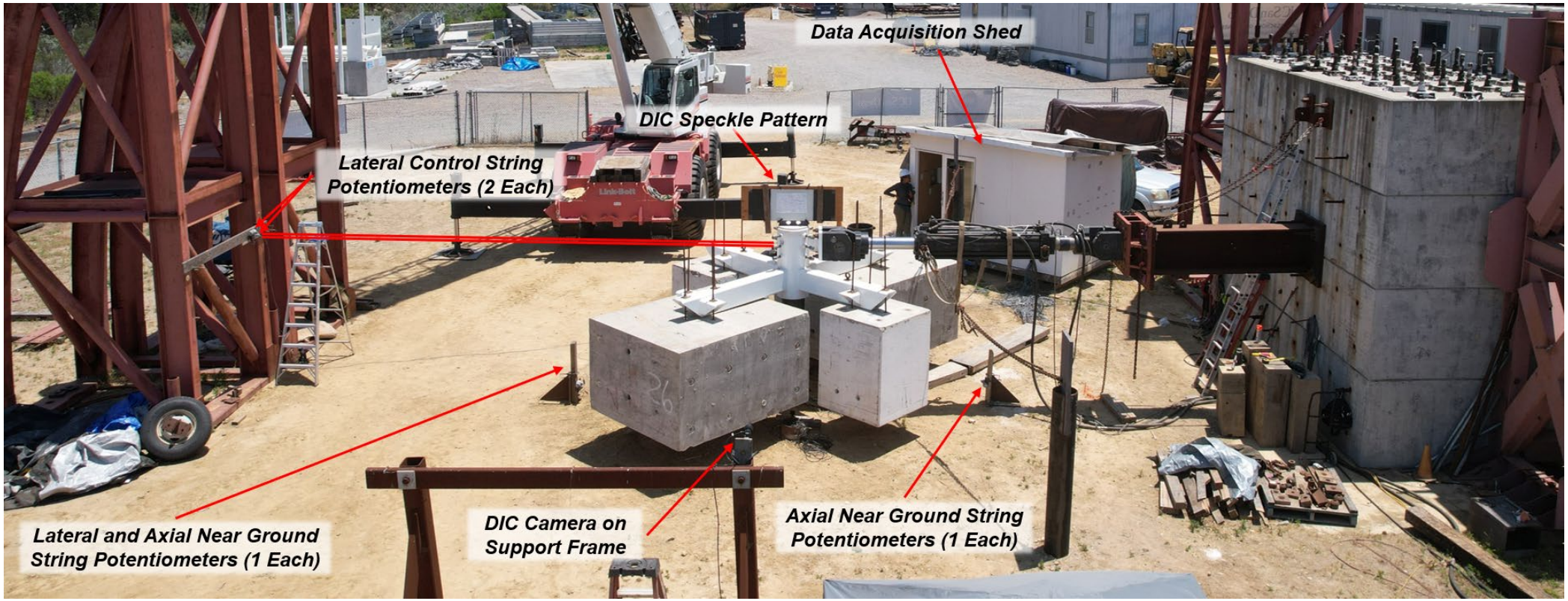

Note: Inclinometer is on the eastern face of the Test 2 pile and therefore, is not shown.

Overall Test Above Ground Instrumentation Test 2

Test Set-Up – Typical Instrumentation Plan

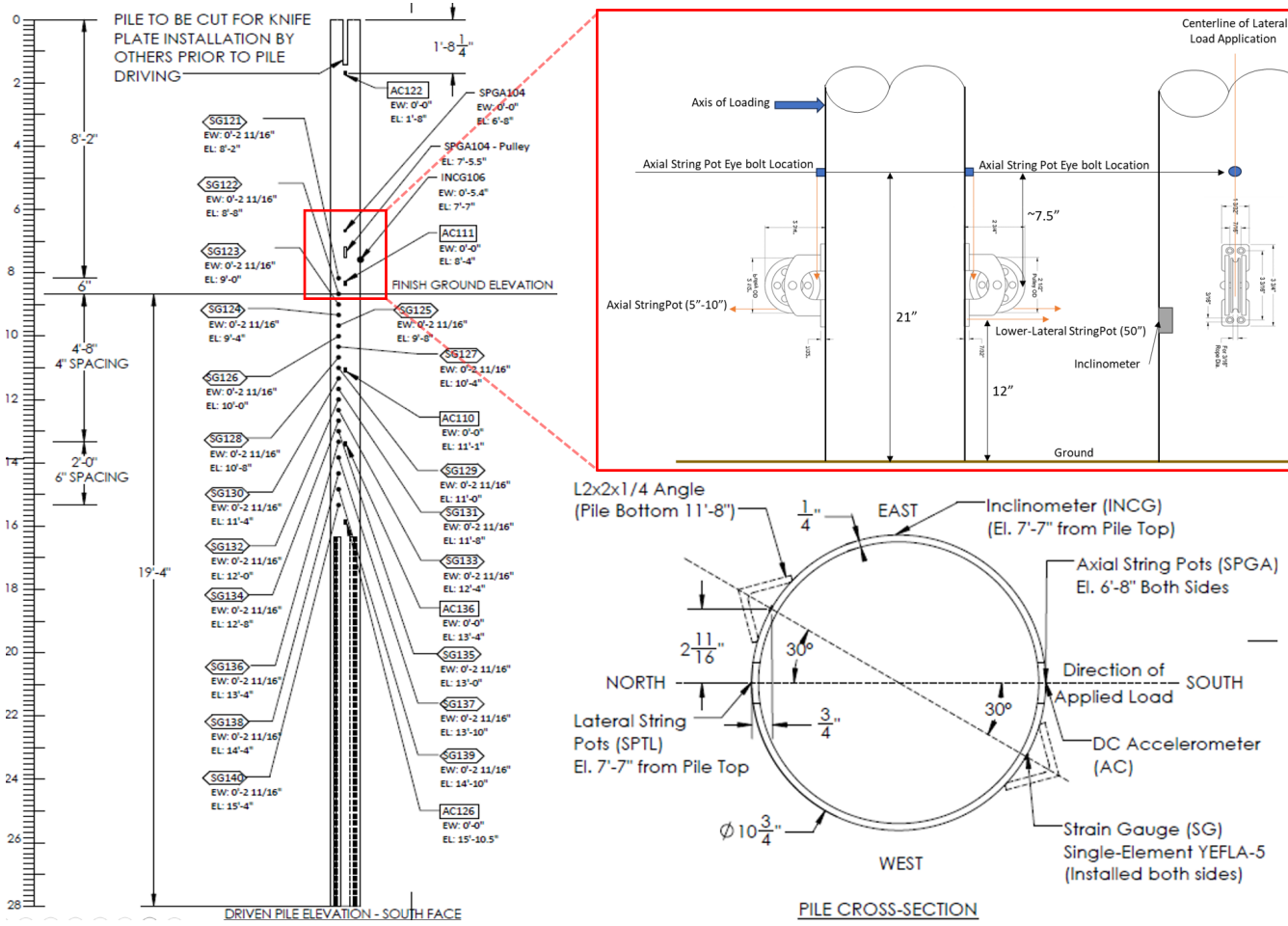

- Single Element Yield Strain Gauges capable of measuring 10% to 15% strains was installed from 0.5-ft above ground to 7-ft below finished ground.
- 4-5 Accelerometers installed at top-of-pile and in-ground up to 7-ft.
- 3 – Lateral String Potentiometers
- 2 – Axial String Potentiometers
- 1 – Near Ground Inclinometer

Note: Locations of Instrumentation are as shown as installed. Excavation and backfill was performed after instrumentation was complete. Elevations for the four tests may differ. Other information such as top of soil elevation from top of pile elevation was measured to confirm. Angle was removed during excavation.

Instrumentation - Strain Gauge

RW-SIDE = Reaction Wall – South Pile Face
BACK = North Face
Elevation +0.0 is Top of Ground Elevation

Test 1				
Strain Gauges				
Label	Location	Label	Location	Elevation
SG101	RW-SIDE	SG121	BACKSIDE	-0.50 ft
SG102	RW-SIDE	SG122	BACKSIDE	0.00 ft
SG103	RW-SIDE	SG123	BACKSIDE	0.33 ft
SG104	RW-SIDE	SG124	BACKSIDE	0.67 ft
SG105	RW-SIDE	SG125	BACKSIDE	1.00 ft
SG106	RW-SIDE	SG126	BACKSIDE	1.33 ft
SG107	RW-SIDE	SG127	BACKSIDE	1.67 ft
SG108	RW-SIDE	SG128	BACKSIDE	2.00 ft
SG109	RW-SIDE	SG129	BACKSIDE	2.33 ft
SG110	RW-SIDE	SG130	BACKSIDE	2.67 ft
SG111	RW-SIDE	SG131	BACKSIDE	3.00 ft
SG112	RW-SIDE	SG132	BACKSIDE	3.33 ft
SG113	RW-SIDE	SG133	BACKSIDE	3.67 ft
SG114	RW-SIDE	SG134	BACKSIDE	4.00 ft
SG115	RW-SIDE	SG135	BACKSIDE	4.33 ft
SG116	RW-SIDE	SG136	BACKSIDE	4.83 ft
SG117	RW-SIDE	SG137	BACKSIDE	5.33 ft
SG118	RW-SIDE	SG138	BACKSIDE	5.83 ft
SG119	RW-SIDE	SG139	BACKSIDE	6.33 ft
SG120	RW-SIDE	SG140	BACKSIDE	6.83 ft

Test 2				
Strain Gauges				
Label	Location	Label	Location	Elevation
SG201	BACK	SG221	RW-SIDE	-0.50 ft
SG202	BACK	SG222	RW-SIDE	0.00 ft
SG203	BACK	SG223	RW-SIDE	0.33 ft
SG204	BACK	SG224	RW-SIDE	0.67 ft
SG205	BACK	SG225	RW-SIDE	1.00 ft
SG206	BACK	SG226	RW-SIDE	1.33 ft
SG207	BACK	SG227	RW-SIDE	1.67 ft
SG208	BACK	SG228	RW-SIDE	2.00 ft
SG209	BACK	SG229	RW-SIDE	2.33 ft
SG210	BACK	SG230	RW-SIDE	2.67 ft
SG211	BACK	SG231	RW-SIDE	3.00 ft
SG212	BACK	SG232	RW-SIDE	3.33 ft
SG213	BACK	SG233	RW-SIDE	3.67 ft
SG214	BACK	SG234	RW-SIDE	4.00 ft
SG215	BACK	SG235	RW-SIDE	4.33 ft
SG216	BACK	SG236	RW-SIDE	4.83 ft
SG217	BACK	SG237	RW-SIDE	5.33 ft
SG218	BACK	SG238	RW-SIDE	5.83 ft
SG219	BACK	SG239	RW-SIDE	6.33 ft
SG220	BACK	SG240	RW-SIDE	6.83 ft

Test 3				
Strain Gauges				
Label	Location	Label	Location	Elevation
SG401	BACK	SG421	RW-SIDE	-0.17
SG402	BACK	SG422	RW-SIDE	0.33
SG403	BACK	SG423	RW-SIDE	0.67
SG404	BACK	SG424	RW-SIDE	1.00
SG405	BACK	SG425	RW-SIDE	1.33
SG406	BACK	SG426	RW-SIDE	1.67
SG407	BACK	SG427	RW-SIDE	2.00
SG408	BACK	SG428	RW-SIDE	2.33
SG409	BACK	SG429	RW-SIDE	2.67
SG410	BACK	SG430	RW-SIDE	3.00
SG411	BACK	SG431	RW-SIDE	3.33
SG412	BACK	SG432	RW-SIDE	3.67
SG413	BACK	SG433	RW-SIDE	4.00
SG414	BACK	SG434	RW-SIDE	4.33
SG415	BACK	SG435	RW-SIDE	4.67
SG416	BACK	SG436	RW-SIDE	5.17
SG417	BACK	SG437	RW-SIDE	5.67
SG418	BACK	SG438	RW-SIDE	6.17
SG419	BACK	SG439	RW-SIDE	6.67
SG420	BACK	SG440	RW-SIDE	7.17

Test 4				
Strain Gauges				
Label	Location	Label	Location	Elevation
SG301	BACKSIDE	SG321	RW-SIDE	-0.17
SG302	BACKSIDE	SG322	RW-SIDE	0.33
SG303	BACKSIDE	SG323	RW-SIDE	0.67
SG304	BACKSIDE	SG324	RW-SIDE	1.00
SG305	BACKSIDE	SG325	RW-SIDE	1.33
SG306	BACKSIDE	SG326	RW-SIDE	1.67
SG307	BACKSIDE	SG327	RW-SIDE	2.00
SG308	BACKSIDE	SG328	RW-SIDE	2.33
SG309	BACKSIDE	SG329	RW-SIDE	2.67
SG310	BACKSIDE	SG330	RW-SIDE	3.00
SG311	BACKSIDE	SG331	RW-SIDE	3.33
SG312	BACKSIDE	SG332	RW-SIDE	3.67
SG313	BACKSIDE	SG333	RW-SIDE	4.00
SG314	BACKSIDE	SG334	RW-SIDE	4.33
SG315	BACKSIDE	SG335	RW-SIDE	4.67
SG316	BACKSIDE	SG336	RW-SIDE	5.17
SG317	BACKSIDE	SG337	RW-SIDE	5.67
SG318	BACKSIDE	SG338	RW-SIDE	6.17
SG319	BACKSIDE	SG339	RW-SIDE	6.67
SG320	BACKSIDE	SG340	RW-SIDE	7.17

Test 3 and 4 Strain Gauge Readings and Elevations

Test #3 Pile Strain Gauge Reading (Prior to Test)						Depth below Ground	
Backside (Northside)			Reaction Wall Side (Southside)			[ft]	[Pile Diameters]
SG401	122.7	2.3	SG421	121.7	2.2	-0.17	
SG402	121.9	2.3	SG422	121.5	2.2	0.33	0.37
SG403	122	2.2	SG423	121.9	2.4	0.67	0.74
SG404	122	2.4	SG424	121.8	2.8	1.00	1.12
SG405	122.2	2.2	SG425	121.8	2.6	1.33	1.49
SG406	121.8	2.2	SG426	121.6	2.2	1.67	1.86
SG407	122.2	2.4	SG427	121.7	3	2.00	2.23
SG408	122.1	2.5	SG428	121.9	2.3	2.33	2.6
SG409	122	2.2	SG429	122.3	2.7	2.67	2.98
SG410	122	2.3	SG430	121.8	2.5	3.00	3.35
SG411	121.7	2.2	SG431	122.5	2.5	3.33	3.72
SG412	122.2	2.3	SG432	122	2.8	3.67	4.09
SG413	121.9	2.3	SG433	123	2.5	4.00	4.47
SG414	0	2.2	SG434	122.1	2.8	4.33	4.84
SG415	121.7	2.4	SG435	121.8	2.2	4.67	5.21
SG416	122	2.8	SG436	121.9	2.6	5.17	5.77
SG417	121.8	2.7	SG437	121.8	2.4	5.67	6.33
SG418	121.7	2.6	SG438	0	2.5	6.17	6.88
SG419	121.8	2.4	SG439	121.9	2.6	6.67	7.44
SG420	0	0	SG440	122.2	2.8	7.17	8

Test #4 Pile Strain Gauge Reading (Prior to Test)						Depth below Ground	
Reaction Wall Side (Southside)			Backside (Northside)			[ft]	[Pile Diameters]
SG301	121.6	2.4	SG321	121.7	2.6	-0.17	
SG302	121.4	2.1	SG322	122.2	2	0.33	0.31
SG303	0	2.1	SG323	121.8	2.2	0.67	0.63
SG304	0	0	SG324	121.7	2.3	1.00	0.94
SG305	121.7	2.5	SG325	0	2.2	1.33	1.25
SG306	121.7	2.1	SG326	121.4	2.6	1.67	1.57
SG307	121.5	2.1	SG327	121.7	2.3	2.00	1.88
SG308	121.5	2	SG328	121.8	2.1	2.33	2.2
SG309	121.5	2.9	SG329	121.7	2.3	2.67	2.51
SG310	121.5	2	SG330	121.7	2.2	3.00	2.82
SG311	0	0	SG331	121.2	2.4	3.33	3.14
SG312	121.6	2.1	SG332	121.8	2.8	3.67	3.45
SG313	Cut at pile	Can save	SG333	121.8	2.3	4.00	3.76
SG314	0	0	SG334	0	0	4.33	4.08
SG315	121.4	2.1	SG335	121.7	2.5	4.67	4.39
SG316	121.6	2.1	SG336	121.8	2.6	5.17	4.86
SG317	121.7	2.9	SG337	122.2	2.7	5.67	5.33
SG318	121.9	2.1	SG338	121.9	2.3	6.17	5.8
SG319	122	2.2	SG339	121.7	2.3	6.67	6.27
SG320	122.1	2.2	SG340	121.7	2.3	7.17	6.75

Instrumentation - Lateral & Axial String Potentiometers

Stringpots	
DAQID	Location
SPTL-101	Top of pile approx. 9.25" from top of pile (North-Side)
SPTL-102	Top of pile approx. 10.75" from top of pile (North-Side)
SPTL-103	Above FG approx. 90.75"" from top of pile (North-Side)
SPGA-104	Above FG approx. 80" from top of pile (North-Side)
SPGA-105	Above FG approx. 80" from top of pile (South-Side)

Sting Pot Eyebolt Installation Position

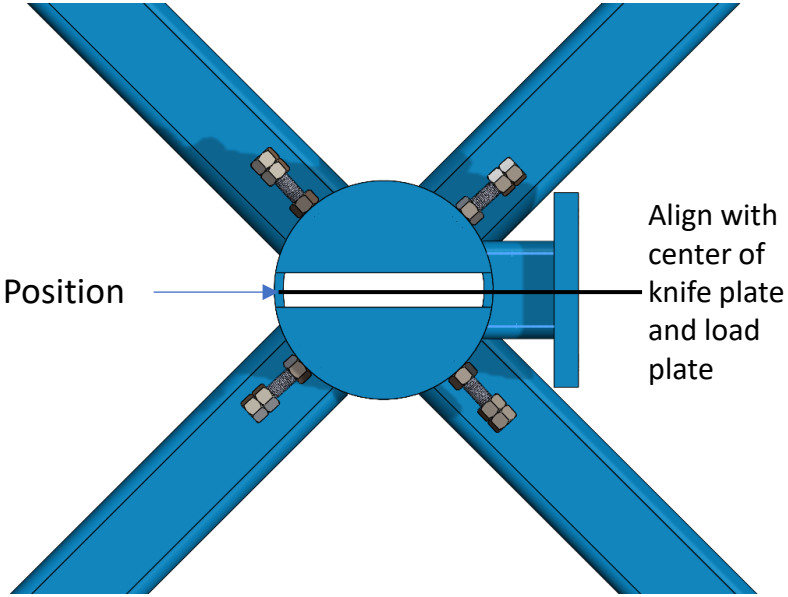

Sting Pot Eyebolt (x2) Installation Position
Minimum 1” apart no more then 3” apart.
(Closer the better)

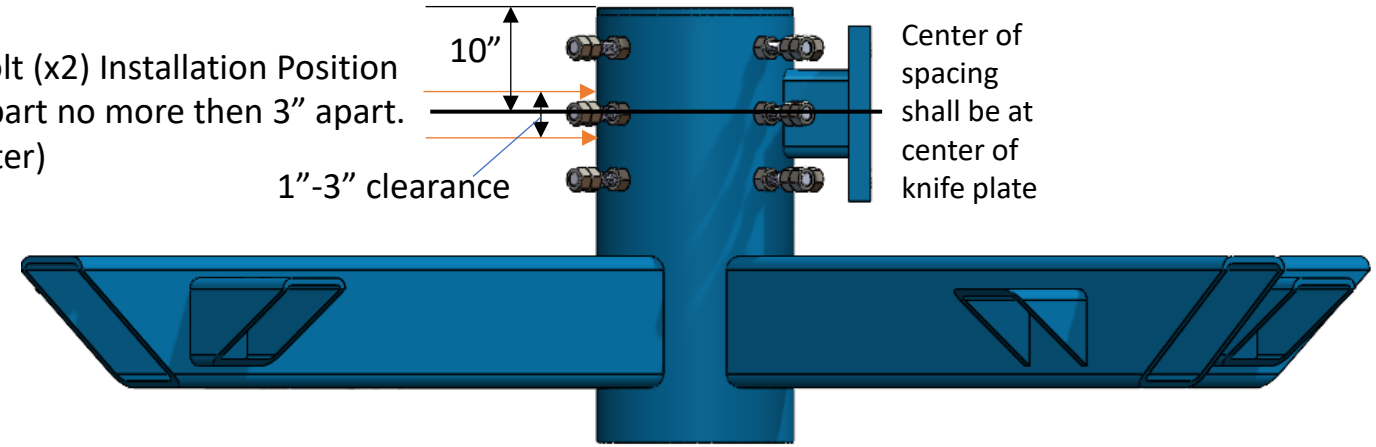

Instrumentation - Top Control String Potentiometers

Instrumentation - Bottom Lateral & Axial String Potentiometers

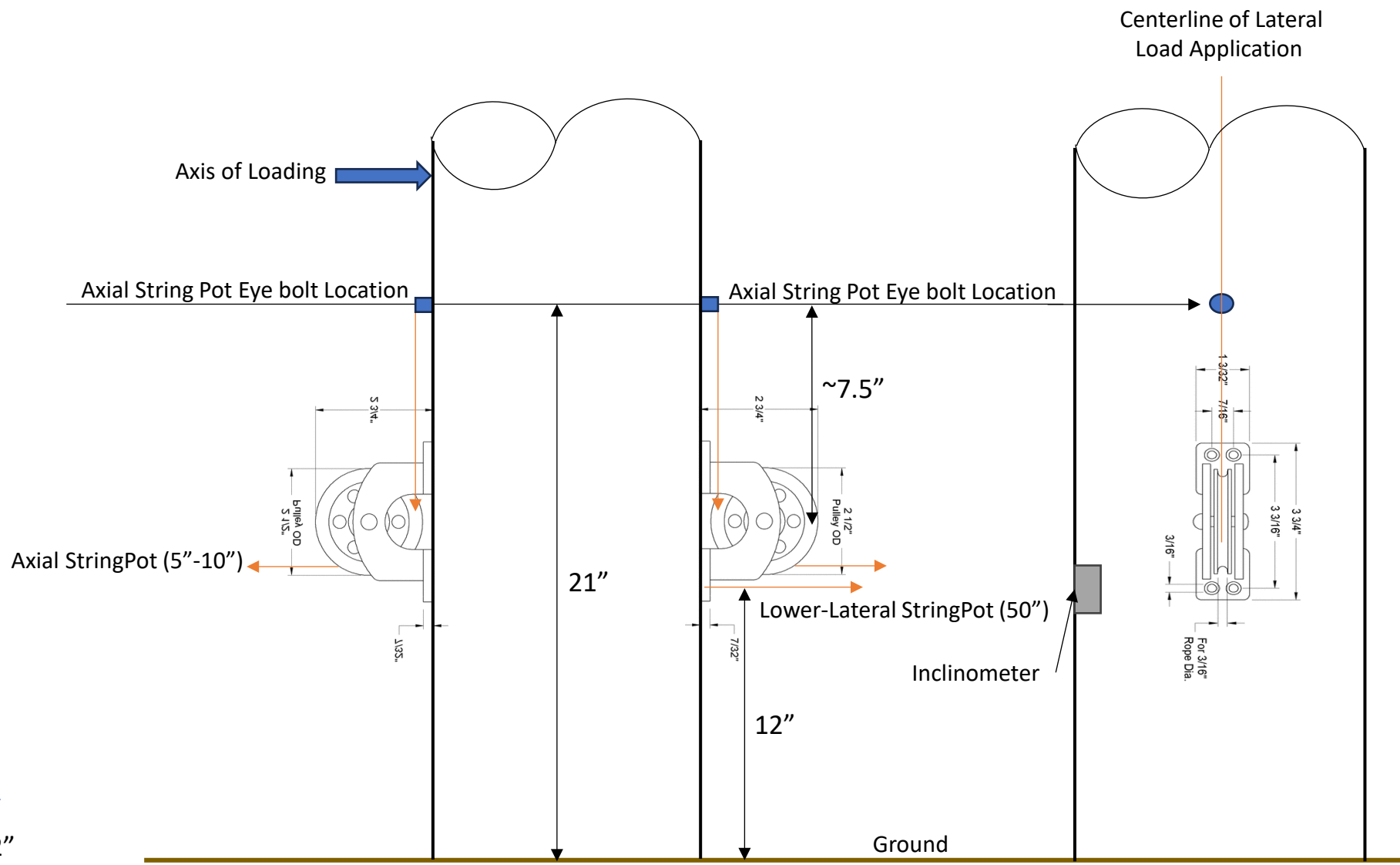

Instrumentation - Bottom Lateral & Axial String Potentiometers

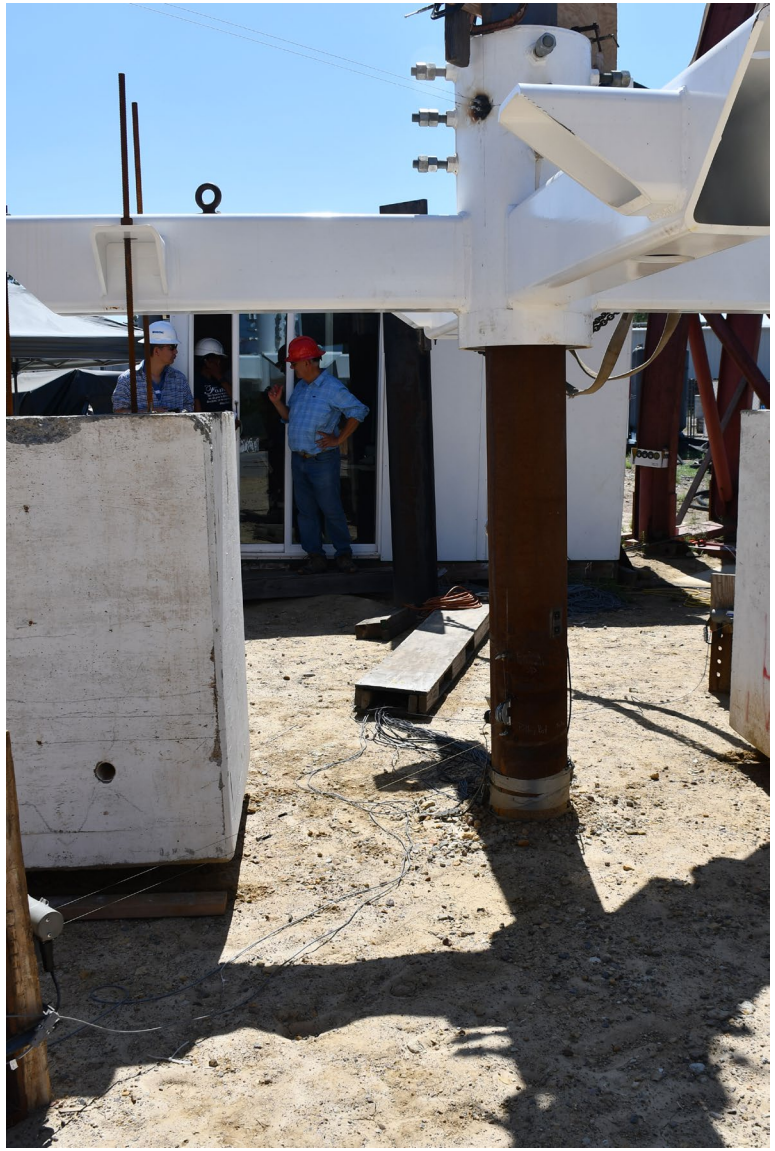

Instrumentation - Inclinometer

Inclinometer	
DAQID	Location
INCG-106	Above FG approx. 90.75" from top of pile (East-Side)

Instrumentation - Accelerometers

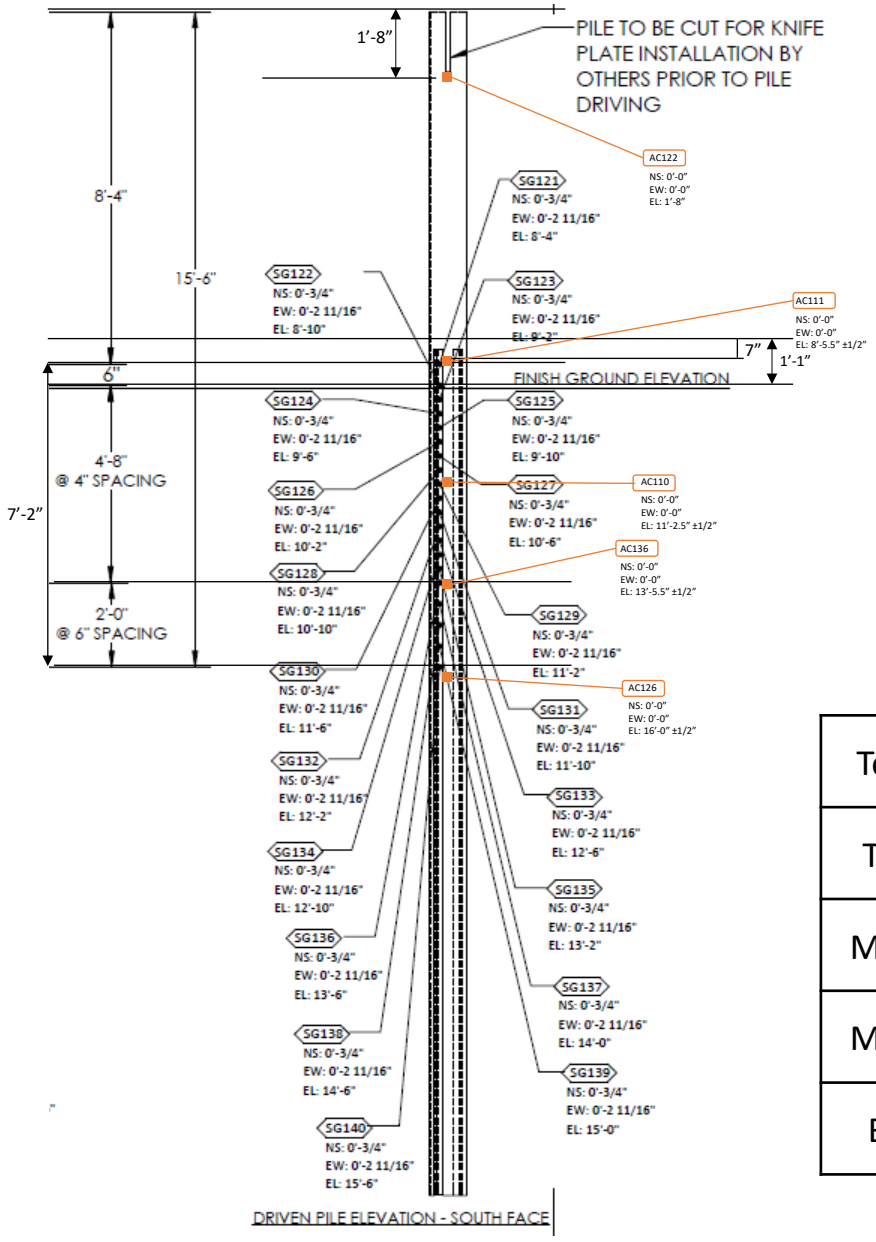

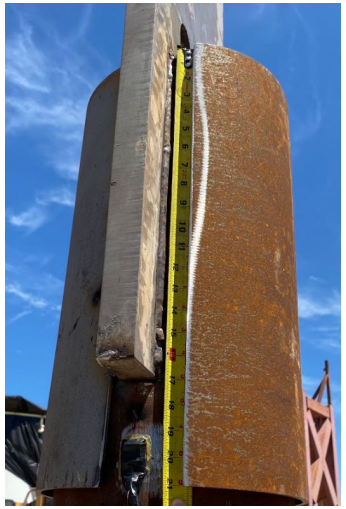

Top-0

Top-1

Mid -2

Top - 0 (20" from Top of the pile)
Top - 1 (8'-5.5" from Top of Pile)
Mid - 2 (11'-2.5" from Top of Pile)
Mid - 3 (13'-5.5" from Top of Pile)
Bot - 4 (16'-0" from Top of Pile)

Mid-3

Bot- 4

Appendix B

Loading Apparatus, Axial Load Concrete Blocks, Miscellaneous Test Drawings

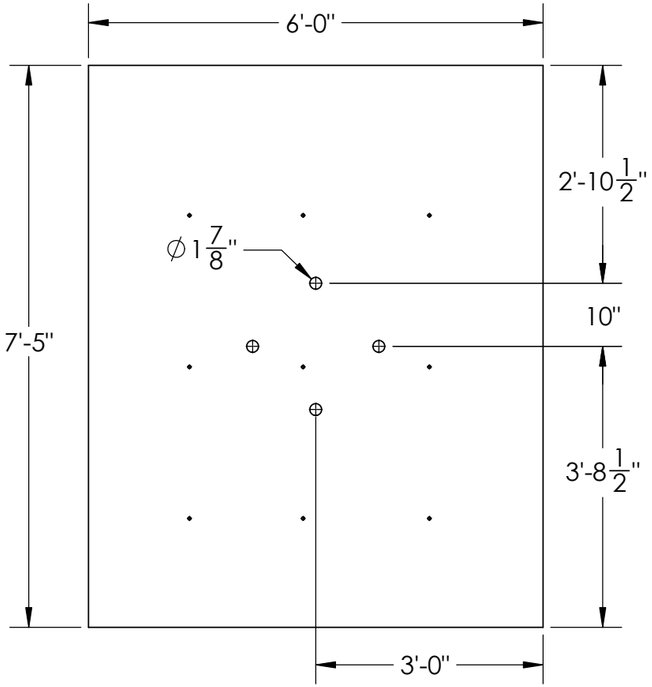

TOP PLAN

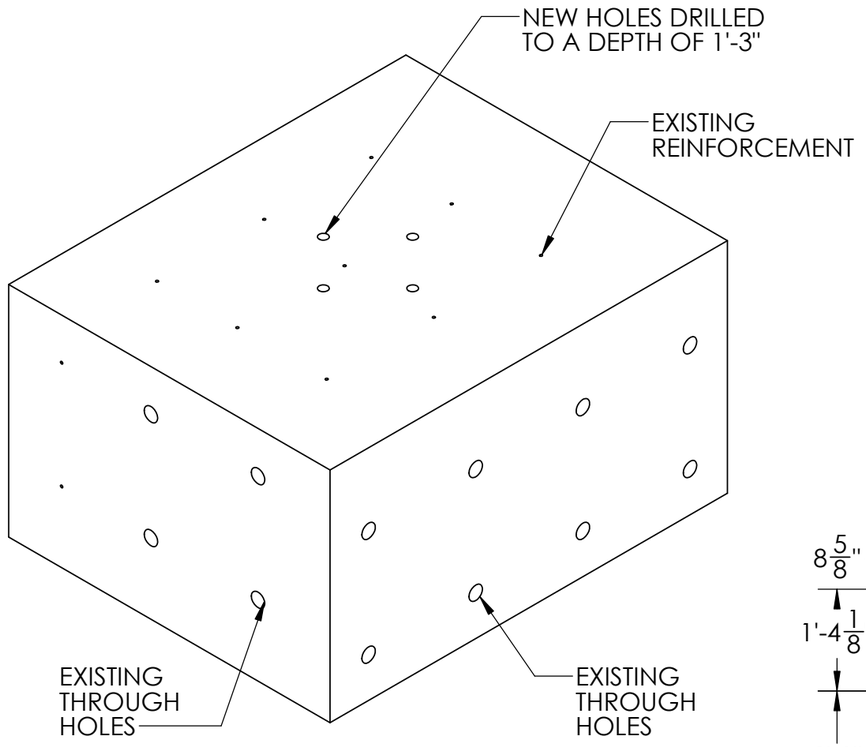

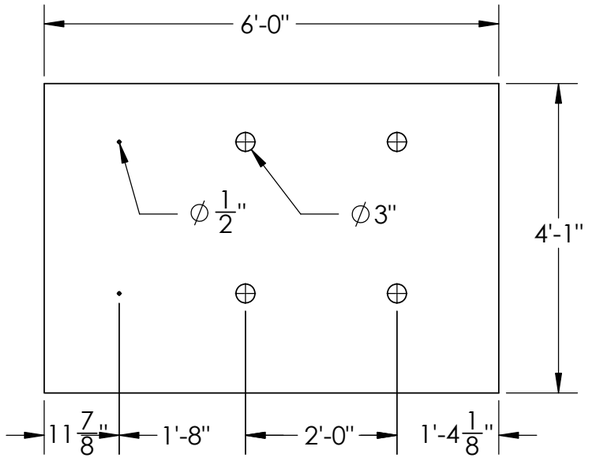

SIDE ELEVATION -1

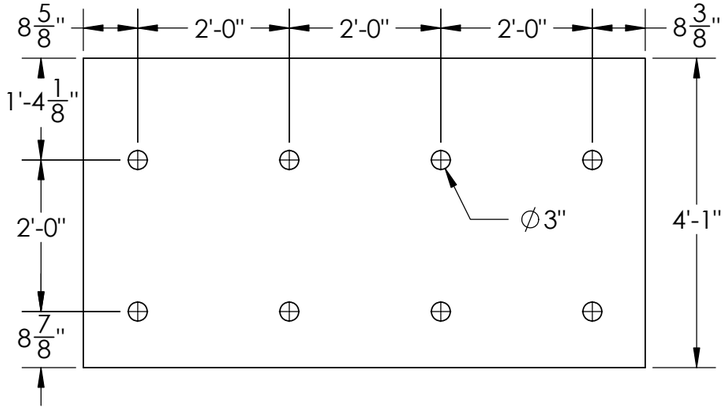

SIDE ELEVATION -2

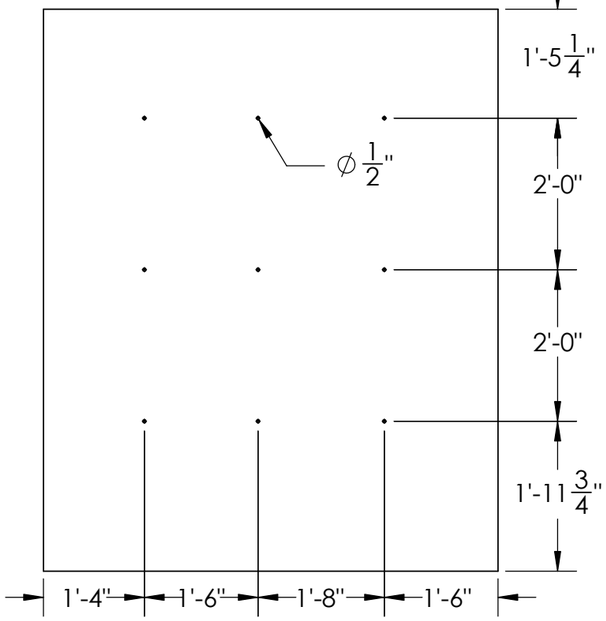

BOTTOM PLAN

PHOTO OF CONCRETE BLOCK

NOTES:
1. CONCRETE BLOCK QUANTITY = 2. HOLE QUANTITY = 4 PER BLOCK.
2. HOLES SHALL BE MINIMUM DIAMETER OF 1.625 INCHES AND 1'-3" DEPTH.
3. EXISTING REINFORCEMENT LOCATIONS ARE UNKNOWN.

UC SAN DIEGO		**ESEC NORTH SOIL PIT STEEL PIPE PILES RESEARCH**	
SHEET SCALE 1:24		TITLE: CONCRETE BLOCK 'Z' CONCRETE CUTTING PLAN	
DRAWN	T. RICHARDS		
CHKD		DATE: 11/10/2022	DRAWING NO.: CD-01
APPRVD		REV:	

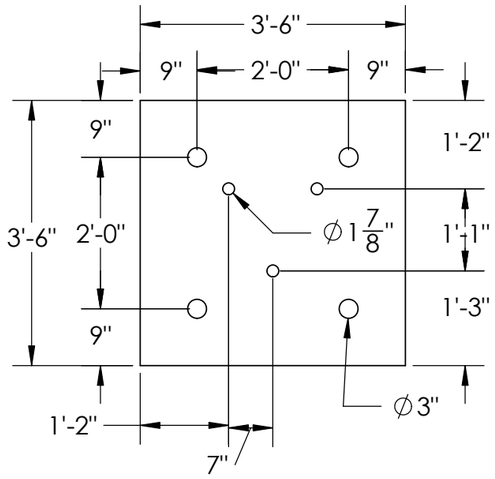

TOP PLAN

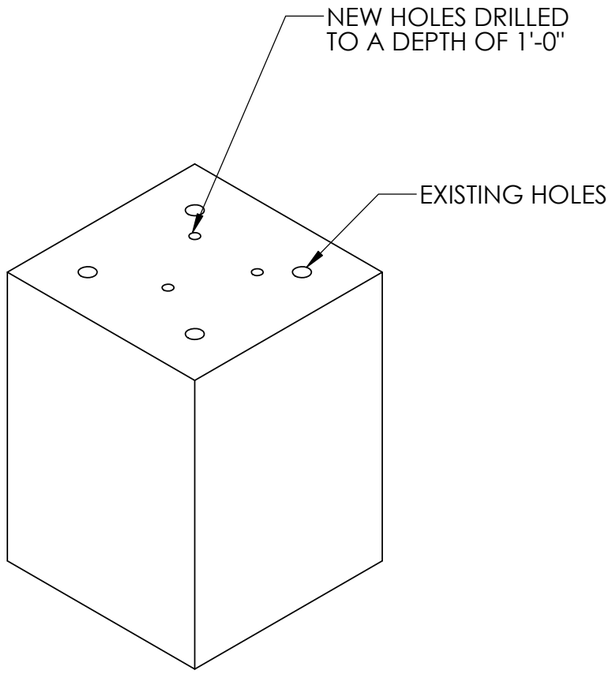

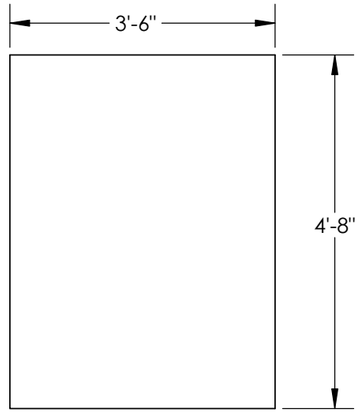

SIDE ELEVATION

PHOTO OF CONCRETE BLOCK

NOTES:
1. CONCRETE BLOCK QUANTITY = 2. HOLE QUANTITY = 3 PER BLOCK.
2. HOLES SHALL BE MINIMUM DIAMETER OF 1.625 INCHES AND 1'-0" DEPTH.
3. EXISTING REINFORCEMENT LOCATIONS AND THROUGHHOLES ARE UNKNOWN.

UC SAN DIEGO		ESEC NORTH SOIL PIT STEEL PIPE PILES RESEARCH	
SHEET SCALE 1:24		TITLE: CONCRETE BLOCK 'A' CONCRETE CUTTING PLAN	
DRAWN	T. RICHARDS		
CHKD		DATE: 12/19/2022	DRAWING NO.: CD-02
APPRVD		REV:	

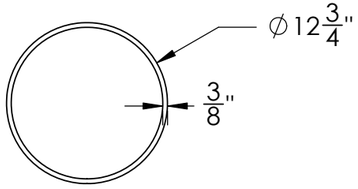

D/t = 34
TEST #4 (NAVFAC)

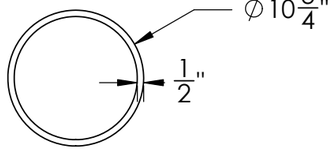

D/t = 22
TEST #3 (NIST)

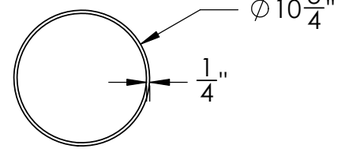

D/t = 43
TEST #2 (NIST)

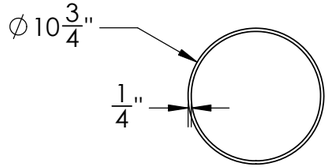

D/t = 43
TEST #1 (NIST)

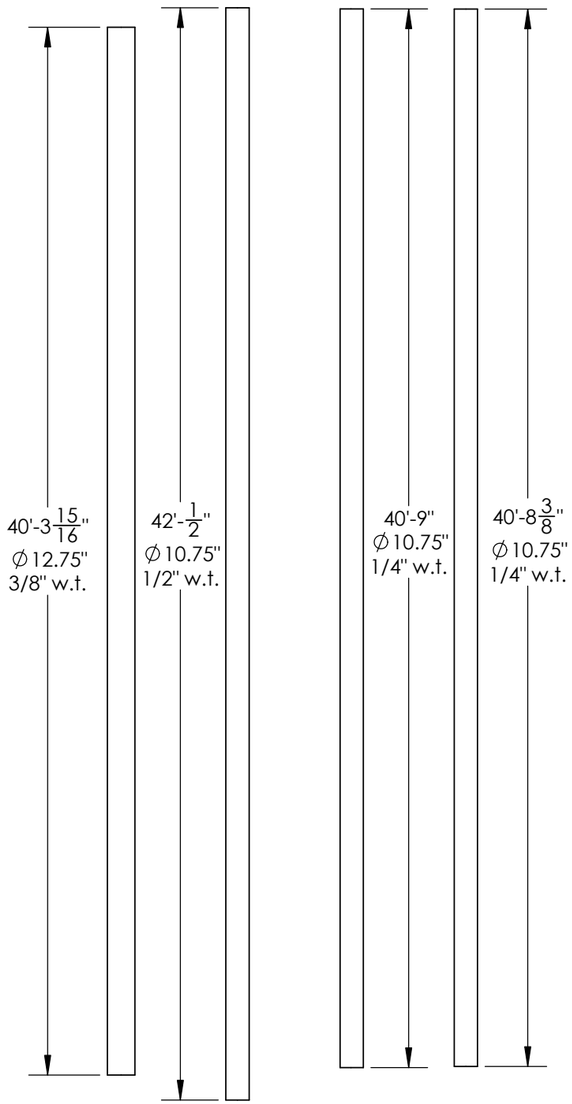

DELIVERED PILE LENGTHS

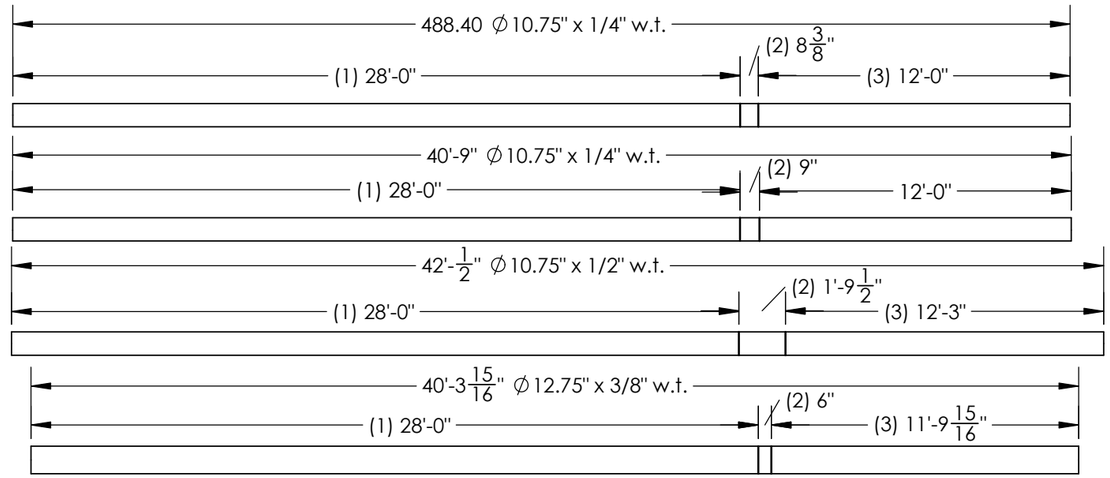

PILE CUT LENGTHS

Research Program	Test No.	OD	w.t.	D/t	Pile Lengths			
					Delivered	(1) Test Pile	(2) Material Testing	(3) Non-Test Pile
		[in]	[in]		[ft]	[ft]	[ft]	[ft]
NIST	1	10.75	0.25	43	40.70	28	0.70	12.00
	2	10.75	0.25	43	40.75	28	0.75	12.00
	3	10.75	0.5	22	42.04	28	1.79	12.25
NAVFAC	4	12.72	0.375	34	40.33	28	0.50	11.83

UC SAN DIEGO		**ESEC NORTH SOIL PIT STEEL PIPE PILES RESEARCH**	
SHEET SCALE 1:70		TITLE: PILE SEGMENT DETAILS	
DRAWN	T. RICHARDS		
CHKD		DATE: 12/11/2022	DRAWING NO.: GN -02
APPRVD		REV:	

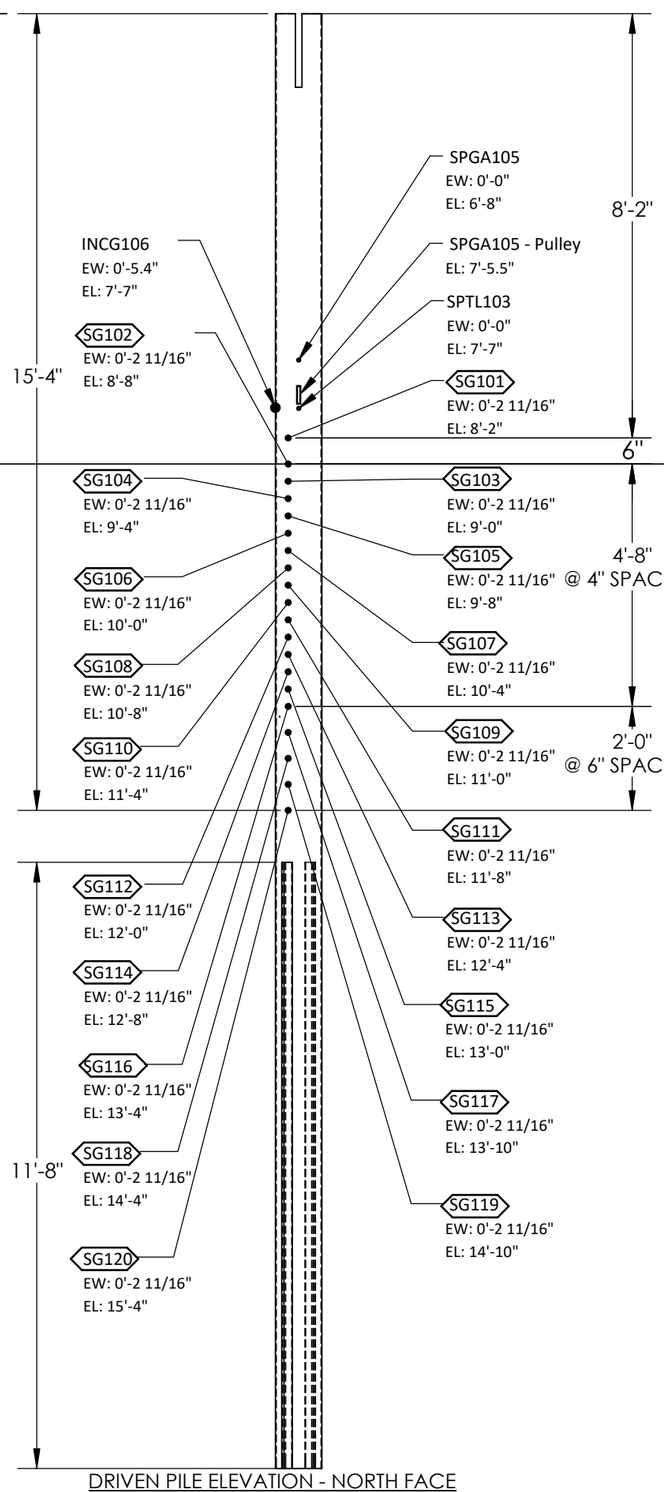

DRIVEN PILE ELEVATION - NORTH FACE

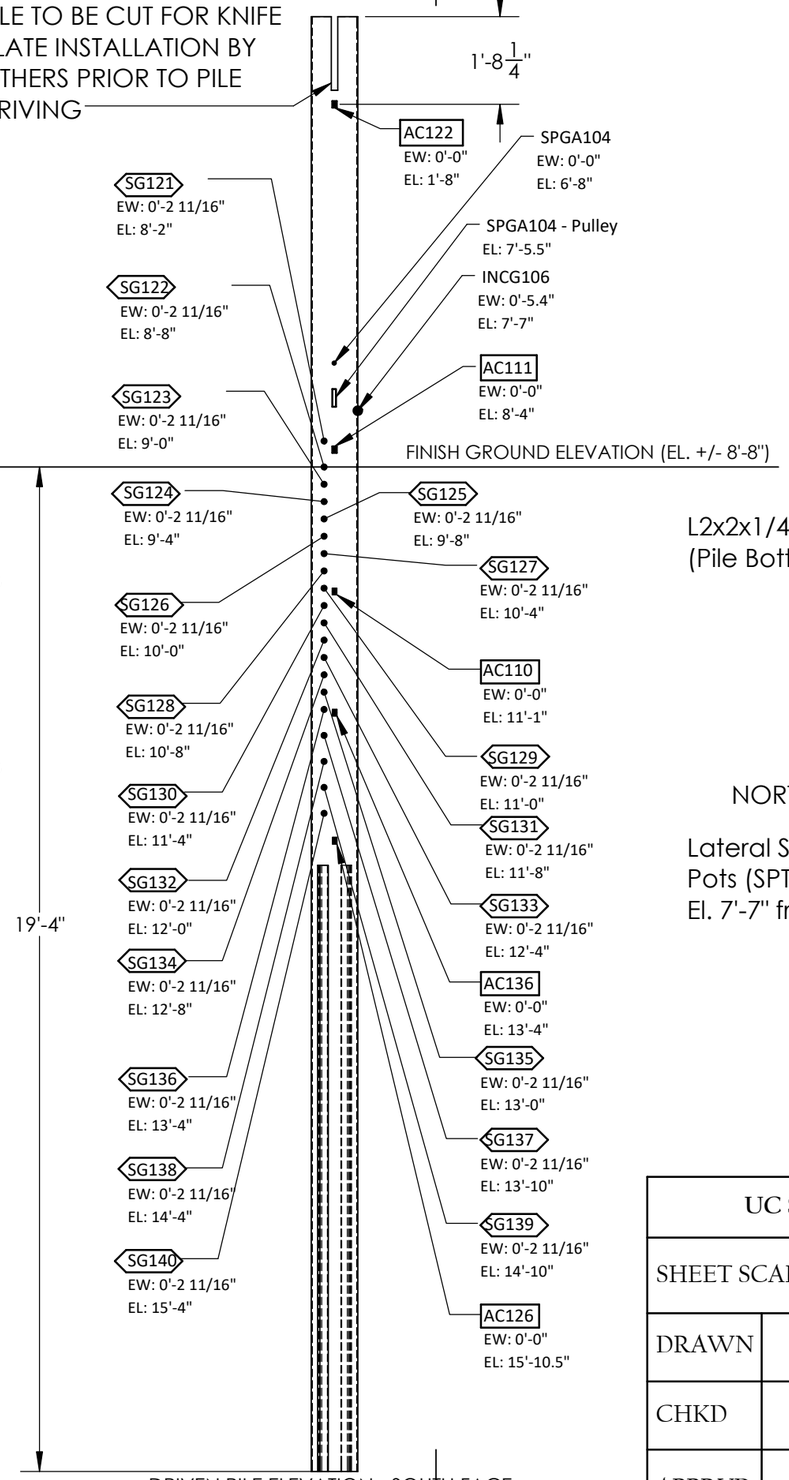

DRIVEN PILE ELEVATION - SOUTH FACE

NOTES:

1. ANGLES SHALL BE WELDED TO THE PILE AT THE FOLLOWING LOCATIONS:
   - PILE TIP TO 24-INCH ABOVE PILE TIP (CONTINUOUS WELD)
   - TACK WELDED (APPROXIMATELY 1-INCH LENGTH) EVERY 12 INCHES.
2. PLATES SHALL BE WELDED (ALL AROUND FILLET WELD) AT THE END OF BOTH ANGLES AT THE PILE TIP. SEE DETAIL 1.

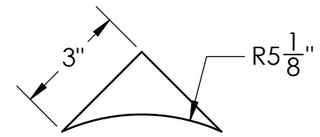

DETAIL 1

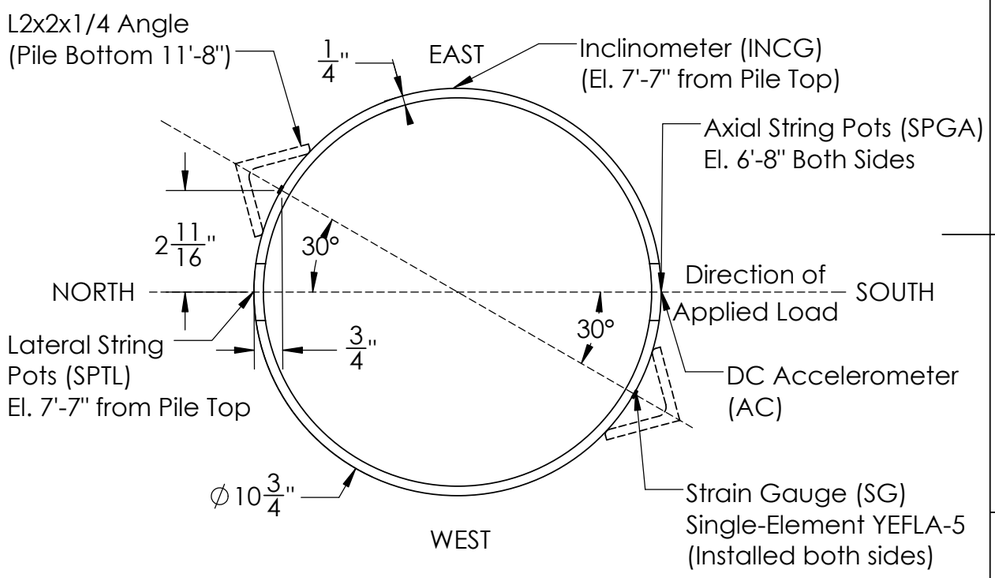

PILE CROSS-SECTION

UC SAN DIEGO		**ESEC NORTH SOIL PIT STEEL PIPE PILES RESEARCH**	
SHEET SCALE 1:35		TITLE: D/t = 43 Test Pile #1 PILE INSTRUMENTATION PLAN (FINAL)	
DRAWN	T. RICHARDS		
CHKD		DATE: 11/28/2023	DRAWING NO.: IP-02
APPRVD		REV:	

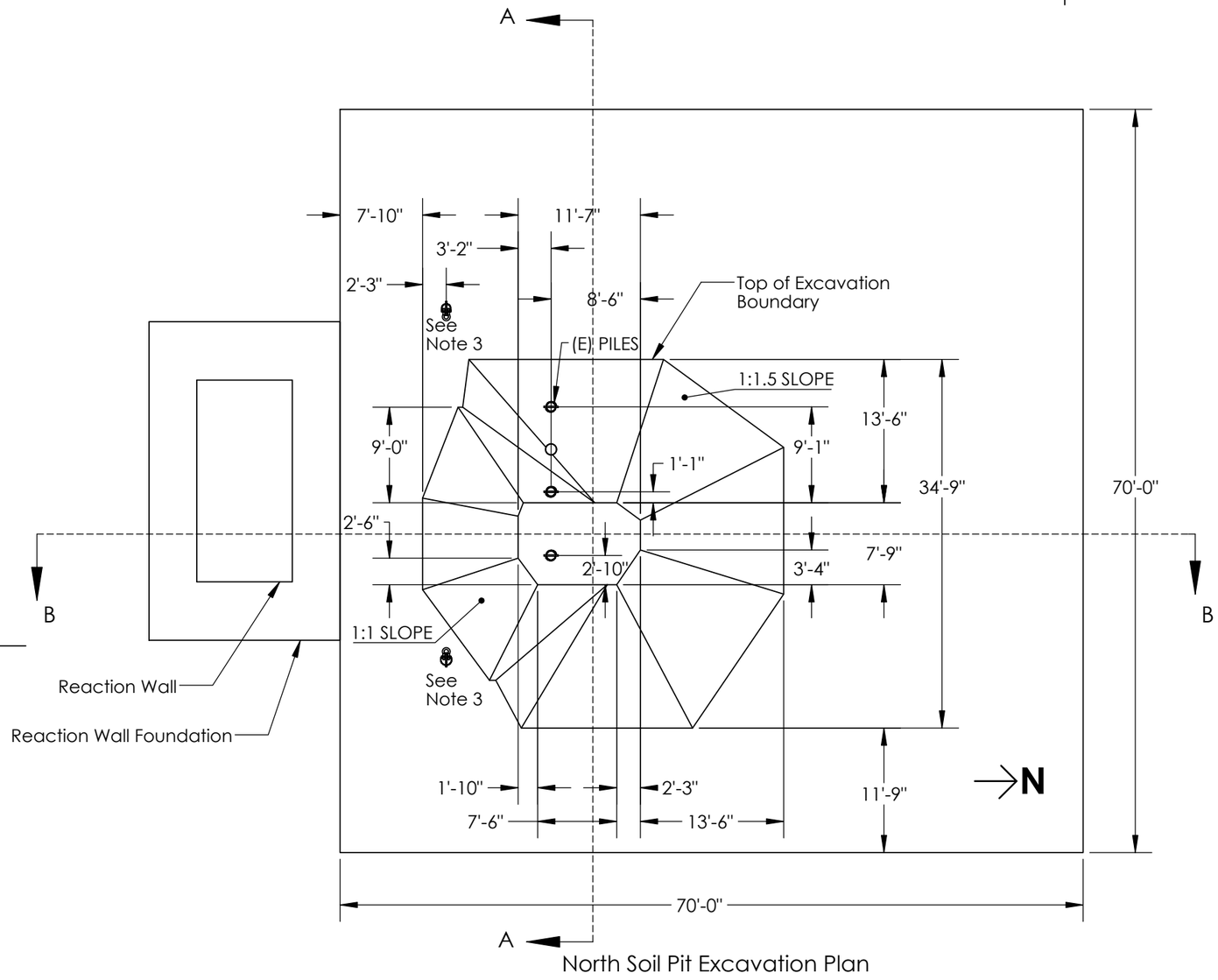

North Soil Pit Excavation Plan

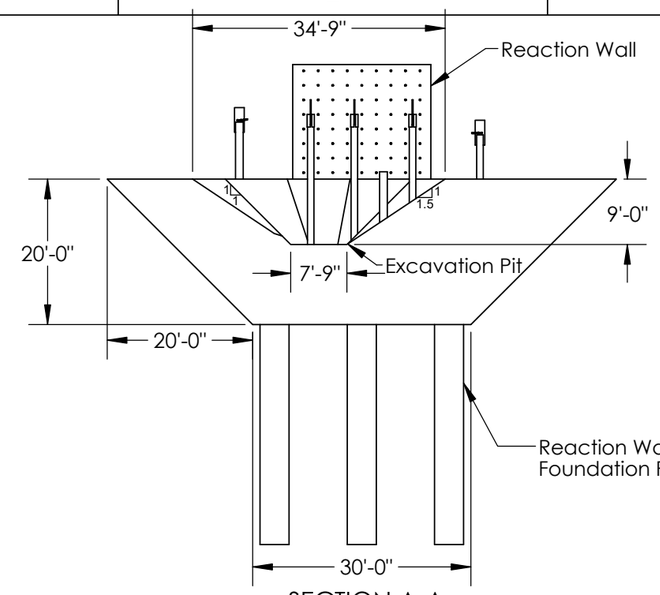

SECTION A-A

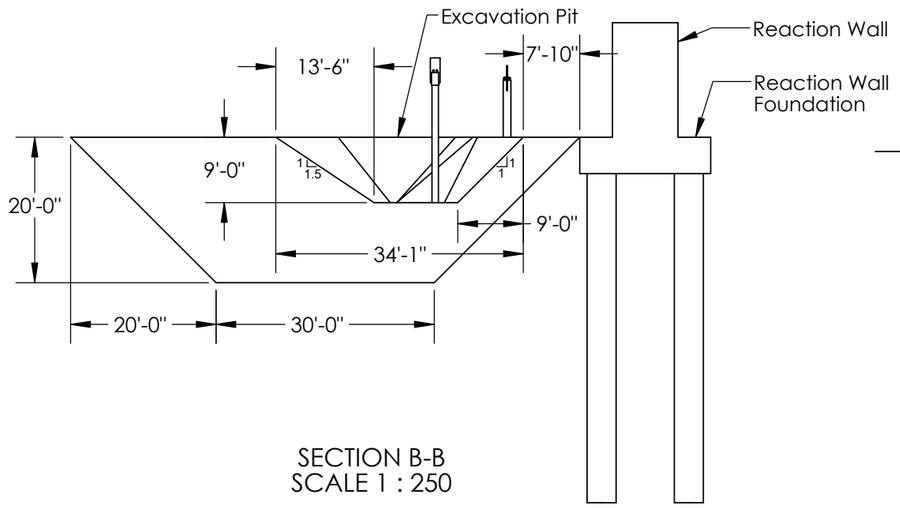

SECTION B-B
SCALE 1 : 250

NOTES:

1. In-situ excavated soils shall be used to backfill the excavation area. Therefore, soil shall be stacked and stored on-site.
2. Excavation shall have a wall slope no steeper than 1.5H:1V, with the exception of the south face to limit undermining the existing short piles which may require a steeper slope, not to exceed 1H:1V. If this can be limited, this is preferred.
3. Soil located within a 1-ft radius (clear distance) of existing piles, within the pit as shown, shall be removed without impacting the piles or causing damage. Contractor shall provide removal methodology.
4. Soil removed along the south excavation wall within 3-ft clear distance from the installed piles shall be removed by hand.
5. Soil shall be backfill after instrumentation, performed by UCSD, is complete. (Estimated time of 2-4 weeks.)
6. Backfill material shall be placed in 8-inch lifts and each lift shall be compacted to 90% of maximum dry density per ASTM D1557.
7. Compaction shall be done by hand-held compactors. Contractor shall provide methodology.
8. Not all piles are extended above finish grade as shown. Three of four piles are cut with less than 2ft exposed above finish ground.

UC SAN DIEGO		**ESEC NORTH SOIL PIT STEEL PIPE PILES RESEARCH**	
SHEET SCALE 1:150		TITLE: NORTH PIT EXCAVATION PLAN JULY 2024	
DRAWN	T. RICHARDS		
CHKD		DATE: 7/22/2024	DRAWING NO.: GN-03
APPRVD		REV:	

LARGE-SCALE STEEL PIPE PILE TESTING
UC SAN DIEGO ENGLEKIRK STRUCTURAL ENGINEERING CENTER

AXIAL LOAD TOP HAT APPARATUS

DRAWING INDEX		
No.	**SHEET**	**TITLE**
1	T-01	COVER SHEET, QUANTITIES & GENERAL NOTES
2	S-01	AXIAL LOAD APPARATUS ASSEMBLY
3	S-02	HSS PIPE JACKET
4	S-03	HSS CROSS BEAM - 1
5	S-04	HSS CROSS BEAM - 2
6	S-05	HSS CROSS BEAM - 3
7	S-06	HSS CROSS BEAM -4
8	S-07	ACTUATOR PLATE
9	S-08	ACTUATOR PLATE CONNECTOR
10	S-09	STEEL CAP PLATE
11	S-10	KNIFE PLATE
12	S-11	12" DIA. SEMI-HSS PIPE SLEEVE
13	S-12	14" DIA. SEMI-HSS PIPE SLEEVE

MATERIAL TAKEOFF				
No.	**COMPONENT**	**SHEET REFERENCE**	**QUANTITY (EA)**	**EST. WEIGHT (LBS)**
1	18" DIA x 3/4" HSS	S-02	1	473
2	12 x 8 x 5/8" HSS	S-03	2	725
3	12 x 8 x 5/8" HSS	S-04	2	864
4	8 x 8 x 5/8" HSS	S-05	4	148
5	8 x 8 x 5/8" HSS	S-06	4	87
6	16" SQ x 2" PLATE	S-07	1	139
7	8 x 8 x 1/2" HSS	S-08	1	22.5
8	18" DIA x 5/8" PLATE	S-09	1	36
9	16" x 41" x 3/2" PLATE	S-10	6	1639
10	12" DIA x 3/8" SEMI-HSS	S-11	6	142
11	14" DIA x 3/8" SEMI-HSS	S-12	2	57
12	1.25" DIA. x 9" LONG THREADED RODS	S-01	12	33
13	HEAVY HEX NUTS (FOR RODS)	S-01	36	29

GENERAL NOTES:

1. ALL ROUND AND RECTANGULAR HSS MEMBERS SHALL BE IN ACCORDANCE WITH ASTM 500 GRADE B, UNLESS OTHERWISE NOTED.
2. PLATES SHALL BE IN ACCORDANCE WITH ASTM A572 GRADE 50.
3. THREADED RODS SHALL BE ASTM F1554 GRADE 55 OR ASTM A307 GRADE B.
4. HARDWARE, NOT OTHERWISE NOTED, SHALL BE ASTM A563.
5. THREADED RODS SHALL BE INSTALLED IN THE FIELD (BY OTHERS).
6. THE HEAVY HEX NUTS (12) LOCATED AT THE EXTERIOR FACE OF THE 18" DIAMETER PIPE SHALL BE SHOP WELDED AS SHOWN IN THE DRAWINGS ON SHEET S-01.
7. KNIFE PLATE AND SEMI-HSS SLEEVES WILL BE INSTALLED IN THE FIELD (BY OTHERS).
8. MINIMUM HOLE DIAMETERS FOR BOLTS SHALL BE IN ACCORDANCE WITH AISC DESIGN SPECIFICATIONS.
9. ALL HOLES SHALL BE CUT IN THE SHOP TO THE DIMENSIONS SHOWN. FABRICATOR SHALL CONTACT THE DESIGNER/ENGINEER IF DIMENSIONS SHOWN ARE INADEQUATE.
10. ALL MATERIAL LISTED IN THE MATERIAL TAKEOFF TABLE SHALL BE INCLUDED IN THE DELIVERY FROM THE MANUFACTURER.
11. ALL WELDING SHALL CONFORM TO THE STRUCTURAL WELDING CODE OF AWS D1-1, LATEST REVISIONS. WELDING ELECTRODES SHALL BE E70XX.
12. ENTIRE AXIAL LOAD APPARATUS AND ITS PARTS SHOWN ON SHEET S-01 SHALL BE COATED WITH FABRICATOR'S STANDARD SHOP PRIMER AND PAINTED WHITE. BOTH SHALL HAVE A MINIMUM APPLIED FILM THICKNESS OF 3MILS.
13. MATERIAL SHALL BE REUSED WHEN POSSIBLE. (I.E. 8X8HSS SHEETS S-05 AND S-07 SHALL BE FABRICATED FROM THE SAME MEMBER.)

UC SAN DIEGO		ESEC NORTH SOIL PIT STEEL PIPE PILES RESEARCH	
SHEET SCALE 1:32		TITLE: COVER SHEET, QUANTITES & NOTES	
DRAWN	T. RICHARDS		
CHKD		DATE: 12/19/2022	DRAWING NO.: T-01
APPRVD		REV:	

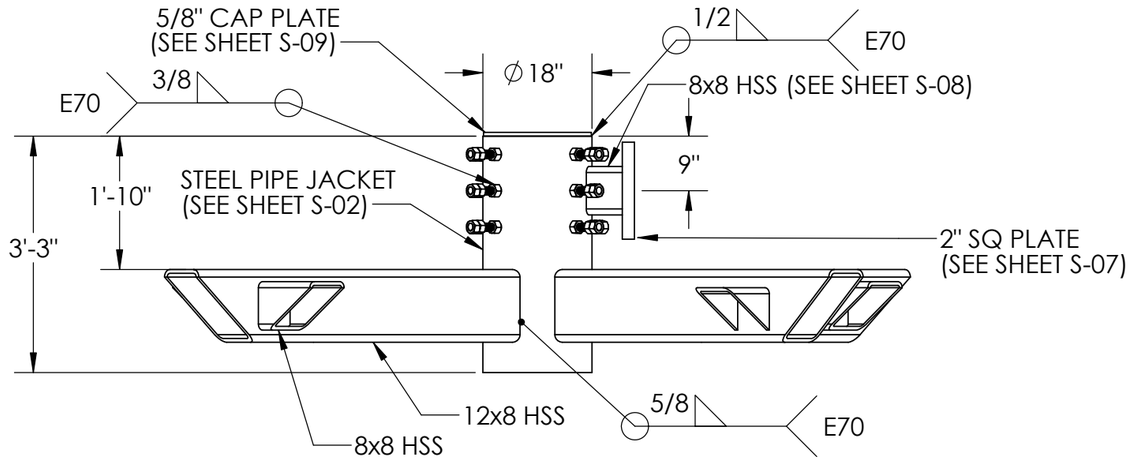

ELEVATION

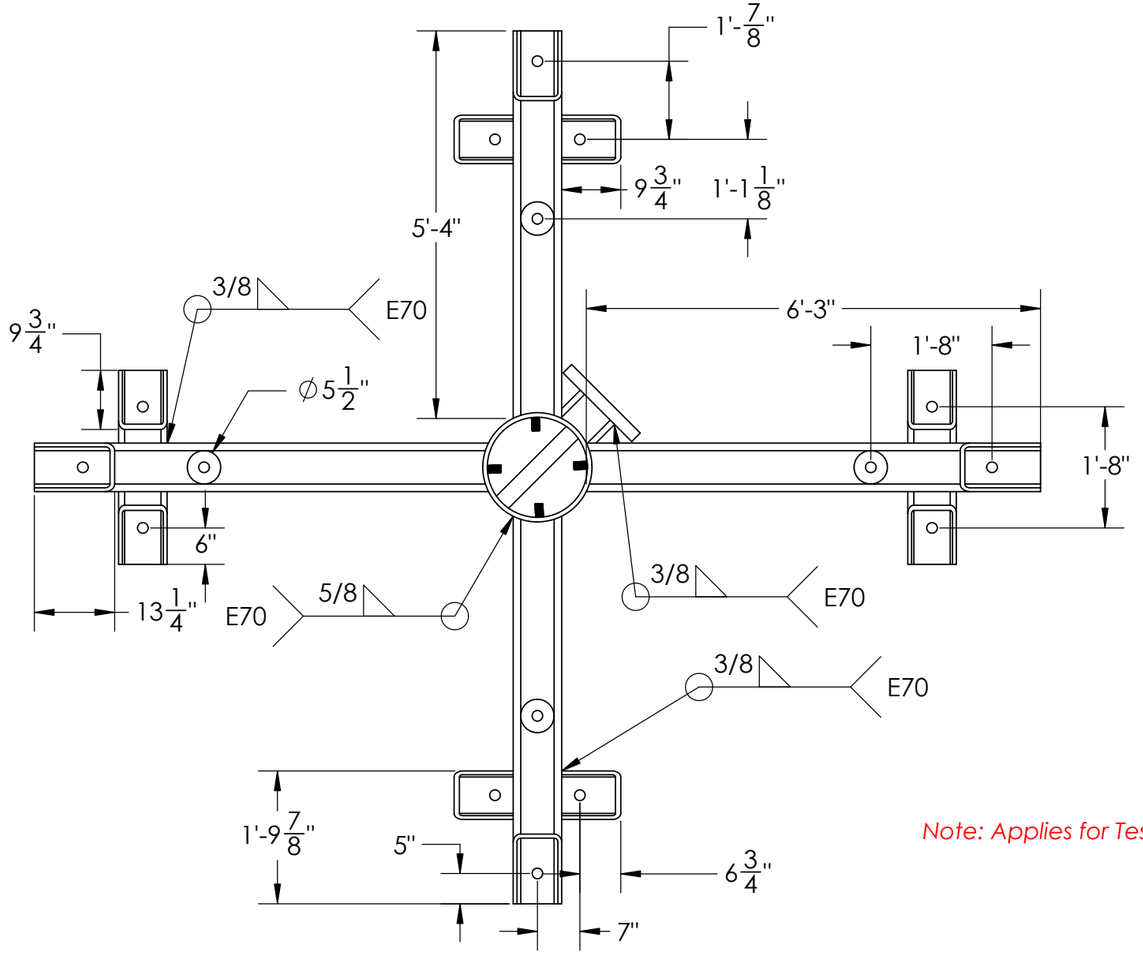

BOTTOM PLAN VIEW

Note: Applies for Test 1 Only.

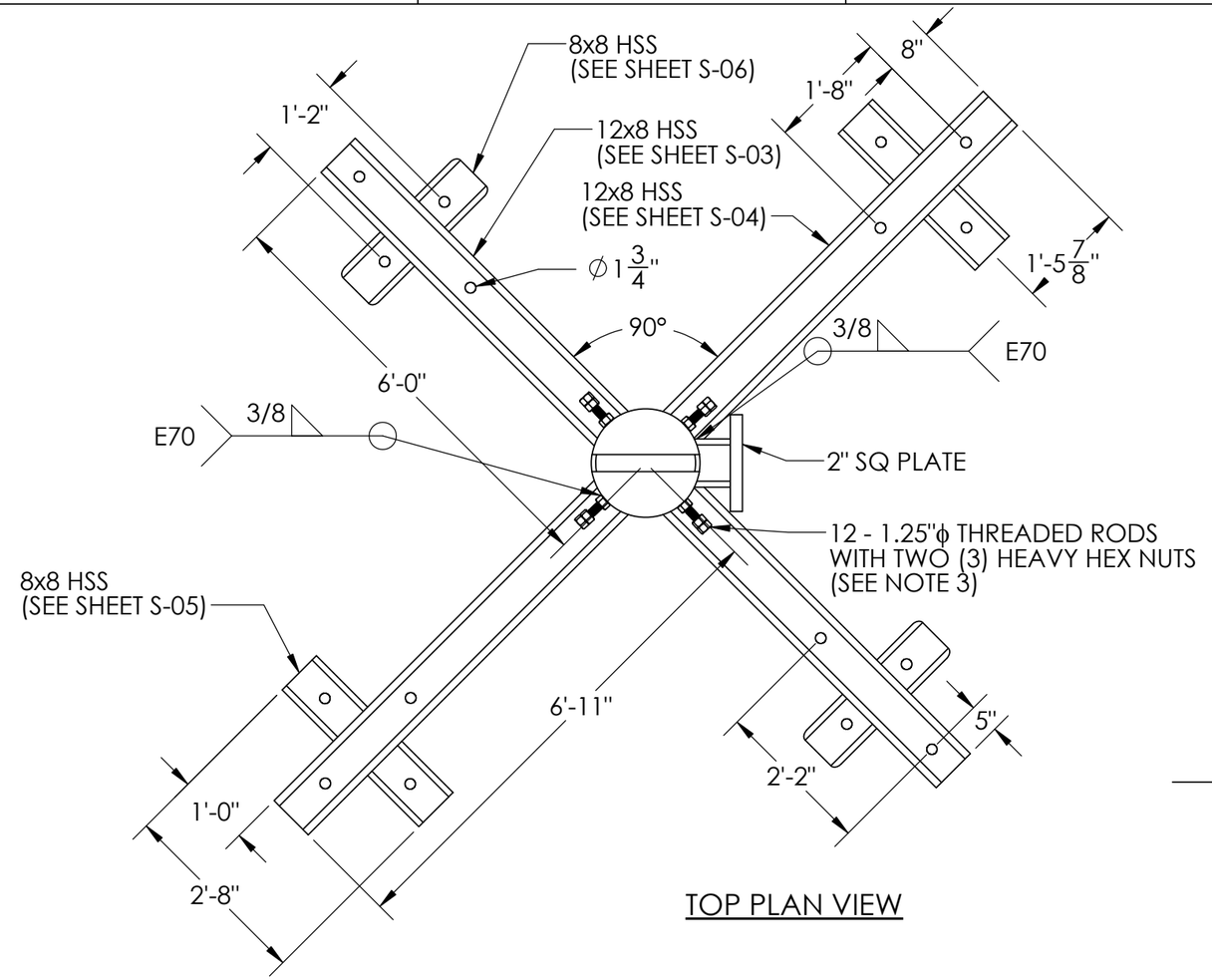

TOP PLAN VIEW

NOTES:

1. REFER TO T-01 FOR GENERAL NOTES.
2. THE WINGS OF THE CANTILEVER BEAMS SHALL BE FABRICATED FROM A SINGLE 8X8 HSS MEMBER. THE CUT-OUT ON S-05 IS THE SECTION OF S-13.
3. THREADED RODS SHALL BE CENTERED IN-LINE WITH THE CENTER AXIS OF THE 12X8 HSS MEMBERS. (SPACED 90-DEG FROM ADJACENT RODS.)

UC SAN DIEGO		ESEC NORTH SOIL PIT STEEL PIPE PILES RESEARCH	
SHEET SCALE 1:25		TITLE: AXIAL LOAD APPARATUS ASSEMBLY	
DRAWN	T. RICHARDS		
CHKD		DATE: 12/19/2022	DRAWING NO.: S-01
APPRVD		REV:	

Note: Applies for Test 2, 3 and 4 Only.

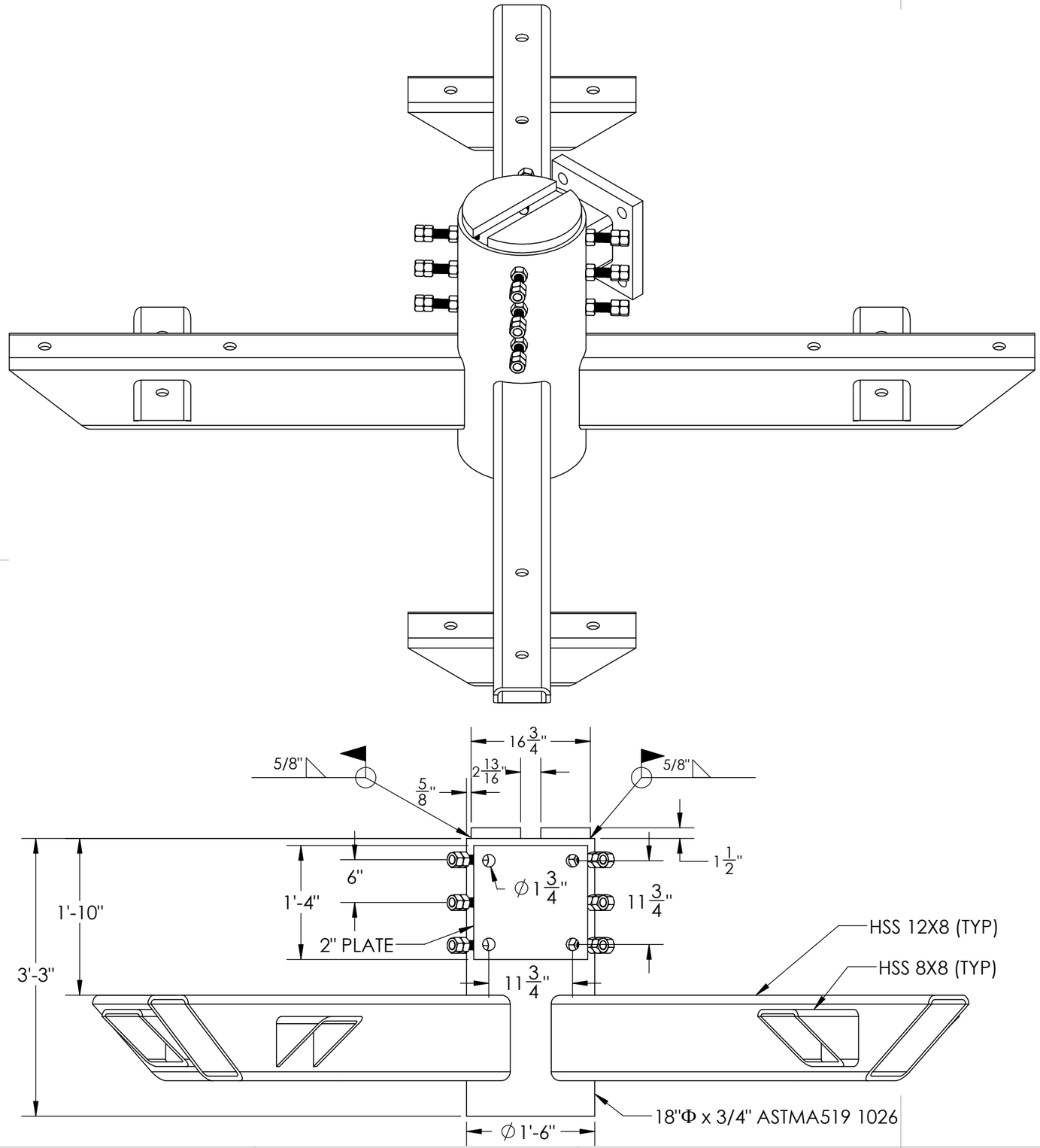

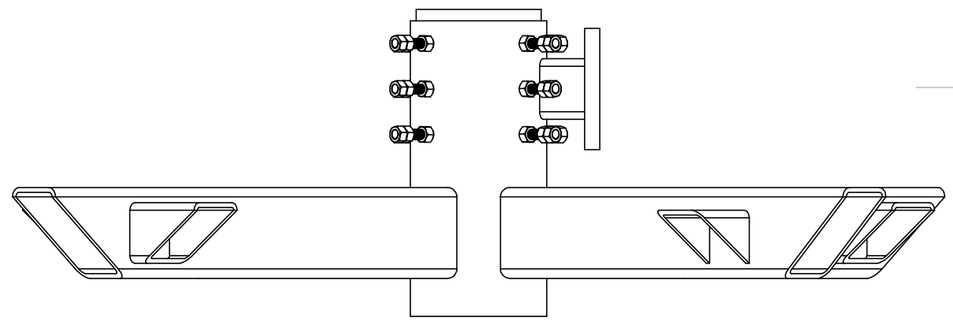

NOTES:

1. REFER TO T-01 FOR GENERAL NOTES.
2. THE WINGS OF THE CANTILEVER BEAMS SHALL BE FABRICATED FROM A SINGLE 8X8 HSS MEMBER. THE CUT-OUT ON S-05 IS THE SECTION OF S-13.
3. THREADED RODS SHALL BE CENTERED IN-LINE WITH THE CENTER AXIS OF THE 12X8 HSS MEMBERS. (SPACED 90-DEG FROM ADJACENT RODS.)

UC SAN DIEGO		ESEC NORTH SOIL PIT STEEL PIPE PILES RESEARCH	
SHEET SCALE 1:16		TITLE: AXIAL LOAD APPARATUS ASSEMBLY	
DRAWN	T. RICHARDS		
CHKD		DATE: 6/12/2024	DRAWING NO.: S-01
APPRVD		REV:	

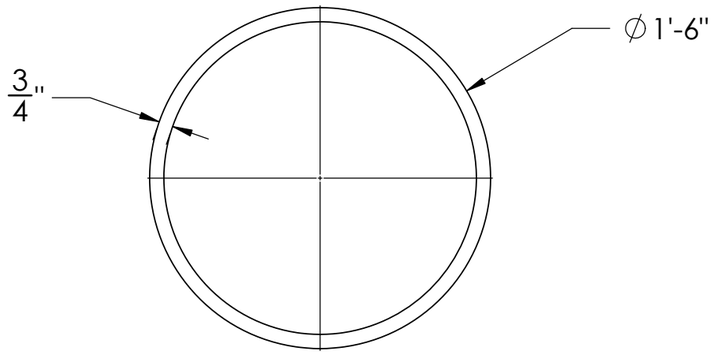

TYPICAL CROSS-SECTION

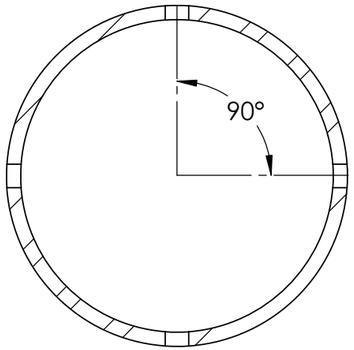

SECTION C-C

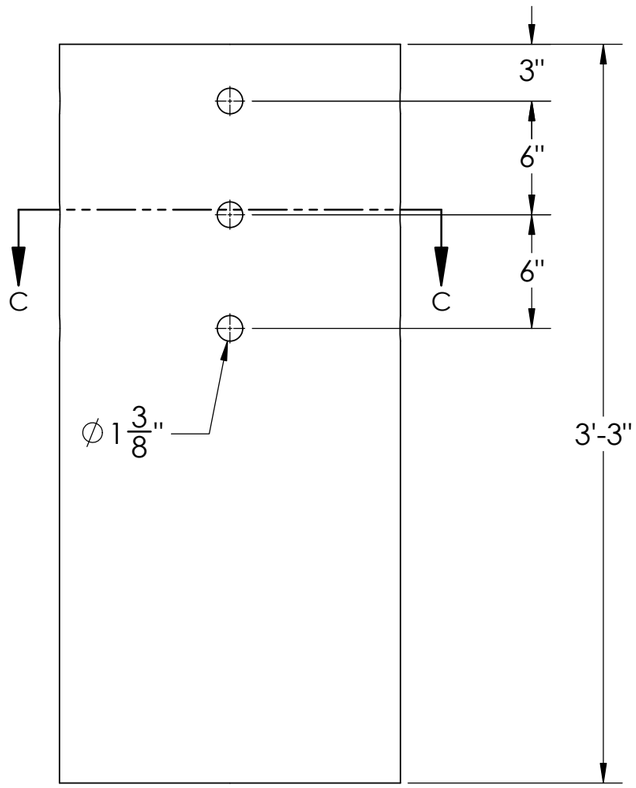

ELEVATION

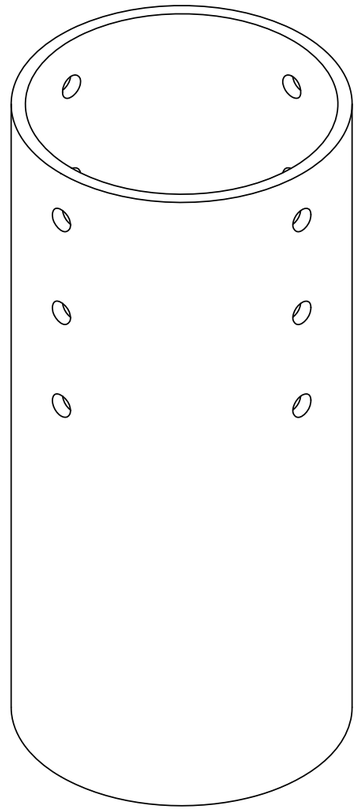

3D ELEVATION

NOTES:

1. REFER TO NOTES ON SHEET S-01.
2. PER EMAIL CONVERSATION DATED 12/19/22, ENGINEER TAKES NO EXCEPTIONS TO PIPE SHOWN ON S-02 TO BE MANUFACTURED IN ACCORDANCE TO ASTM A519 1026 IN LIEU OF ASTM A500 GRADE B.

UC SAN DIEGO		ESEC NORTH SOIL PIT STEEL PIPE PILES RESEARCH	
SHEET SCALE 1:8		TITLE: HSS PIPE JACKET	
DRAWN	T. RICHARDS		
CHKD		DATE: 12/19/2022	DRAWING NO.: S-02
APPRVD		REV:	

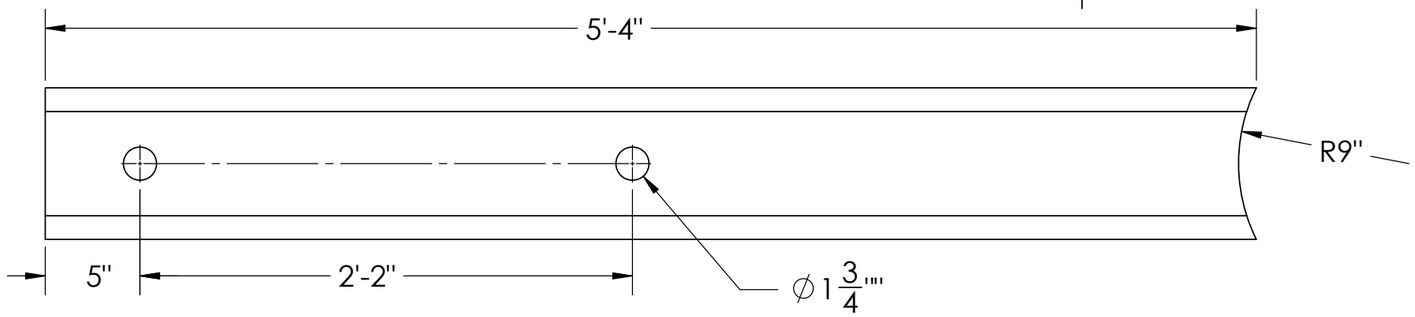

TOP PLAN VIEW

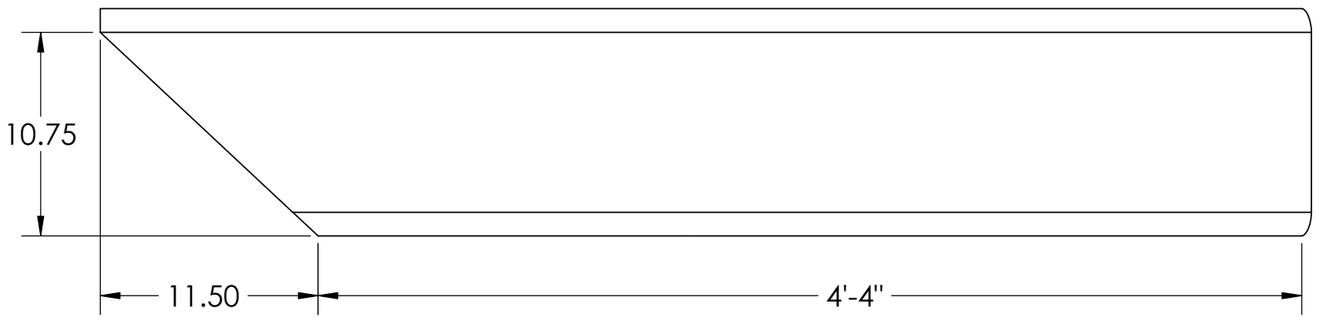

ELEVATION

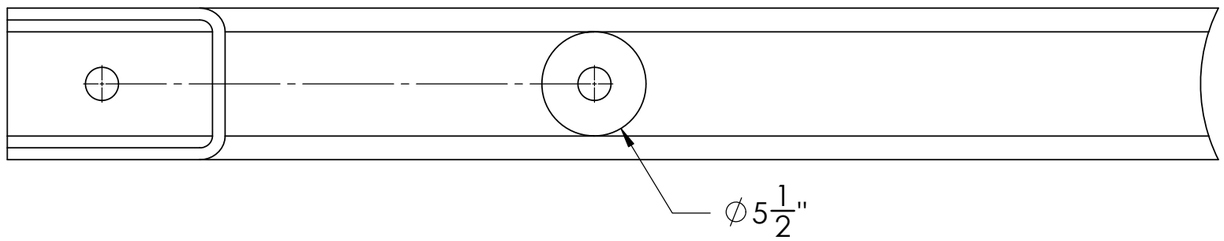

BOTTOM PLAN VIEW

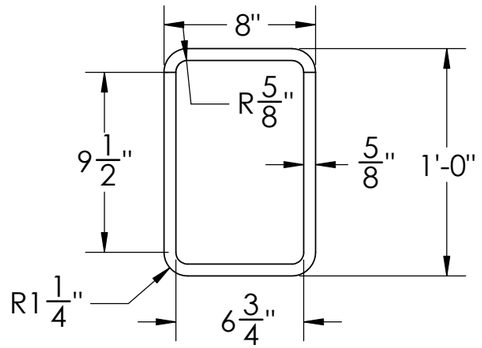

CROSS-SECTION

NOTES:

1. REFER TO NOTES ON SHEET S-01.

UC SAN DIEGO		**ESEC NORTH SOIL PIT STEEL PIPE PILES RESEARCH**	
SHEET SCALE 1:8		TITLE: HSS CROSS BEAM -1	
DRAWN	T. RICHARDS		
CHKD		DATE: 12/19/2022	DRAWING NO.: S-03
APPRVD		REV:	

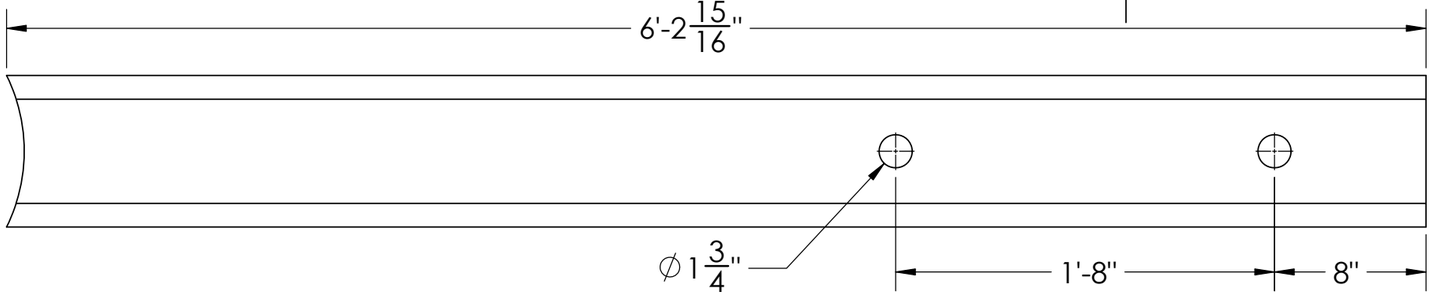

TOP PLAN VIEW

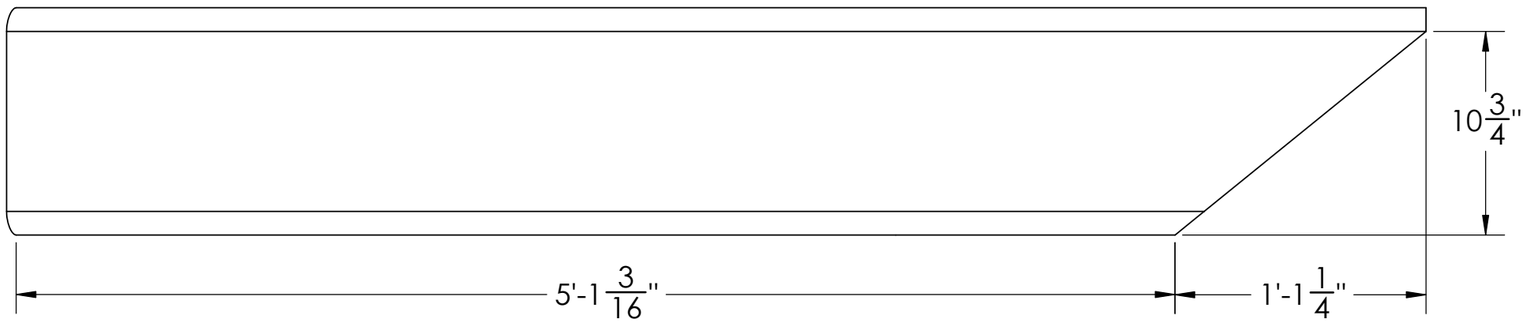

ELEVATION

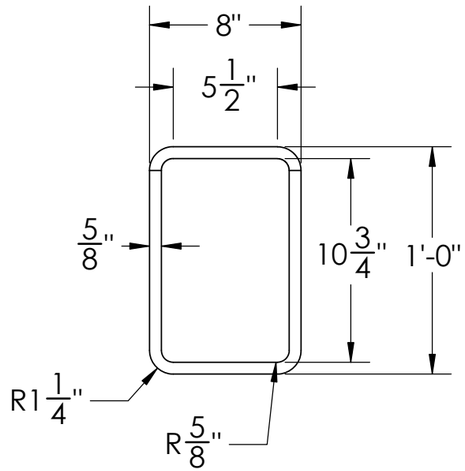

CROSS-SECTION

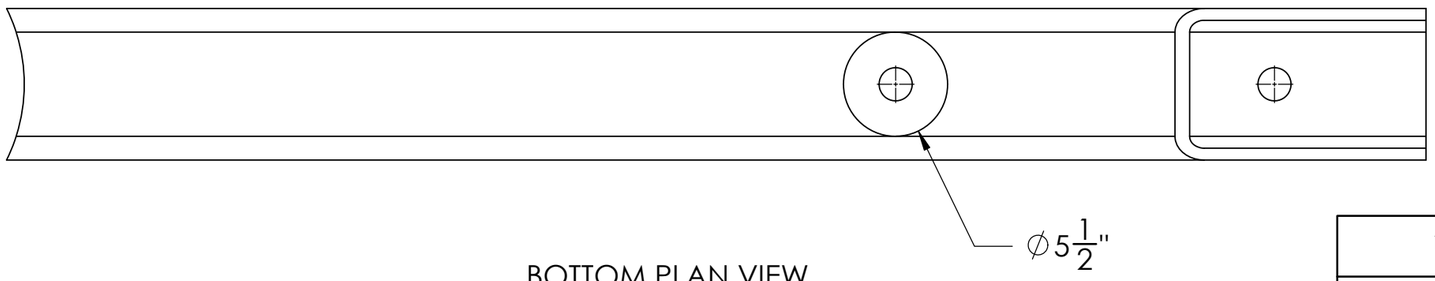

BOTTOM PLAN VIEW

NOTES:

1. REFER TO NOTES ON SHEET S-01.

UC SAN DIEGO		**ESEC NORTH SOIL PIT STEEL PIPE PILES RESEARCH**	
SHEET SCALE 1:8		TITLE: HSS CROSS BEAM - 2	
DRAWN	T. RICHARDS		
CHKD		DATE: 12/19/2022	DRAWING NO.: S-04
APPRVD		REV:	

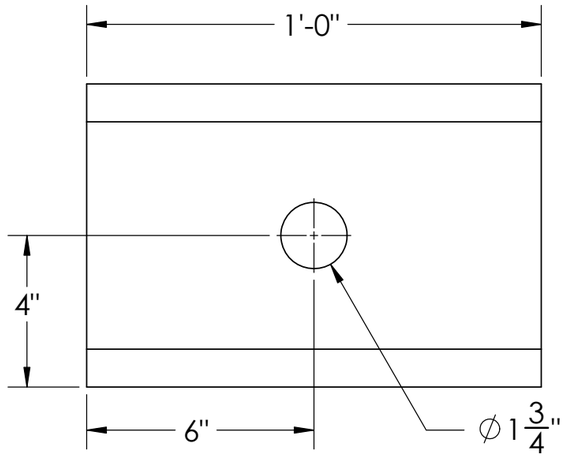

TOP PLAN VIEW

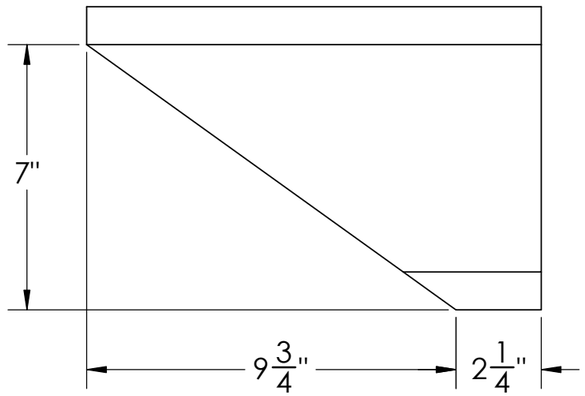

ELEVATION

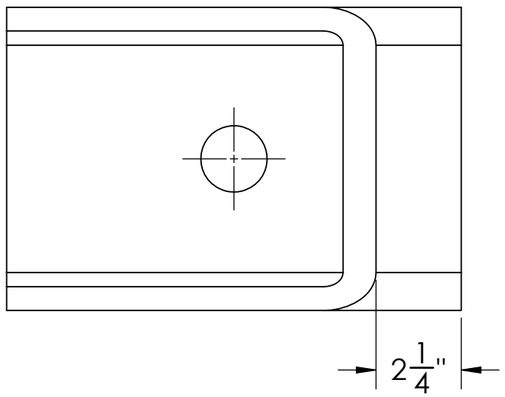

BOTTOM PLAN VIEW

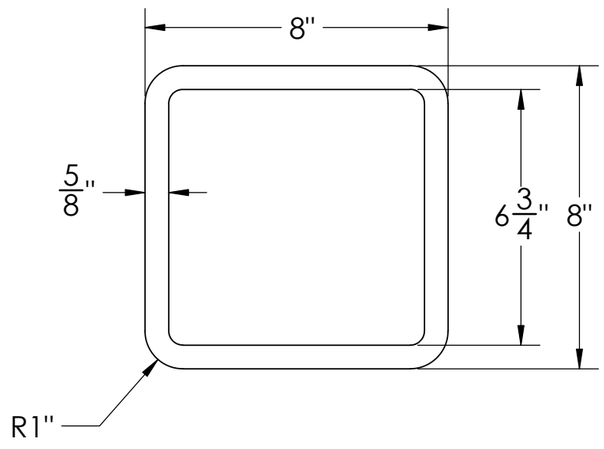

CROSS-SECTION

NOTES:

1. REFER TO NOTES ON SHEET S-01.

UC SAN DIEGO		**ESEC NORTH SOIL PIT STEEL PIPE PILES RESEARCH**	
SHEET SCALE 1:4		TITLE: HSS CROSS BEAM - 3	
DRAWN	T. RICHARDS		
CHKD		DATE: 12/19/2022	DRAWING NO.: S-05
APPRVD		REV:	

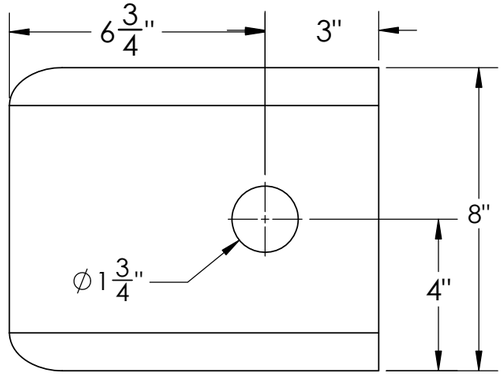

TOP PLAN VIEW

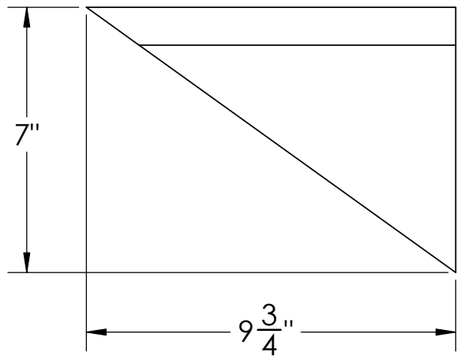

ELEVATION

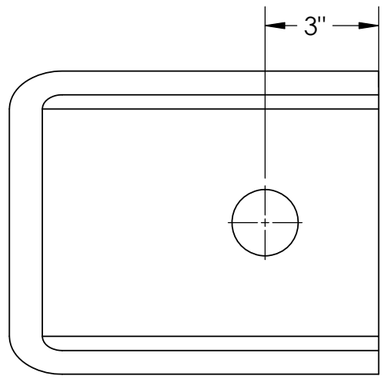

BOTTOM PLAN VIEW

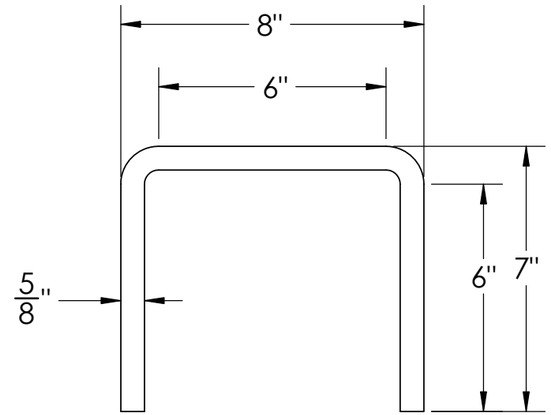

CROSS-SECTION

NOTES:

1. REFER TO NOTES ON SHEET S-01.

UC SAN DIEGO		ESEC NORTH SOIL PIT STEEL PIPE PILES RESEARCH	
SHEET SCALE 1:4		TITLE: HSS CROSS BEAM - 4	
DRAWN	T. RICHARDS		
CHKD		DATE: 12/19/2022	DRAWING NO.: S-06
APPRVD		REV:	

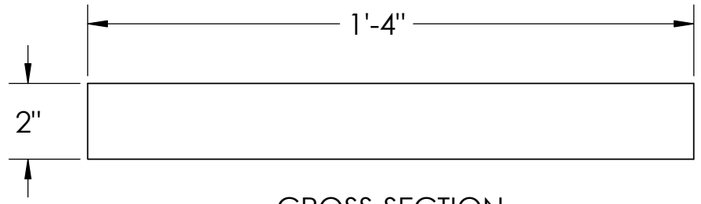

CROSS-SECTION

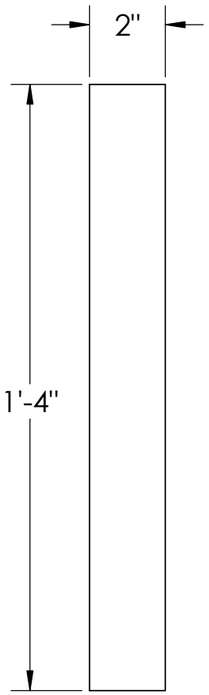

ELEVATION

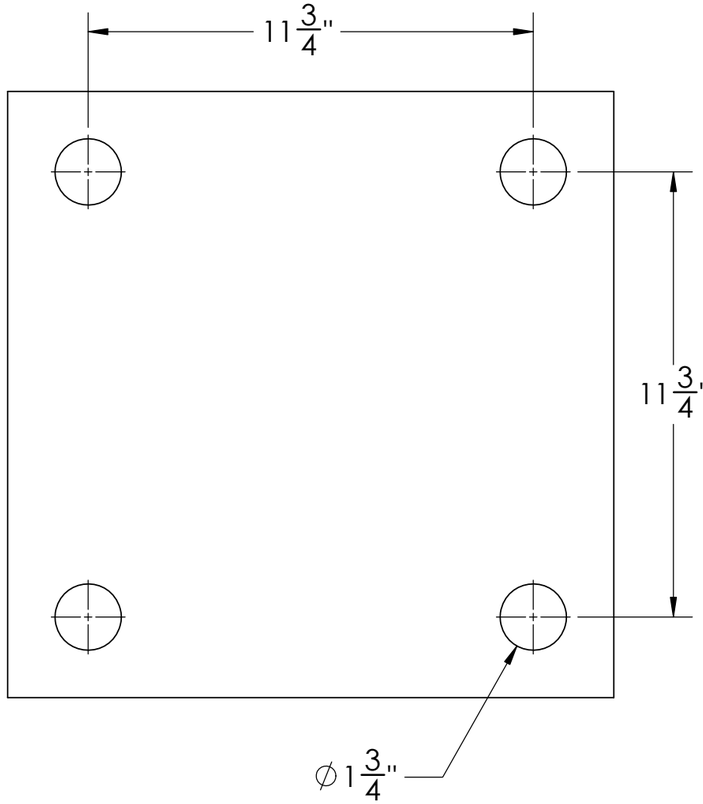

PLAN VIEW

NOTES:
1. REFER TO NOTES ON SHEET S-01.

UC SAN DIEGO		**ESEC NORTH SOIL PIT STEEL PIPE PILES RESEARCH**	
SHEET SCALE 1:4		TITLE: ACTUATOR PLATE	
DRAWN	T. RICHARDS		
CHKD		DATE: 12/19/2022	DRAWING NO.: S-07
APPRVD		REV:	

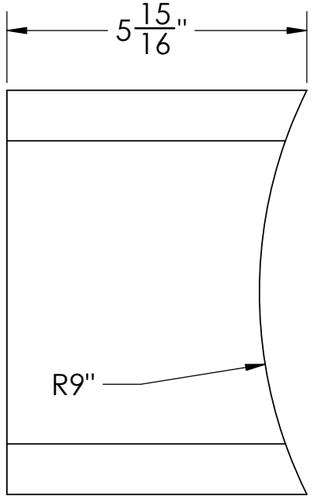

PLAN VIEW

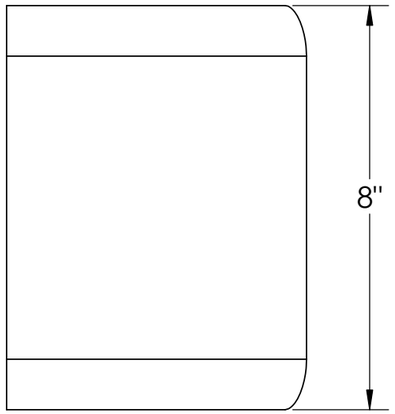

ELEVATION

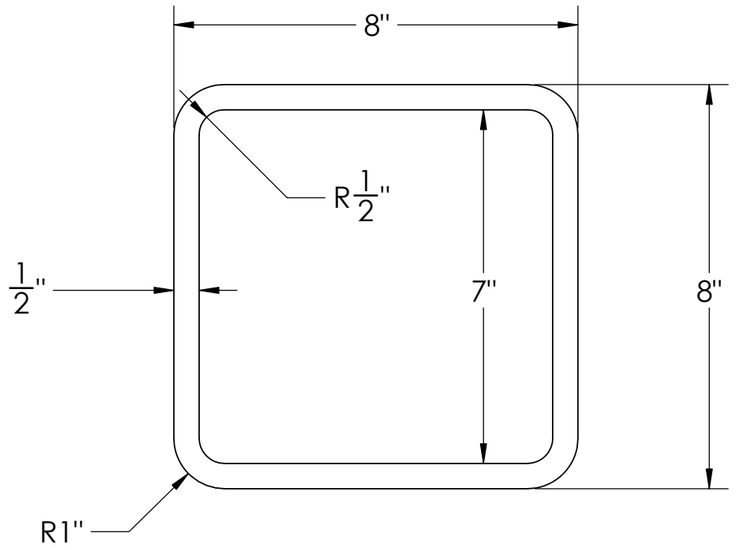

CROSS-SECTION

NOTES:

1. REFER TO NOTES ON SHEET S-01.

UC SAN DIEGO		ESEC NORTH SOIL PIT STEEL PIPE PILES RESEARCH	
SHEET SCALE 1:3		TITLE: ACTUATOR PLATE CONNECTOR	
DRAWN	T. RICHARDS		
CHKD		DATE: 12/19/2022	DRAWING NO.: S-08
APPRVD		REV:	

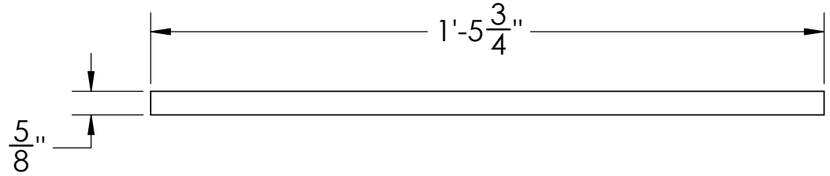

CROSS-SECTION

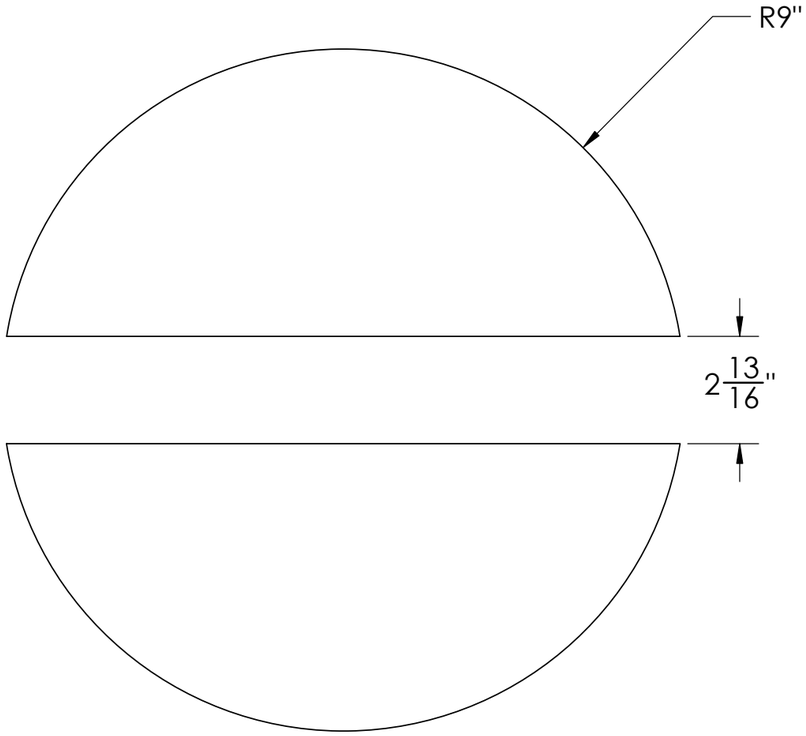

TOP PLAN VIEW

NOTES:

1. REFER TO NOTES ON SHEET S-01.

UC SAN DIEGO		**ESEC NORTH SOIL PIT STEEL PIPE PILES RESEARCH**	
SHEET SCALE 1:4		TITLE: STEEL CAP PLATE	
DRAWN	T. RICHARDS		
CHKD		DATE: 12/19/2022	DRAWING NO.: S-09
APPRVD		REV:	

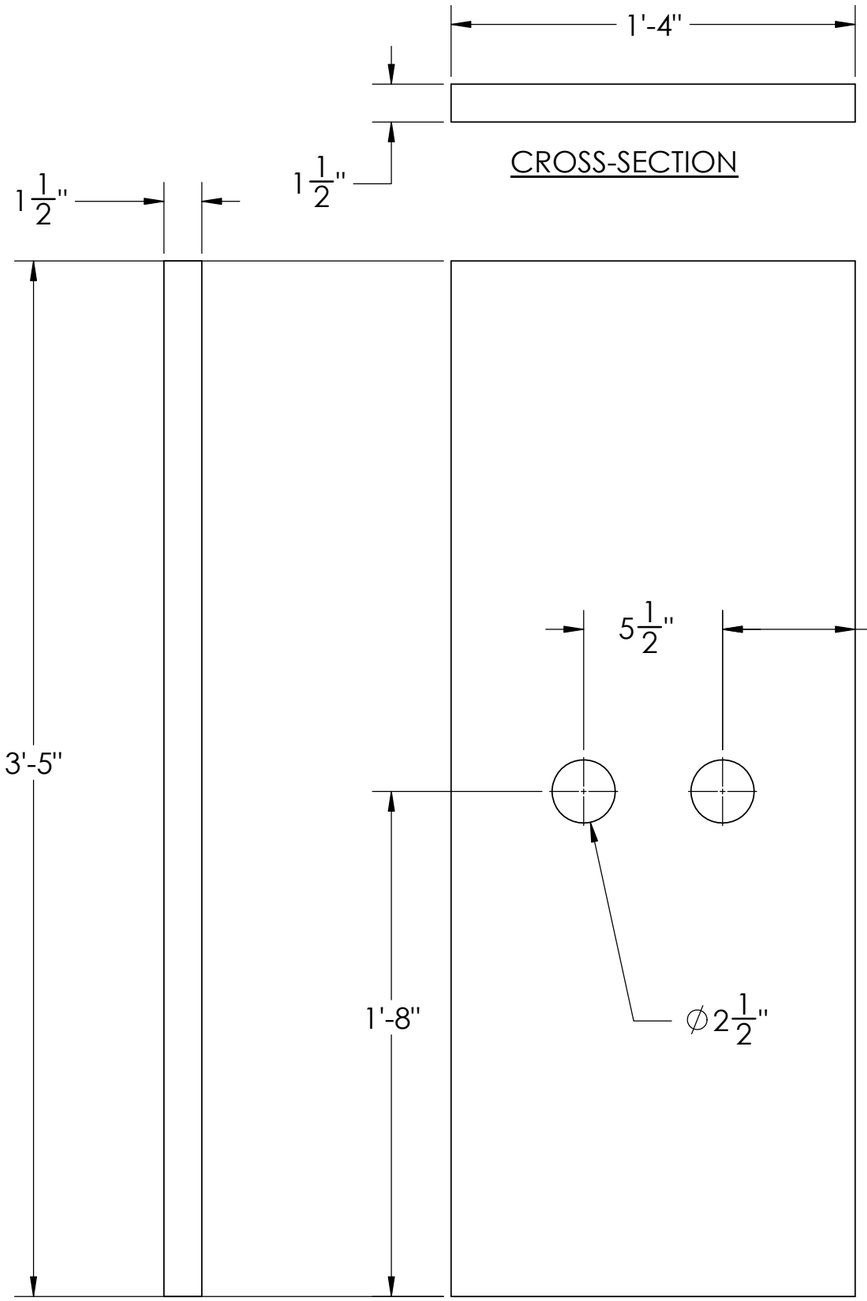

SIDE VIEW

ELEVATION

NOTES:
1. REFER TO NOTES ON SHEET S-01.

UC SAN DIEGO		**ESEC NORTH SOIL PIT STEEL PIPE PILES RESEARCH**	
SHEET SCALE 1:6		TITLE: KNIFE PLATE	
DRAWN	T. RICHARDS		
CHKD		DATE: 12/19/2022	DRAWING NO.: S-10
APPRVD		REV:	

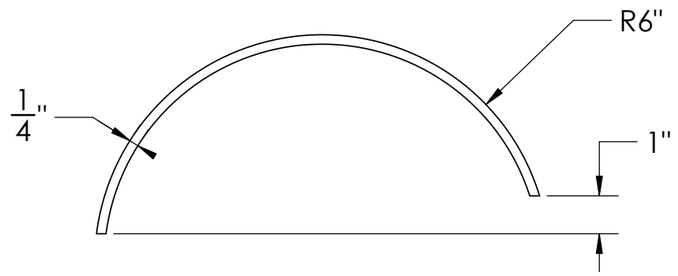

CROSS-SECTION

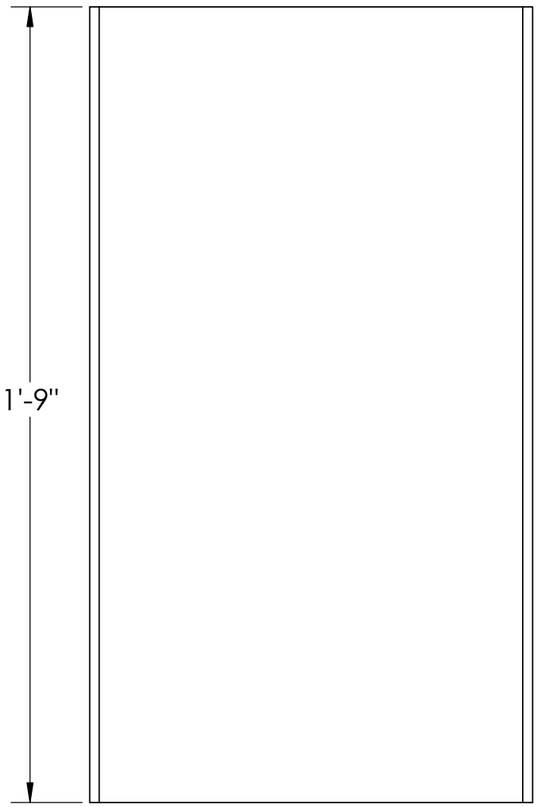

ELEVATION

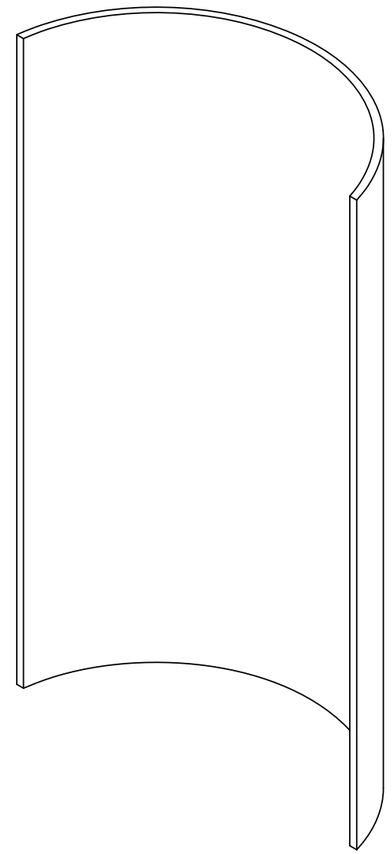

3D ELEVATION

NOTES:

1. REFER TO NOTES ON SHEET S-01.

UC SAN DIEGO		**ESEC NORTH SOIL PIT STEEL PIPE PILES RESEARCH**	
SHEET SCALE 1:4		TITLE: 12" DIA. SEMI-HSS PIPE SLEEVE	
DRAWN	T. RICHARDS		
CHKD		DATE: 12/19/2022	DRAWING NO.: S-11
APPRVD		REV:	

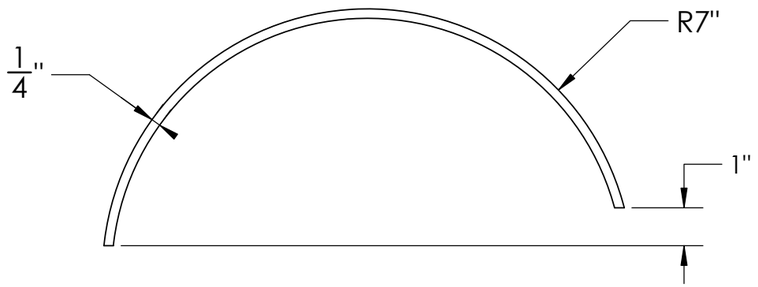

CROSS-SECTION

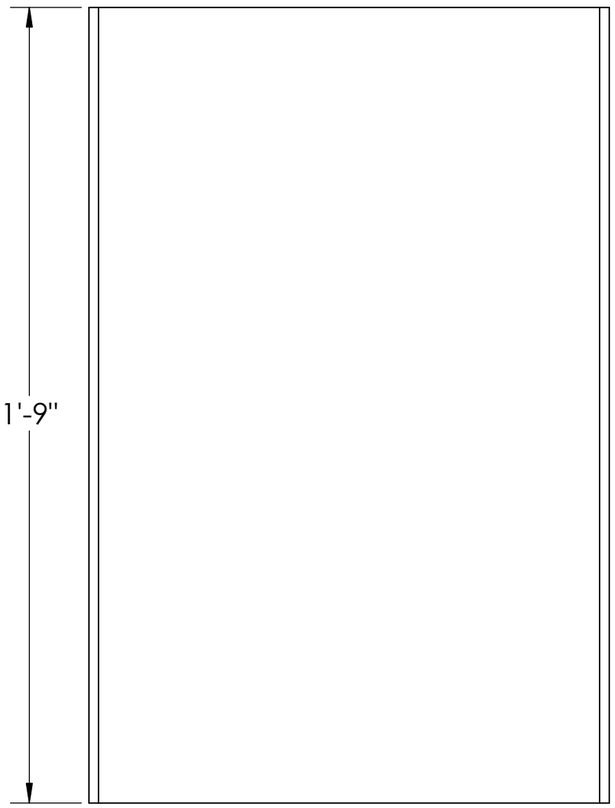

ELEVATION

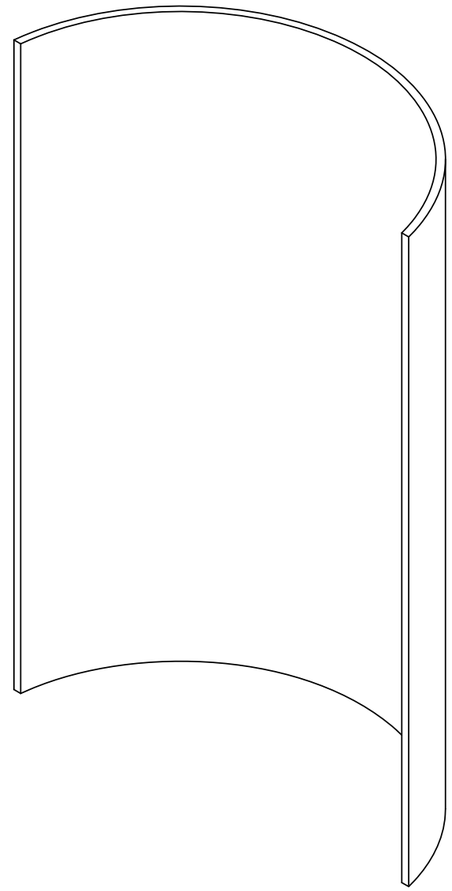

3D ELEVATION

NOTES:

1. REFER TO NOTES ON SHEET S-01.

UC SAN DIEGO		**ESEC NORTH SOIL PIT STEEL PIPE PILES RESEARCH**	
SHEET SCALE 1:4		TITLE: 14" DIA. SEMI-HSS PIPE SLEEVE	
DRAWN	T. RICHARDS		
CHKD		DATE: 12/19/2022	DRAWING NO.: S-12
APPRVD		REV:	

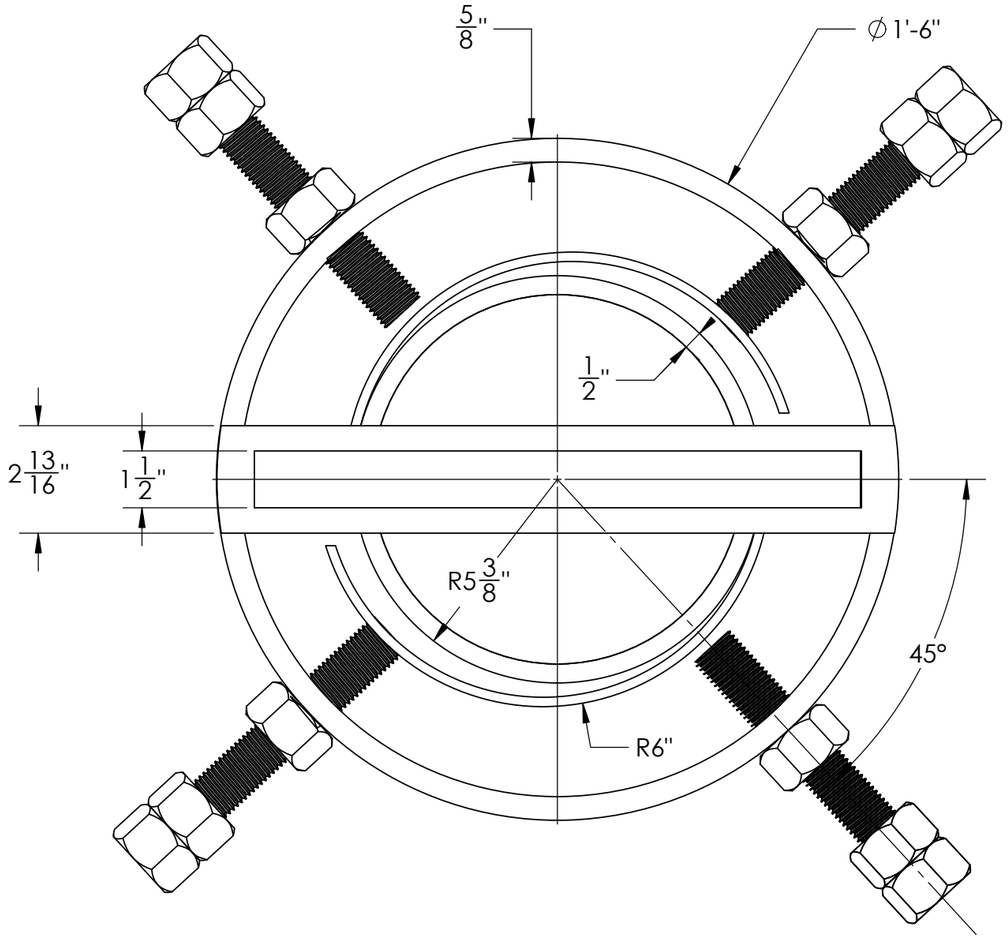

UC SAN DIEGO		ESEC NORTH SOIL PIT STEEL PIPE PILES RESEARCH	
SHEET SCALE 1:4		TITLE: TOP OF PILE CONNECTION DETIAL	
DRAWN	T. RICHARDS		
CHKD		DATE: 12/6/2022	DRAWING NO.: SD-01
APPRVD		REV:	

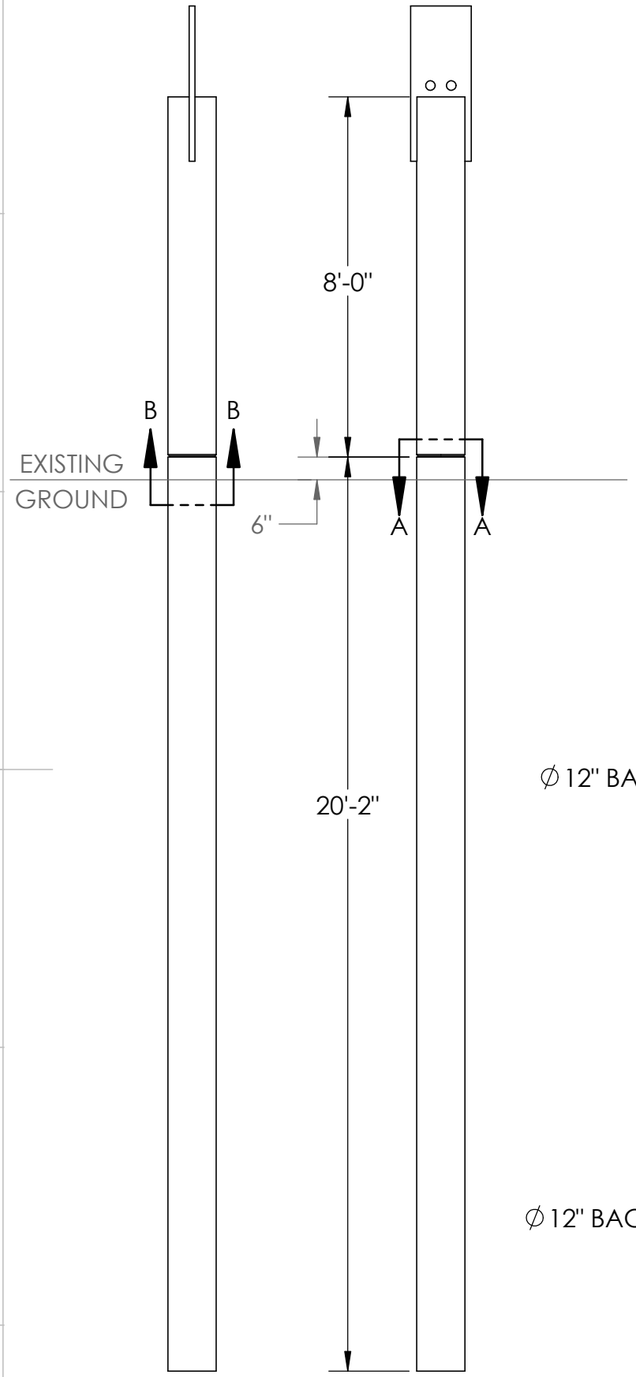

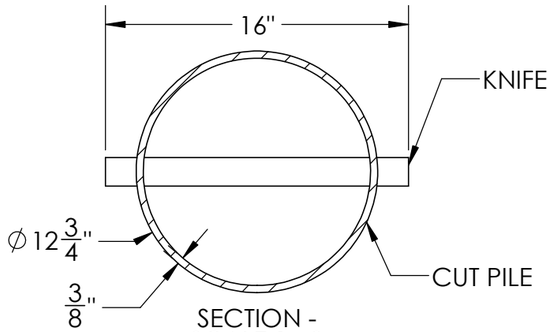

SECTION -
SCALE 1 : 8

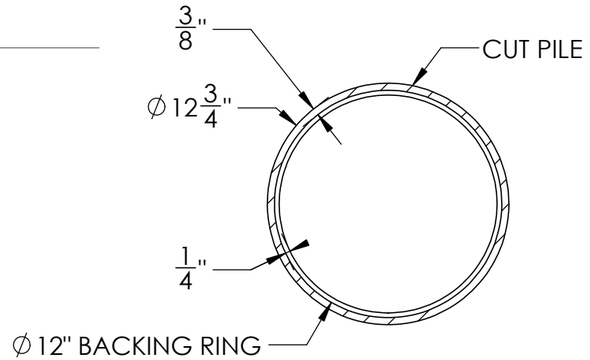

SECTION A-A
SCALE 1 : 8

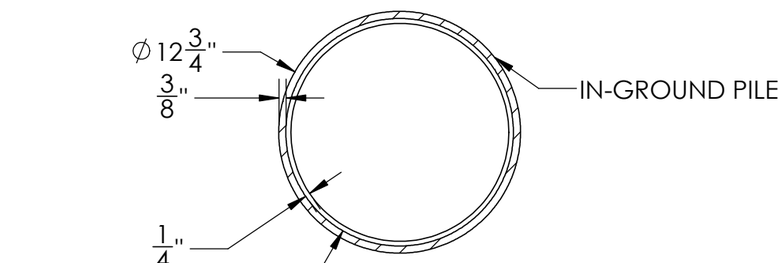

SECTION B-B
SCALE 1 : 8

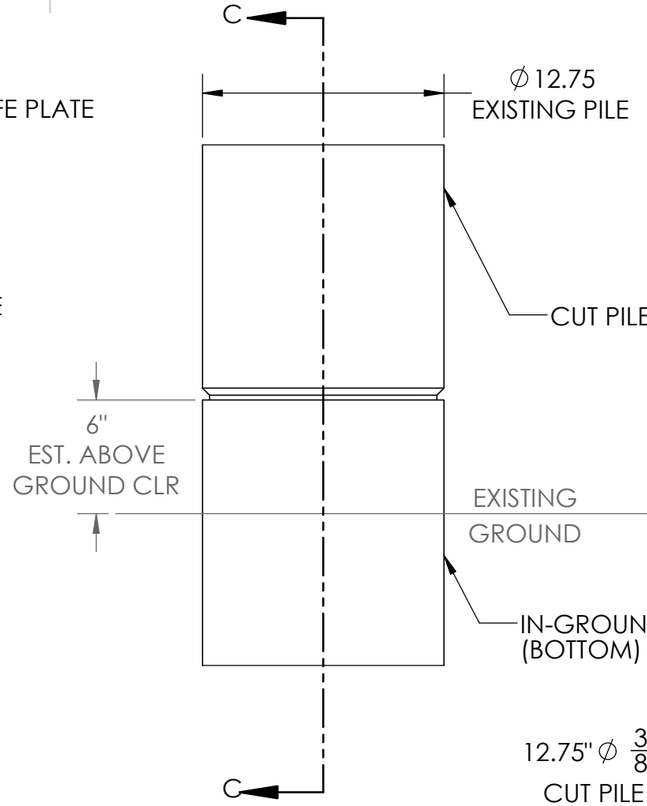

PILE CONNECTION DETAIL

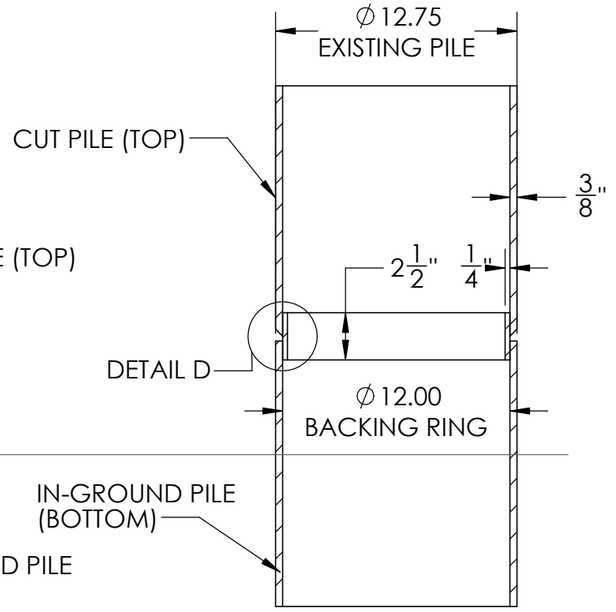

SECTION C-C
SCALE 1 : 8

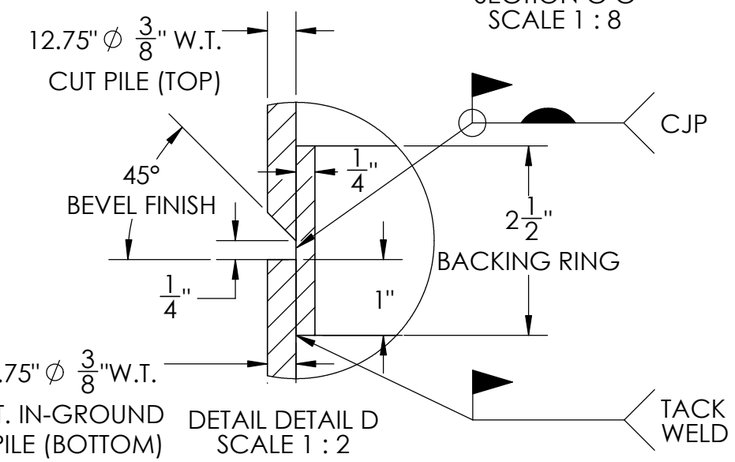

DETAIL DETAIL D
SCALE 1 : 2

NOTES:
1. EXISTING CUT PILE SHALL HAVE A BOTTOM 45 DEGREE BEVEL FINISH. FROM OUTSIDE FACE IN.
2. EXISTING IN-GROUND PILE SHALL BE GRINDED TO A SMOOTH FLAT FINISH
3. BACKING RING SHALL BE BE TACK WELDED TO INTERIOR WALL OF THE IN-GROUND PILE.
4. ALL INSTRUMENTATION WIRES SHALL BE PROTECTED AND SALVAGED DURING WELDING.

UC SAN DIEGO		ESEC NORTH SOIL PIT STEEL PIPE PILES RESEARCH	
SHEET SCALE 1:40		TITLE: PILE TEST #4 12.75" DIAMETER PILE CONNECTION	
DRAWN	T. RICHARDS		
CHKD		DATE: 5/6/2024	DRAWING NO.: SD-02
APPRVD		REV:	

Appendix C

Blind Prediction Documents

https://peer.berkeley.edu/news-and-events/2024-blind-prediction-contest/purpose-and-background

NIST/NSF BLIND PREDICTION CONTEST ON THE IN-GROUND HINGE PERFORMANCE OF STEEL PIPE PILES

SUBMISSIONS DUE November 5th , 2024

Contest Rules

- Contestants may consist of individuals and/or teams.
- An individual can only be involved in a single team.
- If an individual is part of a team the individual cannot enter the competition separately as an individual.
- Multiple teams from a company, a research institution or a university may submit predictions.
- Contestants will submit a single entry of only one of the following two (2) categories:
    - **Limited Analysis:** This category is recommended for practitioners and researchers intending to use simple computational models to capture the main response parameters.
    - **Comprehensive Analysis:** This category is recommended for practitioners and researchers intending to model the test specimens and test setup to capture the full cyclic response of the test specimens and to predict overall and dynamic response parameters.
- There will be one winner for each of the two categories. Each will be evaluated and rewarded separately.
- Results will be presented anonymously except for those of the "winning" entries.
- Questions about the blind prediction contest or details of the single in-ground pile test specimen can be submitted via peer_center@berkeley.edu. Questions should be submitted by October 7, 2024. Questions and answers will be posted on the blind prediction web site.

Contest Schedule

Event	Deadline
Blind Prediction Contest Opens	August 21, 2024
Deadline for Questions	October 7, 2024
Deadline for Submissions	November 5, 2024
Category Winners Notified	November 14, 2024

Provided Information, Assumptions and References

The blind prediction contest website contains the following information:

- Contest Rules
- General Test Information
  - Test Set-up (Pictures and Drawings)
  - Test Specimen Parameters and Material Properties
  - Site Geotechnical Parameters
  - Test Loading Conditions
  - A video of the test. This video demonstrates the cyclic test at a large amplitude displacement. Note: the rate of loading in the video was sped up for viewing convenience.
- Submission Spreadsheet (see below for a detailed description)

Submittal Rules

The individual or team must use the contest submittal spreadsheets provided and input the required values.

Category A. Limited Analysis:

Submit results using the spreadsheet provided:

- Questionnaire Tab: Provide brief description of the method of analysis that clearly explains the structural system and modeling assumptions in no less than 450 words.
- Envelope Tab: Provide the following information
  - Positive Lateral Force (kip) vs. Lateral Displacement (inch) Response Curve at the elevation of applied lateral force at 7'-9" above ground surface. Positive being the loading condition when the pile is being pushed north, away from the reaction wall.
    - Provide the lateral force (kip) at the peak displacements which occur at semi-cycle peaks marked as 25, 29, 33, 37 and 41 in the displacement loading protocol, Figure 10 in the *Information_Assumptions_Reference* document. (5 Total)
  - Determine the in-ground depth z (ft) at the pile's maximum bending moment when the peak lateral force occurs. Note: The depth below ground surface, z, is a negative number. Also provide the peak lateral force and the pile maximum bending moment.
  - Identify the mode of failure which results in softening of the response.

Category B. Comprehensive Analysis:

Submit results using the spreadsheet provided:

- Questionnaire Tab: Provide brief description of the method of analysis that clearly explains the structural system and modeling assumptions in no less than 450 words.
- Free Vibration Tab: The pile was subjected to free vibration testing. For this test, the Axial Load Apparatus was fully fixed on the pile to provide mass. The tire test was performed with only the Axial Load Apparatus applied, no concrete weights applied. An initial maximum lateral displacement of 0.260-inches was measured at the top of the pile due to a single hit with a tire. Compute the fundamental period (sec) of free vibration and the effective viscous damping ratio. The effective viscous damping ratio shall be calculated assuming a free vibration harmonic response decay. Please refer to the *Information_Assumptions_References* document and *Comprehensive Analysis Results Spreadsheet* for details of the free vibration test including the geometry and properties of the loading apparatus.
- Envelope Tab: Provide the following information (graphically and in table)
    - Lateral Force (kip) vs. Lateral Displacement (inch) Response Envelope at the elevation of applied lateral force at 7'-9" above ground surface. Positive being the loading condition when the pile is being pushed north, away from the reaction wall.
        - Provide the lateral force (kip) at the peak displacements which occur at semi-cycle peaks marked as 25, 29, 33, 37 and 41 in the displacement loading protocol, Figure 9 in the *Information_Assumptions_Reference* document. (5 Total)
    - Determine the in-ground depth z (ft) at the pile's maximum bending moment when the peak lateral force occurs. Note: The depth below ground surface, z, is a negative number. Also provide the peak lateral force and the pile maximum bending moment.
    - Identify the mode of failure which results in softening of the response.
- Hysteretic Energy Tab: Calculate the hysteretic energy (kip-in) in cycles 25-26, 33-34 and 37-38. Refer to Figure 10 loading protocol in the *Information_Assumptions_Reference* document and the figure in the *Comprehensive Analysis Results Spreadsheet* for the definition of a cycle. The hysteretic energy shall be taken as the shaded area enclosed by the lateral force vs. lateral displacement loop. Please refer to the *Comprehensive Analysis Results Spreadsheet* for further details.

If necessary, any additional information will be provided at the blind prediction contest website and questions can be submitted by emailing peer_center@berkeley.edu.

Evaluation

Teams and/or individuals are requested to predict the test specimen performance and fill in the tables and values as indicated in the Category A. Limited Analysis Submittal Spreadsheet or the Category B. Comprehensive Analysis Submittal Spreadsheet. The winning team will have the highest total points. In the case of a tie, the winning team will be the one that has the minimum error(s) in Table A-1/Table B-2 of the corresponding submittal sheets.

The following will be scored with a point system as described below, with maximum points for

1. Category A. Limited Analysis Results Spreadsheet — 26 points Max.
2. Category B. Comprehensive Analysis Results Spreadsheet — 42 points Max.

Note: Error is defined as the absolute value of the difference between the measured value from the test and the predicted values input by the contestant, normalized by the absolute value of the measured value from the test.

Questionnaire Tab: Up to 4 points will be assigned. Scoring is similar for both categories.

- 0 points – Incomplete
- 1 point – Less than 50 words and unclear description of methodology
- 2 points - Unclear assumptions and modeling description
- 3 points – Clear modeling description, however assumptions are not provided. OR clear detailed modeling description with assumptions listed, however, exceeds 450 words.
- 4 points – Less than 450 words and clearly describes program/software used, modeling description and outlines modeling assumptions.

Free Vibration Tab: Up to 10 total points for completion of this tab will be assigned. Only scored for Category B. Comprehensive Analysis participants.

- 0.5 pts total for each Table B-1 entry. Each entry will be deducted 0.1pt for every 10% calculated error, up to 50%. If the error is greater than 50%, 0 pts will be assigned for that entry.
- 3 pts total for calculated Fundamental Period. 0.5 pt will be deducted for every 20% calculated error. If the error is greater than 120%, 0 pts will be assigned for that entry.
- 2.5 pts total for calculated Effective Viscous Damping Ratio. 0.5 pt will be deducted for every 20% calculated error. If the error is greater than 180%, 0 pts will be assigned for that entry.

Envelope Tab: Up to 22 points will be assigned. Scoring is similar for both categories.

- 2 pts total for each Table A-1/Table B-2 entry. Each entry will be deducted 0.25pt for every 10% calculated error, up to 50%. If the error is greater than 50%, 0.5 pts will be assigned.
- 3 pts total for Peak Lateral Force value. 0.5 pt will be deducted for every 10% calculated error. If the error is greater than 60%, 0 pts will be assigned for that entry.

- 3 pts total for Pile Maximum Bending Moment value. 0.5 pt will be deducted for every 10% calculated error. If the error is greater than 60%, 0 pts will be assigned for that entry.
- 4 pts total for determined *Depth Below Ground* (ft) value. 0.5 pt will be deducted for every 6-in variation. If the variation is greater than 48-in, 0 pts will be assigned for that entry.
- 2 pts total for Identified mode of failure. 1 pt deduction for correct partial response. 0 pts for incorrect response.

Hysteretic Tab: Up to 6 total points will be assigned. Only scored for Category B. Comprehensive Analysis participants.

- 2 pts total for each Table B-3 entry. Each entry will be deducted 0.5pt for every 20% calculated error, up to 40%. If the error is greater than 40%, 0 pts will be assigned for that entry.

Scoring sheets will not be distributed. The scoring can be made available upon request after November 14, 2024.

General Information - Test Set-Up

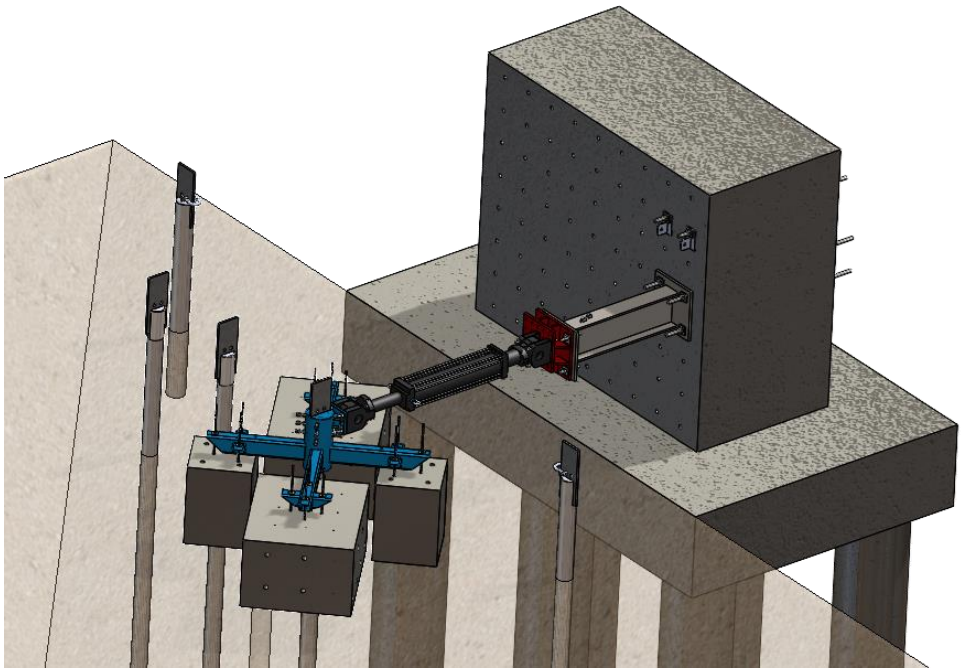

Figure 1: Schematic Rendering of Pile Test

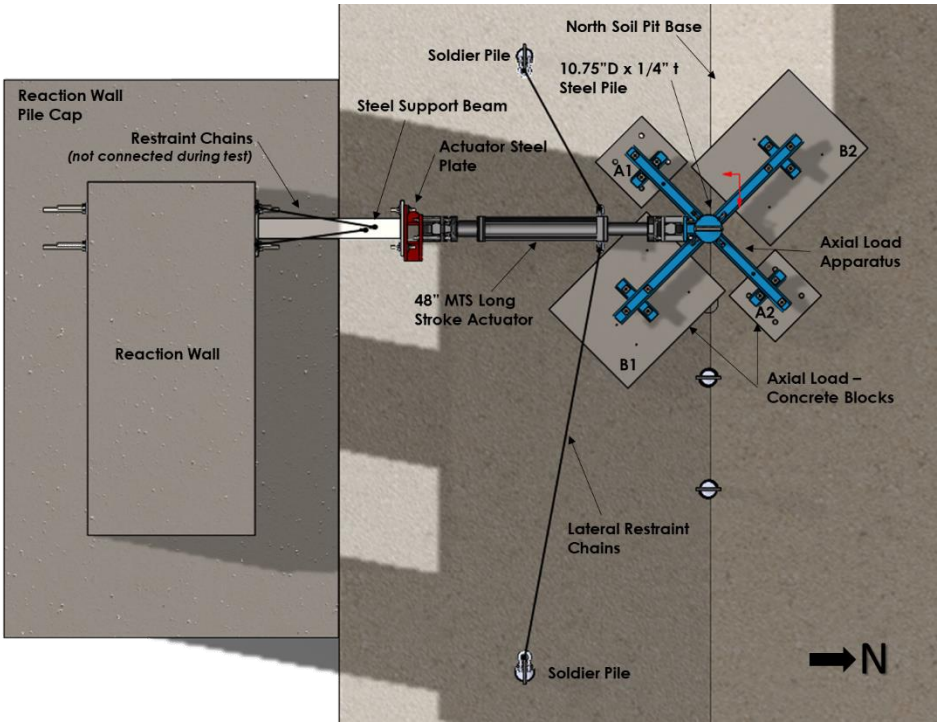

Figure 2: Schematic Plan of Pile Test Set-Up

Figure 3: Overview Pile Test Set-Up

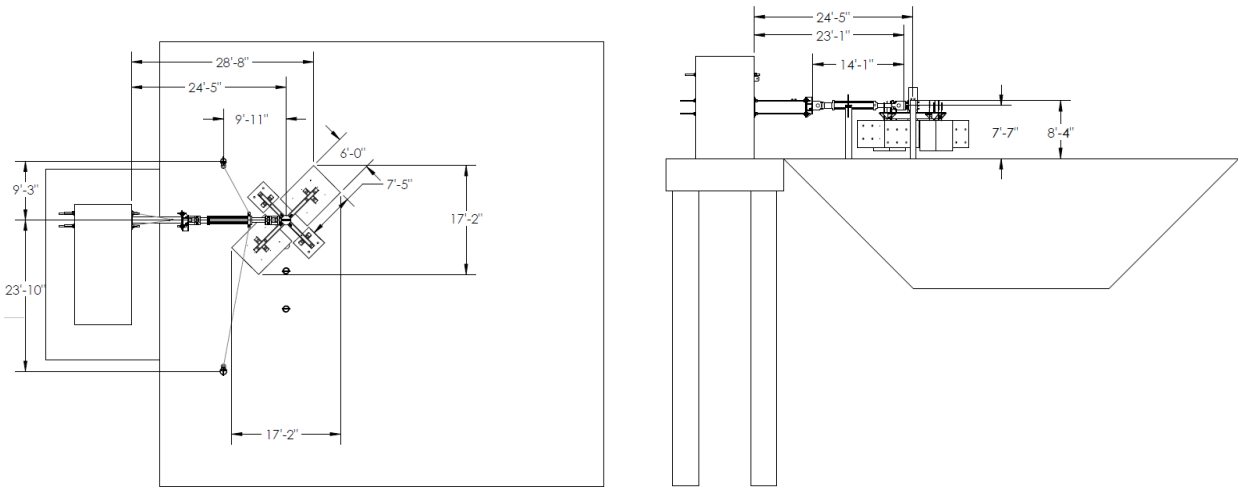

(a) Plan View (b) Elevation View

Figure 4: Test-Setup Schematic Drawings

Note: Field dimensions vary slightly up to +/- 6". For the lateral load test, the height of the top of pile from top of ground was measured in the field as 100.5 inches. Thus, the lateral load was applied at 91.5 inches (7.625 ft) above the ground elevation.

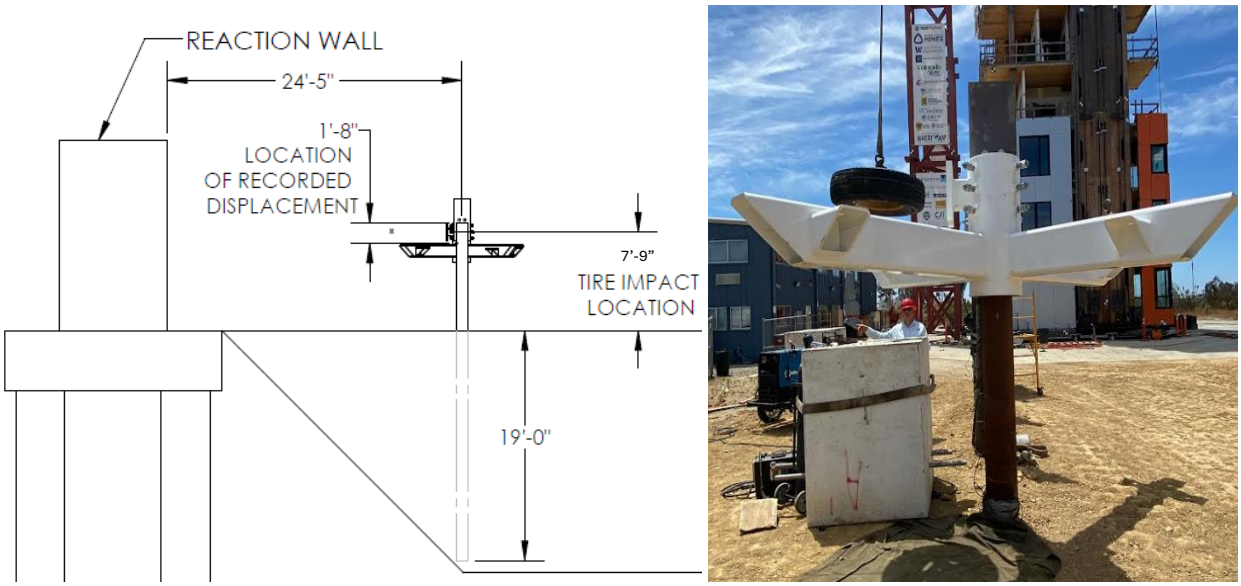

(a) Free Vibration Test Schematic (b) Test Set-Up Before Single Force Hit

Figure 5: Free Vibration Test

Note: Measurements provided in all figures are estimates and can vary in field within +/- 6-inches.

General Information – Test Specimen Parameters & Material Properties

Table 1: Specimen Parameters and Material Properties

Pile (Nominal Dim.)		**Total Pile Length**	**Approx. In-Ground Pile Depth**	**Approx. Above Ground Pile Height[3]**	**Top of Soil Plug Depth[4]**
D	t[1,2]				
[in]	[in]	[ft]	[ft]	[ft]	[ft]
10.75	0.25	28	19.67	8.33	12.97

Notes:
[1] Pile thickness varied +/- 2% along length of pile
[2] The pile specimen is specified according to API 5L X52 PSL2.
[3] Measured above ground height of the pile from the top of in-situ soil.
[4] Measured depth of the soil plug from the top of the pile.

Material Properties –

Material Testing using coupons from the pile specimen was performed to obtain the material properties. Refer to the provided Excel file with stress-strain curve.

General Information – Site Geotechnical Parameters

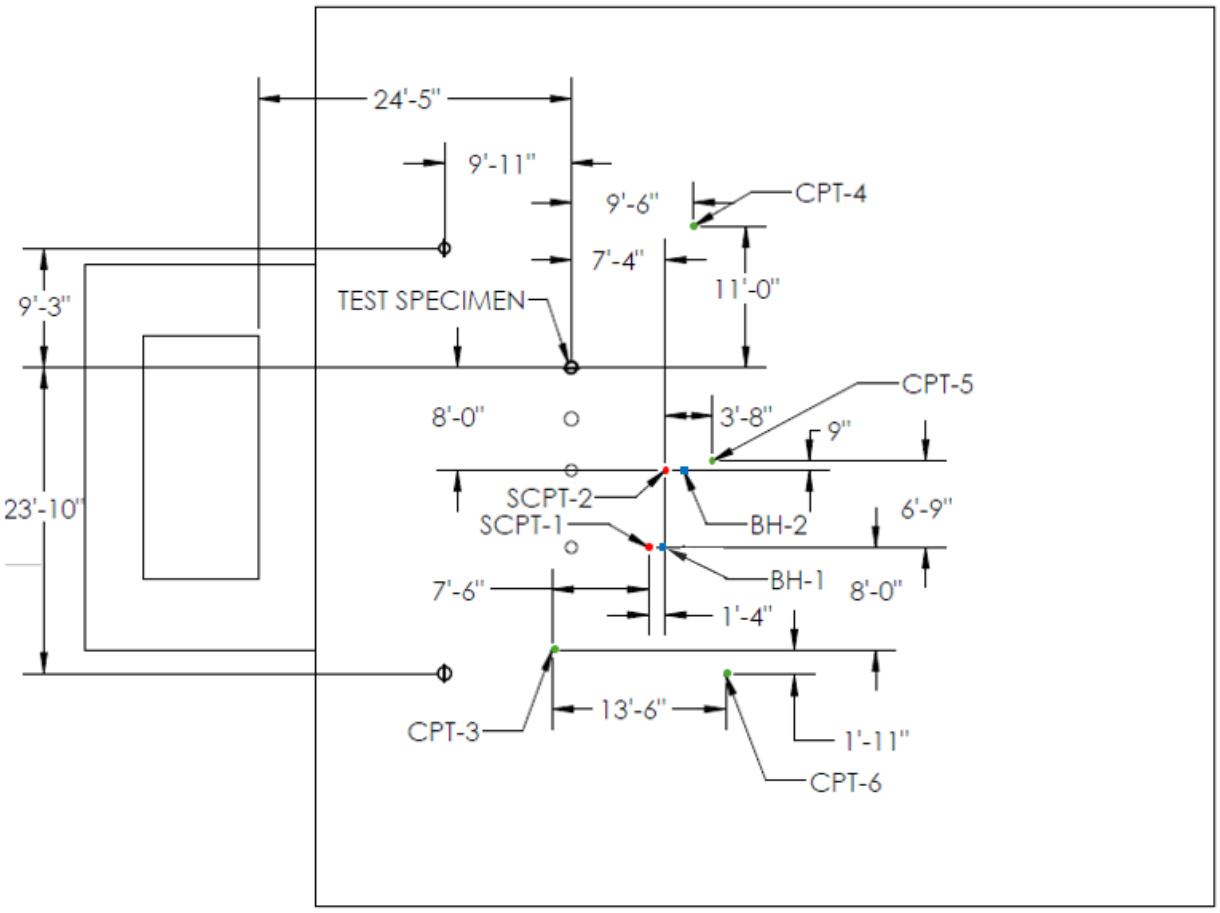

Figure 6: CPT/SCPT and Boring General Locations

The following is available under the Geotechnical Information:

- Cone Penetration Tests (CPTs)
- Seismic CPTs
- Boring Logs
- Soil Laboratory Tests

General Information – Test Loading Conditions

Axial loading included:

- Steel Loading Frame Apparatus
  - Geometry – Figure 7
  - Mass properties – Figure 8
- 2 pairs of reinforced concrete blocks (Table 2) – 72 kips
- Lateral loading was applied using a 48-inch long stroke MTS actuator (Figure 9) – 5.2 kips

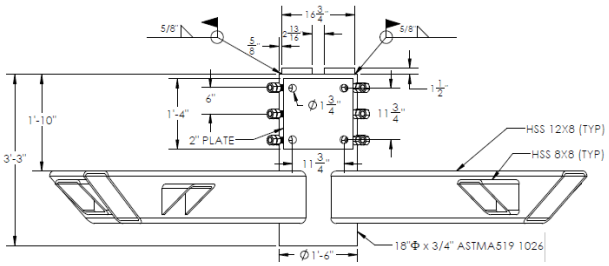

(A) Elevation View

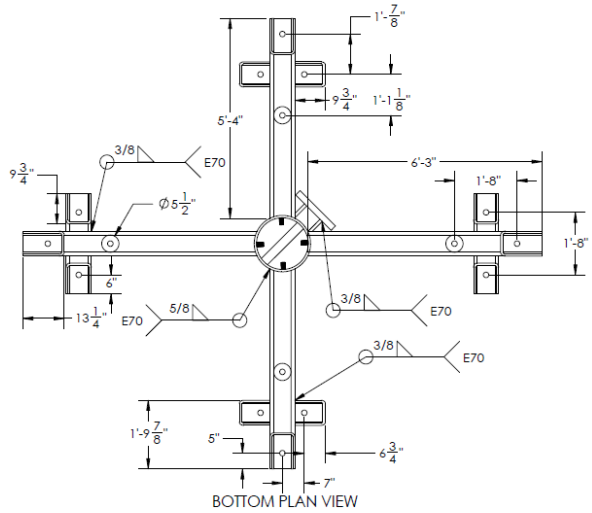

(b) Bottom Plan View

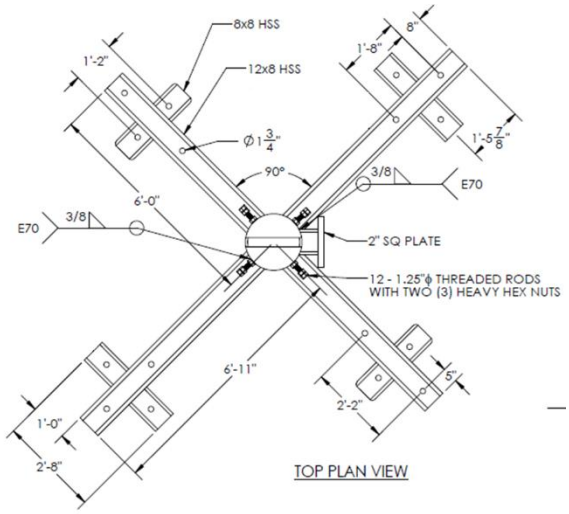

(c) Top Plan View

Figure 7: Steel Loading Apparatus Drawings

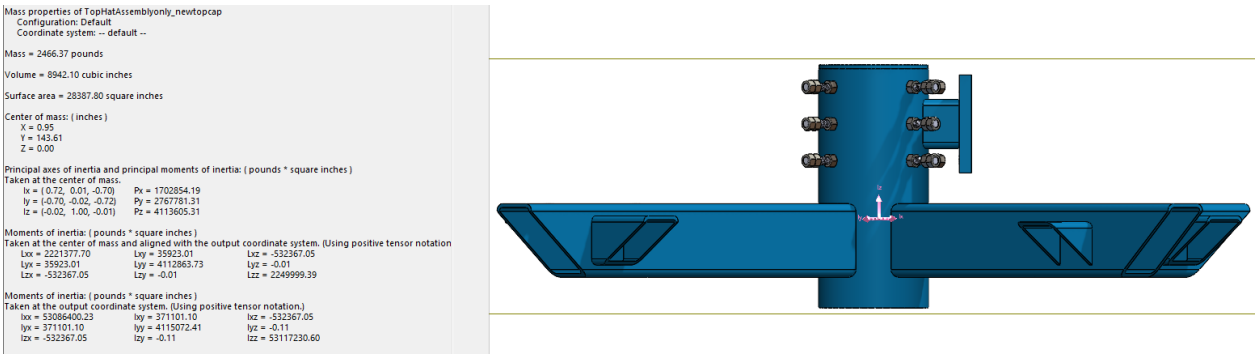

Figure 8: Steel Loading Apparatus Mass Properties per SolidWorks

Table 2: Axial Concrete Block Applied Loading

Description	Unit	A - Blocks	B - Blocks
Block Height	ft	4.7	4.1
Block Width	ft	3.5	6
Block Length	ft	3.5	7.4
Individual Block Weight	kips	8.58	27.26
Number of Blocks	-	2	2
Total Block Pair Weight	kips	17.15	54.51
Approximate Applied Weight (Rounded)	kips	72	

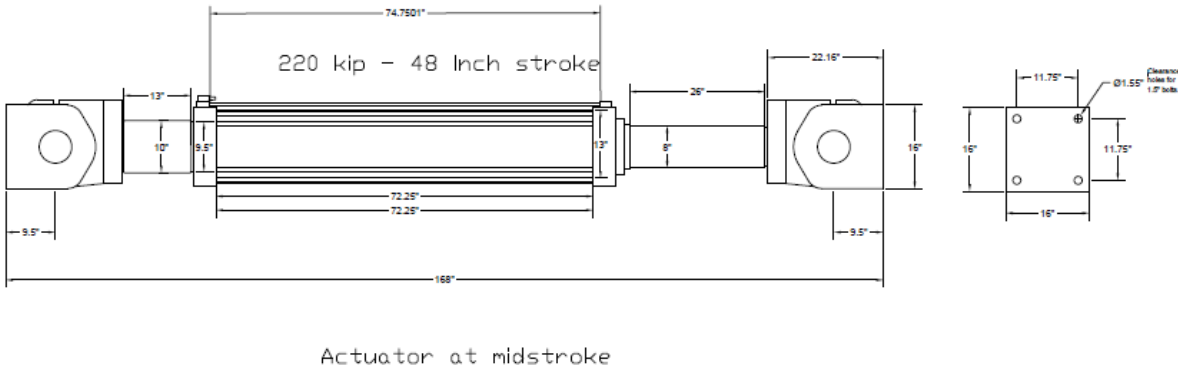

Actuator at midstroke

Figure 9: 220kip (48-inch) Long Stroke MTS Actuator Dimensions

Due to the pin of the actuator being eccentric to the pile centerline, the specimen experiences an initial moment before the application of the lateral load. This moment is determined as (5.2 kip/2) * (20.65").

Note: For free vibration testing, the Axial Load Apparatus was fully fixed on the pile to provide mass.

General Information – Free Vibration Loading

The free vibration test considered the test specimen with only the steel loading frame firmly placed on top of the pile. Refer to Figure 5. A vehicular spare tire was used to hit the pile at the center of the 2-inches thick square plate on the steel apparatus, approximately 9-inches below pile top. Accelerations were recorded at 20-inches from the pile top and converted to displacements. A maximum lateral displacement of 0.260-inches was recorded at 20-inches from the pile top. The pile remains elastic during the free vibration tests.

General Information – Lateral Loading Protocol

Each cycle considers two (2) consecutive target displacement cycles with the same amplitude. Refer to Figure 10 and Table 3.

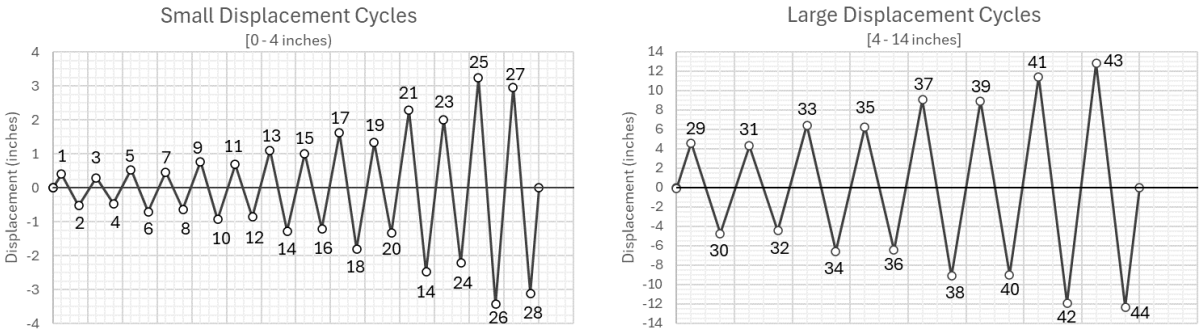

(a) Small Displacement up to Semi-Cycle 28 (b) Large Displacement from Semi-Cycle 29 to 44

Figure 10: Lateral Loading Protocol

Table 3: Cyclic Lateral Loading Protocol Table

Description	Cycle	Semi-Cycle Peak	Peak Displacement
Small Displacement [0 – 4 in)	1	1	0.40
		2	-0.52
		3	0.29
		4	-0.47
	2	5	0.54
		6	-0.70
		7	0.47
		8	-0.63
	3	9	0.77
		10	-0.93
		11	0.69
		12	-0.86
	4	13	1.10
		14	-1.27
		15	1.01
		16	-1.20
	5	17	1.61
		18	-1.80
		19	1.33
		20	-1.33
	6	21	2.29
		22	-2.48
		23	2.02
		24	-2.22
	7	25	3.23
		26	-3.43
		27	2.97
		28	-3.11
Large Displacement [4 – 14in]	8	29	4.58
		30	-4.75
		31	4.31
		32	-4.44
	9	33	6.42
		34	-6.56
		35	6.26
		36	-6.44
	10	37	9.07
		38	-9.12
		39	8.93
		40	-8.98
	11	41	11.43
		42	-11.93
		43	12.82
		44	-12.33

Stress [ksi]	Strain, ε_s [-]
-4.75E-05	-1.786074
0.000793	23.56367
0.001813	53.0108
0.002861	79.91583
0.004021	72.95806
0.006097	71.44068
0.008586	71.44184
0.011075	71.44301
0.013564	71.44417
0.016052	71.44533
0.018541	71.44649
0.02103	71.44766
0.023518	71.44882
0.026007	71.44998
0.028496	71.45114
0.030985	71.45231
0.033473	71.45347
0.036652	72.53127
0.040036	73.61634
0.043388	74.42739
0.046746	75.06354
0.050079	75.63479
0.053431	76.15313
0.056863	76.6115
0.060131	77.05271
0.063478	77.42286
0.066828	77.79044
0.070216	78.06392
0.073559	78.37744
0.07687	78.58105
0.080213	78.79828
0.083566	78.99218
0.086912	79.16884
0.090283	79.31212
0.093635	79.48874
0.096951	79.56522
0.10031	79.65542
0.103655	79.78612
0.10704	79.87037
0.110358	79.93089
0.113691	79.99555
0.117033	80.06249
0.120398	80.1256
0.123744	80.104
0.127091	80.22088
0.130481	80.16504
0.133845	80.25699
0.137152	80.24339
0.140516	80.25602
0.143799	80.24539
0.147168	80.25471
0.150206	80.2467
0.152307	80.19537
0.154408	80.14404

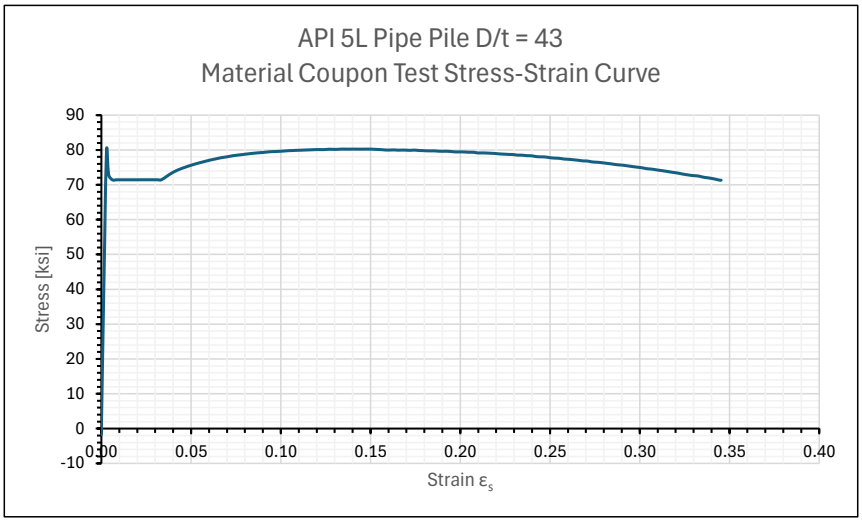

0.156516	80.0829
0.158699	79.99243
0.160872	79.98802
0.162997	80.0311
0.165224	79.95506
0.167451	79.97944
0.169748	79.96132
0.172064	79.90584
0.174375	79.9722
0.176721	79.87171
0.179009	79.82651
0.181303	79.76523
0.183574	79.74896
0.185917	79.74223
0.188288	79.64672
0.190547	79.64005
0.192946	79.63368
0.195397	79.54157
0.197664	79.43986
0.199952	79.46567
0.20241	79.43061
0.204827	79.35653
0.207329	79.34774
0.209775	79.15207
0.212123	79.1655
0.214619	79.1277
0.217036	79.06059
0.219498	78.99508
0.222009	78.8703
0.224569	78.80635
0.226991	78.72828
0.22934	78.69319
0.231873	78.52422
0.234452	78.51592
0.237174	78.3696
0.239721	78.33991
0.242305	78.10945
0.244769	78.04076
0.247383	77.99896
0.249941	77.79444
0.252537	77.67761
0.255221	77.61043
0.257864	77.39968
0.260471	77.32723
0.263219	77.18589
0.265798	77.05005
0.268409	76.86431
0.270866	76.83041
0.27357	76.57428
0.276265	76.48953
0.279054	76.34281
0.281818	76.16087
0.284553	75.98799
0.28732	75.76976
0.290121	75.66316
0.292752	75.48547
0.29557	75.27181
0.29839	75.08014

0.301139	74.90373
0.303972	74.63347
0.306816	74.50342
0.309701	74.2637
0.31262	74.05532
0.315308	73.83842
0.318215	73.59871
0.321097	73.38471
0.323999	73.08355
0.326717	72.85777
0.329641	72.65607
0.332519	72.54087
0.335555	72.18215
0.338562	71.96406
0.341561	71.69133
0.344442	71.34178
0.345353	71.32074

Submitted by:

Date:

Affliation/Company/Institution:

Provide brief description of the method of analysis that clearly explains the structural system and modeling assumptions in no less than 450 words:

Submitted by: 0 Date: 0

Affliation/Company/Institution: 0

Note: This is only required for Comprehensive Analysis

Pile was subjected to free vibration testing. Maximum lateral displacement of 0.260-inches was applied at the top of the pile. For free vibration testing, the Axial Load Apparatus was fully fixed on the pile to provide mass. Compute the fundamental period of free vibration and the viscous damping ratio.

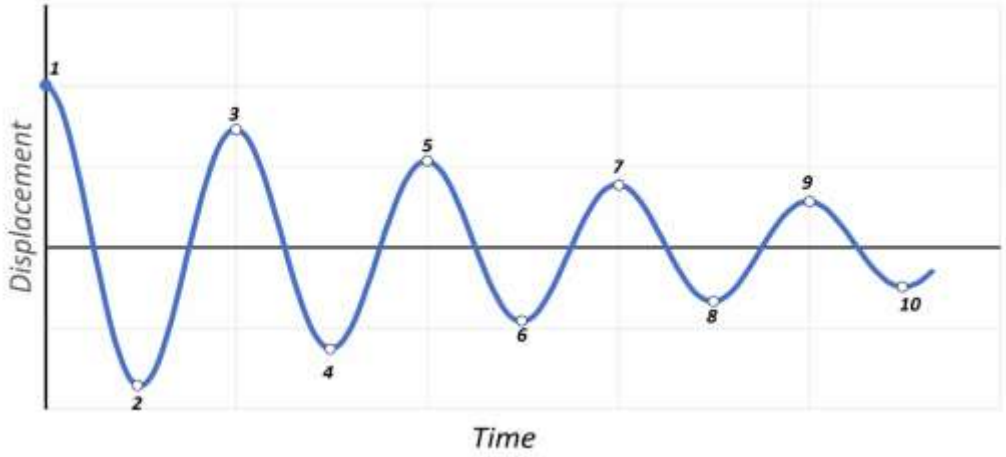

The effective viscous damping ratio shall be calculated assuming a free vibration harmonic response decay, as shown above. Fill in the table below.

Table B-1: Displacement Decay

Peak	Time (s)	Displ. (in)
1	0.000	0.260
2	0.125	
3	0.240	
4	0.365	
5	0.490	
6	0.615	
7	0.740	
8	0.860	
9	0.975	
10	1.115	

Fundamental Period : secs

Effective Viscous Damping Ratio:

Submitted by: 0 Date: 0

Affliation/Company/Institution: 0

Response Envelope: Provide the following information

Lateral Force (kip) vs. Lateral Displacement (inch) Response Envelope at elevation of applied lateral force at 7'-9" above ground surface.

Lateral Force (kip) vs. Lateral Displacement (inch) Response Envelope

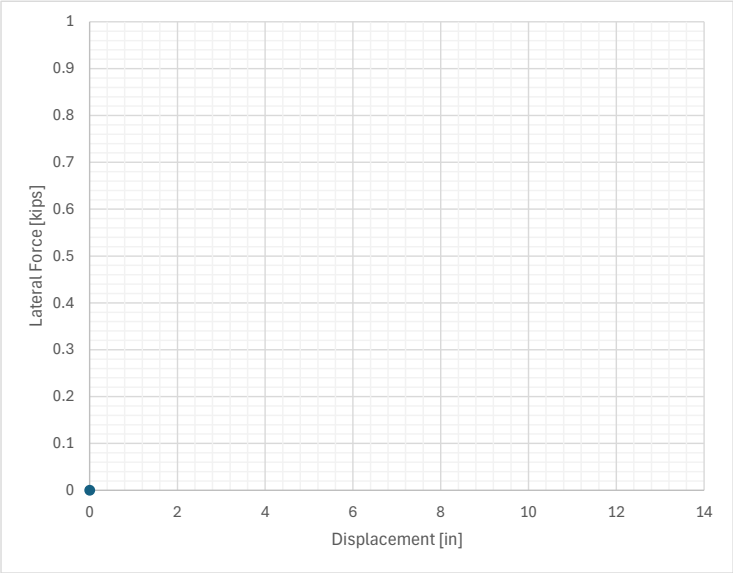

Table B-2 Response Envelope

Provide the lateral force at the peak displacement amplitude shown below:

Sub-Cycle Peaks	Lateral Displacement Amplitude	Lateral Force
	in	kip
-	0	0
25	3.23	
29	4.58	
33	6.42	
37	9.07	
41	11.43	

Note: Sub-Cycles peaks numbering is provided in the *Information_Assumptions_References* document.

In-ground depth z at the pile's maximum bending moment when the peak lateral force occurs.

Note: The depth below ground surface, z, is a negative number.

i. Peak Lateral Force (+ Push North) kip

Pile Maximum Bending Moment kip-ft

Depth below ground ft

Pile Diameters 0.0

Identify the mode of failure which results in softening of the response.

Submitted by: 0 Date: 0

Affliation/Company/Institution: 0

Table B-3 Hysteretic Energy

Calculate the hysteretic energy in the following cycles:

Cycle	Hystertic Energy
	kip-in
25 - 26	
33 - 34	
37 - 38	

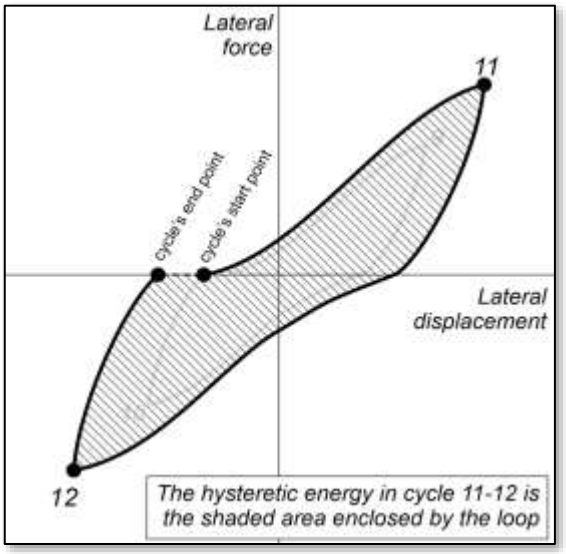

Note: Semi-Cycles peaks numbering is provided in the *Information_Assumptions_References* document

SUMMARY

OF

CONE PENETRATION TEST DATA

Project:

ESEC Englekirk Structural Engineering Center North Soil Pit
10201 Pomerado Road
San Diego, CA
April 16, 2024

Prepared for:

Mr. Jose Restrepo
University of California, San Diego (UCSD)
Structural Engineering Department (SME 341H)
9500 Gilman Drive
La Jolla, CA 92093
Office (909) 730-3307

Prepared by:

KEHOE TESTING & ENGINEERING
5415 Industrial Drive
Huntington Beach, CA 92649-1518
Office (714) 901-7270 / Fax (714) 901-7289
www.kehoetesting.com

TABLE OF CONTENTS

SUMMARY
OF
CONE PENETRATION TEST DATA

1. INTRODUCTION

This report presents the results of a Cone Penetration Test (CPT) program carried out for the ESEC Englekirk Structural Engineering Center North Soil Pit project located at 10201 Pomerado Road in San Diego, California. The work was performed by Kehoe Testing & Engineering (KTE) on April 16, 2024. The scope of work was performed as directed by University of California, San Diego (UCSD) personnel.

2. SUMMARY OF FIELD WORK

The fieldwork consisted of performing CPT soundings at six locations to determine the soil lithology. A summary is provided in **TABLE 2.1**.

LOCATION	DEPTH OF CPT (ft)	COMMENTS/NOTES:
SCPT-1	25	
SCPT-2	25	
CPT-3	25	
CPT-4	25	
CPT-5	25	
CPT-6	25	

TABLE 2.1 - Summary of CPT Soundings

3. FIELD EQUIPMENT & PROCEDURES

The CPT soundings were carried out by **KTE** using an integrated electronic cone system manufactured by Vertek. The CPT soundings were performed in accordance with ASTM standards (D5778). The cone penetrometers were pushed using a 30-ton CPT rig. The cone used during the program was a 15 cm^2 cone with a cone net area ratio of 0.83. The following parameters were recorded at approximately 2.5 cm depth intervals:

- Cone Resistance (qc)
- Sleeve Friction (fs)
- Dynamic Pore Pressure (u)
- Inclination
- Penetration Speed

At locations SCPT-1 & SCPT-2, shear wave measurements were obtained at various depths. The shear wave is generated using an air-actuated hammer, which is located inside the front jack of the CPT rig. The cone has a triaxial geophone, which recorded the shear wave signal generated by the air hammer.

The above parameters were recorded and viewed in real time using a laptop computer. Data is stored at the KTE office for up to 2 years for future analysis and reference. A complete set of baseline readings was taken prior to each sounding to determine temperature shifts and any zero load offsets. Monitoring base line readings ensures that the cone electronics are operating properly.

4. CONE PENETRATION TEST DATA & INTERPRETATION

The Cone Penetration Test data is presented in graphical form in the attached Appendix. These plots were generated using the CPeT-IT program. Penetration depths are referenced to ground surface. The soil behavior type on the CPT plots is derived from the attached CPT SBT plot (Robertson, "Interpretation of Cone Penetration Test…", 2009) and presents major soil lithologic changes. The stratigraphic interpretation is based on relationships between cone resistance (qc), sleeve friction (fs), and penetration pore pressure (u). The friction ratio (Rf), which is sleeve friction divided by cone resistance, is a calculated parameter that is used along with cone resistance to infer soil behavior type. Generally, cohesive soils (clays) have high friction ratios, low cone resistance and generate excess pore water pressures. Cohesionless soils (sands) have lower friction ratios, high cone bearing and generate little (or negative) excess pore water pressures.

The CPT data files have also been provided. These files can be imported in CPeT-IT (software by GeoLogismiki) and other programs to calculate various geotechnical parameters.

It should be noted that it is not always possible to clearly identify a soil type based on qc, fs and u. In these situations, experience, judgement and an assessment of the pore pressure data should be used to infer the soil behavior type.

If you have any questions regarding this information, please do not hesitate to call our office at (714) 901-7270.

Sincerely,

KEHOE TESTING & ENGINEERING

Steven P. Kehoe
President

04/30/24-jg-4363-4

APPENDIX

Kehoe Testing and Engineering
714-901-7270
steve@kehoetesting.com
www.kehoetesting.com

Project: **UCSD . ESEC Englekirk Structural Engineering Center North Soil Pit**
Location: **10201 Pomerado Rd, San Diego, CA**

SCPT-1
Total depth: 25.00 ft, Date: 4/16/2024

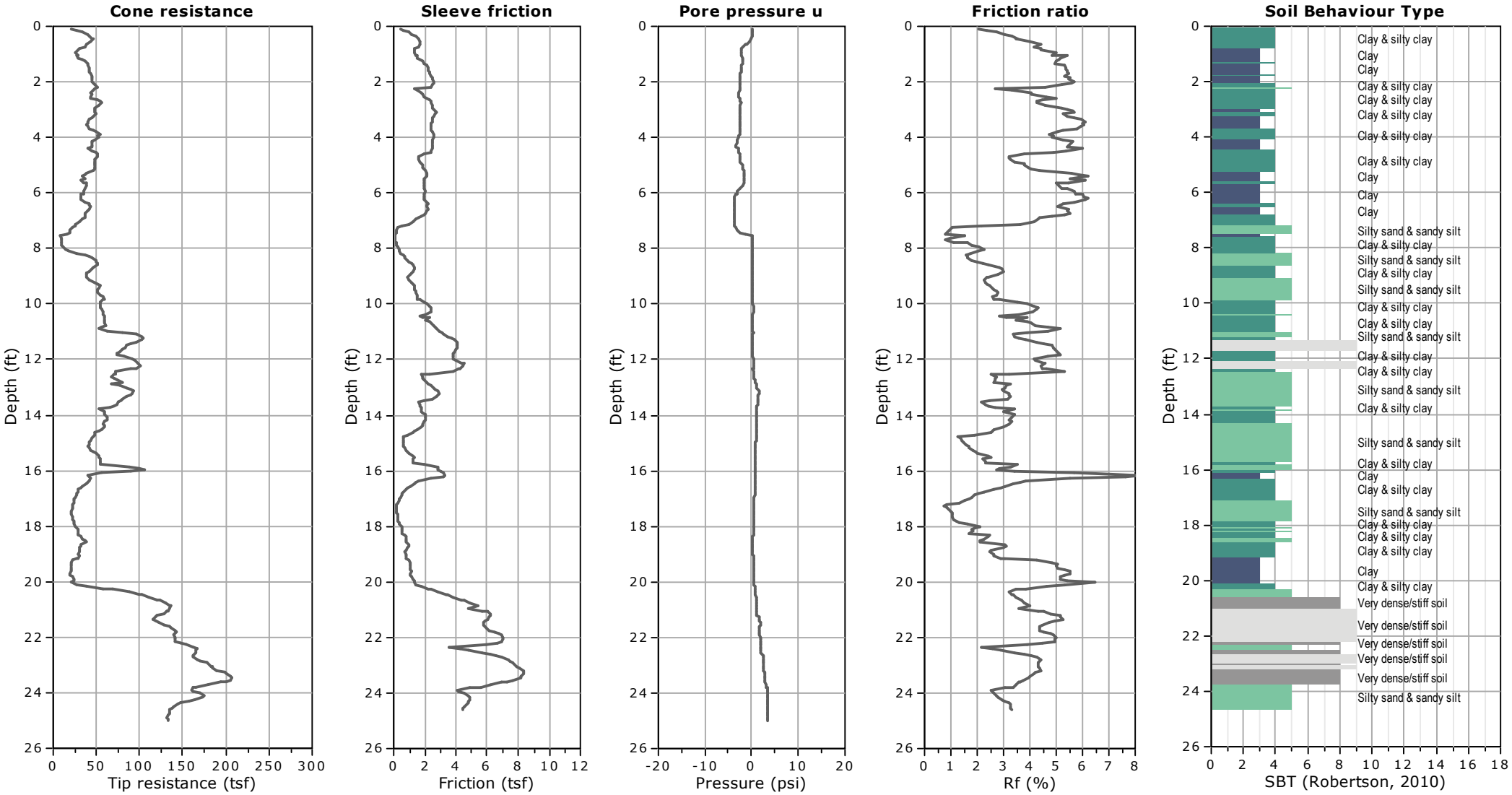

Kehoe Testing and Engineering
714-901-7270
steve@kehoetesting.com
www.kehoetesting.com

Project: **UCSD . ESEC Englekirk Structural Engineering Center North Soil Pit**
Location: **10201 Pomerado Rd, San Diego, CA**

SCPT-2
Total depth: 25.00 ft, Date: 4/16/2024

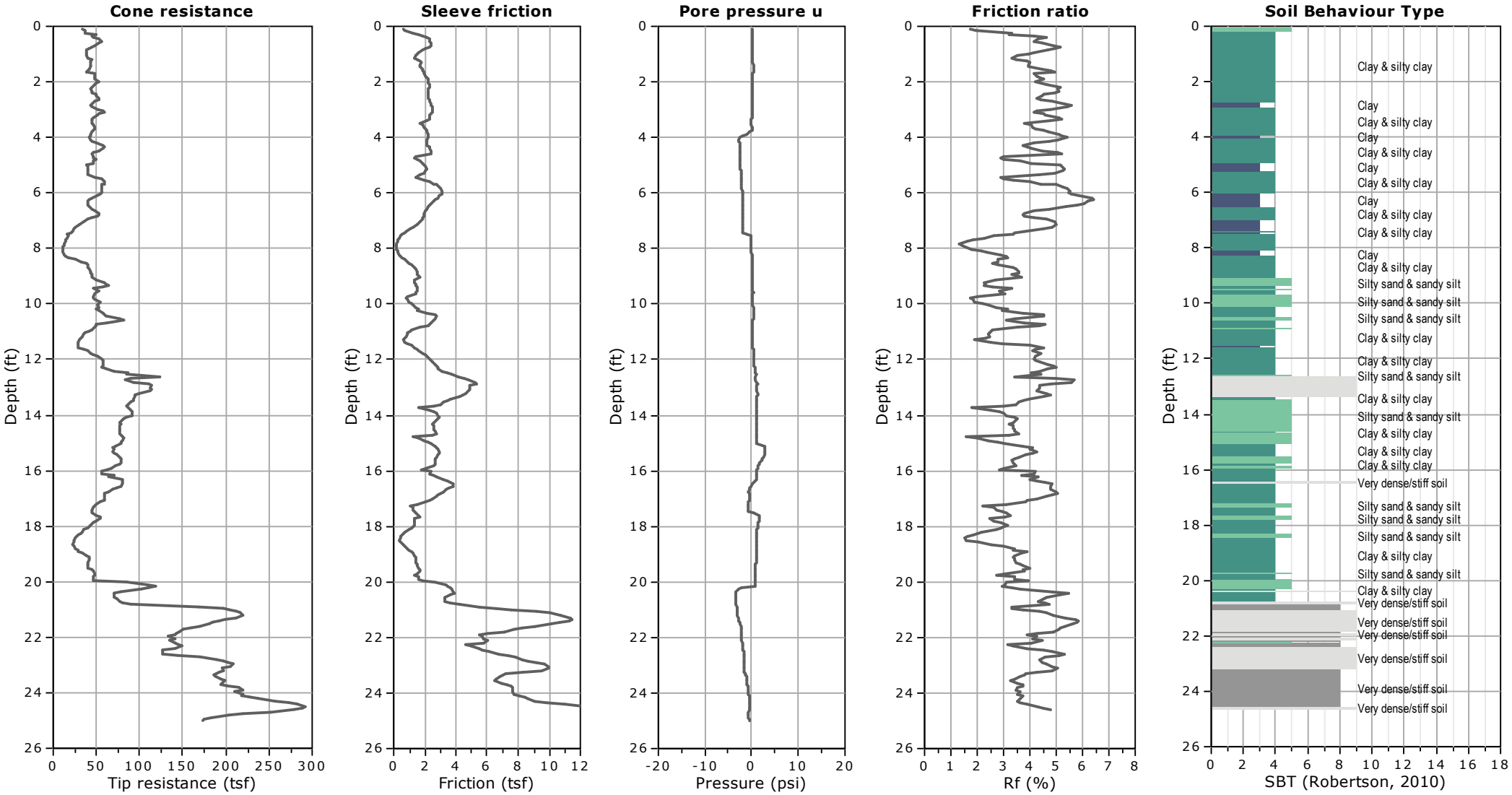

Kehoe Testing and Engineering
714-901-7270
steve@kehoetesting.com
www.kehoetesting.com

Project: **UCSD . ESEC Englekirk Structural Engineering Center North Soil Pit**
Location: **10201 Pomerado Rd, San Diego, CA**

CPT-3
Total depth: 25.07 ft, Date: 4/16/2024

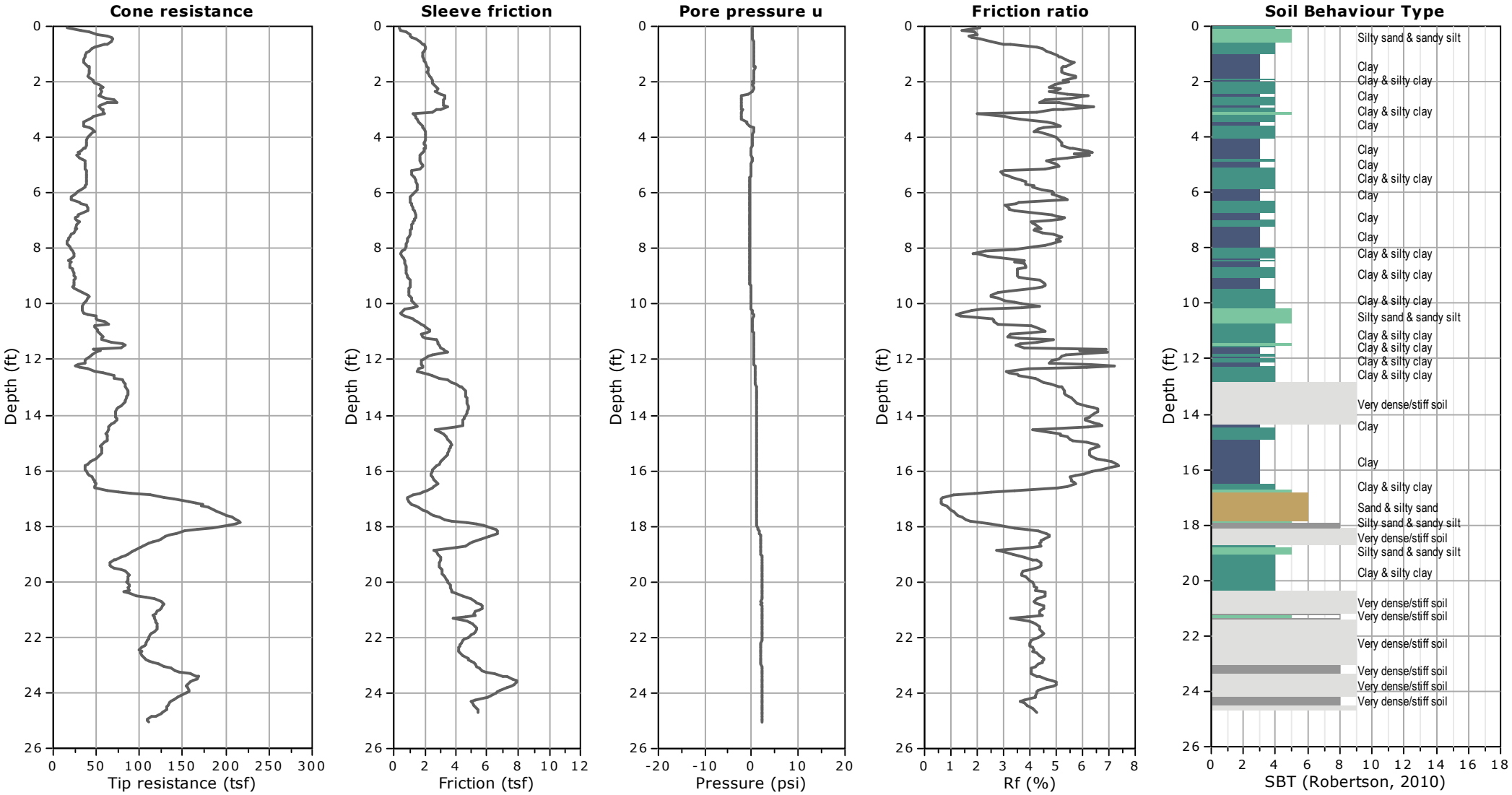

TABLE B-1 SUMMARY OF LABORATORY TEST RESULTS

Project No. : *21-601* **Project Name :** UCSD Steel Pile Research

Boring No .	Sample No.	Sample Depth (ft)	Soil Identification (group symbol) ASTM D2488/D2487	Moisture Content ASTM D2216 (%)	Total Unit Weight ASTM D2937 (pcf)	Pocket Penetrometer (tsf)	Torvane Shear (tsf)	Grain Size Distribution GR:SA:FI (%)	Sand Equivalent (CT-217)	Atterberg Limits ASTM D4318 (LL/PL/PI)	Soil-Minimum Resistivity CT-643 (ohm-cm)	Soil-pH CT-643	Soil-Soluble Sulfate Content CT-417 (ppm)	Soil-Moisture Free Chloride Content CT-422 (ppm)
BH-1	*D-1*	0	SC	13.8	126.0			9:45:46		28/17/11				
BH-1	*T-2*	2.5	SC	11.7	136.6			9:48:43						
BH-1	*D-3*	5	SC	15.3	126.5			7:49:42		27/15/12				
BH-1	*T-4*	7.5	SC-SM	11.6	119.3			3:65:32		23/16/7				
BH-1	*D-5*	10	SC	13.6	130.2			1:62:31		24/16/8				
BH-1	*D-6*	12.5	SC	10.8	117.8			2:70:28						
BH-1	*D-7*	15	SC-SM	14.2	124.4			2:62:36		23/17/6				
BH-1	*D-9*	20	SC	12.9	126.8			0:75:25						
BH-2	*D-1*	0	SC	13.4	126.4			6:47:47		28/16/12				
BH-2	*T-2*	2.5	SC	11.8	131.9			7:53:40						
BH-2	*D-3*	5	SC	14.6	130.2			4:50:46		26/15/11				
BH-2	*T-4*	7.5	SC-SM	11.4	117.7			3:64:33		23/16/7				
BH-2	*D-5*	10	CL to SC	13.5	125.4			0:65:35		23/16/7				
BH-2	*D-6*	12.5	SC	11.3	124.5			3:66:31						
BH-2	*D-7*	15	SC	14.3	130.8			1:58:41		24/14/10				
BH-2	*D-9*	20	SC	12.7	129.8			0:74:26						

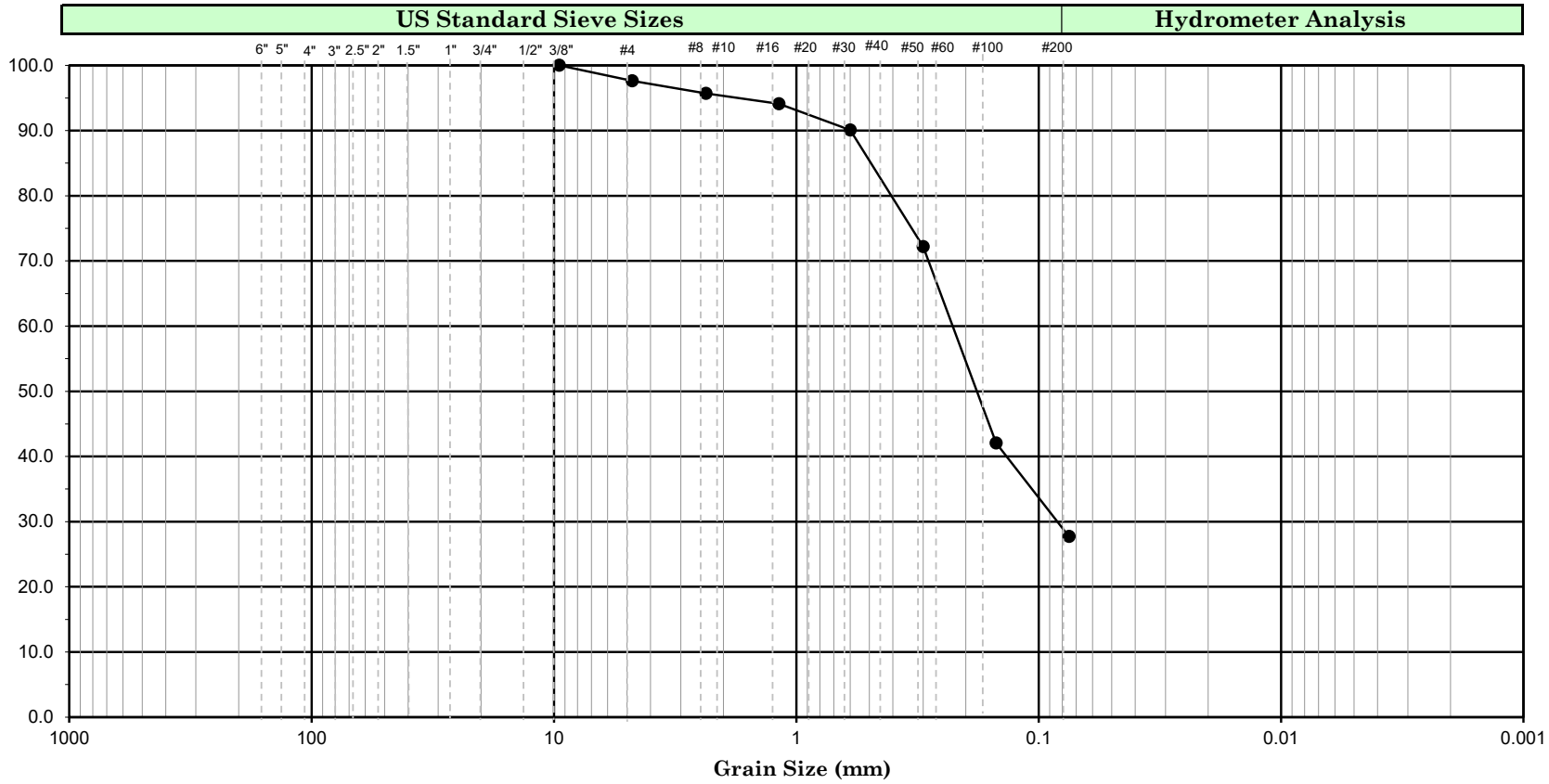

Cobbles	Gravel		Sand			Silt or Clay
	Coarse	Fine	Coarse	Medium	Fine	

Symbol	Boring Number	Sample Number	Depth (ft)		Depth (m)		Soil Color	Soil Description	U.S.C.S.
●	BH-1	D-6	12.5				yellowish brown with brown	Clayey sand	SC
Remark									

Earth Mechanics, Inc.
Geotechnical and Earthquake Engineering

UCSD Steel Pile Research

Project No. : 21-601

Date : 05/05/24

GRAIN SIZE ANALYSIS

(ASTM D-7928)

Figure No. :

Cobbles	Gravel		Sand			Silt or Clay
	Coarse	Fine	Coarse	Medium	Fine	

Symbol	Boring Number	Sample Number	Depth (ft)		Depth (m)		Soil Color	Soil Description	U.S.C.S.
●	BH-1	D-9	20				yellowish brown	Clayey sand	SC
Remark									

Earth Mechanics, Inc.
Geotechnical and Earthquake Engineering

UCSD Steel Pile Research

Project No. : *21-601*

Date : *05/05/24*

GRAIN SIZE ANALYSIS
(ASTM D-7928)

Figure No. :

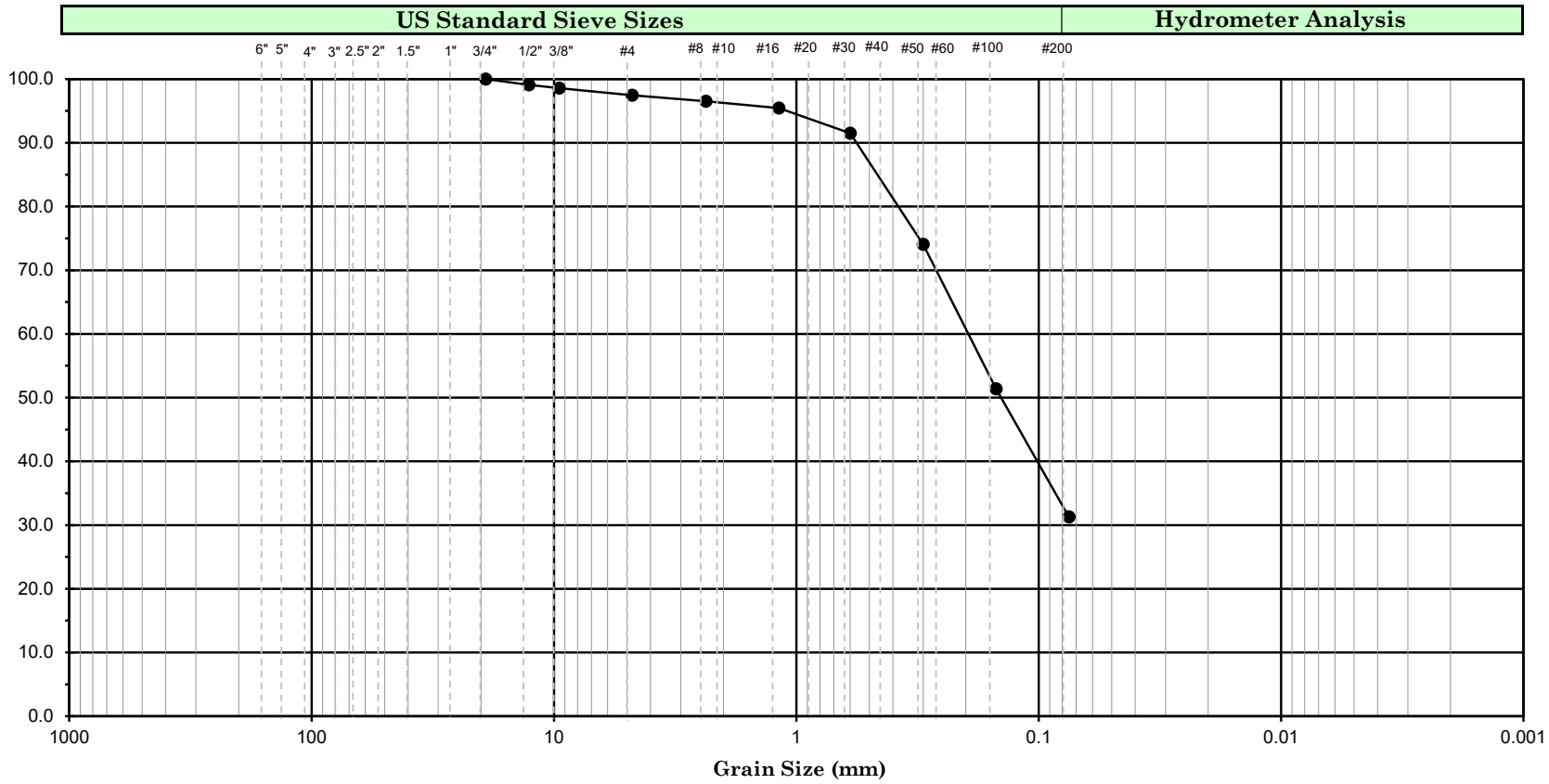

Cobbles	Gravel		Sand			Silt or Clay
	Coarse	Fine	Coarse	Medium	Fine	

Symbol	Boring Number	Sample Number	Depth (ft)		Depth (m)		Soil Color	Soil Description	U.S.C.S.
●	BH-2	D-6	12.5				mottled yellowish brown, white, light gray	Clayey sand	SC
Remark									

Earth Mechanics, Inc.
Geotechnical and Earthquake Engineering

UCSD Steel Pile Research

Project No. : 21-601

Date : 05/05/24

GRAIN SIZE ANALYSIS
(ASTM D-7928)

Figure No. :

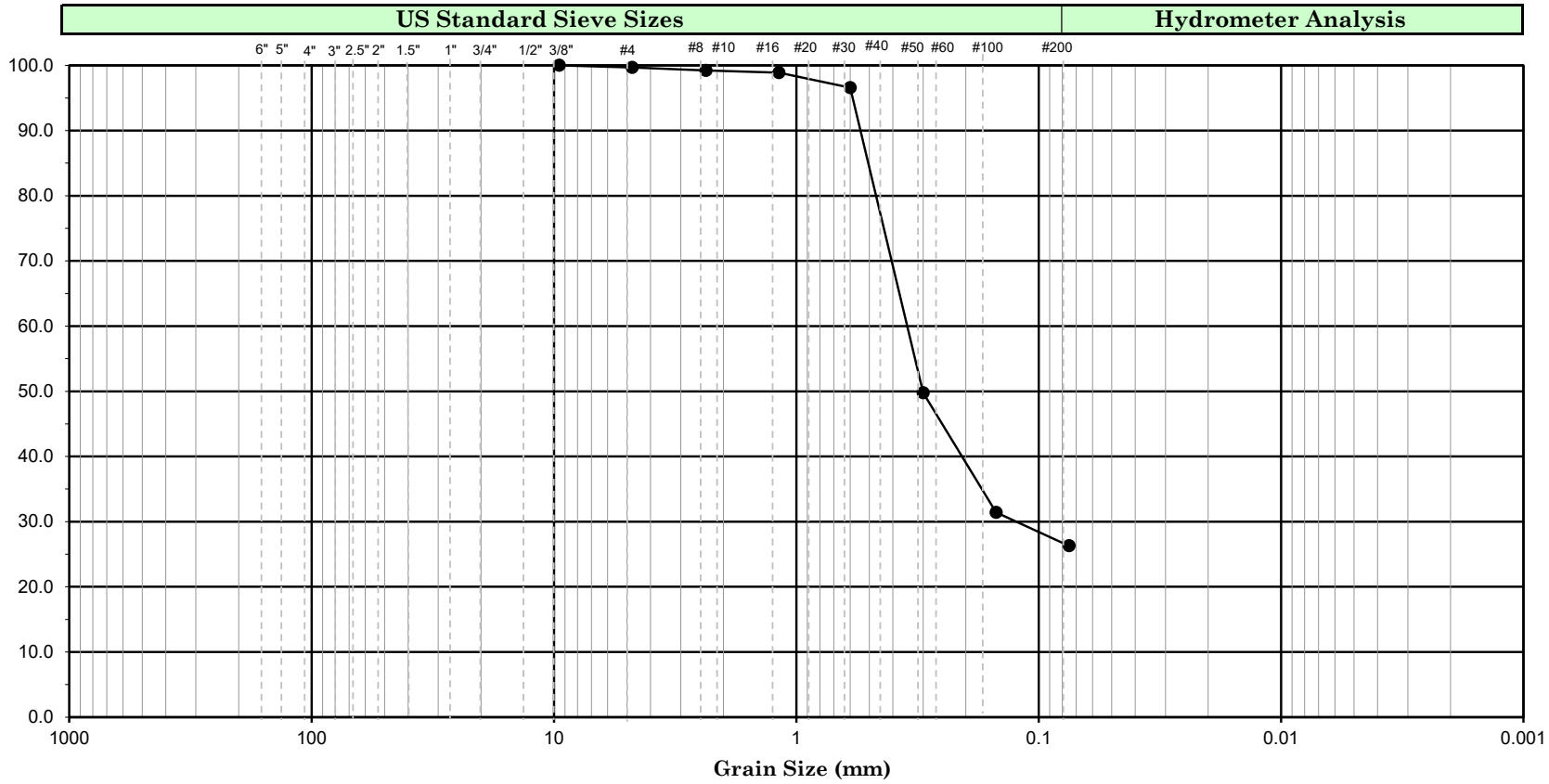

Cobbles	Gravel		Sand			Silt or Clay
	Coarse	Fine	Coarse	Medium	Fine	

Symbol	Boring Number	Sample Number	Depth (ft)		Depth (m)		Soil Color	Soil Description	U.S.C.S.
●	BH-2	D-9	20				dark yellowish brown	Clayey sand	SC
Remark									

Earth Mechanics, Inc.
Geotechnical and Earthquake Engineering

UCSD Steel Pile Research

Project No. : 21-601

Date : 05/05/24

GRAIN SIZE ANALYSIS

(ASTM D-7928)

Figure No. :

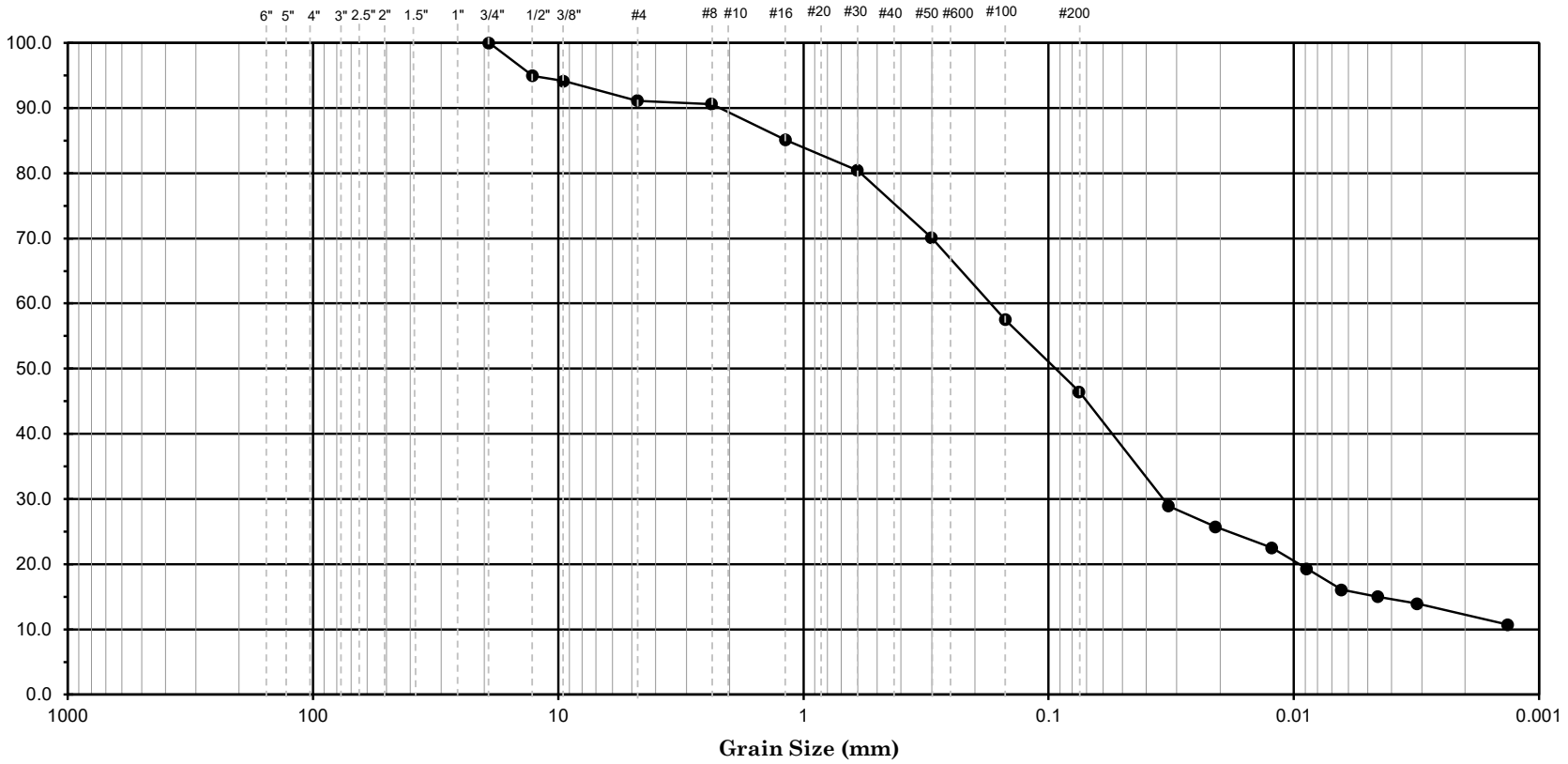

Cobbles	Gravel		Sand			Silt or Clay
	Coarse	Fine	Coarse	Medium	Fine	

Symbol	Boring Number	Sample Number	Depth (ft)	Depth (m)	Soil Color	Soil Description	U.S.C.S.
●	BH-1	D-1	0.0		yellowish brown with brown	Clayey sand	SC
Remark							

Earth Mechanics, Inc.
Geotechnical and Earthquake Engineering

UCSD Steel Pile Research

Project No. : 21-601

Date : 05/24/24

GRAIN SIZE ANALYSIS

(ASTM D 6913 ASTM D 7928)

Figure No. :

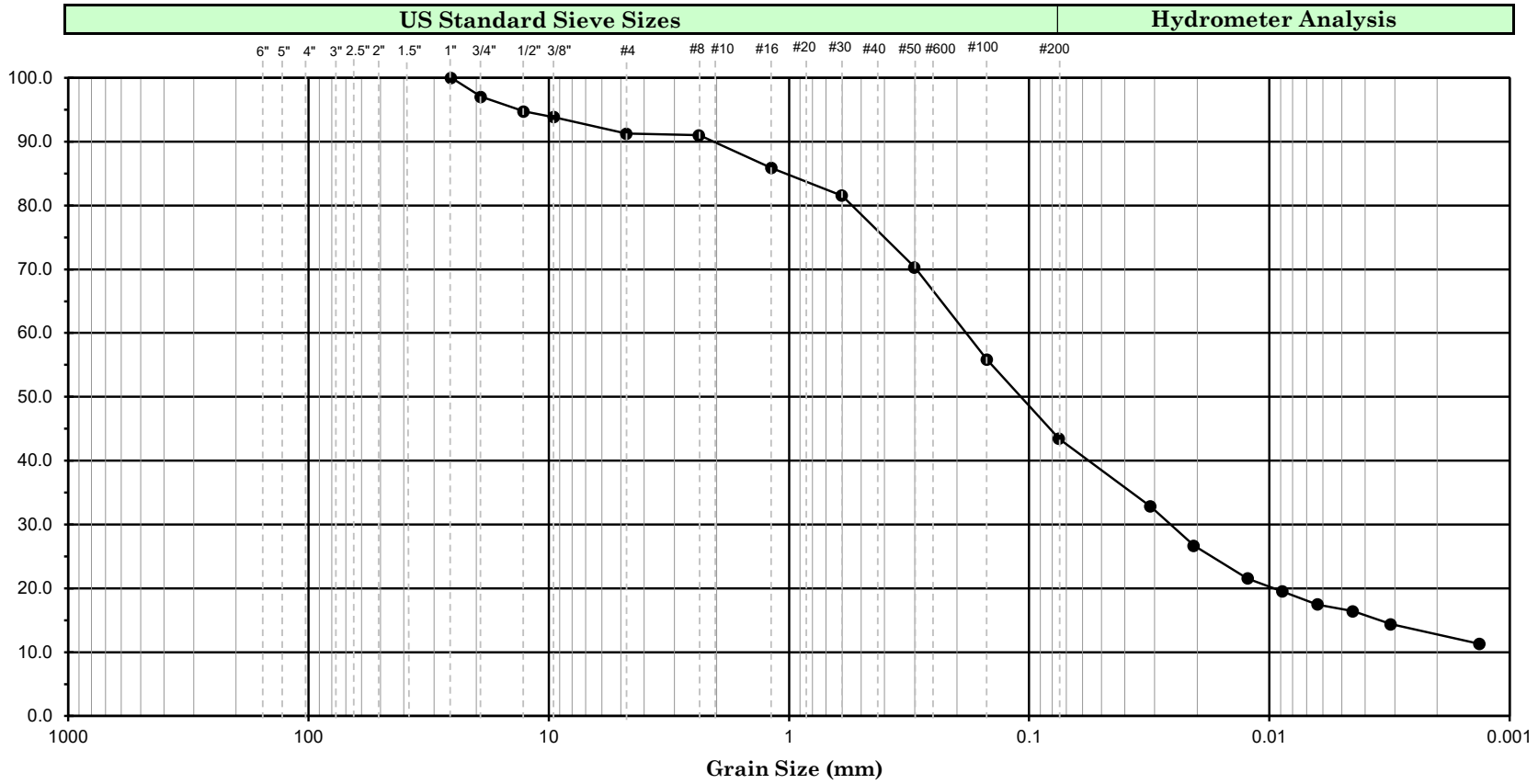

Cobbles	Gravel		Sand			Silt or Clay
	Coarse	Fine	Coarse	Medium	Fine	

Symbol	Boring Number	Sample Number	Depth (ft)	Depth (m)	Soil Color	Soil Description	U.S.C.S.
●	BH-1	T-2	2.5		yellowish brown with brown	Clayey sand	SC
Remark							

Earth Mechanics, Inc.
Geotechnical and Earthquake Engineering

UCSD Steel Pile Research

Project No. : 21-601

Date : 05/24/24

GRAIN SIZE ANALYSIS

(ASTM D 6913 ASTM D 7928)

Figure No. :

Cobbles	Gravel		Sand			Silt or Clay
	Coarse	Fine	Coarse	Medium	Fine	

Symbol	Boring Number	Sample Number	Depth (ft)	Depth (m)	Soil Color	Soil Description	U.S.C.S.
●	BH-1	D-3	5.0		yellowish brown	Clayey sand	SC
Remark							

Earth Mechanics, Inc.
Geotechnical and Earthquake Engineering

UCSD Steel Pile Research

Project No. : 21-601

Date : 05/24/24

GRAIN SIZE ANALYSIS

(ASTM D 6913 ASTM D 7928)

Figure No. :

Cobbles	Gravel		Sand			Silt or Clay
	Coarse	Fine	Coarse	Medium	Fine	

Symbol	Boring Number	Sample Number	Depth (ft)	Depth (m)	Soil Color	Soil Description	U.S.C.S.
●	BH-1	T-4	7.5		yellowish brown	Silty clayey sand	SC-SM
Remark							

Earth Mechanics, Inc.
Geotechnical and Earthquake Engineering

UCSD Steel Pile Research

Project No. : 21-601

Date : 05/24/24

GRAIN SIZE ANALYSIS

(ASTM D 6913 ASTM D 7928)

Figure No. :

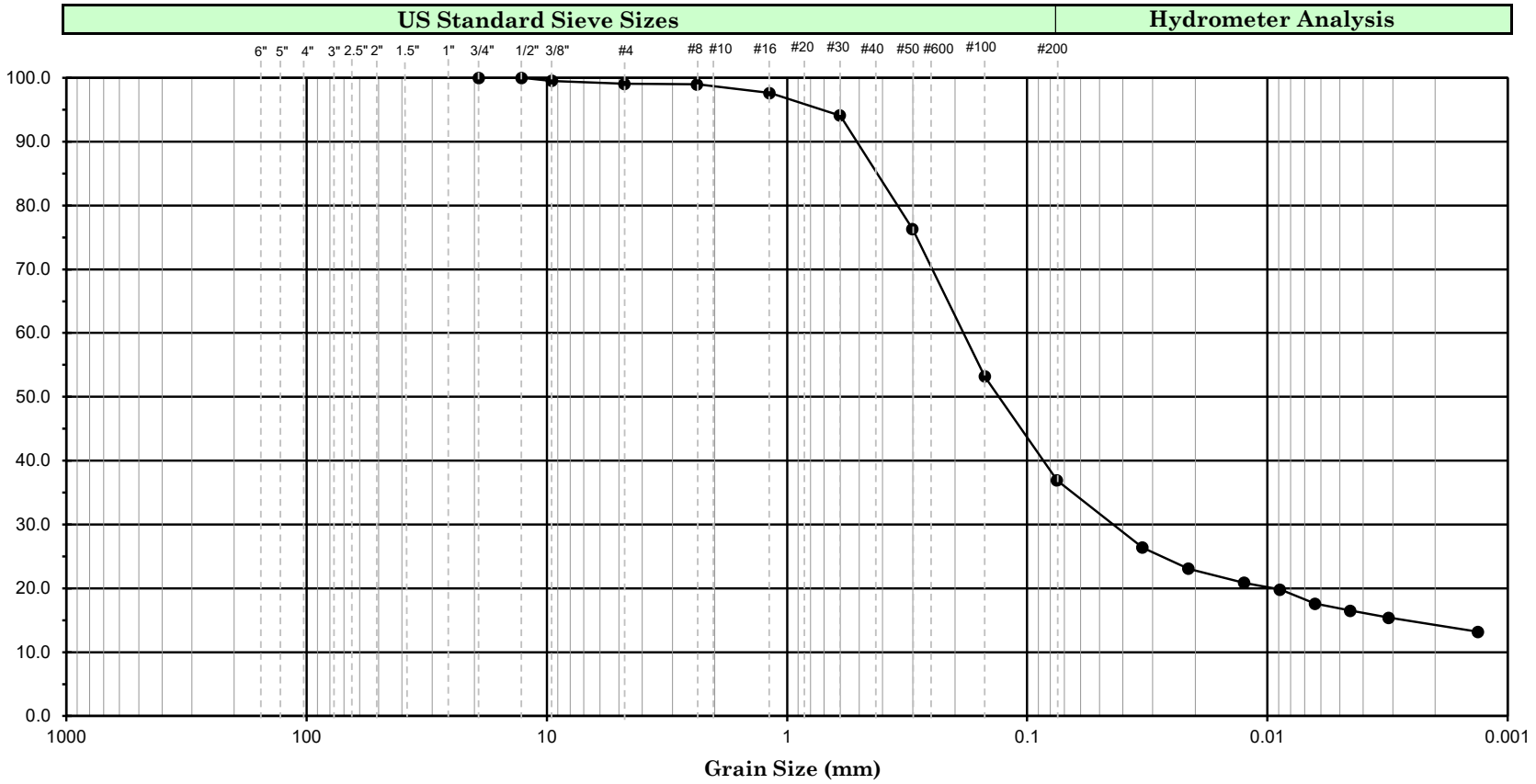

Cobbles	Gravel		Sand			Silt or Clay
	Coarse	Fine	Coarse	Medium	Fine	

Symbol	Boring Number	Sample Number	Depth (ft)	Depth (m)	Soil Color	Soil Description	U.S.C.S.
●	BH-1	D-5	10.0		yellowish brown	Clayey sand	SC
Remark							

Earth Mechanics, Inc.
Geotechnical and Earthquake Engineering

UCSD Steel Pile Research

Project No. : 21-601

Date : 05/24/24

GRAIN SIZE ANALYSIS

(ASTM D 6913 ASTM D 7928)

Figure No. :

Cobbles	Gravel		Sand			Silt or Clay
	Coarse	Fine	Coarse	Medium	Fine	

Symbol	Boring Number	Sample Number	Depth (ft)	Depth (m)	Soil Color	Soil Description	U.S.C.S.
●	BH-1	D-7	15.0		yellowish brown	Silty clayey sand	SC-SM
Remark							

Earth Mechanics, Inc.
Geotechnical and Earthquake Engineering

UCSD Steel Pile Research

Project No. : 21-601

Date : 05/24/24

GRAIN SIZE ANALYSIS

(ASTM D 6913 ASTM D 7928)

Figure No. :

Cobbles	Gravel		Sand			Silt or Clay
	Coarse	Fine	Coarse	Medium	Fine	

Symbol	Boring Number	Sample Number	Depth (ft)	Depth (m)	Soil Color	Soil Description	U.S.C.S.
●	BH-2	D-1	0.0		yellowish brown	Clayey sand	SC
Remark							

Earth Mechanics, Inc.
Geotechnical and Earthquake Engineering

UCSD Steel Pile Research

Project No. : 21-601

Date : 05/24/24

GRAIN SIZE ANALYSIS

(ASTM D 6913 ASTM D 7928)

Figure No. :

Cobbles	Gravel		Sand			Silt or Clay
	Coarse	Fine	Coarse	Medium	Fine	

Symbol	Boring Number	Sample Number	Depth (ft)	Depth (m)	Soil Color	Soil Description	U.S.C.S.
●	BH-2	T-2	2.5		yellowish brown with brown	Clayey sand	SC
Remark							

Earth Mechanics, Inc.
Geotechnical and Earthquake Engineering

UCSD Steel Pile Research

Project No. : 21-601

Date : 05/24/24

GRAIN SIZE ANALYSIS

(ASTM D 6913 ASTM D 7928)

Figure No. :

Cobbles	Gravel		Sand			Silt or Clay
	Coarse	Fine	Coarse	Medium	Fine	

Symbol	Boring Number	Sample Number	Depth (ft)	Depth (m)	Soil Color	Soil Description	U.S.C.S.
●	BH-2	D-3	5.0		yellowish brown	Clayey sand	SC
Remark							

Earth Mechanics, Inc.
Geotechnical and Earthquake Engineering

UCSD Steel Pile Research

Project No. : 21-601

Date : 05/24/24

GRAIN SIZE ANALYSIS

(ASTM D 6913 ASTM D 7928)

Figure No. :

Cobbles	Gravel		Sand			Silt or Clay
	Coarse	Fine	Coarse	Medium	Fine	

Symbol	Boring Number	Sample Number	Depth (ft)	Depth (m)	Soil Color	Soil Description	U.S.C.S.
●	BH-2	T-4	7.5		yellowish brown	Silty clayey sand	SC-SM
Remark							

Earth Mechanics, Inc.
Geotechnical and Earthquake Engineering

UCSD Steel Pile Research

Project No. : 21-601

Date : 05/24/24

GRAIN SIZE ANALYSIS

(ASTM D 6913 ASTM D 7928)

Figure No. :

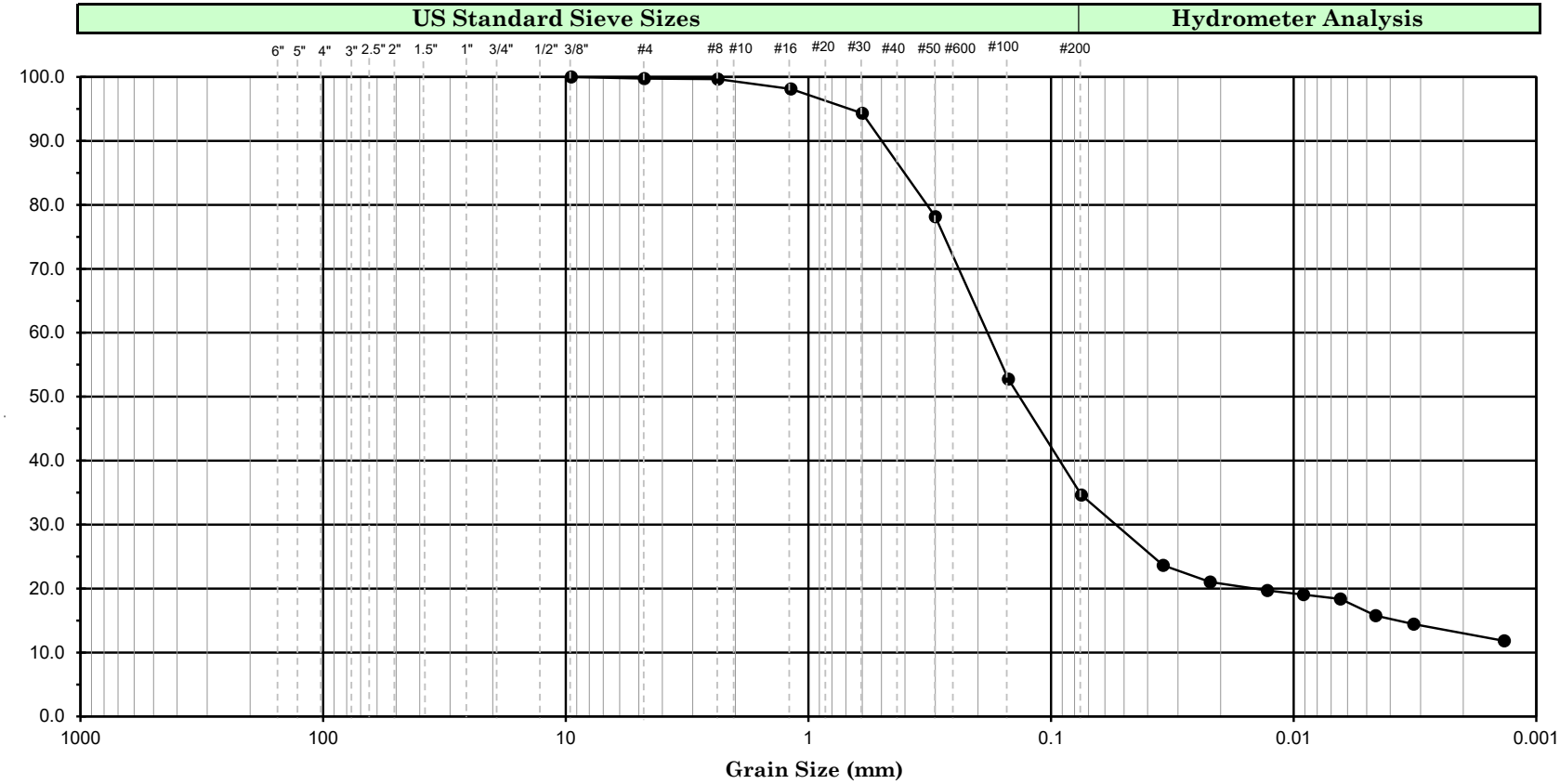

Cobbles	Gravel		Sand			Silt or Clay
	Coarse	Fine	Coarse	Medium	Fine	

Symbol	Boring Number	Sample Number	Depth (ft)	Depth (m)	Soil Color	Soil Description	U.S.C.S.
●	BH-2	D-5	10.0		yellowish brown	Silty clayey sand	SC-SM
Remark							

Earth Mechanics, Inc.
Geotechnical and Earthquake Engineering

UCSD Steel Pile Research

Project No. : 21-601

Date : 05/24/24

GRAIN SIZE ANALYSIS

(ASTM D 6913 ASTM D 7928)

Figure No. :

Cobbles	Gravel		Sand			Silt or Clay
	Coarse	Fine	Coarse	Medium	Fine	

Symbol	Boring Number	Sample Number	Depth (ft)	Depth (m)	Soil Color	Soil Description	U.S.C.S.
●	BH-2	D-7	15.0		yellowish brown	Clayey sand	SC
Remark							

Earth Mechanics, Inc.
Geotechnical and Earthquake Engineering

UCSD Steel Pile Research

Project No. : 21-601

Date : 05/24/24

GRAIN SIZE ANALYSIS

(ASTM D 6913 ASTM D 7928)

Figure No. :

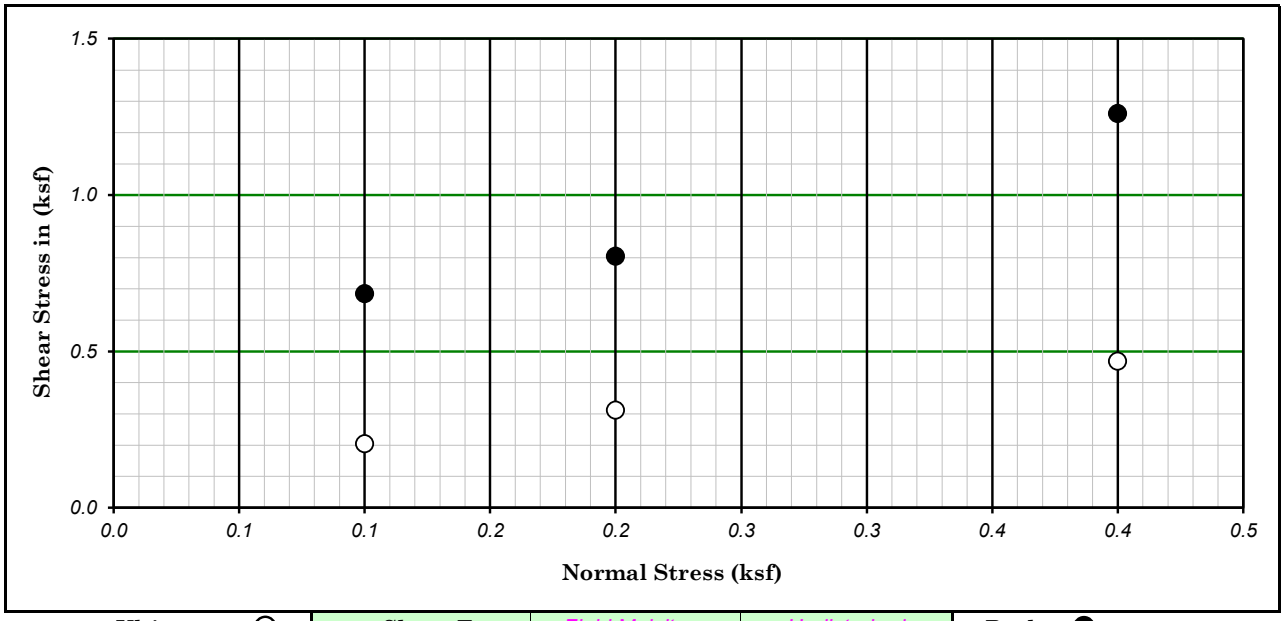

Ultimate : ○	Shear Type :	Field Moisiture	Undisturbed	Peak : ●

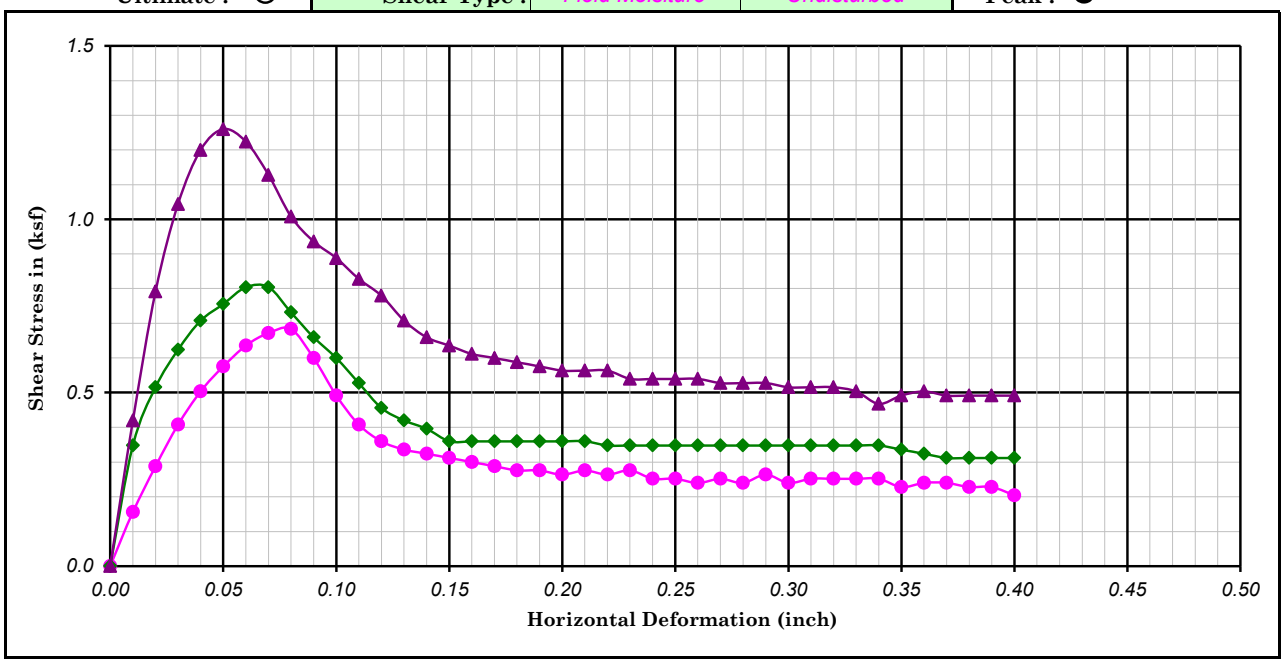

Boring No. : BH-1		Strength Intercept (C) :	0.46	(ksf)	Peak	0.13	(ksf)	Ultimate
Sample No. : D-1			21.8	(kPa)		6.0	(kPa)	
Depth (ft/m) : 0.0	0.00	Friction Angle (ϕ) :	63	Degree		41	Degree	
Description : Yellowish brown, CLAYEY SAND (SC)					Shear Rate (inch/minute) :		0.02	

SYMBOL	MOISTURE CONTENT (%)	DRY DENSITY (pcf)	DRY DENSITY (kN/m^3)	VOID RATIO	NORMAL STRESS (ksf)	NORMAL STRESS (kPa)	PEAK STRESS (ksf)	PEAK STRESS (kPa)	ULTIMATE STRESS (ksf)	ULTIMATE STRESS (kPa)
●	13.80	105.80	16.65	0.59	0.10	4.79	0.68	32.75	0.20	9.77
◆	14.61	111.75	17.59	0.51	0.20	9.58	0.80	38.50	0.31	14.94
▲	14.51	114.18	17.97	0.48	0.40	19.15	1.26	60.33	0.47	22.41

Earth Mechanics, Inc.
Geotechnical and Earthquake Engineering

UCSD Steel Pile Research

DIRECT SHEAR TEST

(ASTM D-3080)

Project No. : 21-601

Date : 05/22/24

Figure No.

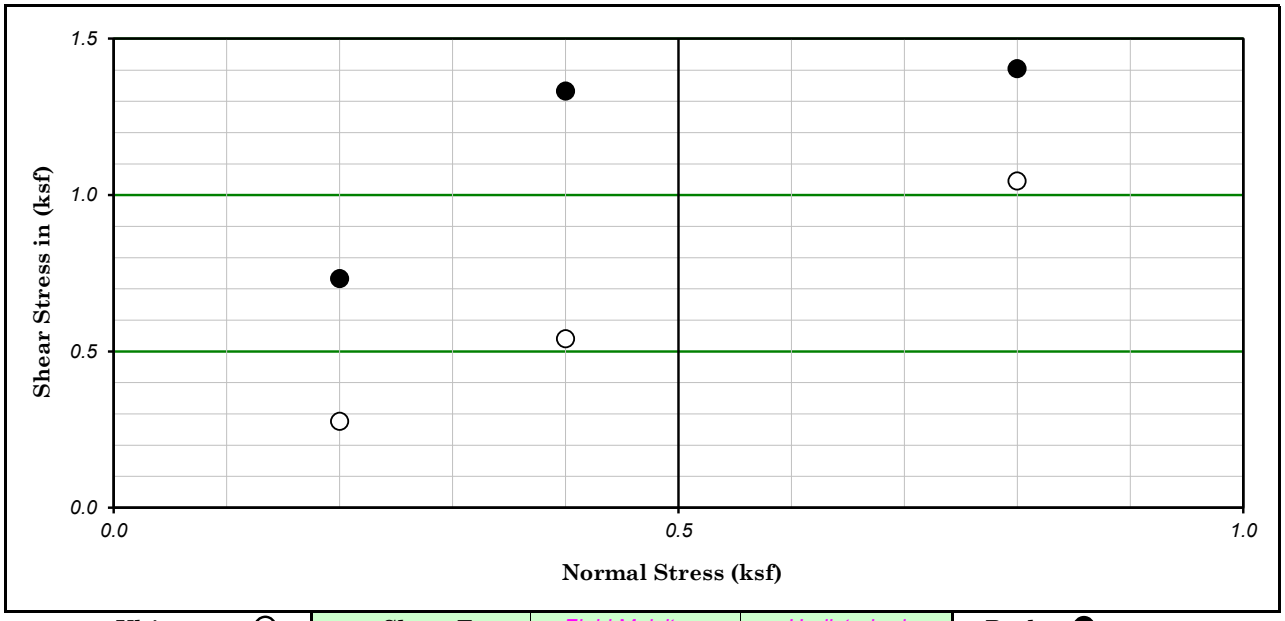

Ultimate : ○	Shear Type :	Field Moisiture	Undisturbed	Peak : ●

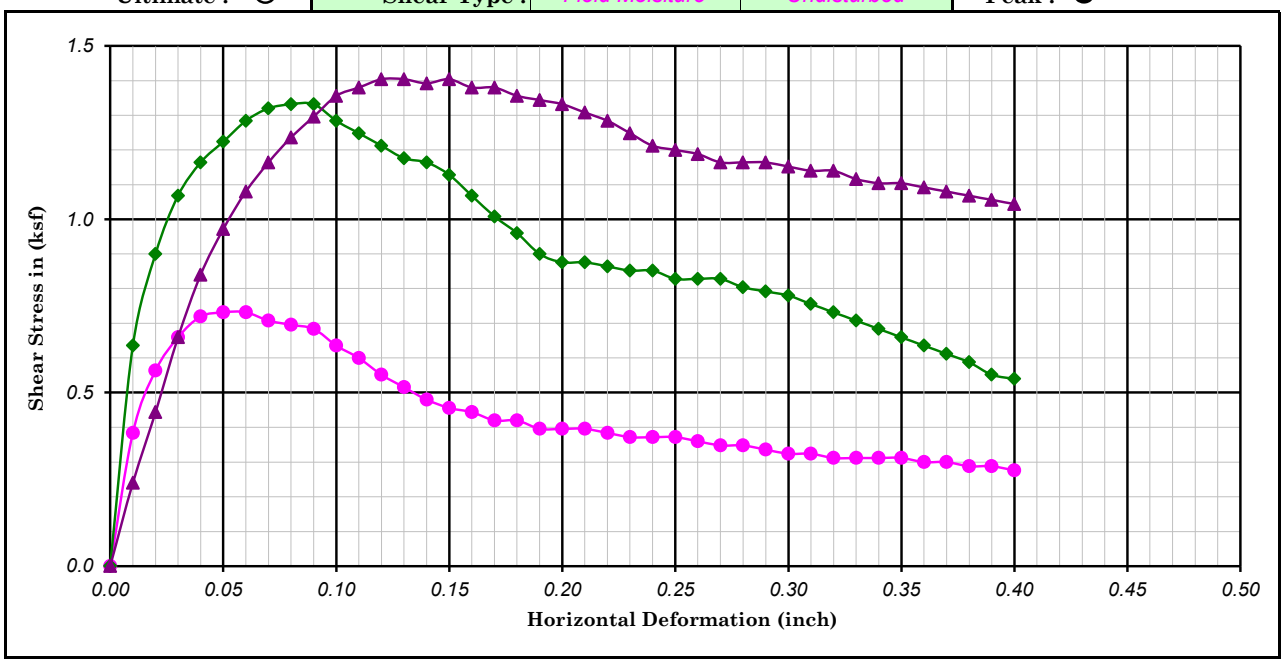

Boring No. : BH-1		Strength Intercept (C) :	0.70	(ksf)	Peak	0.02	(ksf)	Ultimate
Sample No. : T-2			33.3	(kPa)		1.1	(kPa)	
Depth (ft/m) : 2.5	0.00	Friction Angle (ϕ) :	45	Degree		45	Degree	
Description : Yellowish brown, CLAYEY SAND (SC)					Shear Rate (inch/minute) :		0.02	

SYMBOL	MOISTURE CONTENT (%)	DRY DENSITY (pcf)	DRY DENSITY (kN/m^3)	VOID RATIO	NORMAL STRESS (ksf)	NORMAL STRESS (kPa)	PEAK STRESS (ksf)	PEAK STRESS (kPa)	ULTIMATE STRESS (ksf)	ULTIMATE STRESS (kPa)
●	12.63	115.62	18.20	0.46	0.20	9.58	0.73	35.05	0.28	13.21
◆	12.22	117.59	18.51	0.43	0.40	19.15	1.33	63.78	0.54	25.86
▲	12.22	112.04	17.64	0.50	0.80	38.30	1.40	67.22	1.04	49.99

Earth Mechanics, Inc.
Geotechnical and Earthquake Engineering

UCSD Steel Pile Research

DIRECT SHEAR TEST

(ASTM D-3080)

Project No. : 21-601

Date : 05/22/24

Figure No.

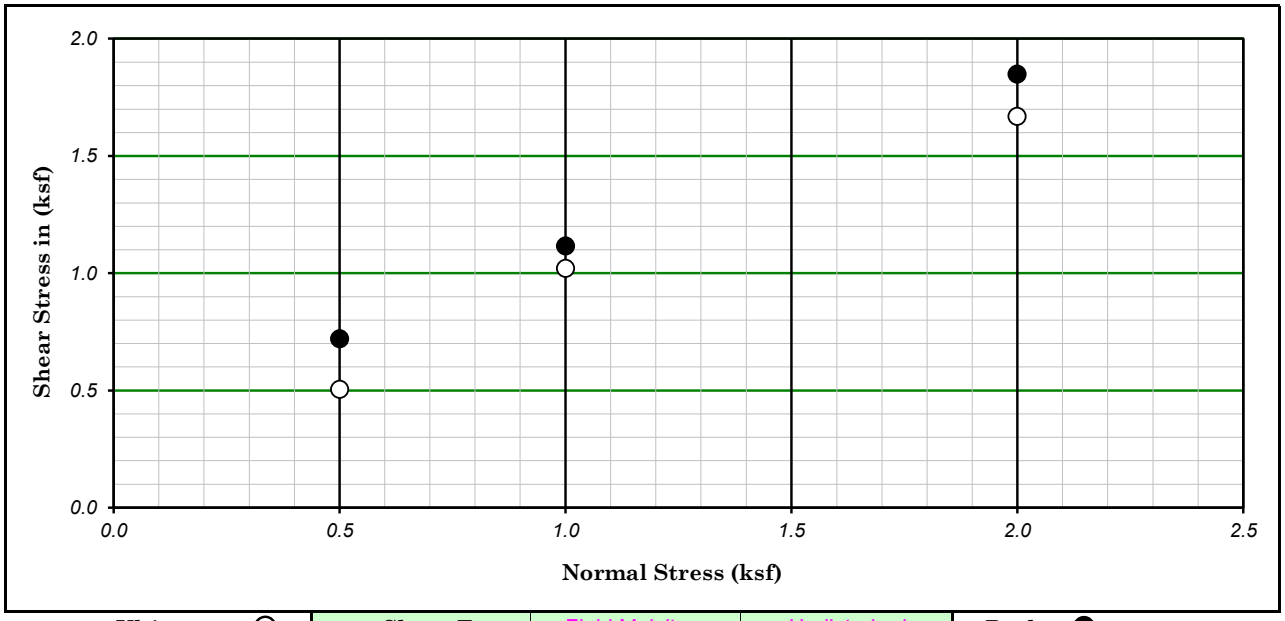

Ultimate : ○	Shear Type :	Field Moisiture	Undisturbed	Peak : ●

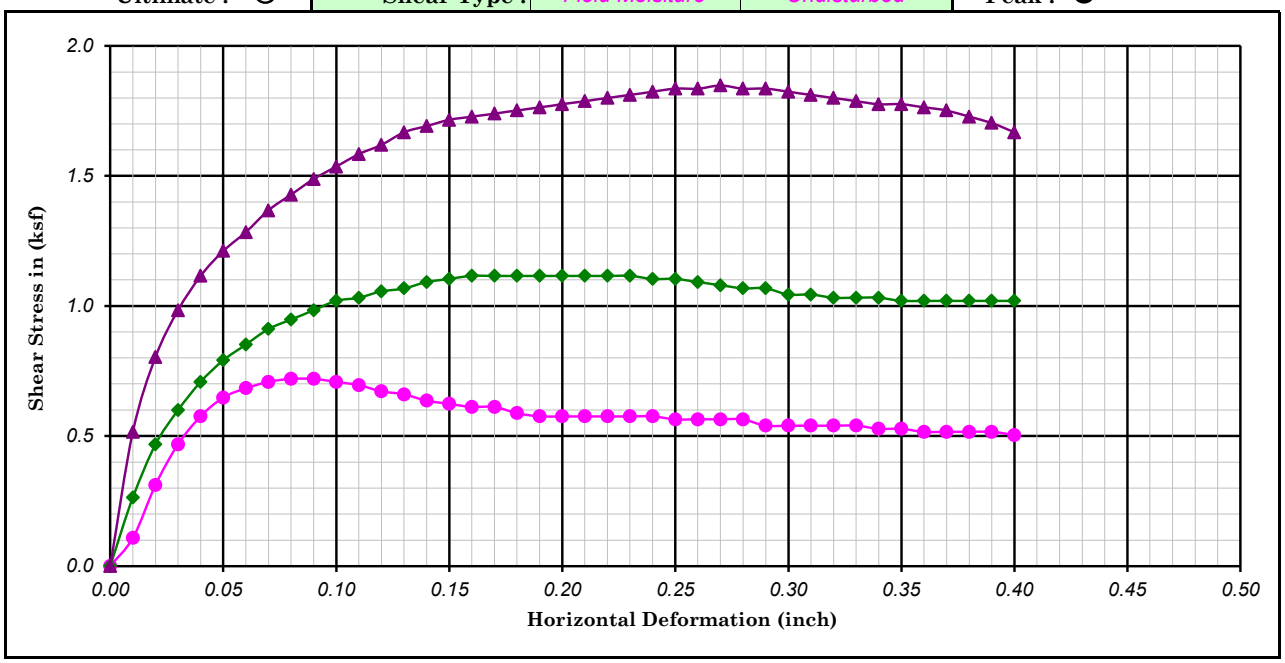

Boring No. : BH-1		Strength Intercept (C) :	0.35	(ksf)	Peak	0.18	(ksf)	Ultimate
Sample No. : T-4			16.9	(kPa)		8.6	(kPa)	
Depth (ft/m) : 7.5	0.00	Friction Angle (ϕ) :	37	Degree		37	Degree	
Description : Yellowish brown, SILTY CLAYEY SAND (SC-SM)					Shear Rate (inch/minute) :		0.02	

SYMBOL	MOISTURE CONTENT (%)	DRY DENSITY (pcf)	DRY DENSITY (kN/m^3)	VOID RATIO	NORMAL STRESS (ksf)	NORMAL STRESS (kPa)	PEAK STRESS (ksf)	PEAK STRESS (kPa)	ULTIMATE STRESS (ksf)	ULTIMATE STRESS (kPa)
●	11.01	102.64	16.16	0.64	0.50	23.94	0.72	34.47	0.50	24.13
◆	11.12	106.46	16.76	0.58	1.00	47.88	1.12	53.43	1.02	48.84
▲	10.73	104.10	16.39	0.62	2.00	95.76	1.85	88.48	1.67	79.86

Earth Mechanics, Inc.
Geotechnical and Earthquake Engineering

UCSD Steel Pile Research

DIRECT SHEAR TEST

(ASTM D-3080)

Project No. : 21-601

Date : 05/22/24

Figure No.

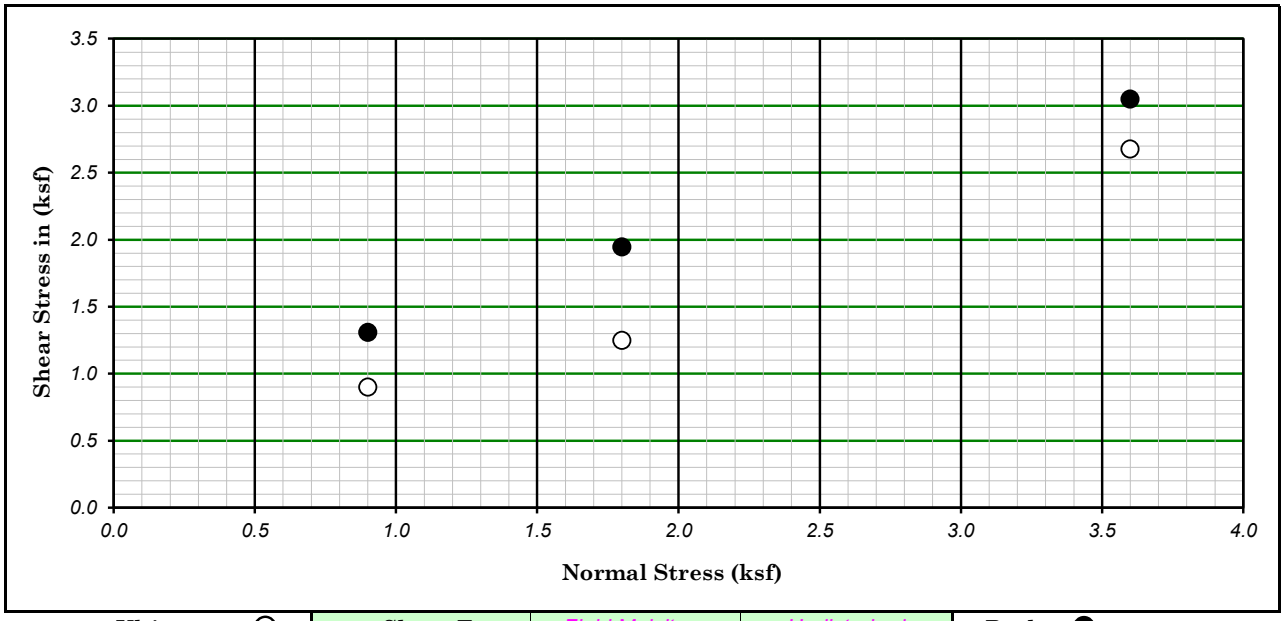

Ultimate : ○ | Shear Type : Field Moisiture | Undisturbed | Peak : ●

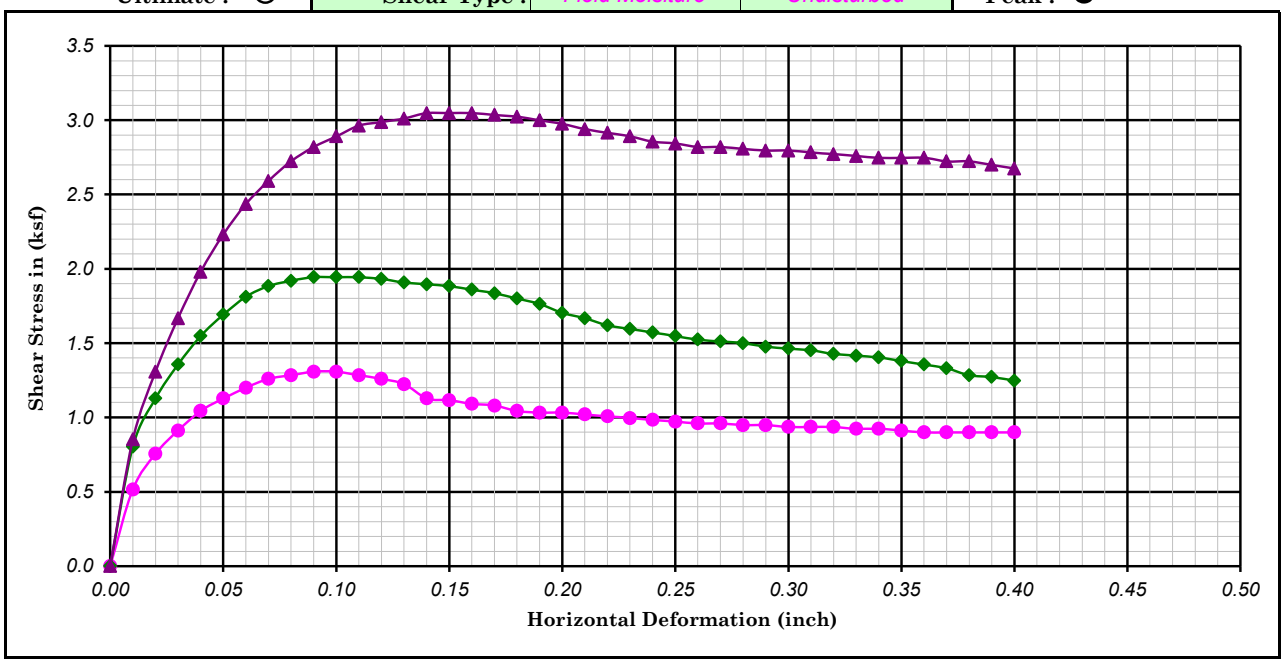

Boring No. : BH-1	Strength Intercept (C) :	0.76	(ksf)	Peak	0.19	(ksf)	Ultimate
Sample No. : D-7		36.20	(kPa)		8.91	(kPa)	
Depth (ft/m) : 15.0 / 0.00	Friction Angle (ϕ) :	33	Degree		33	Degree	

Description : Yellowish brown, SILTY CLAYEY SAND (SC-SM) — Shear Rate (inch/minute) : 0.02

SYMBOL	MOISTURE CONTENT (%)	DRY DENSITY (pcf)	DRY DENSITY (kN/m^3)	VOID RATIO	NORMAL STRESS (ksf)	NORMAL STRESS (kPa)	PEAK STRESS (ksf)	PEAK STRESS (kPa)	ULTIMATE STRESS (ksf)	ULTIMATE STRESS (kPa)
●	14.19	101.85	16.03	0.65	0.90	43.09	1.31	62.63	0.90	43.09
◆	13.13	109.95	17.31	0.53	1.80	86.18	1.94	93.08	1.25	59.75
▲	13.53	109.08	17.17	0.55	3.60	172.37	3.05	145.94	2.68	128.13

Earth Mechanics, Inc.
Geotechnical and Earthquake Engineering

UCSD Steel Pile Research

DIRECT SHEAR TEST

(ASTM D-3080)

Project No. : 21-601 | Date : 05/22/24 | Figure No.

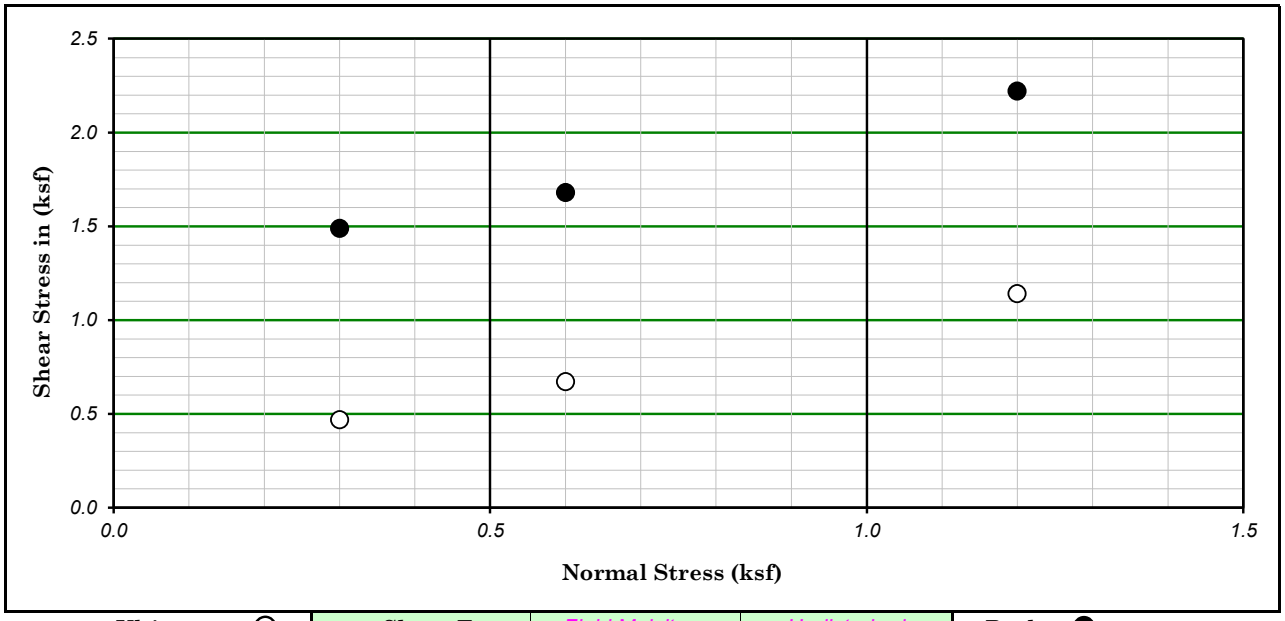

Ultimate : ○	Shear Type :	Field Moisiture	Undisturbed	Peak : ●

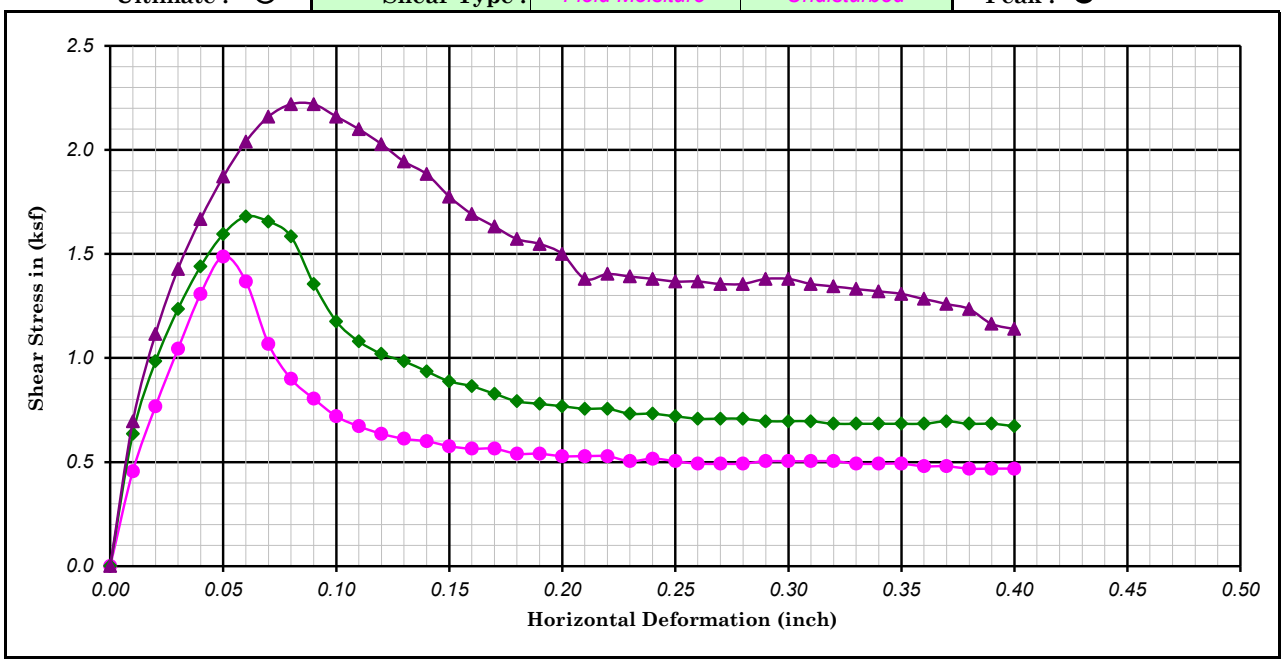

Boring No. : BH-2		Strength Intercept (C) :	1.22	(ksf)	Peak	0.23	(ksf)	Ultimate	
Sample No. : D-3			58.3	(kPa)		11.2	(kPa)		
Depth (ft/m) : 5.0	0.00	Friction Angle (ϕ) :	40	Degree		37	Degree		
Description : Yellowish brown with brown, CLAYEY SAND (SC)					Shear Rate (inch/minute) :		0.02		

SYMBOL	MOISTURE CONTENT (%)	DRY DENSITY (pcf)	DRY DENSITY (kN/m^3)	VOID RATIO	NORMAL STRESS (ksf)	NORMAL STRESS (kPa)	PEAK STRESS (ksf)	PEAK STRESS (kPa)	ULTIMATE STRESS (ksf)	ULTIMATE STRESS (kPa)
●	14.59	120.60	18.98	0.40	0.30	14.36	1.49	71.25	0.47	22.41
◆	12.16	114.73	18.06	0.47	0.60	28.73	1.68	80.44	0.67	32.18
▲	12.65	113.18	17.81	0.49	1.20	57.46	2.22	106.29	1.14	54.58

Earth Mechanics, Inc.
Geotechnical and Earthquake Engineering

UCSD Steel Pile Research

DIRECT SHEAR TEST

(ASTM D-3080)

Project No. : 21-601

Date : 05/22/24

Figure No.

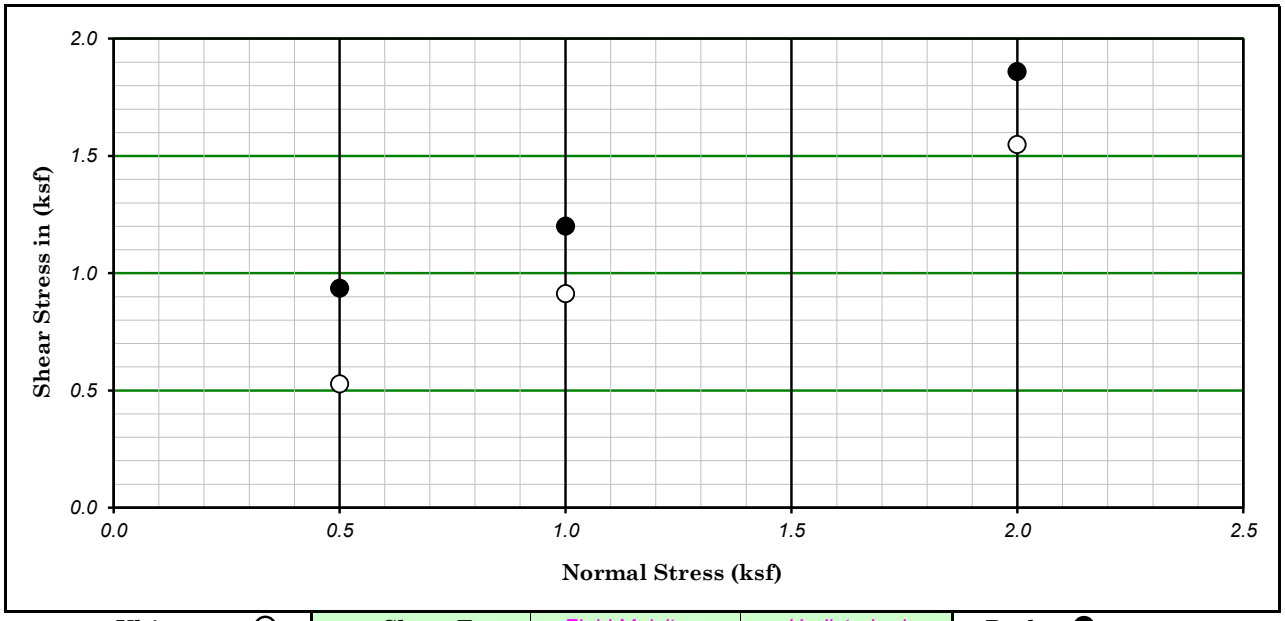

Ultimate : ○	Shear Type :	Field Moisiture	Undisturbed	Peak : ●

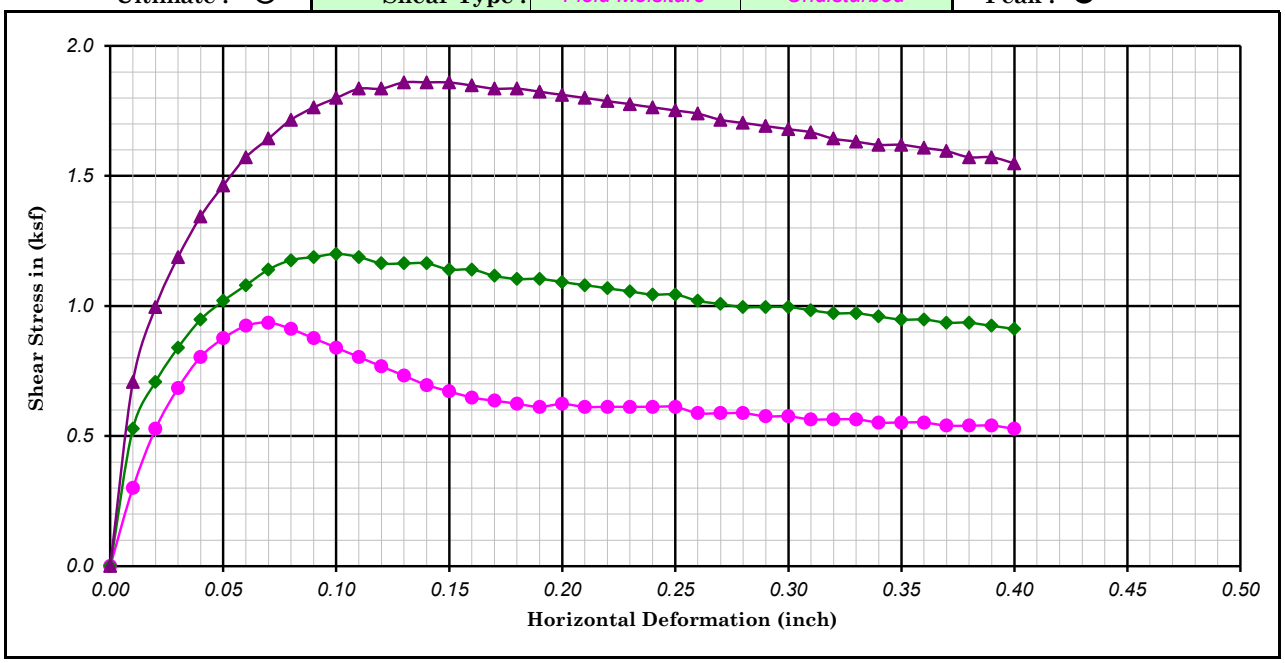

Boring No. : BH-2		Strength Intercept (C) :	0.61	(ksf)	Peak	0.21	(ksf)	Ultimate
Sample No. : T-4			29.0	(kPa)		10.1	(kPa)	
Depth (ft/m) : 7.5	0.00	Friction Angle (ϕ) :	32	Degree		32	Degree	
Description : Yellowish brown, SILTY CLAYEY SAND (SC-SM)					Shear Rate (inch/minute) :		0.02	

SYMBOL	MOISTURE CONTENT (%)	DRY DENSITY (pcf)	DRY DENSITY (kN/m^3)	VOID RATIO	NORMAL STRESS (ksf)	NORMAL STRESS (kPa)	PEAK STRESS (ksf)	PEAK STRESS (kPa)	ULTIMATE STRESS (ksf)	ULTIMATE STRESS (kPa)
●	11.97	106.19	16.71	0.59	0.50	23.94	0.94	44.82	0.53	25.28
◆	11.09	110.44	17.38	0.53	1.00	47.88	1.20	57.46	0.91	43.67
▲	11.34	108.97	17.15	0.55	2.00	95.76	1.86	89.06	1.55	74.12

Earth Mechanics, Inc.
Geotechnical and Earthquake Engineering

UCSD Steel Pile Research

DIRECT SHEAR TEST

(ASTM D-3080)

Project No. : 21-601

Date : 05/22/24

Figure No.

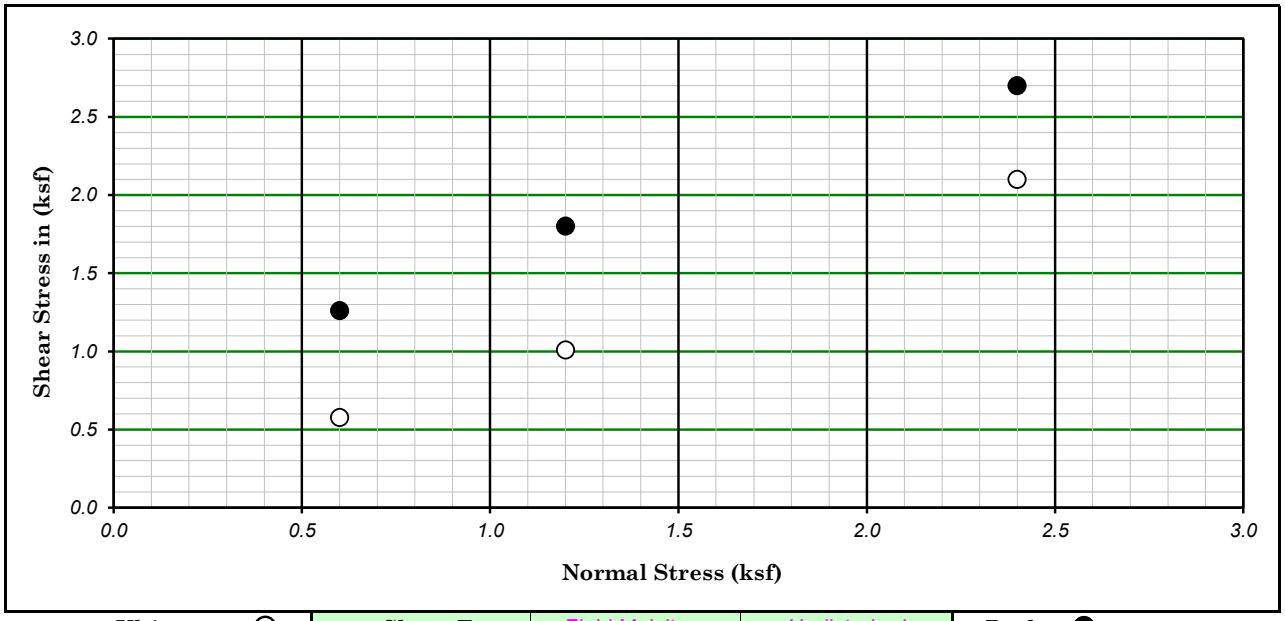

Ultimate : ○	Shear Type :	Field Moisiture	Undisturbed	Peak : ●

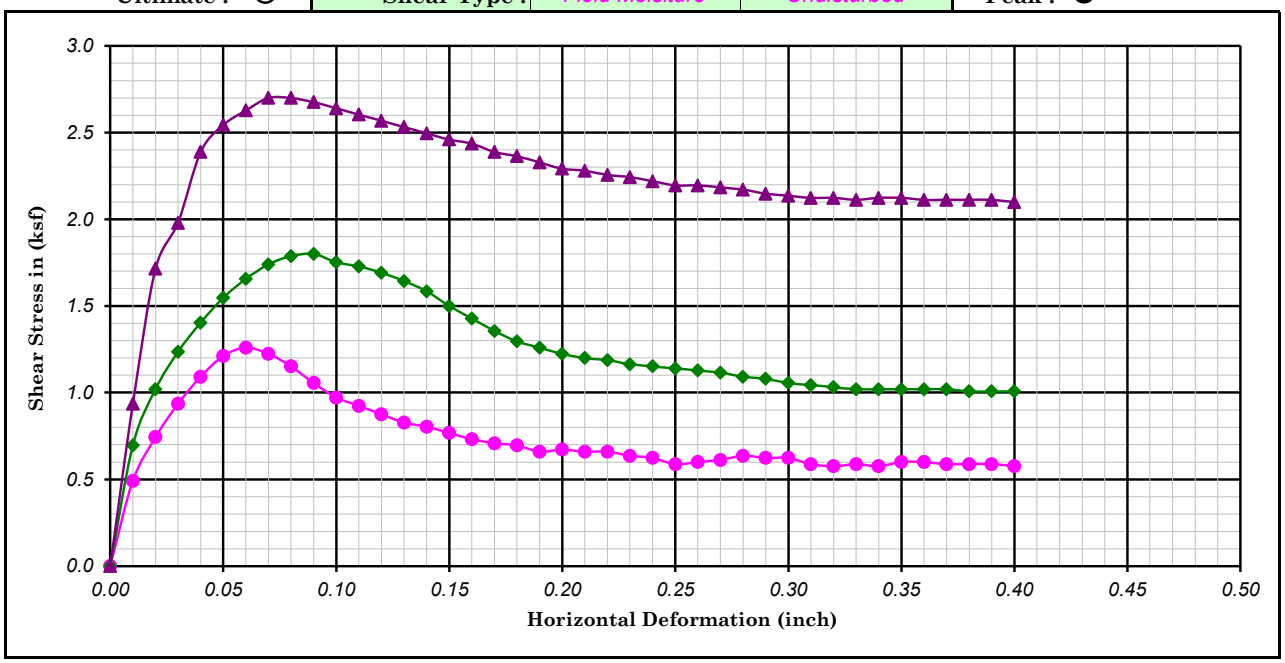

Boring No. : BH-2		Strength Intercept (C) :	0.81	(ksf)	Peak	0.03	(ksf)	Ultimate	
Sample No. : D-5			38.8	(kPa)		1.4	(kPa)		
Depth (ft/m) : 10.0	0.00	Friction Angle (ϕ) :	38	Degree		38	Degree		
Description : Yellowish brown, SILTY CLAYEY SAND (SC-SM)					Shear Rate (inch/minute) :		0.02		

SYMBOL	MOISTURE CONTENT (%)	DRY DENSITY (pcf)	DRY DENSITY (kN/m^3)	VOID RATIO	NORMAL STRESS (ksf)	NORMAL STRESS (kPa)	PEAK STRESS (ksf)	PEAK STRESS (kPa)	ULTIMATE STRESS (ksf)	ULTIMATE STRESS (kPa)
●	13.74	114.62	18.04	0.47	0.60	28.73	1.26	60.33	0.58	27.58
◆	12.46	109.89	17.30	0.53	1.20	57.46	1.80	86.18	1.01	48.26
▲	11.94	112.26	17.67	0.50	2.40	114.91	2.70	129.28	2.10	100.55

Earth Mechanics, Inc.
Geotechnical and Earthquake Engineering

UCSD Steel Pile Research

DIRECT SHEAR TEST

(ASTM D-3080)

Figure No.

Project No. : 21-601

Date : 05/22/24

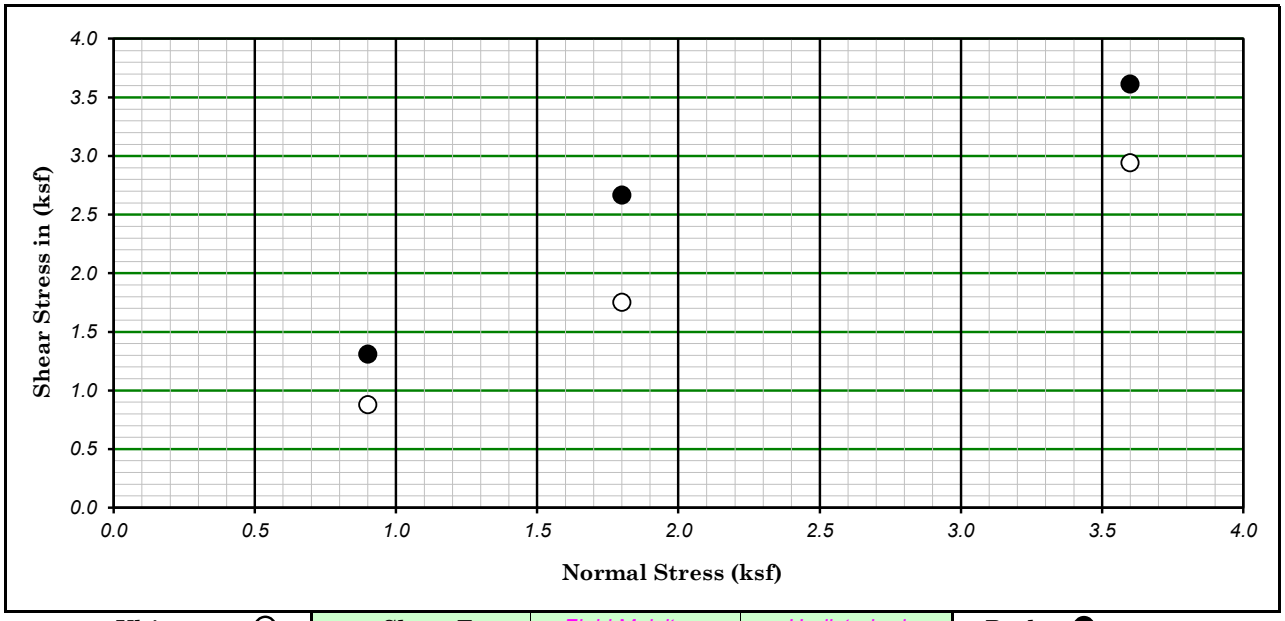

Ultimate : ○ | Shear Type : Field Moisiture | Undisturbed | Peak : ●

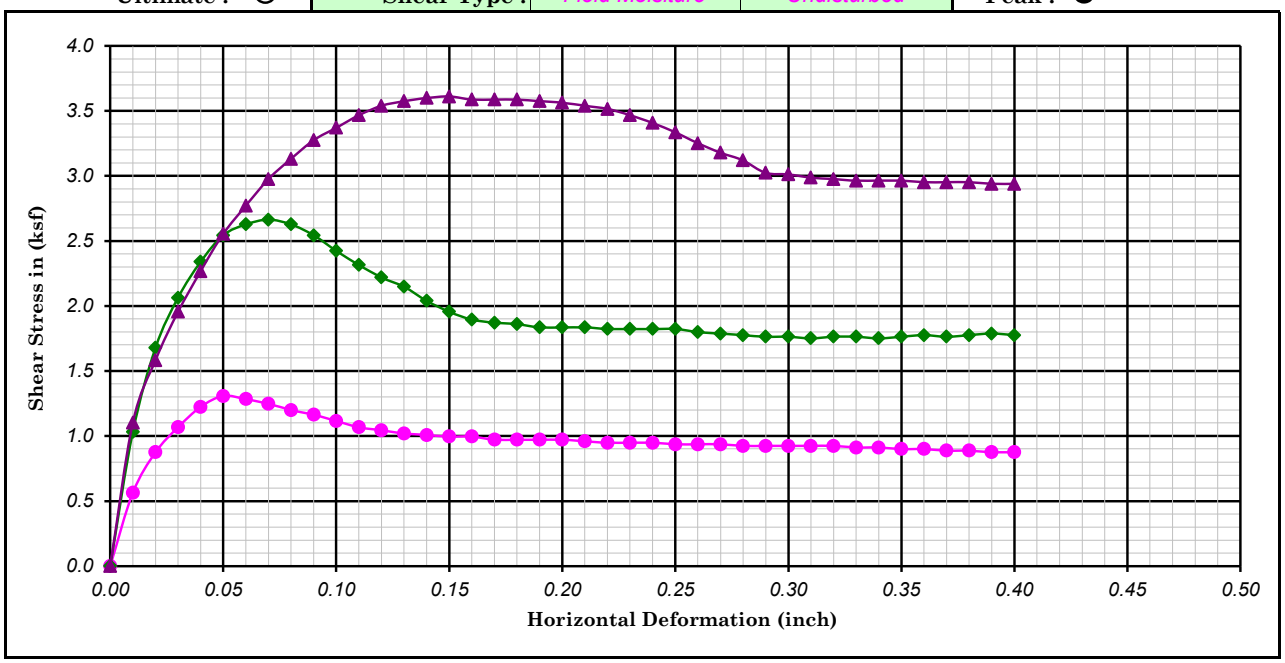

Boring No. : BH-2	Strength Intercept (C) :	0.83	(ksf)	Peak	0.28	(ksf)	Ultimate
Sample No. : D-7		39.9	(kPa)		13.5	(kPa)	
Depth (ft/m) : 15.0 / 0.00	Friction Angle (ϕ) :	39	Degree		37	Degree	

Description : Dark yellowish brown , CLAYEY SAND (SC) — Shear Rate (inch/minute) : 0.02

SYMBOL	MOISTURE CONTENT (%)	DRY DENSITY (pcf)	DRY DENSITY (kN/m^3)	VOID RATIO	NORMAL STRESS (ksf)	NORMAL STRESS (kPa)	PEAK STRESS (ksf)	PEAK STRESS (kPa)	ULTIMATE STRESS (ksf)	ULTIMATE STRESS (kPa)
●	14.29	114.01	17.95	0.48	0.90	43.09	1.31	62.63	0.88	41.94
◆	14.36	120.36	18.94	0.40	1.80	86.18	2.66	127.55	1.75	83.89
▲	13.70	116.06	18.27	0.45	3.60	172.37	3.61	172.94	2.94	140.77

Earth Mechanics, Inc.
Geotechnical and Earthquake Engineering

UCSD Steel Pile Research

DIRECT SHEAR TEST

(ASTM D-3080)

Project No. : 21-601 | Date : 05/22/24 | Figure No.

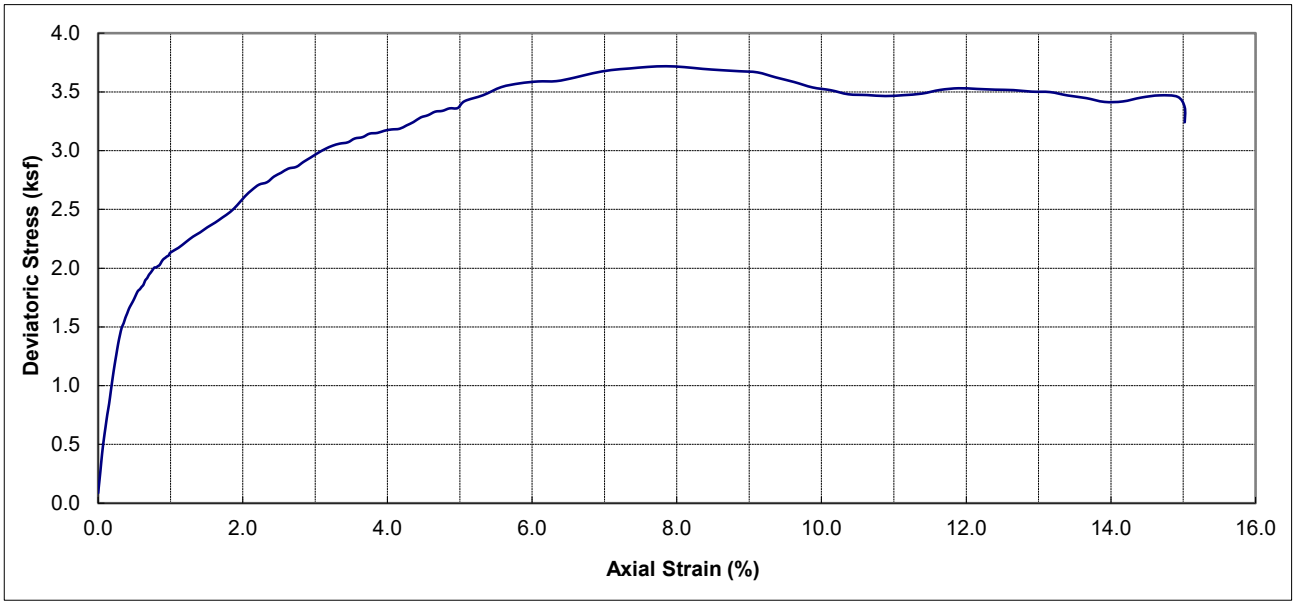

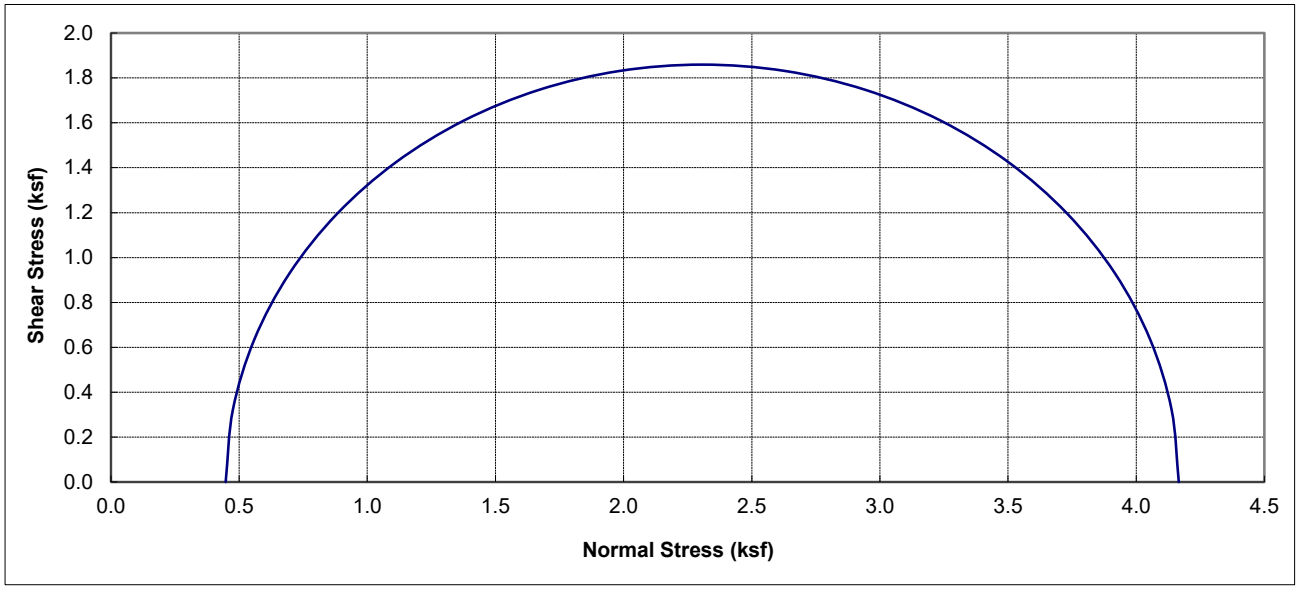

Boring No.	Sample No.	Depth (ft)	Soil Type	Dry Density (pcf)	Moisture Content (%)	Conf. Stress (ksf)	Max Dev. Stress (ksf)	Initial Saturation (%)
BH-1	D-3	5	Yellowish brown with brown, CLAYEY SAND (SC)	112.6	13.64	0.45	3.72	74.3

Earth Mechanics, Inc.
Geotechnical and Earthquake Engineering

UCSD Steel Pile Research

UNCONSOLIDATED UNDRAINED TEST
(ASTM D2850)

Project No. : 21-601

Date : 05/13/24

Figure No. :

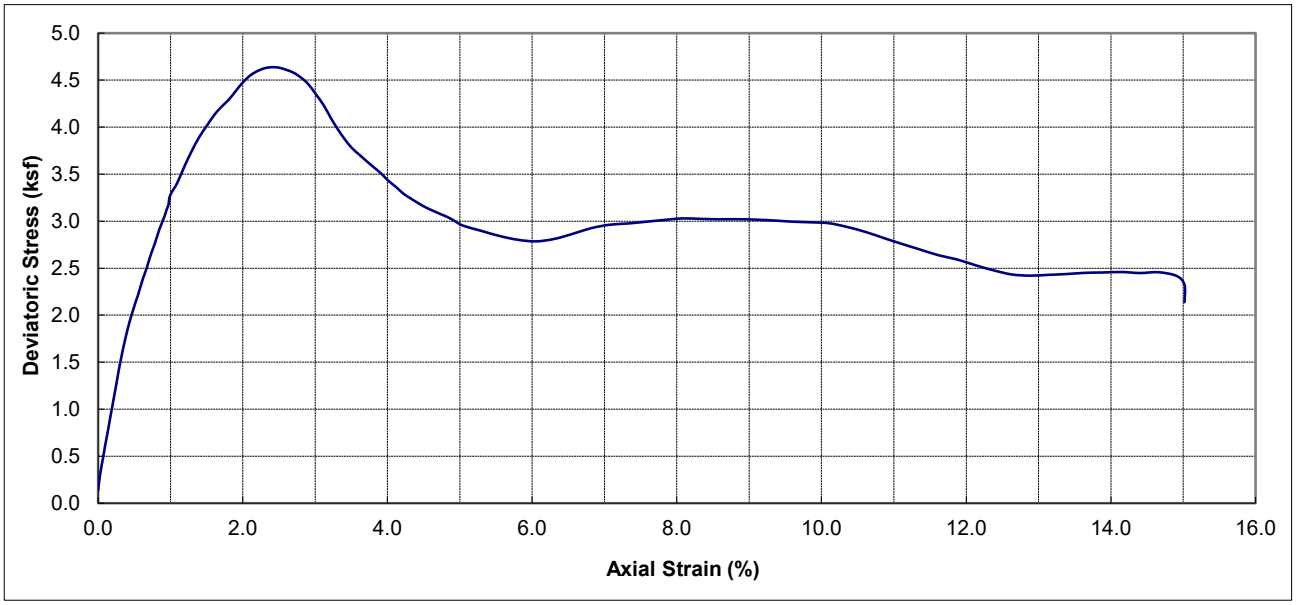

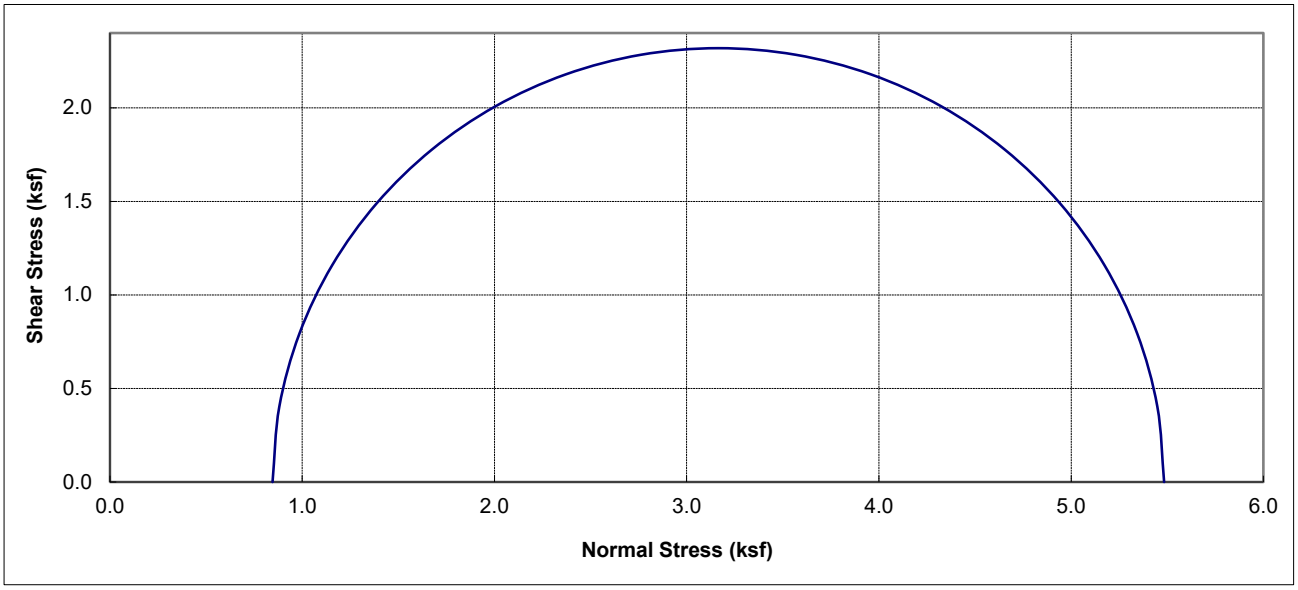

Boring No.	Sample No.	Depth (ft)	Soil Type	Dry Density (pcf)	Moisture Content (%)	Conf. Stress (ksf)	Max Dev. Stress (ksf)	Initial Saturation (%)
BH-1	D-5	10	Yellowish brown, SILTY CLAYEY SAND (SC-SM)	112.7	15.31	0.85	4.64	83.5

Earth Mechanics, Inc. Geotechnical and Earthquake Engineering	UCSD Steel Pile Research
	UNCONSOLIDATED UNDRAINED TEST (ASTM D2850) Figure No. :
Project No. : 21-601	Date : 05/13/24

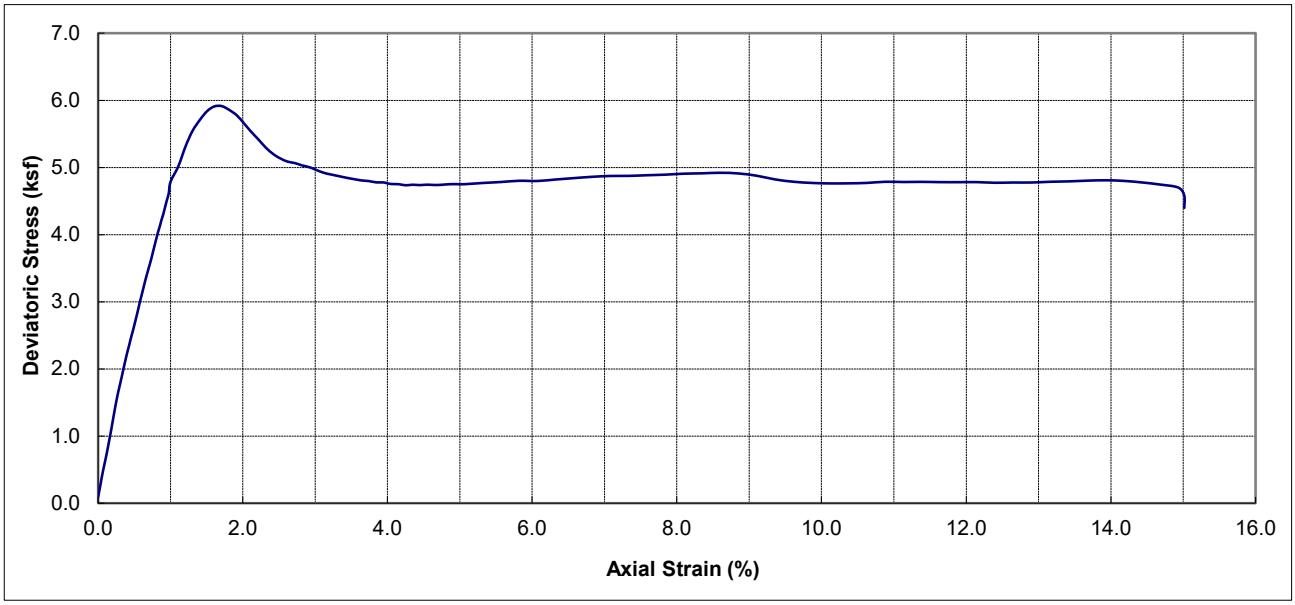

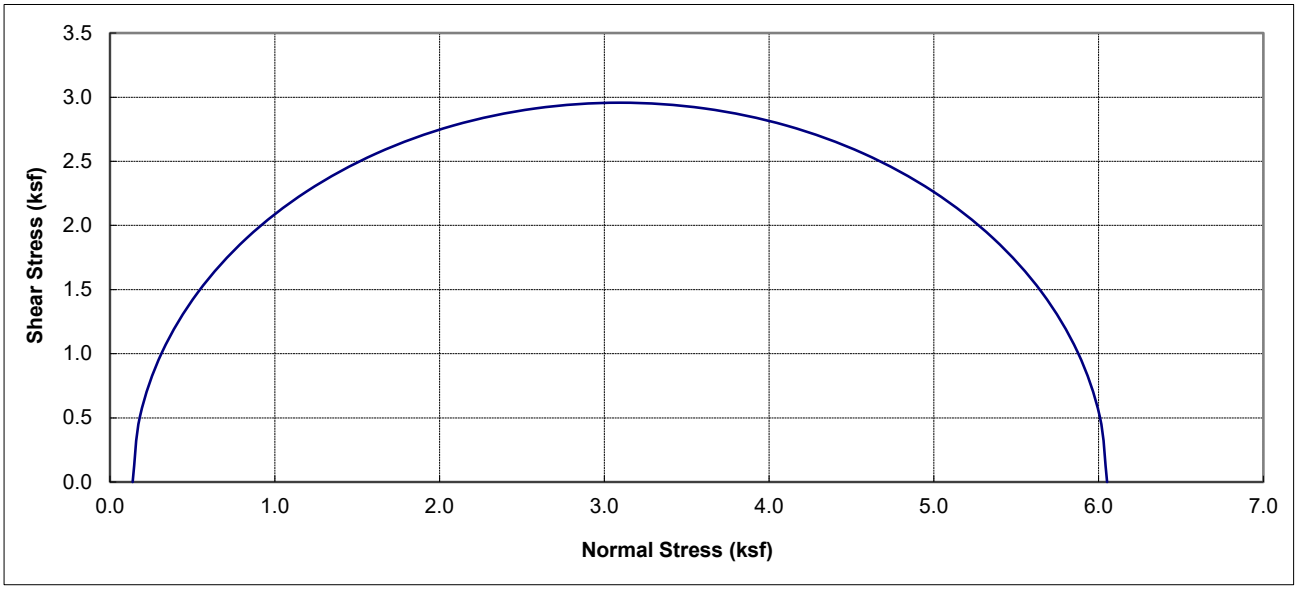

Boring No.	Sample No.	Depth (ft)	Soil Type	Dry Density (pcf)	Moisture Content (%)	Conf. Stress (ksf)	Max Dev. Stress (ksf)	Initial Saturation (%)
BH-2	D-1	0	Yellowish brown, CLAYEY SAND (SC)	114.7	13.42	0.14	5.91	77.2

Earth Mechanics, Inc.
Geotechnical and Earthquake Engineering

UCSD Steel Pile Research

UNCONSOLIDATED UNDRAINED TEST
(ASTM D2850)

Project No. : 21-601

Date : 05/13/24

Figure No. :

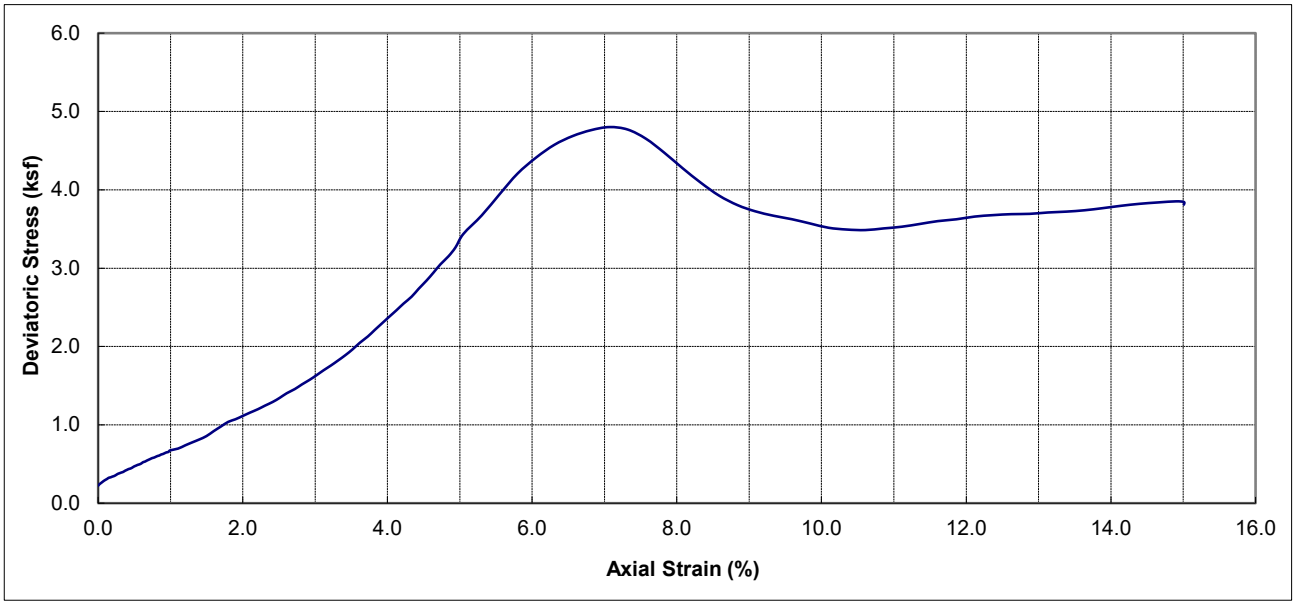

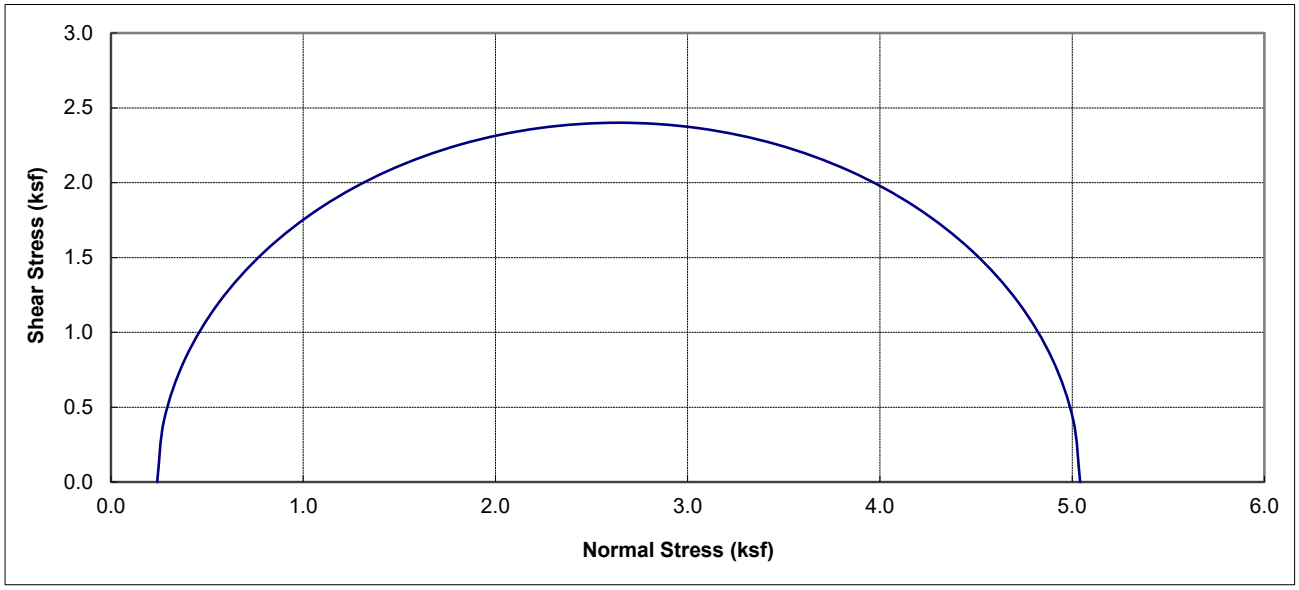

Boring No.	Sample No.	Depth (ft)	Soil Type	Dry Density (pcf)	Moisture Content (%)	Conf. Stress (ksf)	Max Dev. Stress (ksf)	Initial Saturation (%)
BH-2	T-2	2.5	Yellowish brown, CLAYEY SAND (SC)	115.1	11.82	0.24	4.80	68.7

Earth Mechanics, Inc. Geotechnical and Earthquake Engineering	UCSD Steel Pile Research
	UNCONSOLIDATED UNDRAINED TEST (ASTM D2850) Figure No. :
Project No. : 21-601	Date : 05/17/24

Kehoe Testing and Engineering
714-901-7270
rich@kehoetesting.com
www.kehoetesting.com

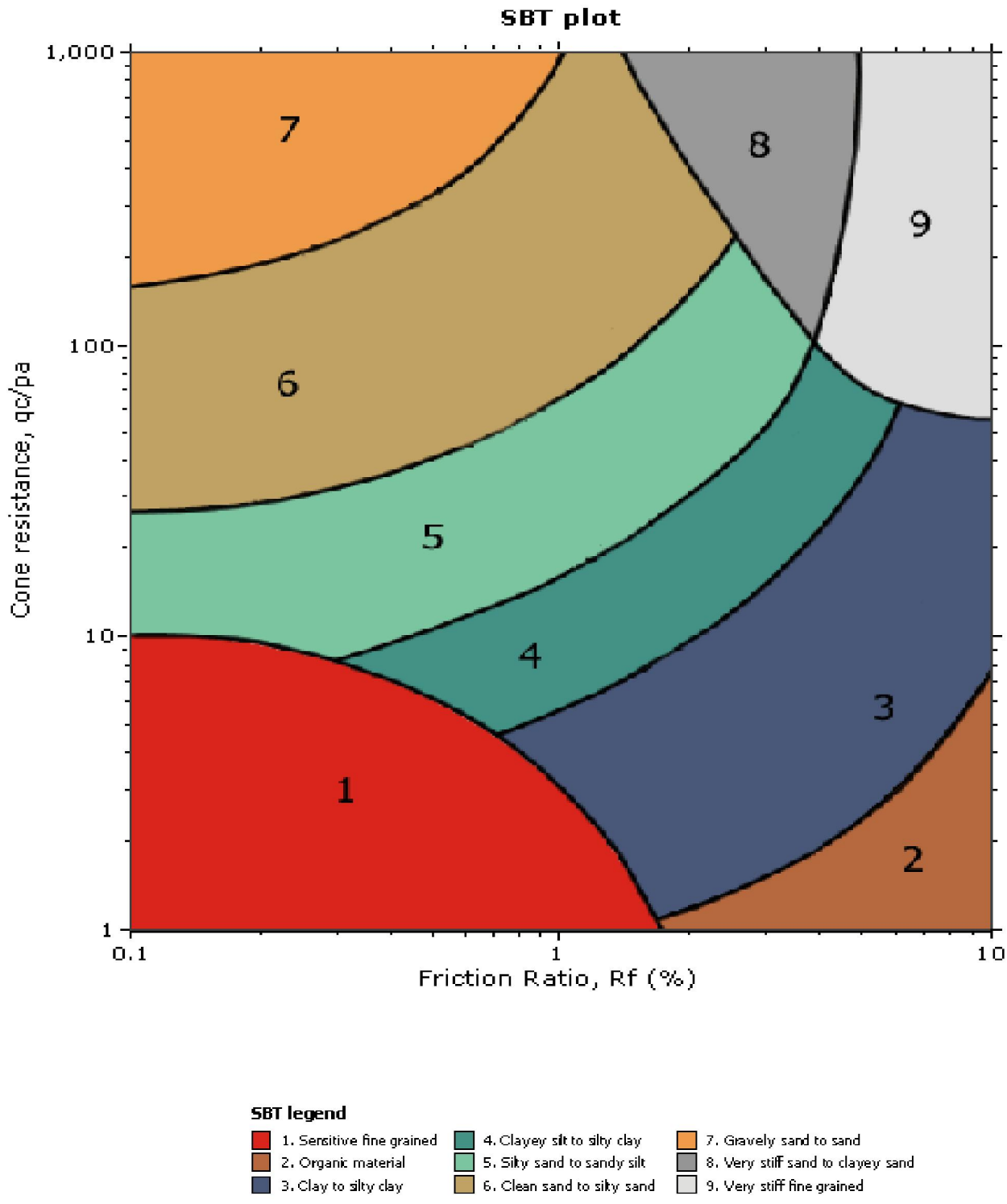

UCSD
ESEC Englekirk Structural Engr. Center North Soil Pit
San Diego, CA

CPT Shear Wave Measurements

Location	Tip Depth (ft)	Geophone Depth (ft)	Travel Distance (ft)	S-Wave Arrival (msec)	S-Wave Velocity from Surface (ft/sec)	Interval S-Wave Velocity (ft/sec)
SCPT-1	2.49	1.49	2.49	2.76	904	
	4.99	3.99	4.46	5.56	803	703
	7.51	6.51	6.81	8.24	826	876
	10.04	9.04	9.26	12.08	766	638
	12.50	11.50	11.67	15.72	743	663
	15.03	14.03	14.17	18.30	774	969
	17.52	16.52	16.64	20.96	794	928
	20.01	19.01	19.11	23.56	811	952
	22.51	21.51	21.60	25.16	859	1555
	25.03	24.03	24.11	26.62	906	1719
SCPT-2	2.53	1.53	2.52	2.88	874	
	4.99	3.99	4.46	5.78	772	671
	7.51	6.51	6.81	8.56	796	844
	10.01	9.01	9.23	11.96	772	711
	12.50	11.50	11.67	15.60	748	671
	15.03	14.03	14.17	18.20	779	961
	17.49	16.49	16.61	21.18	784	818
	20.01	19.01	19.11	24.20	790	829
	22.51	21.51	21.60	26.44	817	1111
	25.00	24.00	24.08	27.92	863	1676

Shear Wave Source Offset - 2 ft

S-Wave Velocity from Surface = Travel Distance/S-Wave Arrival
Interval S-Wave Velocity = (Travel Dist2-Travel Dist1)/(Time2-Time1)

SPT CAL

SPT HAMMER ENERGY MEASUREMENTS

Prepared for;
Tri-County Drilling
9631 Candida St
San Diego, CA 92126

(858) 271-0099

Energy Measurement Test for Dynamic Penetrometers
Standard Penetration Tests (SPT)

Date: 10/05/2023

Location: San Diego, CA

Prepared by;

SPT CAL
5512 Belem Dr
Chino Hills, CA 91709

909-730-2161
bc@sptcal.com

Drill: Rig 77

Energy Transfer Ratio = 80.4% @ 43.9 blows per minute

Hammer Energy Measurements performed per ASTM D4633 using an approved and calibrated SPT Analyzer 8G from Pile Dynamics, Inc. meeting the criteria of ASTM D4633-05 and per the process defined in ASTM D4633-05, The process and equipment requirements followed per ASTM D4633-05 meet the criteria of ASTM D4633-16.

GROUP SYMBOLS AND NAMES

Graphic / Symbol	Group Names
GW	Well-graded GRAVEL Well-graded GRAVEL with SAND
GP	Poorly graded GRAVEL Poorly graded GRAVEL with SAND
GW-GM	Well-graded GRAVEL with SILT Well-graded GRAVEL with SILT and SAND
GW-GC	Well-graded GRAVEL with CLAY (or SILTY CLAY) Well-graded GRAVEL with CLAY and SAND (or SILTY CLAY and SAND)
GP-GM	Poorly graded GRAVEL with SILT Poorly graded GRAVEL with SILT and SAND
GP-GC	Poorly graded GRAVEL with CLAY (or SILTY CLAY) Poorly graded GRAVEL with CLAY and SAND (or SILTY CLAY and SAND)
GM	SILTY GRAVEL SILTY GRAVEL with SAND
GC	CLAYEY GRAVEL CLAYEY GRAVEL with SAND
GC-GM	SILTY, CLAYEY GRAVEL SILTY, CLAYEY GRAVEL with SAND
SW	Well-graded SAND Well-graded SAND with GRAVEL
SP	Poorly graded SAND Poorly graded SAND with GRAVEL
SW-SM	Well-graded SAND with SILT Well-graded SAND with SILT and GRAVEL
SW-SC	Well-graded SAND with CLAY (or SILTY CLAY) Well-graded SAND with CLAY and GRAVEL (or SILTY CLAY and GRAVEL)
SP-SM	Poorly graded SAND with SILT Poorly graded SAND with SILT and GRAVEL
SP-SC	Poorly graded SAND with CLAY (or SILTY CLAY) Poorly graded SAND with CLAY and GRAVEL (or SILTY CLAY and GRAVEL)
SM	SILTY SAND SILTY SAND with GRAVEL
SC	CLAYEY SAND CLAYEY SAND with GRAVEL
SC-SM	SILTY, CLAYEY SAND SILTY, CLAYEY SAND with GRAVEL
PT	PEAT
	COBBLES COBBLES and BOULDERS BOULDERS

Graphic / Symbol	Group Names
CL	Lean CLAY Lean CLAY with SAND Lean CLAY with GRAVEL SANDY lean CLAY SANDY lean CLAY with GRAVEL GRAVELLY lean CLAY GRAVELLY lean CLAY with SAND
CL-ML	SILTY CLAY SILTY CLAY with SAND SILTY CLAY with GRAVEL SANDY SILTY CLAY SANDY SILTY CLAY with GRAVEL GRAVELLY SILTY CLAY GRAVELLY SILTY CLAY with SAND
ML	SILT SILT with SAND SILT with GRAVEL SANDY SILT SANDY SILT with GRAVEL GRAVELLY SILT GRAVELLY SILT with SAND
OL	ORGANIC lean CLAY ORGANIC lean CLAY with SAND ORGANIC lean CLAY with GRAVEL SANDY ORGANIC lean CLAY SANDY ORGANIC lean CLAY with GRAVEL GRAVELLY ORGANIC lean CLAY GRAVELLY ORGANIC lean CLAY with SAND
OL	ORGANIC SILT ORGANIC SILT with SAND ORGANIC SILT with GRAVEL SANDY ORGANIC SILT SANDY ORGANIC SILT with GRAVEL GRAVELLY ORGANIC SILT GRAVELLY ORGANIC SILT with SAND
CH	Fat CLAY Fat CLAY with SAND Fat CLAY with GRAVEL SANDY fat CLAY SANDY fat CLAY with GRAVEL GRAVELLY fat CLAY GRAVELLY fat CLAY with SAND
MH	Elastic SILT Elastic SILT with SAND Elastic SILT with GRAVEL SANDY elastic SILT SANDY elastic SILT with GRAVEL GRAVELLY elastic SILT GRAVELLY elastic SILT with SAND
OH	ORGANIC fat CLAY ORGANIC fat CLAY with SAND ORGANIC fat CLAY with GRAVEL SANDY ORGANIC fat CLAY SANDY ORGANIC fat CLAY with GRAVEL GRAVELLY ORGANIC fat CLAY GRAVELLY ORGANIC fat CLAY with SAND
OH	ORGANIC elastic SILT ORGANIC elastic SILT with SAND ORGANIC elastic SILT with GRAVEL SANDY ORGANIC elastic SILT SANDY ORGANIC elastic SILT with GRAVEL GRAVELLY ORGANIC elastic SILT GRAVELLY ORGANIC elastic SILT with SAND
OL/OH	ORGANIC SOIL ORGANIC SOIL with SAND ORGANIC SOIL with GRAVEL SANDY ORGANIC SOIL SANDY ORGANIC SOIL with GRAVEL GRAVELLY ORGANIC SOIL GRAVELLY ORGANIC SOIL with SAND

FIELD AND LABORATORY TESTS

C	Consolidation (ASTM D 2435-04)
CL	Collapse Potential (ASTM D 5333-03)
CP	Compaction Curve (CTM 216 - 06)
CR	Corrosion, Sulfates, Chlorides (CTM 643 - 99; CTM 417 - 06; CTM 422 - 06)
CU	Consolidated Undrained Triaxial (ASTM D 4767-02)
DS	Direct Shear (ASTM D 3080-04)
EI	Expansion Index (ASTM D 4829-03)
M	Moisture Content (ASTM D 2216-05)
OC	Organic Content (ASTM D 2974-07)
P	Permeability (CTM 220 - 05)
PA	Particle Size Analysis (ASTM D 422-63 [2002])
PI	Liquid Limit, Plastic Limit, Plasticity Index (AASHTO T 89-02, AASHTO T 90-00)
PL	Point Load Index (ASTM D 5731-05)
PM	Pressure Meter
PP	Pocket Penetrometer
R	R-Value (CTM 301 - 00)
SE	Sand Equivalent (CTM 217 - 99)
SG	Specific Gravity (AASHTO T 100-06)
SL	Shrinkage Limit (ASTM D 427-04)
SW	Swell Potential (ASTM D 4546-03)
TV	Pocket Torvane
UC	Unconfined Compression - Soil (ASTM D 2166-06) Unconfined Compression - Rock (ASTM D 2938-95)
UU	Unconsolidated Undrained Triaxial (ASTM D 2850-03)
UW	Unit Weight (ASTM D 4767-04)
VS	Vane Shear (AASHTO T 223-96 [2004])
WA	Wash Analysis (ASTM D 1140-97)

SAMPLER GRAPHIC SYMBOLS

- Standard Penetration Test (SPT)
- Standard California Sampler
- Modified California Sampler
- Shelby Tube
- Piston Sampler
- NX Rock Core
- HQ Rock Core
- Bulk Sample
- Other (see remarks)

DRILLING METHOD SYMBOLS

- Auger Drilling
- Rotary Drilling
- Dynamic Cone or Hand Driven
- Diamond Core

WATER LEVEL SYMBOLS

- First Water Level Reading (during drilling)
- Static Water Level Reading (short-term)
- Static Water Level Reading (long-term)

Earth Mechanics, Inc.
Geotechnical and Earthquake Engineering

BORING RECORD LEGEND

UCSD Steel Pile Research.gpj

Project Number: 21-601	Date: 4-29-24	SHEET 1 of 2

CONSISTENCY OF COHESIVE SOILS

Descriptor	Unconfined Compressive Strength (tsf)	Pocket Penetrometer (tsf)	Torvane (tsf)	Field Approximation
Very Soft	< 0.25	< 0.25	< 0.12	Easily penetrated several inches by fist
Soft	0.25 - 0.50	0.25 - 0.50	0.12 - 0.25	Easily penetrated several inches by thumb
Medium Stiff	0.50 - 1.0	0.50 - 1.0	0.25 - 0.50	Can be penetrated several inches by thumb with moderate effort
Stiff	1.0 - 2.0	1.0 - 2.0	0.50 - 1.0	Readily indented by thumb but penetrated only with great effort
Very Stiff	2.0 - 4.0	2.0 - 4.0	1.0 - 2.0	Readily indented by thumbnail
Hard	> 4.0	> 4.0	> 2.0	Indented by thumbnail with difficulty

APPARENT DENSITY OF COHESIONLESS SOILS

Descriptor	SPT N_{60} - Value (blows / foot)
Very Loose	0 - 4
Loose	5 - 9
Medium Dense	10 - 29
Dense	30 - 49
Very Dense	> 50

MOISTURE

Descriptor	Criteria
Dry	Absence of moisture, dusty, dry to the touch
Moist	Damp but no visible water
Wet	Visible free water, usually soil is below water table

PERCENT OR PROPORTION OF SOILS

Descriptor	Criteria
Trace	Particles are present but estimated to be less than 5%
Few	5 to 10%
Little	15 to 25%
Some	30 to 45%
Mostly	50 to 100%

SOIL PARTICLE SIZE

Descriptor		Size
Boulder		> 12 inches
Cobble		3 to 12 inches
Gravel	Coarse	3/4 inch to 3 inches
	Fine	No. 4 Sieve to 3/4 inch
Sand	Coarse	No. 10 Sieve to No. 4 Sieve
	Medium	No. 40 Sieve to No. 10 Sieve
	Fine	No. 200 Sieve to No. 40 Sieve
Silt and Clay		Passing No. 200 Sieve

PLASTICITY OF FINE-GRAINED SOILS

Descriptor	Criteria
Nonplastic	A 1/8-inch thread cannot be rolled at any water content.
Low	The thread can barely be rolled, and the lump cannot be formed when drier than the plastic limit.
Medium	The thread is easy to roll, and not much time is required to reach the plastic limit; it cannot be rerolled after reaching the plastic limit. The lump crumbles when drier than the plastic limit.
High	It takes considerable time rolling and kneading to reach the plastic limit. The thread can be rerolled several times after reaching the plastic limit. The lump can be formed without crumbling when drier than the plastic limit.

CEMENTATION

Descriptor	Criteria
Weak	Crumbles or breaks with handling or little finger pressure.
Moderate	Crumbles or breaks with considerable finger pressure.
Strong	Will not crumble or break with finger pressure.

NOTE:
This legend sheet provides descriptors and associated criteria for required soil description components only. Refer to Caltrans Soil and Rock Logging, Classification, and Presentation Manual (2022 Edition), Section 2, for tables of additional soil description components and discussion of soil description and identification.

REF = Refusal; During drilling seating interval (first 6-inch interval) is not achieved.

SPT CAL

SPT HAMMER ENERGY MEASUREMENTS

Prepared for;
Tri-County Drilling
9631 Candida St
San Diego, CA 92126

(858) 271-0099

Energy Measurement Test for Dynamic Penetrometers
Standard Penetration Tests (SPT)

Date: 10/05/2023

Location: San Diego, CA

Prepared by;

SPT CAL
5512 Belem Dr
Chino Hills, CA 91709

909-730-2161
bc@sptcal.com

Drill: Rig 77

Energy Transfer Ratio = 80.4% @ 43.9 blows per minute

Hammer Energy Measurements performed per ASTM D4633 using an approved and calibrated SPT Analyzer 8G from Pile Dynamics, Inc. meeting the criteria of ASTM D4633-05 and per the process defined in ASTM D4633-05, The process and equipment requirements followed per ASTM D4633-05 meet the criteria of ASTM D4633-16.

LOGGED BY	BEGIN DATE	COMPLETION DATE	BOREHOLE LOCATION	HOLE ID
WD	4-19-24	4-19-24	Northing: ft Easting: ft	BH-1
DRILLING CONTRACTOR				SURFACE ELEVATION (MLLW)
TriCounty Drilling				
DRILLING METHOD			DRILL RIG	BOREHOLE DIAMETER
Hollow-Stem Auger			Dietrich D-120	8"
SAMPLER TYPE(S) AND SIZE(S) (ID)			SPT HAMMER TYPE	HAMMER EFFICIENCY, ERi
Mod Cal (2.4"), Shelby (2.87"), SPT (1.4")			Automatic Hammer 140 lb 30 inch drop	80.4%
GROUNDWATER DEPTH: DURING DRILLING				TOTAL DEPTH OF BORING
Not Encountered				26.5 ft

ELEVATION (ft)	DEPTH (ft)	Material Graphics	DESCRIPTION	Sample Location	Sample Number	Blows per 6 in.	Blows per foot	Recovery (%)	RQD (%)	Moisture Content (%)	Dry Unit Weight (pcf)	Shear Strength (tsf)	Drilling Method	Casing Depth	Remarks
	0		CLAYEY SAND (SC); medium dense; yellowish brown; moist; about 9% fine GRAVEL, max. 1/2 in. dia.; about 45% fine SAND; about 46% low plasticity fines; weak cementation.		D-1	8 8 11	19	100		13.8	110.7				DS, PI, PA
	3		About 9% fine GRAVEL; about 48% fine SAND; about 43% low plasticity fines; weak cementation.		T-2			100		11.7	122.3				DS, PA
	5		About 7% fine GRAVEL, max. 3/8 in. dia.; about 49% fine SAND; about 42% low plasticity fines; weak cementation.		D-3	8 11 13	24	100		15.3	109.7				PI, UU, PA
	8		SILTY, CLAYEY SAND (SC-SM); yellowish brown; moist; about 3% fine GRAVEL, max. 3/8 in. dia.; about 65% fine SAND; about 32% low plasticity fines; weak cementation.		T-4			100		11.6	106.9				DS, PI, PA
	10		CLAYEY SAND (SC); medium dense; yellowish brown; moist; about 1% fine GRAVEL, max. 3/8 in. dia.; about 62% fine SAND; about 31% low plasticity fines; weak cementation.		D-5	7 11 18	29	100		13.6	114.6				PI, UU, PA
	13		About 2% fine GRAVEL, max. 0.187 in. dia.; about 70% fine SAND; about 28% low plasticity fines; weak cementation.		D-6	10 16 20	36	100		10.8	106.3				PA
	15		SILTY, CLAYEY SAND (SC-SM); medium dense; yellowish brown; moist; about 2% fine GRAVEL, max. 3/8 in. dia.; about 62% fine SAND; about 36% low plasticity fines; weak cementation.		D-7	5 6 10	16	100		14.2	108.9				DS, PI, PA
	18				S-8	3 7 9	16	28							
	20		CLAYEY SAND (SC); dense; yellowish brown; moist; about 75% medium to fine SAND; about 25% low plasticity fines; weak cementation.		D-9	7 20 36	56	100		12.9	112.3				PA
	23		Poorly-graded SAND very dense; yellowish brown; moist; mostly medium to fine SAND; trace nonplastic fines; weak cementation; TERRACE DEPOSITS (Qt).		S-10	12 25 34	59	44							
	25														

(continued)

ELEVATION (ft)	DEPTH (ft)	Material Graphics	DESCRIPTION	Sample Location	Sample Number	Blows per 6 in.	Blows per foot	Recovery (%)	RQD (%)	Moisture Content (%)	Dry Unit Weight (pcf)	Shear Strength (tsf)	Drilling Method	Casing Depth	Remarks
	25		Poorly-graded SAND *(continued)*.		S-11	13 28 35	63	44							
	26														
	27		Bottom of borehole at 26.5 ft bgs. Notes:												
	28														
	29														
	30														
	31														
	32														
	33														
	34														
	35														
	36														
	37														
	38														
	39														
	40														
	41														
	42														
	43														
	44														
	45														
	46														
	47														
	48														
	49														
	50														
	51														
	52														
	53														
	54														
	55														

LOGGED BY	BEGIN DATE	COMPLETION DATE	BOREHOLE LOCATION	HOLE ID
WD	4-19-24	4-19-24	Northing: ft Easting: ft	BH-2
DRILLING CONTRACTOR				SURFACE ELEVATION (MLLW)
TriCounty Drilling				
DRILLING METHOD			DRILL RIG	BOREHOLE DIAMETER
Hollow-Stem Auger			Dietrich D-120	8"
SAMPLER TYPE(S) AND SIZE(S) (ID)			SPT HAMMER TYPE	HAMMER EFFICIENCY, ERi
Mod Cal (2.4"), Shelby (2.87"), SPT (1.4")			Automatic Hammer 140 lb 30 inch drop	80.4%
GROUNDWATER DEPTH: DURING DRILLING				TOTAL DEPTH OF BORING
Not Encountered				26.5 ft

ELEVATION (ft)	DEPTH (ft)	Material Graphics	DESCRIPTION	Sample Location	Sample Number	Blows per 6 in.	Blows per foot	Recovery (%)	RQD (%)	Moisture Content (%)	Dry Unit Weight (pcf)	Shear Strength (tsf)	Drilling Method	Casing Depth	Remarks
	0		CLAYEY SAND (SC); medium dense; yellowish brown; moist; about 6% fine GRAVEL, max. 1/2 in. dia.; about 47% fine SAND; about 47% low plasticity fines; weak cementation.		D-1	9 10 11	21	100		13.4	111.5				PI, UU, PA
	3		About 7% fine GRAVEL, max. 3/4 in. dia.; about 53% fine SAND; about 40% low plasticity fines; weak cementation.		SH-2			100		11.8	118.0				UU, PA
	5		About 4% fine GRAVEL, max. 1/2 in. dia.; about 50% fine SAND; about 46% low plasticity fines; weak cementation.		D-3	7 12 18	30	100		14.6	113.6				DS, PI, PA
	8		SILTY, CLAYEY SAND (SC-SM); medium dense; yellowish brown; moist; about 3% fine GRAVEL, max. 1/2 in. dia.; about 64% fine SAND; about 33% low plasticity fines; weak cementation.		SH-4			100		11.4	105.7				DS, PI, PA
	10		About 65% fine SAND; about 35% low plasticity fines; weak cementation.		D-5	6 9 8	17	100		13.5	110.5				DS, PI, PA
	13		CLAYEY SAND (SC); medium dense; yellowish brown; moist; about 3% fine GRAVEL, max. 1/2 in. dia.; about 66% fine SAND; about 31% low plasticity fines; weak cementation.		D-6	14 19 23	42	100		11.3	111.9				PA
	15		About 1% fine GRAVEL, max. 3/8 in. dia.; about 58% fine SAND; about 41% low plasticity fines; weak cementation.		D-7	10 15 24	39	100		14.3	114.4				DS, PI, PA
	18				S-8	5 5 8	13	44							
	20		About 74% fine SAND; about 26% low plasticity fines; weak cementation.		D-9	11 20 38	58	100		12.7	115.2				PA
	21		Poorly-graded SAND dense; yellowish brown; moist; mostly medium to fine SAND; trace nonplastic fines; weak cementation; TERRACE DEPOSITS (Qt).												
	23		Very dense; mostly fine SAND.		S-10	20 43 50/5"		67							
	25														

(continued)

ELEVATION (ft)	DEPTH (ft)	Material Graphics	DESCRIPTION	Sample Location	Sample Number	Blows per 6 in.	Blows per foot	Recovery (%)	RQD (%)	Moisture Content (%)	Dry Unit Weight (pcf)	Shear Strength (tsf)	Drilling Method	Casing Depth	Remarks
	25		Poorly-graded SAND *(continued)*.		S-11	30 28 45	73	100							
	26														
	27		Bottom of borehole at 26.5 ft bgs. Notes:												
	28														
	29														
	30														
	31														
	32														
	33														
	34														
	35														
	36														
	37														
	38														
	39														
	40														
	41														
	42														
	43														
	44														
	45														
	46														
	47														
	48														
	49														
	50														
	51														
	52														
	53														
	54														
	55														